Springer ThesesRecognizing Outstanding Ph.D. Research

Alessandro Manacorda

Lattice Models for Fluctuating Hydrodynamics in Granular and Active Matter



Springer Theses

Recognizing Outstanding Ph.D. Research

Aims and Scope

The series "Springer Theses" brings together a selection of the very best Ph.D. theses from around the world and across the physical sciences. Nominated and endorsed by two recognized specialists, each published volume has been selected for its scientific excellence and the high impact of its contents for the pertinent field of research. For greater accessibility to non-specialists, the published versions include an extended introduction, as well as a foreword by the student's supervisor explaining the special relevance of the work for the field. As a whole, the series will provide a valuable resource both for newcomers to the research fields described, and for other scientists seeking detailed background information on special questions. Finally, it provides an accredited documentation of the valuable contributions made by today's younger generation of scientists.

Theses are accepted into the series by invited nomination only and must fulfill all of the following criteria

- They must be written in good English.
- The topic should fall within the confines of Chemistry, Physics, Earth Sciences, Engineering and related interdisciplinary fields such as Materials, Nanoscience, Chemical Engineering, Complex Systems and Biophysics.
- The work reported in the thesis must represent a significant scientific advance.
- If the thesis includes previously published material, permission to reproduce this must be gained from the respective copyright holder.
- They must have been examined and passed during the 12 months prior to nomination.
- Each thesis should include a foreword by the supervisor outlining the significance of its content.
- The theses should have a clearly defined structure including an introduction accessible to scientists not expert in that particular field.

More information about this series at http://www.springer.com/series/8790

Alessandro Manacorda

Lattice Models for Fluctuating Hydrodynamics in Granular and Active Matter

Doctoral Thesis accepted by the University of Sapienza, Rome, Italy



Author
Dr. Alessandro Manacorda
Department of Physics
University of Sapienza
Rome, Italy

Supervisor
Dr. Andrea Puglisi
University of Sapienza
Rome, Italy

ISSN 2190-5053 ISSN 2190-5061 (electronic) Springer Theses ISBN 978-3-319-95079-2 ISBN 978-3-319-95080-8 (eBook) https://doi.org/10.1007/978-3-319-95080-8

Library of Congress Control Number: 2018946591

© Springer International Publishing AG, part of Springer Nature 2018

This work is subject to copyright. All rights are reserved by the Publisher, whether the whole or part of the material is concerned, specifically the rights of translation, reprinting, reuse of illustrations, recitation, broadcasting, reproduction on microfilms or in any other physical way, and transmission or information storage and retrieval, electronic adaptation, computer software, or by similar or dissimilar methodology now known or hereafter developed.

The use of general descriptive names, registered names, trademarks, service marks, etc. in this publication does not imply, even in the absence of a specific statement, that such names are exempt from the relevant protective laws and regulations and therefore free for general use.

The publisher, the authors, and the editors are safe to assume that the advice and information in this book are believed to be true and accurate at the date of publication. Neither the publisher nor the authors or the editors give a warranty, express or implied, with respect to the material contained herein or for any errors or omissions that may have been made. The publisher remains neutral with regard to jurisdictional claims in published maps and institutional affiliations.

Printed on acid-free paper

This Springer imprint is published by the registered company Springer International Publishing AG part of Springer Nature

The registered company address is: Gewerbestrasse 11, 6330 Cham, Switzerland



Supervisor's Foreword

The Ph.D. thesis of Dr. Alessandro Manacorda deals with the theoretical foundations of hydrodynamic models for granular flows and active matter. These systems are considered among the most prominent examples of complex fluids, where the collective many-particle behavior can be surprising with respect to the simplicity of the single-particle dynamics. The work of Dr. Manacorda has been carried out at the Physics Department of the University of Rome "Sapienza" in association with the Institute for Complex Systems of the Italian Consiglio Nazionale delle Ricerche (CNR-ISC). The granular part of the thesis project was setup in collaboration with Prof. Antonio Prados of the University of Sevilla, where Dr. Manacorda has also spent a few months of his Ph.D. period.

Granular and active systems are examples of soft matter, in the broad meaning of condensed matter states where fluctuations are relevant. However, they are not relegated to the microscopic world, but can be encountered along a wide range of spatial and temporal scales. Indeed, granular matter is made of solid grains of size from tens of microns up to centimeters or even meters (as in rocks found in planetary rings), and active matter includes not only microscopic swimmers and ratchets (such as actin filaments, bacteria, sperms.) but also large groups of macroscopic animals such as fishes and birds. This brings to the fore a fundamental property of fluctuations in granular and active matter, that is, their intrinsic out-of-equilibrium nature. In both granular and active fluids, one has a flow of energy coming from some external driving device (an externally vibrated box in the granular case, some internal energy storage in the active case) which animates the system and is eventually dissipated in the environment. This energy current prevents the use of the equilibrium tools of statistical mechanics, such as the equilibrium ensembles or the free energies. Logically, the theoretical investigation of those systems needs to perform a backward step with respect to equilibrium statistical mechanics: We need to return to kinetic theory and work with time-dependent (and time-asymmetrical) equations for probabilities. In order to simplify the theory, we can look for some coarse-graining procedure, typically focusing on a few observables or fields which evolve slowly in space and time. Another crucial aspect of both granular and active fluids is their "small" size, in terms of number of elementary constituents which can be as small as a few hundreds in several physical examples. As a consequence, the amplitude of fluctuations of coarse-grained variables can be much more important than in a fluid made of 10^{20} molecules. The coarse-graining procedures, therefore, should include some description of fluctuations and this—in a non-equilibrium system—represents an unsolved challenge that puts the work of this thesis at the frontier of theoretical physics.

The main theoretical new results presented in this thesis, all published in peer-reviewed papers, concern the introduction of new lattice models for a granular fluid (Chaps. 4 and 5) or an active fluid (Chap. 6) and the derivation—in both cases through simplifying assumptions such as Molecular Chaos and Local Equilibrium—of continuum hydrodynamic equations with noises coherent with the microscopic probabilistic prescriptions. The derived equations, validated through comparison with numerical Monte Carlo simulations of the lattice models, have also been studied analytically in order to deduce interesting collective regimes and phases. In certain cases, the analytical study of the microscopic model has gone beyond the local equilibrium assumption, producing interesting results about spatial and temporal correlations.

My opinion is that the value of this thesis is not limited to the new results, but is enriched by the first three chapters which provide an excellent introduction to the main subjects of this investigation, that are the physics of granular matter, the physics of active matter, and the general theory of fluctuating hydrodynamics. This opening discussion takes roughly half of the length of this thesis and constitutes a complete guide for students or researchers coming from other fields. Most importantly, these first chapters offer an interesting perspective about the physical and mathematical features shared by granular and active matter, in particular with respect to their continuum (hydrodynamic) description. A unifying picture of active and granular flows is rarely considered in the literature and therefore constitutes a conceptual key point of this thesis.

Rome, Italy April 2018 Dr. Andrea Puglisi

Abstract

This thesis is the result of my research work as a Ph.D. student at Rome University Sapienza, under the supervision of Dr. Andrea Puglisi, and in collaboration with Dr. Antonio Lasanta, Prof. Antonio Prados and Carlos A. Plata from Sevilla University. The goal of the thesis is the formulation of the fluctuating hydrodynamics in granular and active matter by means of lattice models in the non-equilibrium framework.

The contents of the thesis are the following: Chap. 1 is an introduction to the physics of granular and active matter, where the definitions and the main phenomenology of granular and active systems are reviewed.

Chapter 2 reviews the fundamental theoretical tools for the study of granular and active systems. The formulation of kinetic theory for conservative interactions is given and later applied to the granular case, introducing some of the most important granular states. The modelization of active matter is also discussed, introducing the most important models formulated in the last years to reproduce self-propulsion and active interactions. The last section analyzes some key experiments showing a possible active behavior for driven granular systems.

Chapter 3 is dedicated to hydrodynamics. The classic formulation of hydrodynamics through the Chapman–Enskog approach is sketched and later applied to the granular case and the study of its hydrodynamical instabilities. An overview of hydrodynamics in active matter is given and compared with previous cases. Finally, the mostly studied lattice models for conservative and dissipative statistical systems are reviewed.

Chapter 4 introduces a granular lattice model to investigate the fluctuating hydrodynamics of shear modes: The hydrodynamic equations are derived from microscopic dynamics through a continuum limit. Depending on the boundary conditions, the model is able to reproduce several granular states and is predictive about their hydrodynamic instabilities.

Chapter 5 describes the properties of the granular model introduced when molecular chaos assumption is abandoned. It is shown how velocity correlations and energy fluctuations can be directly computed from microscopic dynamics,

X Abstract

explaining the divergence of numerical results from the uncorrelated case previously studied.

Chapter 6 introduces a lattice model of active matter. The procedure of previous chapters is used to include self-propelled particles in d > 1, leading to the observation of collective behavior. The linear stability of the disordered state is studied together with the fluctuations of hydrodynamic currents.

The Appendices contain the derivation of analytical results for the granular model presented in Chaps. 4 and 5 (Appendix A) and for the active model of Chap. 6 (Appendix B). Appendix C contains a list of link to videos, aimed at a novel reader to illustrate the phenomenology introduced in Part I.

Many results presented in Part II of this thesis have been already published in journal articles; the research work is here presented in a detailed and consequential manner. The interested reader can refer to:

- Chapter 4: A. Manacorda, C. A. Plata, A. Lasanta, A. Puglisi, and A. Prados. Lattice models for granular-like velocity fields: hydrodynamic description. *J. Stat. Phys.*, 164(4):810–841, Aug 2016.
- Chapter 5: C. A. Plata, A. Manacorda, A. Lasanta, A. Puglisi, and A. Prados. Lattice models for granular-like velocity fields: finite-size effects. *J. Stat. Mech.* (*Theor. Exp.*), 2016(9):093203, 2016.
- Chapter 6: A. Manacorda and A. Puglisi. Lattice model to derive the fluctuating hydrodynamics of active particles with inertia. *Physical Review Letters*, 119(20):208003, 2017.

List of Publications

- [1] Alessandro Manacorda, Andrea Puglisi, and Alessandro Sarracino. Coulomb friction driving Brownian motors. *Communications in Theoretical Physics*, 62 (4):505, 2014.
- [2] Antonio Lasanta, Alessandro Manacorda, Antonio Prados, and Andrea Puglisi. Fluctuating hydrodynamics and mesoscopic effects of spatial correlations in dissipative systems with conserved momentum. *New J. Phys.*, 17:083039, 2015.
- [3] Alessandro Manacorda, Carlos A. Plata, Antonio Lasanta, Andrea Puglisi, and Antonio Prados. Lattice models for granular-like velocity fields: Hydrodynamic description. *J. Stat. Phys.*, 164(4):810–841, Aug 2016.
- [4] C A Plata, A Manacorda, A Lasanta, A Puglisi, and A Prados. Lattice models for granular-like velocity fields: finite-size effects. *J. Stat. Mech. (Theor. Exp.)*, 2016(9):093203, 2016.
- [5] A. Manacorda and A. Puglisi. Lattice model to derive the fluctuating hydrodynamics of active particles with inertia. *Phys. Rev. Lett.*, 119:208003, Nov 2017.

Acknowledgements

My first gratitude is to Andrea Puglisi, my advisor and master of physics, who ceaselessly guided me in my education as a physicist and inseparably as a man. In these years, I could appreciate his willingness and patience—even in front of my common oddities—combined with the various theoretical, numerical, and experimental perspective which he is able to combine in his investigation, a quality that fascinated me from the very beginning. I hope that this thesis will correspond some of the expectations that we had together when we started this path already five years ago, and that it may become useful in the future and be the first of many works together.

Subsequently, I thank those who shared with me the most important steps of my scientific work: first of all Antonio Lasanta, being its presence a source of discussions and debates always useful during his stay in Rome, together with his friendly and energetic spirit. I thank Prof. Antonio Prados, who inspired and educated me in these years with his meticulousness and perseverance, and who constantly followed the development of my thesis. I also thank Carlos A. Plata, that I had the pleasure to meet in Sevilla and to have as a co-worker, who stimulated me to do my best whole interlacing our results. His scientific curiosity and his welcoming have been very precious to me, together with the whole crew in Sevilla, thank you all!

During my Ph.D., the TNT group in Rome has constantly been my scientific reference point. I want to thank in particular Luca Cerino for the stimulating discussions and the support that he gave me little by little while we carried on our theses. I thank Angelo Vulpiani for his availability and his help and suggestions, both for scientific questions and future perspectives, and for being not only a strong physicist but an inspiring thinker; and I thank Alessandro Sarracino, who has been fundamental to understand many physical arguments beyond my expertise, being a stimulating and curious speaker. Thanks also to Umberto Marini Bettolo Marconi for the preliminary discussions about our active matter model, which guided us at the beginning of our research. Thanks to Giorgio Pontuale, Alberto Petri, Andrea Baldassarri, Mario Alberto Annunziata, Fabio Cecconi, and Massimo Cencini for

xiv Acknowledgements

their welcoming in the last years, with a special dedication to Andrea Gnoli, which I always admire for his kindness and grace.

This thesis has been mostly developed in Room 413, which I could share with many young physicist struggling with their Ph.D. studies between 2013 and 2017. I especially want to thank Fabrizio Antenucci, for the pleasure of his knowledge both in scientific discussions and human dialogue, and Daniele Conti for the debates and the support given: I hope that sooner or later he will manage to become a better crosser.

I also thank my room neighbors Massimiliano Viale and Stefania Melillo that have been a fundamental moral support while I was drowning writing the thesis. Their solidarity, curiosity, and empathy have been precious, as Massimiliano shows through the generosity that he uses in playing football.

This thesis concludes an important period of my life, started ten years ago when I became a student of Rome's Physics Department. From the beginning, I have had extraordinary fellows. First of all, I want to thank Marco Sciannamea, because writing this thesis would have been very harder without his presence. It has been beautiful spending these months helping each other writing our theses, as it could be more than ten years ago. I thank also Alessandro Calandri, Riccardo Junior Buonocore, and Ferdinando Randisi, special friends and passionate scientists, for the friendship going on across long distances but always united. I want to particularly thank Ferdinando for his giraffe, too.

I want to thank all my friends that supported me until now and in the last years, and for the sake of conciseness I can only name you: Michele Angelo Cecchi, Daniele Mezzalira, Maria Beatrice Bongiovanni, Gaia Benzi, Francesca Romana Calandrelli, Carlotta Taschini, Ludovica Zaccagnini, Kalipso Trevisiol, and Federica D'Alessio ... thank you all, you know why.

I thank my former comrades of the CUS, for the common path shared and for having been a very important part of my life and formation until the last years. I want to especially thank Maria Giordano, Dario Renzi, Manu Voto, Francesca Raineri, Micol Drago, and Marcin Trycz. I hope that also if we took a different direction the past will be a treasure to guide us in the future.

While I was writing this thesis, on May 28, 2017, Francesco Totti retired from football, but his inventions and genius still inspire us today any time we need to feel brave and free. Grazie, Francesco: for the years spent watching you, for the dreams that you embodied for me and many more, for the creation of new geometries and dynamics of time and space, and for the inspiration that will last in the future.

Thanks to Nerina Marcon and Emanuela Salciccia for having been two special teachers for me, the former for inflaming my heart with the passion for science—without any rebate for the young student that I was—and the latter for the confidence and the ambition instilled since ten years ago until now.

I thank my parents, for the ceaseless love and support that allowed me to get where I am, for the goodwill and serenity that they imparted to me, giving me the possibility to live my life and make my choices, not necessarily understanding them. I thank my sister for being always my great sister, and for the many moments when she made me grow, listening to me and making me more aware.

Acknowledgements xv

Finally, my main gratitude goes to my grandparents for all the love that they gave me, with their stories and their antithetical characters. I thank Valeria for having been a unique example of gentleness, and Giuliano for showing me how a man with value and eminence can also be sensitive. I thank Carlo for the confidence and the passion that he always infused in me, hoping to have partially reciprocated the dedication that he made me ten years ago. And I thank Silvia for being the most extraordinary grandma of the world, for the strength, determination, and love that she gives to her grandchildren, which I have the privilege to be. Altogether they formed my cultural background, being at the origin of many of my vocations and fascinations. This thesis is dedicated to them.

Rome, Italy May 2018 Dr. Alessandro Manacorda

Contents

Part I Granular and Active Matter

1	Introduction				
	1.1	What is Granular Matter			
	1.2		9		
		1.2.1 Granular Pressure, Internal Stresses, Jamming	9		
	1.3	Granular Flows	2		
		1.3.1 Rapid Granular Flows	2		
	1.4	What is Active Matter	6		
		1.4.1 Active Phenomenology	7		
		1.4.2 Living Systems	1		
		1.4.3 Non-living Systems	4		
	Refe	rences	6		
2	The	oretical Models of Granular and Active Matter	1		
	2.1	Kinetic Theory of Rapid Granular Flows	1		
		2.1.1 From Liouville to Boltzmann Equation	2		
		2.1.2 Inelastic Collisions and Granular Boltzmann Equation 3	8		
		2.1.3 The Homogeneous Cooling State and Haff's Law 4	2		
		2.1.4 Steady State Representation	5		
		2.1.5 Driven Granular Systems	6		
		2.1.6 Inelastic Maxwell Molecules 4	7		
	2.2	Active Models	9		
		2.2.1 The Kuramoto Model	2		
		2.2.2 The Vicsek Model	4		
		2.2.3 Active Brownian Particles and Run-and-Tumble			
		Dynamics	7		
		2.2.4 Active Ornstein–Uhlenbeck Particles 5	9		
	2.3	Grains and Active Particles 6	1		
	Refe	rences	3		

xviii Contents

3	Hyd	rodyna	amic Description and Lattice Models	67
	3.1	Hydro	odynamics	68
		3.1.1	Conservative Interactions	68
		3.1.2	Granular Hydrodynamics	74
		3.1.3	Hydrodynamic Instabilities and the HCS	76
		3.1.4	Active Hydrodynamics	80
	3.2	Fluctu	ating Hydrodynamics	82
	3.3	Lattice	e Models	87
		3.3.1	Conservative Models	88
		3.3.2	Dissipative Models	93
	Refe	erences		96
Pa	rt II		uating Hydrodynamics of Granular and Active Matter:	
	_			
4			Lattice: Fluctuating Hydrodynamics	101
	4.1		tion of the Model	102
		4.1.1	Master Equation for the Lattice Model	103
		4.1.2	Physical Interpretation	105
		4.1.3	Evolution Equation for the One-Particle Distribution	106
	4.2		dynamics	107
		4.2.1	Microscopic Balance Equations	107
		4.2.2	Balance Equations in the Continuum Limit	109
	4.3	-	cally Relevant States	111
		4.3.1	The Homogeneous Cooling State	112
		4.3.2	The Uniform Shear Flow Steady State	114
		4.3.3	The Couette Flow Steady State	116
		4.3.4	Validity of the Hydrodynamic Description	118
	4.4		ating Hydrodynamics	118
		4.4.1	Definition of Fluctuating Currents	118
		4.4.2	Noise Correlations	119
		4.4.3	Cross-Correlations of the Noises and Gaussianity	122
	4.5		rical Results	124
		4.5.1	General Simulation Strategy	124
		4.5.2	Homogeneous and Non-homogeneous Cooling	124
		4.5.3	Uniform Shear Flow State	125
		4.5.4	The Couette Flow State	128
		4.5.5	Fluctuating Currents	131
	Refe	erences		132

Contents xix

5	Gra	nular I	Lattice: Beyond Molecular Chaos	135				
	5.1	Pertur	bative Solution for Temperature and Correlations	136				
	5.2 Temperature and Correlations Evolution: Multiple-Scale							
		Analy	sis	139				
	5.3	Total	Energy Fluctuations and Multiscaling	142				
	Refe	rences		147				
6	Active Lattice Fluctuating Hydrodynamics							
	6.1	Defini	tion of the Model	150				
		6.1.1	Microscopic Ingredients	150				
		6.1.2	Physical Interpretation	151				
		6.1.3	Microscopic Balance Equations	152				
	6.2	Hydro	odynamic Limit	155				
		6.2.1	Homogeneous Fixed Points	160				
		6.2.2	Stability Analysis of the Disordered State	162 164				
	6.3 Fluctuating Hydrodynamics							
	6.4	Nume	rical Results	166				
		6.4.1	General Simulation Strategy	166				
		6.4.2	Swarming Instability	167				
		6.4.3	Clustering Instability	168				
		6.4.4	Finite-Size Effects Near the Transition	169				
		6.4.5	Fluctuating Currents	170 171				
	References							
7	Con	clusion	s	173				
Aŗ	pend	ix A: A	Analytical Results for the Granular Model	177				
Aŗ	pend	ix B: A	Analytical Results for the Active Model	195				
Αŗ	pend	ix C: V	Videos	199				

Part I Granular and Active Matter

Chapter 1 Introduction



Like lesser birds on the four winds Like silver scrapes in May Now the sands become a crust And most of you have gone away

(Blue Öyster Cult)

Granular and active matter are among the most studied systems in out of equilibrium statistical physics.

The study of out of equilibrium systems is still under development and represents one of the most important progresses of statistical physics in the last century. At the end of the 19th century, equilibrium statistical physics had developed the main tools to investigate the physical properties of macroscopic systems as a statistical consequence of their macroscopic behavior. The development of the kinetic theory has related the time evolution and the equilibrium values of thermodynamic observables such as temperature and pressure to the microscopic dynamics of the enormous number of particles constituting the material of observation. The existence of conservation laws such as the energy conservation principle is the basis to define the tendency to equilibrium normally observed in gases and liquids: no matter the initial configuration of the system, the microscopic dynamics of the system leads it to a macroscopic equilibrium state with a given probability distribution of its dynamical coordinates, namely the positions and velocities of the particles of a gas, determined by the Boltzmann formula $e^{-\beta H}$ for Hamiltonian systems. The existence of an equilibrium state allows to introduce the Gibbs ensembles description and define thermodynamical functions such as the Helmoltz free energy, the entropy and so on.

However, out of equilibrium systems are ubiquitous. First, every system at equilibrium can be driven out of it from a perturbation, inducing a heat or mass current into the system, developing spatial gradients coupled with a temporal evolution of thermodynamical quantities. This is what ceaselessly happens in *transport processes*, e.g. when a fluid is flowing under a pressure gradient or an electric current arises because of the application of a voltage. Nonequilibrium phenomena are involved in a large amount of research fields, such as climate dynamics, chemical reactions, biological physics and applications of physics to economics and social science. The basis of nonequilibrium statistical physics rely on probability and stochastic processes theory: while on one hand the huge number of microscopic components forbid any possibility of analytical computation of their motion one by one, on the other hand it allows to use limit theorems such as the Law of Large Numbers or the Central Limit Theorem, getting more precise predictions as the number of microscopic particles increase. The most ambitious goal of statistical physics is to derive the probability distribution of the microscopic variables of the considered system: if this is achieved, the computation of macroscopic observables is generally almost straightforward.

Granular and active matter are two kinds of out of equilibrium statistical systems. Granular matter is everything that is made of grains, like powders, sand, cereals, pills etc. A grain is a solid particle following the laws of classical mechanics and interacting among each other through dissipative collisions. The last feature is what actually makes granular matter out of equilibrium, differentiating it from colloidal particles which follow classical mechanics but undergo elastic collisions. A system can be at equilibrium if a phase-space trajectory and its time-reversed one have the same probability to occur a priori. It will be shown that dissipation makes it impossible for granular materials. Therefore, being out of equilibrium in granular matter is not the consequence of a perturbation but rather an *intrinsic* property of the physical system. This is possible because the granular description introduces a coarse-graining of the system at a mesoscopic scale, disregarding the microscopic degrees of freedom involved in collisions and absorbing the dissipated kinetic energy, restoring the energy conservation principle at a more fundamental level. Nevertheless, the description introduced has revealed to be of practical use to describe the main properties of granular materials. Research on granulars started from the observation of many unknown features in industrial devices: the observation that pressure and stress propagation followed a rather different behavior from elastic materials inaugurated a new research area, with many possible interactions with engineering problems such as the transport of grains, the mixing or separation of different kind of powders, the prevention of avalanches and the diffusion of fluids into a granular material.

Active matter is every system composed by many self-propelled units. The most natural examples are animals: their biological structure provide them the motility, i.e. the capability to sustain a state of motion by converting the chemical energy stored into kinetic energy. As it will be shown, the research has identified a plethora of active systems, including humans which obviously move across the space. Active matter exhibits a spectacular behavior when the units coordinate themselves and give rise to collective motion: this is what we observe when fishes move together in

huge schools, travelling across the sea and defending from predators, or when birds coordinate their motion forming amazing flocks. Thus, active matter phenomena are the combination of the individual self-propulsion of the units with the reciprocal interactions established among them. Living units are very complex systems, and the derivation of interaction rules from their biological properties is currently out of reach. Therefore, research on active matter in the last two decades focused on the proposal of minimal models capable to reproduce the main features of collective motion observed in experiments.

Granular and active matter share two main properties:

- they are both intrinsically out of equilibrium: indeed, active matter continuously converts internal energy absorbed somehow from the environment-in kinetic energy to sustain its state of motion; furthermore, when moving in a viscous fluid or substrate, kinetic energy is dissipated all along the motion. This implies the presence of continuous balance of energy injection/dissipation during the motion of the particle. The same balance occurs in a driven granular gas: to avoid the global "cooling" of granular motion caused by collisions, one can inject energy in a granular media through some mechanical process, like shearing or shaking the granular. Therefore, granular and active matter seem to have a *specular behavior*: while the former loses kinetic energy in its free motion and needs to absorb it from the environment, the latter vice versa "creates" kinetic energy from stored internal energy and dissipates it interacting with the environment.
- grains and active units are generally *small systems*: even if in some physical situations they can be made of $N \sim 10^5$ particles, this number is quite far from Avogadro's number $N_A \sim 10^{23}$. Therefore, the validity of limit theorems is more delicate, the *fluctuations* become relevant and can usually be compared with the magnitude of macroscopic quantities of the system. A probabilistic approach must not disregard them but rather include them in a more accurate description.

The specularity between granular and active particles is not an invention of this thesis: many studies have connected the two, and several experiments on shaken nematic or polar rods have shown their "active behavior". Actually, it is established that driven *asymmetrical* granular particles can behave as active units, because nematic or polar interactions can produce an alignment and increase of velocity correlations leading to some collective motion. Nevertheless, what has been observed numerically-and confirmed analytically in this thesis-is that dissipative granular collisions are sufficient to create velocity correlations leading a granular system to an ordered motion, even for apolar and isotropic particles.

There are several possible descriptions when looking at granular and active matter: we are interested in their *hydrodynamic description*. Namely, a granular material or an active system can be treated as a *fluid*, where each unit is analogous to a molecule of the fluid and the dynamical observables are the macroscopic fields of density, velocity and temperature, defined from classical hydrodynamic description of molecular fluids. This representation allows to recognize many collective phenomena of granular and active motion such as vortex formation, clustering, swarming and so on. Hydrodynamics is deeply related to kinetic theory, providing a statistical derivation of

macroscopic observables without the need of equilibrium assumptions. Furthermore, in the last decades the theory of *fluctuating hydrodynamics* has started, aiming at reintroducing in hydrodynamic theory all the fluctuations which are typically neglected when considering systems with a huge number of particles. However, fluctuating hydrodynamics of nonequilibrium systems often relies on equilibrium assumptions; otherwise, some successful attempts of rigorous derivation for nonequilibrium systems have been done, but represent a very hard technical challenge and therefore are limited to some specific cases.

1.1 What is Granular Matter

Every physical system made by a large amount of macroscopic or mesoscopic particles, called *grains*, is a granular material: typical examples are sand, dust, pills, seeds, as well as iceberg groups and Saturn rings-see Fig. 1.1 [1, 2]. Granular matter is ubiquitous in everyday life: when we transport food, build houses, stock products, project industrial processes and so on. Understanding its qualities has a great importance to predict and reproduce the behavior of such materials.

Granular materials share the following properties:

- grains are *macroscopic*: they follow the laws of classical mechanics and have a large number of internal degrees of freedom, which one does not directly observe during experiments;
- grains are solid: they occupy a volume which is excluded to other grains during their motion:
- grains interact by means of *dissipative interactions*: because of the presence of internal degrees of freedom, after a collision the total energy of two particles is partially dissipated, mainly because of grains deformation, as heat. Therefore friction occurs at the first level of description for a granular fluid;
- the temperature doesn't affect granular dynamics, i.e. grains can always be considered at T=0. Indeed, since grains are macroscopic their mechanical energy is typically many order of magnitude larger than their internal energy, namely $mv^2 \gg k_B T$ for a particle moving with velocity v. In kinetic theory a *granular temperature* can be introduced from statistical properties of granular motion, but it has nothing to do with room temperature.

Let us try to explain their physical meaning: since a granular material is made by many particles, statistical mechanics is the principal theoretic tool to understand its behavior. However, even if all the above-stated properties are quite general, one can see that a granular material is intrinsically different from an elastic fluid or a solid: the classic nature of grains makes the law of quantum mechanics unnecessary, and therefore the correct statistical representation must consider classic observables and interactions. Of course, each grain is made by atoms following the laws of quantum mechanics, but at this stage the grains are the "elementary particles" of our system.



Fig. 1.1 Several examples of granular materials. From top to bottom: sand dunes, color powders and iceberg group (left column), charcoal, cereals and legumes, Saturn rings (right column). Credit: NASA/JPL-Caltech/Space Science Institute

Another key feature to understand granular dynamics is the role of *inelasticity*: it is known that elastic collisions are not an ideal case in physics but they ceaselessly occurs between atoms and molecules because of energy conservation. Since grains have many internal degrees of freedom, after a collision they can distort and even break into more parts; these processes need energy which comes from the kinetic energy of grains, which therefore decreases after a collision. Typically, the inelasticity is measured by the *restitution coefficient* α (see Sect. 2.1), which ranges from 1 in the elastic case to 0 when collisions are totally inelastic.

The dissipative nature of interactions has lots of consequences in granular physics; one of the most important, which will be persistently remarked all along this thesis, is that granular matter is intrinsically *out of equilibrium*: the lack of energy conservation at this level of description imply that the phase-space trajectories are not symmetric

under time reversal. This is evident in the case of granular cooling, when energy dissipation leads the system to a metastable state where all the grains stop with zero kinetic energy-see Sect. 2.1.3.

The only way to avoid the inevitable cooling of a freely evolving granular gas is to *drive* the system by supplying power from outside: this is done both theoretically and experimentally by means of some shaking or shearing mechanism. These drivings provide a continuous injection/dissipation of energy in the system leading to a *non equilibrium steady state* (NESS).

The reader must then move away from classical concepts elaborated in statistical mechanics, and forget about the temperature as a physical parameter of the reservoir surrounding the system. From now on, only granular temperature is considered, which depends on kinetic energy of grains and generally coincides with the variance of their velocity (if $m=k_B=1$). Driving devices act as a thermostat, forcing the granular velocity distribution toward a given temperature. Typically, when considering a shaken granular gas subject to the force of gravity, the shaking acceleration needs to be larger than the gravity acceleration g, so that a grain colliding with a wall in the bottom gets the kinetic energy to reach the maximum height of the physical system. The energies involved in this process are then kinetic energy and gravitational potential energy. Furthermore, from now on materials with elastic interactions will be indicated as elastic materials, as distinct from granular materials which are always inelastic.

All the properties above-stated define a granular material: evidently they are not independent one from another but deeply related – the dissipation is the consequence of the mesoscopic space scale chosen, which is possible only in classical mechanics. There is another feature which does not define a granular material but occurring in almost all granular systems: the *number of particles* is large, typically ranging from 10² to 10⁵ in most experiments and physical systems studied, therefore statistical mechanics description is adopted because following the individual motion of each particle is impossible at a theoretical level. However, if compared with molecular materials, containing an Avogadro's number of particles $N_A \sim 10^{23}$, the number of grains is very small. This is a crucial property: indeed statistical mechanics makes plentiful use of the thermodynamic limit $N \to \infty$, to exploit limit theorems such as Law of large numbers and Central limit theorem. This can be done in granular matter as well, but fluctuations become very relevant when compared with molecular systems. Therefore, their theoretical and experimental description is a key point to understand granular dynamics: this is typically carried on by means of mathematical tools such as stochastic equations and large deviations theory. The goal of this thesis is to formulate a hydrodynamic description of granular and active matter capable to accounting for large fluctuations: this kind of theory is called *fluctuating* hydrodynamics, and will be described in Sect. 3.2.

1.2 Granular States 9

1.2 Granular States

Here some particular properties of granular materials at rest are reviewed: the reader may find a more detailed and complete overview in [1, 3], with a comparison between granular phases (solid, liquid, gases). The aim of the present section is to introduce some characteristic granular properties underlining their differences with molecular materials and show their connections with equilibrium statistical physics, when they can be done.

1.2.1 Granular Pressure, Internal Stresses, Jamming

When a silo is filled with a granular, the pressure at the bottom grows with the height of the filling in a rather different form from a classic fluid: indeed, a Newtonian fluid follows the Stevin's law [4]

$$p_v(h) = \rho g h \,, \tag{1.1}$$

with p_v the vertical pressure, ρ the density of the fluid, g the gravity acceleration and h the height of the fluid column above the position of measurement. The pressure in a granular material follows a different law, discovered by H. A. Janssen in 1895 [5], i.e.

$$p_v(h) = \Lambda \rho g - (\Lambda \rho g - p_v(0))e^{-h/\Lambda}, \qquad (1.2)$$

where Λ is a characteristic length of the order of the cylinder radius R. The Janssen's law accounts for saturation in granular cylinders, which guarantees a constant flow rate in a hourglass. Janssen himself gave a first derivation, with the following assumptions:

- 1. the vertical pressure p_v is constant in the horizontal plane;
- 2. the horizontal pressure p_h is proportional to the vertical pressure, i.e. $K = p_h/p_v$ constant in space;
- 3. the wall friction $f = \mu p_h$ sustains the vertical load at contact with the wall;
- 4. the granular material has constant density ρ at all heights.

The mechanical equilibrium of a granular disk of radius R and height dh therefore reads

$$\pi R^2 \frac{dp_v}{dh} dh + 2\pi R \mu K p_v dh = \pi R^2 \rho g dh , \qquad (1.3)$$

leading to

$$\frac{dp_v}{dh} + \frac{p_v}{\Lambda} = \rho g \,, \tag{1.4}$$

where $\Lambda = R/(2\mu K)$. Janssen's law in Eq. (1.2) is the corresponding solution with boundary condition $p_v(0)$.

The previous assumptions are not obvious: the first one is generally false because the pressure depends also on the radial distance from the cylinder axis, while the second assumption should be justified from constitutive relations, relying on microscopical features of the model. Nevertheless, the Janssen's law is a good first step to go beyond elastic fluids laws. The vertical and horizontal pressure are connected with *stresses*: in an elastic fluid at equilibrium, it is known that the stress tensor is uniform, isotropic and diagonal. This is not what actually happens in granular materials: every grain discharges its load to underlying grains, creating long force chains and propagating the stress in random directions depending on the specific configuration at rest. An experimental and numerical observation of force chains is shown in Fig. 1.2.

Another remarkable phenomenon revealed by experiments on granular statics are *pressure fluctuations*: when a container is poured several times with a granular material, the pressure at its bottom can change of more than 20% between two distinct realizations [7]. Furthermore when considering a single pouring, the distribution of stresses in the bulk or at the bottom of the silo shows an exponential tail [8].

Internal pressure behavior is directly related with *sound propagation* in granular mediums: it has been experimentally shown by Liu and Nagel [9] that when the bulk is perturbed by a harmonic force (4 Hz) the fluctuations can be very large, with a

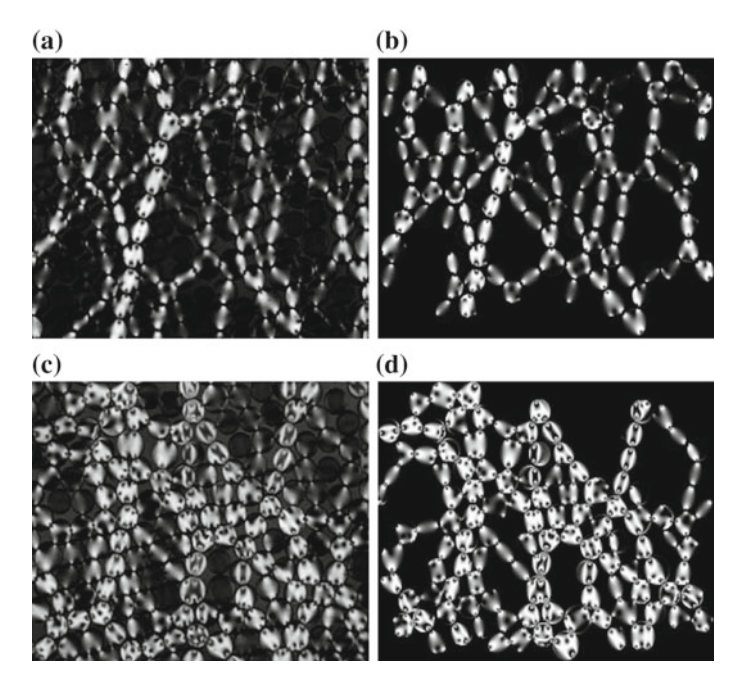


Fig. 1.2 Force chains in a granular material, experimental observations (**a**, **c**) and numerical simulations (**b**, **d**). Grains are photoelastic birefringent disks subjected to pure shear (top pair) or isotropic compression (bottom pair) [6]

1.2 Granular States 11

power-law spectrum $f^{-\alpha}$ where $\alpha = 2.2 \pm 0.05$. Also, the same authors observed that the sound group velocity can reach 5 times the phase velocity and that changing the amplitude of vibration gives rise to an hysteretic behavior [10].

As it has been shown, the pressure acts on granular particles in a quite different way from an elastic medium, because of the formation of long-ranged threadlike force chains and the presence of strong fluctuations, signature of the strong disorder in the bulk of the medium. A consequence of these features is the phenomenon of *arch formation*: when a granular is flowing through a hopper, the flow can suddenly stop because of the formation of a stable arch over the opening, able to sustain the entire load of the grains overhead (see Fig. 1.3). This phenomenon is a very well known experience in everyday life: many times, when pouring a granular substance from one container to another, if the outlet is too small the grains spontaneously stop pouring and one typically needs to shake the medium to start again. Generally speaking, the transition occurring when vibrated or flowing granular particles get stuck together in a single compact aggregate is called *jamming transition*.

In 1961, Beverloo et al. experimentally found the existence of a critical opening size below which jamming occurs [12]; more recently [13], experiments have shown the quantitative behavior of the jamming probability in function of the opening parameter d = R/D > 1 and the hopper angle φ , where R is the diameter of the outlet and D is the radius of monodisperse spherical grains (see Fig. 1.4a). This effect has recently been studied in experiments by Tang and Behringer [14, 15]:

The jamming transition is a typical example of a granular *phase transition*, although being out of equilibrium this has not the same meaning of equilibrium transitions, where a free energy can be defined and the transition shifts the system from an equilibrium state to another. The jamming transition has been investigated theoretically [16–19] and experimentally [20, 21], leading to a strong comparison with liquid-glass transition in glassy systems. Specifically, a phase diagram can be written in terms of granular temperature, packing fraction and external stress [18]. When considering the behavior of dense packing of granular particles flowing down a rough, inclined plane, it has been shown that the tilt angle behaves as a control parameter in analogy with the temperature T in the glass transition [19]. Furthermore, experiments in a 2d granular system of photoelastic bidisperse disks with

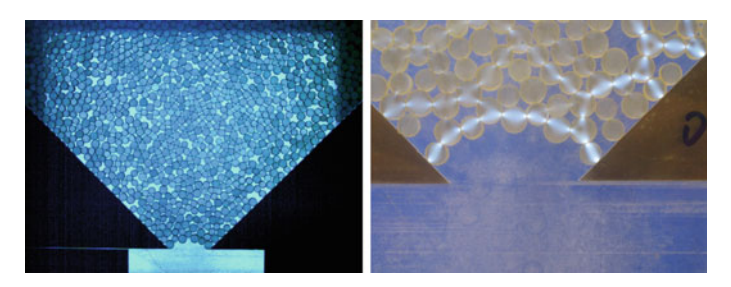


Fig. 1.3 Arch formation and granular jamming. Left panel shows how a concave arch supports the whole granular above it. Right panel shows arch forces near the outlet [11]

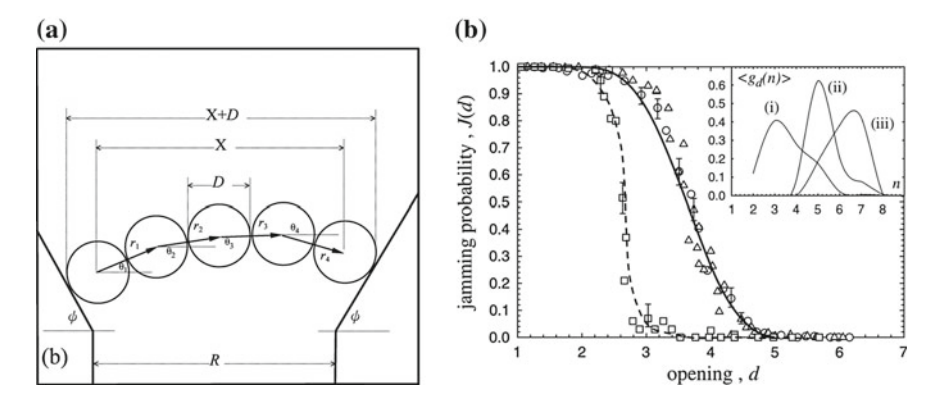


Fig. 1.4 Probability of jamming for a granular flowing through a hopper [13], experimental setup (left) and jamming transition (right). The jamming probability j(d) is plotted versus the opening parameter d, for three hopper angles $\phi = 34^{\circ}$ (circles), 60° (triangles) and 75° (squares). The solid line is a theoretical prediction provided by the authors, the dashed line is a guide to the eye for the $\phi = 75^{\circ}$ case [13]

moving walls have shown a power-law behavior of the mean contact number Z and the granular pressure P above the critical value of packing fraction $\phi_c = 0.8422$, namely $Z \sim P \sim (\phi - \phi_c)^\beta$, with $0.5 < \beta < 0.6$ [21]. All the cited studies converged in stating that in granular jamming a critical behavior is actually observed, even though granular materials are far from equilibrium.

1.3 Granular Flows

When a granular material is flowing, two kinds of regime can occur: *slow* or *rapid* flow. While in the former the grains are always in contact with their neighbors and interact frictionally for macroscopic times, in the latter they typically move ballistically between two inelastic collisions, which are instantaneous events. The rapid or slow behavior is generally governed by the granular density, its typical acceleration and boundary conditions. In rapid granular flows the analogy with kinetic representation describing elastic gases is strong: in the next sections it will be shown how a kinetic theory can be built from microscopic interactions, leading to a macroscopic picture of granular flow and to hydrodynamics. In this section some characteristic features of rapid granular flows are introduced.

1.3.1 Rapid Granular Flows

Many experiments have been made to investigate the behavior of *sheared* and *shaken* granular fluids [22]. Two kinds of experimental setups can be distinguished:

1.3 Granular Flows 13

• Couette rheology, consisting of a granular medium placed between two cylindrical walls with the same axis, and rotating one or both of them to induce a shear formation in the granular. The physical parameters are the distance between the cylinders, the rotational speed and the packing fraction of the granular.

• Shakers, consisting of a granular medium in a container whose one or more walls are vibrated. Typical parameters of these systems are the vibrations amplitude A and the frequency ω , which can be compared with gravity acceleration g through the vibration parameter $\Gamma = A\omega^2/g$: when $\Gamma > 1$, the vibration is strong enough to produce many phenomena that will be described below. The transition from slow to rapid granular flow induced by vibration is often called *vibrofluidization*.

In both cases the shear or the shaking can be sufficient to lead the system to a stationary state, i.e. to avoid the inelastic cooling. However, tuning the above-stated parameters the granular medium can change qualitatively its features, moving from a slow granular motion to a fluidized state of rapid flow. Here some characteristic phenomena of granular fluids are reviewed:

- Stress fluctuations: it has already been mentioned that in granular statics stresses are not homogeneous and exhibit strong fluctuations; when a 2d bidisperse granular is sheared in a Couette geometry, a strengthening/softening transition has been observed [23]. Below a threshold value of the packing fraction $\phi_c \simeq 0.776$, stress fluctuations are small, the granular is compressible and stress chains are long and radial; above this value strong fluctuations occurs, compressibility becomes large and the network of stress chains becomes tangled and dense.
- Slow convection and size segregation: when a granular is shaken or sheared, convection takes place. If the granular is heterogeneous, size segregation occurs as well. These features are known for a long time and have been recently investigated in experiments with Couette cylinders [24] and vertically vibrated granulars [25]: larger particles use to rise to the top of the granular medium during its motion, carried by convective cells formation. This effect is also known as the *Brazil-nut effect*, because when opening a box of cereals it is common to find the larger ones (Brazil-nuts) at the top [26]. Further experiments have shown that size segregation depends on relative diameter, density and shaking frequency: indeed, at low frequencies segregation is governed by inertia and convection, and denser particles rise faster. On the other hand, at high frequencies the granular is fluidized and there is no convection, so an intruder sinks if it is denser than the surrounding grains, and buoys up otherwise [25].
- **Pattern formation**: experiments have shown the formation of surface waves patterns in vertically vibrated granular layers [27–30], which exhibit various and fascinating textures (see Fig. 1.5a) depending on the set of parameters of the granular system: vibration frequency, vibration parameter Γ, size of the system, size and shape of the grains, and so on. This behavior has been associated also to the presence of *oscillons*, namely spatially localized excitations with the propensity to assemble into molecular or crystalline structures, see Fig. 1.5b [31].

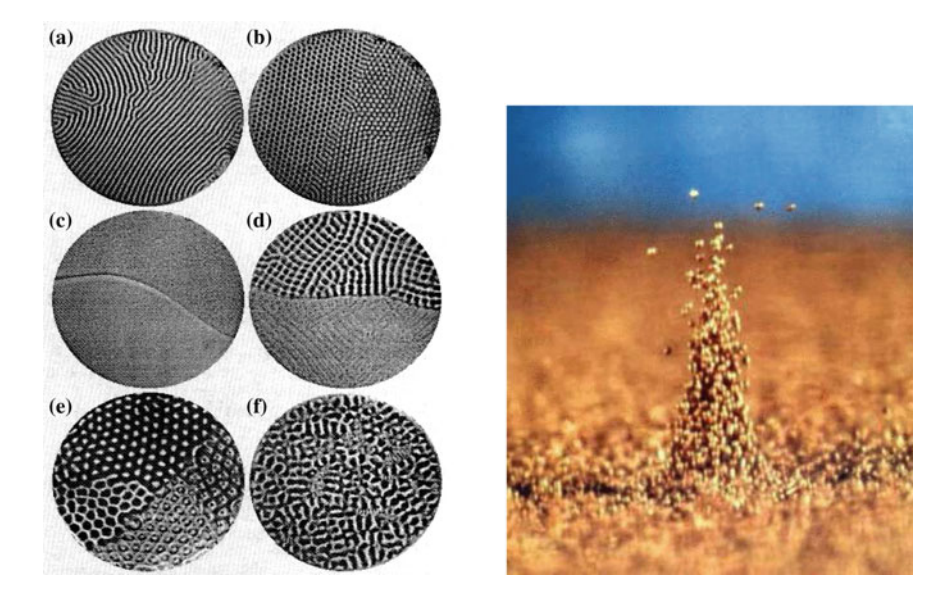


Fig. 1.5 Left: patterns in a vertically vibrated granular layer: **a** stripes, **b**, **e** hexagons, **c** flat with kink, **d** competing squares and stripes and **f** disorder [29]. Right: an oscillon, a solitary standing wave on the surface of a vibrated granular layer [27]

- Clustering: cluster formation in granular fluids has been analyzed numerically and theoretically in granular cooling [32] and later observed experimentally in shaken systems [33–36]. Clustering is not observed in elastic fluids, and is carried on by inelastic collisions: actually in a dense region the granular temperature decreases faster than in a dilute one because collisions are dissipative, yielding a decrease of the granular pressure: the pressure gradient created leads then to a migration towards the dense region. Therefore, once a density fluctuation appears, the dense region will attract other particles and grow, unless some hydrodynamic mechanism intervene to scatter particles faster than the clustering process [32]. A numerical sketch of a granular cluster is shown in Fig. 1.6a. Clustering appears as a hydrodynamic instability of the homogeneous cooling state of a granular medium, related to the shear instability: the study and analysis of instabilities will play a crucial role in Part II of this thesis. Finally, in above-cited experiments [33, 34] a transition has been observed when the number of particles is increased, moving from a gas-like behavior to a collective solid-like behavior: the latter is shown in Fig. 1.6b.
- Non-Gaussian velocities: velocity distributions in granular fluids are often non-Gaussian. This feature has been observed in numerical simulations and confirmed by experiments [35, 38, 39], which have proved a strong connection between clustering and velocity distributions [40]. Indeed, when particles cluster, *inelastic collapse* can occur [41, 42], namely particles stuck together because of inelastic

1.3 Granular Flows 15

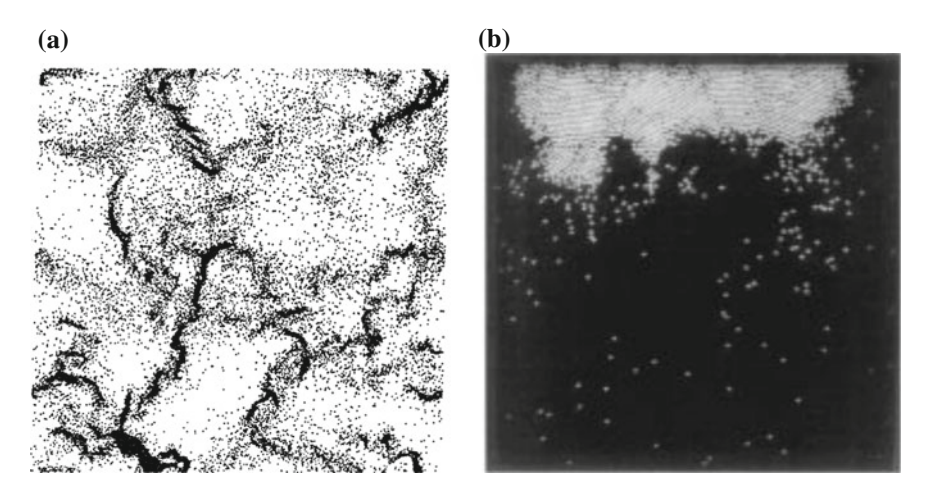
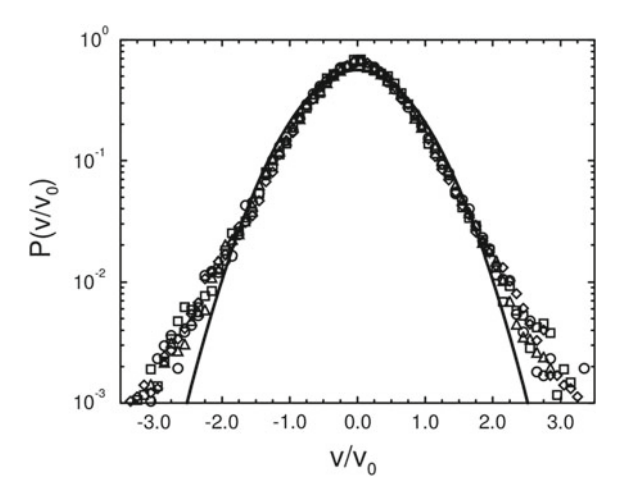


Fig. 1.6 Clustering: a snapshot of a clustered granular system in numerical simulations [32], b cluster formation in a granular fluid shaken by the horizontal wall at the bottom [37]

Fig. 1.7 Horizontal velocity distributions in a vertically vibrated granular monolayer, rescaled by the second moment, for different vibration amplitudes Γ [38]



collisions and start moving at the same parallel velocity. Clustering and inelastic collapse create regions with high density and low velocities, resulting in nearly exponential tails in the velocity distribution, see Fig. 1.7. In a different experiment [43], velocity distributions revealed exponential tails in a cooling state and $\exp(-v^{3/2})$ tails in a driven state, verifying theoretical predictions in [44]. Nevertheless, non-Gaussianity can be observed in absence of clustering as well: a successive experiment measured the horizontal velocity distribution of a vertically vibrated vertical monolayer, obtaining again a $\exp(-v^{3/2})$ velocity distribution also without clustering.

• **Velocity correlations**: strong long-range velocity correlations between granular particles have been revealed in experiments with dense granular gases [45], similar to the setup of [35] used to investigate non-Gaussian distributions. Furthermore, recent experiments studied velocity structure factors in a quasi-2*d* vertically vibrated horizontal granular monolayer by means of fluctuating hydrodynamics (see Sect. 3.2), confirming the validity of the theory [46, 47]. The experiments also displayed a correlation length which increases with the packing fraction.

• Thermal convection: very recently, an experiment on a vibrofluidized granular gas has shown the existence of a convection mechanism driven by the inelastic interactions with the walls of the container where the granular is shaken [48]. We already discussed the case of slow convection, which is generally a phenomenon driven by bulk buoyancy for slow flows. Experiments and simulations considered the case of a vibrated granular gas on a 2d inclined plane: the bottom wall is shaking the gas with accelerations much greater than the effective gravity. The presence of inelastic vertical walls is the key point of the establishment of thermal convection: since energy is dissipated at the boundaries, an horizontal temperature gradient is induced: thus, in any steady state of the system there must be a flow and, since the system is closed in the horizontal, the flow will be convective.

The granular features above-described have been chosen among the main studied and will be recalled in the following of this thesis; nevertheless, several outstanding features and applications of granular flows have been investigated in the last years, such as *granular jets* [49], *stick-slip frictional properties* [50, 51], a granular *Leidenfrost effect* [52], Kovacs-like memory effects [53–55] and *granular ratchets* [56–59] - see also Sect. 2.3. In Appendix C one can found several links to videos showing many of these granular effects.

Many of these studies converged in giving an experimental validation of kinetic theory [60–62]: the latter will be the starting point of our theoretical investigation, and will be introduced in Chap. 2

1.4 What is Active Matter

Many biological living units have the ability to move themselves in a fluid medium, converting an internally stored energy into kinetic energy by means of some biochemical process: this is what we call an *active particle*. When considering physical systems, one usually determines the motion of a particle through the resultant of the forces acting on it, thinking at the particle as a passive unity; on the contrary, active particles typically generate on their own a force to attain a certain state of motion: this force is called *self-propulsion*. Self-propulsion is made possible by the interaction of the active particle with a substrate or a surrounding fluid: actually, the momentum of an active unit is not conserved during its motion, but it must be so when considering

both the particle and the environment. For instance, human beings are active particles: we convert our chemical energy stored as ATP into kinetic energy through our muscular activity, being able to change our velocity intensity and orientation, but we can do it only in presence of a reacting medium, i.e. when walking on the ground or when swimming in the water, unless there is some mass exchange acting like a jet propulsion, which will be disregarded here. This principle obviously holds for any kind of active particle that we will see below, such as animals, bacteria, robots and so on.

When many active particles move together in a united system we talk about active matter. In this case the particles are not just self-propelling themselves but also interacting among them. Active matter can be observed in several circumstances in everyday life: bird flocks fly together in the sky; fish schools swim almost like a single object, defending from predators; sheep herds graze together, and also human beings use to walk together in more or less crowded environments, see Fig. 1.8. The interactions between active particles give rise to collective motion, i.e. individual units coherently move and form outstanding patterns and shapes: this phenomenon is also known as *flocking*, a general notion standing for the formation of order in an active matter system. Biological systems with active behavior are ubiquitous, and their complete review is far beyond the aim of this thesis. Some reviews already exist [63– 66] where a wider and more detailed outlook on active systems, phenomenology and models is given. A list of the most experimentally studied systems includes macromolecules, bacteria colonies, amoeba, cells, insects, fishes, birds, mammals and humans [63]. Furthermore, active matter can be also composed by non-living units: actually, there exist several systems [63, 64] where particles absorb energy from a substrate where chemical, thermal or electrostatic gradients are induced; where the units are activated by some external field (typically the electromagnetic field); where the units contain a stored energy that can be converted in kinetic energy; or finally where the walls of the substrate are shaken and the asymmetry of the particles' geometry induces a self-propulsion mechanism [64]. The main goal of all these setups is to generate a self-propulsion mechanism mimicking the self-propulsion characteristic of living systems. In the last Sect. 1.4.3 some of these systems are reviewed, like Janus particles, nano-swimmers, simple robots or vibrated polar granular particles: the latter represent a bridge between granular and active matter, which will be examined carefully. In Appendix C a collection of links to videos is reported to show the experimental behavior of some discussed systems.

1.4.1 Active Phenomenology

It is useful to introduce the typical phenomena of collective motion before presenting the most studied active systems: indeed, a quantitative characterization of collective behavior is needed to analyze it and compare several phases and systems. An important feature is the presence of phase transitions, which are expected in active matter even though the system is out of equilibrium. Phase transitions occur when a macroscopic quantity named *order parameter* suddenly changes under a

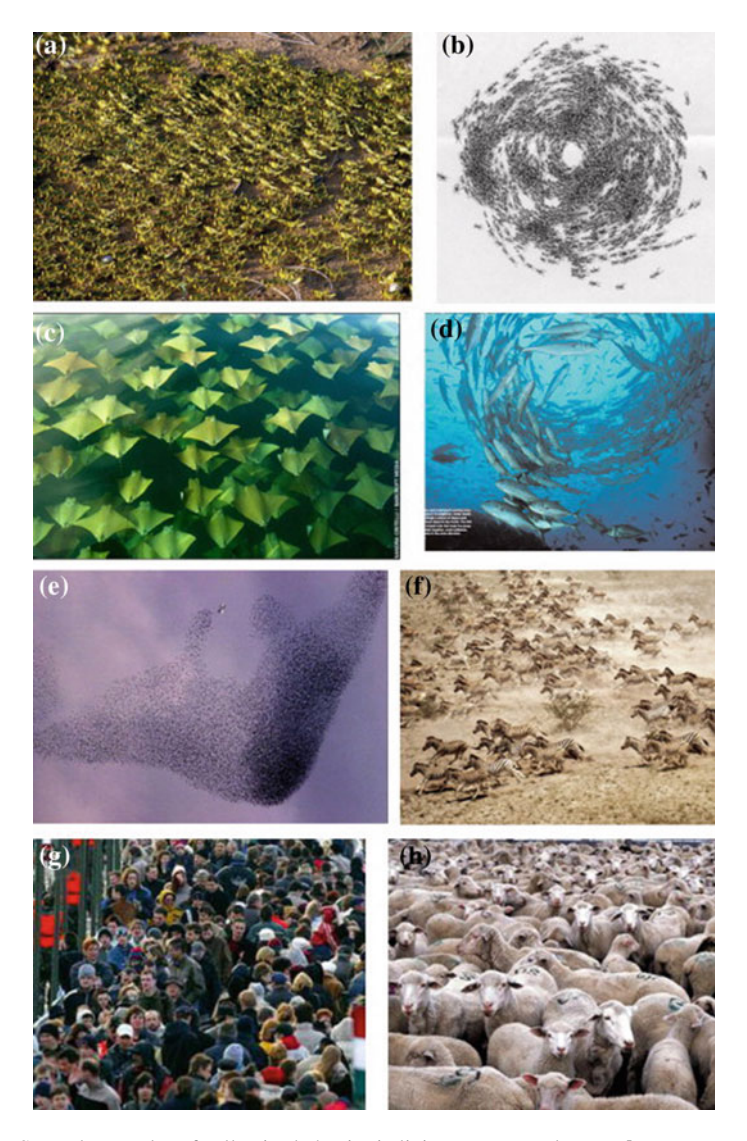


Fig. 1.8 Several examples of collective behavior in living systems: \mathbf{a} locusts, \mathbf{b} army ants, \mathbf{c} golden rays, \mathbf{d} fishes forming a vortex, \mathbf{e} starlings flocking, \mathbf{f} a herd of zebra, \mathbf{g} people walking in a street, \mathbf{h} sheep hanging around [63]

variation of an external variable, usually called *control parameter*. Typical examples of phase transitions at equilibrium are the condensation of a gas turning into liquid or the spontaneous magnetization of a ferromagnet, both happening if the temperature is decreased below a *critical value*. In these cases, the order parameters are respectively the mass density and the magnetization, while the control parameter is the temperature. The liquid-gas transition is called a *first-order* transition, because the order parameter discontinuously changes at the critical point; on the

1.4 What is Active Matter 19

contrary, the spontaneous magnetization is called a *second-order* transition, because the order parameter continuously changes with the temperature. What kind of phases are observed in active matter, and what are the order parameters involved?

First of all, many active systems show **swarming**, that is when a macroscopic fraction of the units move with the same orientation of the velocity. Such a state can be reached in interacting systems where, after an interaction, the particles tend to correlate their velocities aligning their orientations. An order parameter indicating the presence of swarming is given by [63]

$$r = \frac{1}{Nv_0} \left| \sum_{i=1}^{N} \mathbf{v}_i \right| , \tag{1.5}$$

where N is the number of the particles, v_0 their mean speed and \mathbf{v}_i the velocity of the ith particle. The swarming parameter r vanishes for disordered motion (uniform distribution of velocity orientations, particles going in all directions as in a molecular gas) while r=1 for perfect swarming, i.e. active units move together in the same direction without fluctuations. The particles spontaneously align their velocities in a given direction, breaking the continuous rotational symmetry of the system, similarly to what happens in the Heisenberg model of ferromagnetism. Here, the transition from disorder to swarming is governed by the competition between an aligning mechanism and the noise of the process: while aligning interactions force the system towards a swarming, ordered state (as the ferromagnetic interaction does in the Ising or Heisenberg model), the noise given by self-propulsion or interactions with the surroundings increases the disorder. This competition will be clarified in Sect. 2.2.

The swarming state implies a strong correlation between the velocity orientation of the active units. Furthermore, even without formation of collective motion, interactions of active units can give rise to a **leader-follower** behavior, consisting in an asymmetric relation between units when the motion of unit i (the leader) anticipates the motion of another unit j (the follower). This behavior can be observed through the directional correlation function

$$c_{ij}(\tau) = \langle \mathbf{v}_i(t) \cdot \mathbf{v}_j(t+\tau) \rangle , \qquad (1.6)$$

quantifying the degree of correlation between the velocity of unit i and j after a time delay τ , where the average $\langle \cdots \rangle$ is over the starting time t. The time τ_{ij}^* at which the directional correlation function shows a maximum is the *time delay* of the particle j with respect to the motion of particle i. If $\tau_{ij}^* > 0$ one can identify the unit i as the leader and j as the follower, and vice versa for $\tau_{ij}^* < 0$, recalling that $c_{ij}(\tau) = c_{ji}(-\tau)$ [63].

Another typical active phase is **clustering**: as discussed for granular materials, also active systems can form clusters during their motion. Indeed, even in presence of purely repulsive interactions, two colliding particles can get blocked by the persistence of their motion (see Fig. 1.9). When a third particle collides with them, they grow into a cluster which is attractive under certain conditions [64]. The particles

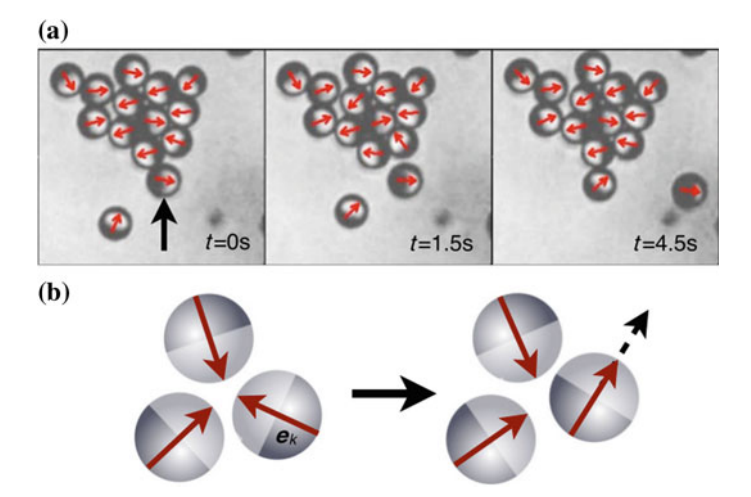


Fig. 1.9 Clustering of self-propelled Janus particles. Top panel: snapshots of experimental system where the projected orientations of the caps are resolved (red arrows). Bottom panel: sketch of the self-trapping mechanism (left). Rotational diffusion is the only way that particles have to escape from the cluster [67]

become very correlated because of the continuous interactions between them. A measure of local spatial ordering can be given by the radial distribution function q(r)

$$g(r) = \frac{V}{4\pi r^2 N^2} \left\langle \sum_{i \neq j} \delta(r - r_{ij}) \right\rangle, \qquad (1.7)$$

giving the unit density ρ at distance r from a particle placed at the origin, namely $\rho(r) = ng(r)$, being n the averaged number density n = N/V [63]. When a cluster grows in a dilute system, the local density sharply increases and deviates from n. The radial density distribution moves from a single-peaked to a double-peaked shape, signaling the presence of a dense clustered region and a dilute region, which is called a *phase separation* (see below) [68, 69]. An order parameter C can be defined as

$$C = \frac{\langle N_c \rangle}{N} \,, \tag{1.8}$$

where N_c is the number of units belonging to the larger cluster, so that $C \ll 1$ in absence of clustering and $C \to 1$ when clustering is present [67]. Clustered units can move together in the same direction, giving rise to a swarming state, or form a static cluster where they ceaselessly collide and the excluded volume prevent them to escape the cluster. In the latter case, self-clustering can lead also to **self-jamming** [64], i.e. particles get stuck together in one or more regions behaving like a solid: they become able to support a shear, and a probe particle in the active medium

feels a dramatical increase of viscosity when moving from a dilute to a jammed zone. The viscosity exhibits strong spatial fluctuations signaling the presence of jamming.

Phase separation in active matter is the consequence of an intrinsically non-equilibrium mechanism called **motility-induced phase separation** (MIPS), which is absent in the Brownian motion of particles at thermal equilibrium or for colloidal particles without attractive interactions. It has been shown [70] that for some kind of isotropic active particles one has a stationary one-particle distribution $P_s(\mathbf{r}, \mathbf{u}) \propto 1/v(\mathbf{r})$, being \mathbf{u} the velocity orientation and $v(\mathbf{r})$ the space-dependent average speed field, which is the effect of self-propulsion. Therefore, the local density $\rho(\mathbf{r})$ decreases as the self-propulsion increases and one can define a constitutive relation $v(\rho)$. Slower particles tend to accumulate and MIPS arises when the decrease of the speed with the density is steep enough to make an uniform suspension unstable, leading to a coexistence of an active motile gas with a dense liquid of low motility [71].

Finally, active systems are far from the thermodynamical limit, thus fluctuations play an important role in their dynamics. A common phenomenon observed are **giant number fluctuations** (GNF): for some systems of self-propelled units, the fluctuations of the number of particles linearly scale with the number of units N of an increasing region, in contrast with classic fluctuations in equilibrium systems scaling as \sqrt{N} [66].

1.4.2 Living Systems

There exist a plethora of active systems studied in the last decades by physicist and biologists, exhibiting many other features beyond the ones above introduced; the present section contains an overview of the most studied, specifying how the phenomena explained above are actually observed in living systems.

• **Bacteria**: bacterial colonies are one of the simplest systems made of a large number of interacting organisms and displaying a non-trivial macroscopic behavior. *Escherichia coli* is one of the most studied bacteria since the observation of traveling bands when seeking an optimal environment [72]. Further studies observed the presence of collective motion patterns such as super-diffusion, rotating and highly-correlated turbulent states.

The motion of *E. coli* has shown for the first time another important dynamics, which is known as *run-and-tumble* motion [64]: the bacteria follow a ballistic, constant speed motion (run) until they suddenly change their direction of motion (tumble), starting with another run in the new direction. This motion has been studied in several models and will be described in Sect. 2.2.3.

Further experiments on a morphotype of *Bacillus subtilis* at high concentration, see Fig. 1.10, showed the existence of a collective phase called "Zooming BioNematics" [73], where cell clusters move together in a swarming state at speeds

22 1 Introduction

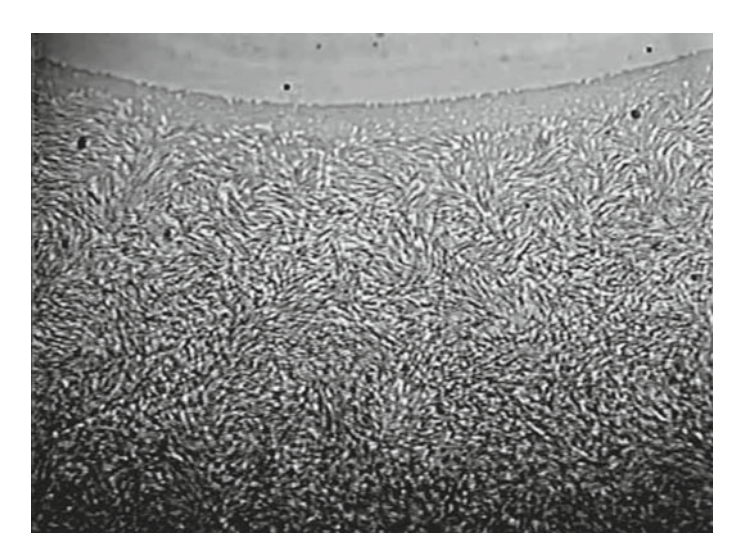


Fig. 1.10 Collective dynamics of swimming *B. subtilis* cells [73]

larger than the average speed of a single bacterium. Giant number fluctuations are present.

Some species spread very efficiently in a medium: this ability has been investigated experimentally [74], and it has been found that certain bacteria (*Myxococcus xanthus*) regularly reverse their direction, coming back to the colony and thus walking against a density gradient. This behavior, a waste of energy and time at first sight, actually contributes to the alignment of swarming cells, reducing the probability of collisions and consequently the "active viscosity" of the medium.

• **Fishes**: fishes are commonly known to form *shoals* or *schools*, two different collective behaviors. The former indicates when fishes aggregate together, moving without a collective order (no swarming) and many species can be included. In the latter, fishes coherently move in the same direction (swarming), and can be then considered a special case of shoal. A shoal can also suddenly organize into a school and vice versa depending on the momentary activity, such as escaping predators, feeding, resting or traveling [75].

Recording the trajectories of individual fishes in schools, both individual and collective behavior have been studied. Depending on the density of units, a transition from disorder to correlated motion has been found [76]. Also, observations on *Notemigonus Crysoleucas* trajectories produced data about the structure of the interactions in schools: the latter don't seem to be governed by an alignment rule but rather by a speed regulation which is the crucial ingredient of interactions, while the alignment only modulates the strength of speed regulation. Furthermore, it has been claimed that fish interactions are not pairwise, but rather multiple-bodies interactions more suitable to explain the observed dynamics [77].

Fish schools are a system of great interest for *decision making processes* into collective motion, e.g. trying to understand if there is a leader fish or a kind of consensus, and how the size of the school influences decision making. Some experiments have shown the ability of groups of fishes to influence the entire school, or that single fishes responded when a threshold number of conspecifics performed a particular behavior (*quorum responses*). Nevertheless, the comprehension of decision making and leader-follower behavior is still under debate.

- Bird flocks: birds flying together usually form spectacular flocks exhibiting great order in their collective behavior, giving rise to highly-coordinated motion patterns, see Fig. 1.11a. These have been studied for thirty years, but in the last decade the most important experimental observations have been carried out on Sturnus vulgaris, European Starlings, observing flocks containing up to 2600 units: tracking the position and velocity of each bird, it was possible to reconstruct the dynamics of the network through the spatial distribution of nearest neighbors of each bird, which is represented in Fig. 1.11b. In the same experiment [78], it has been observed that birds interact with their 6-7 closest neighbors - "topological interaction" - instead of those within a certain distance - "metrical interaction". Different kinds of interaction give rise to different models, especially concerning the role of density in flocks. On the contrary, further experiments concerning various species [79] suggested that the range of interaction did not change with density. Experiments focused on velocity correlations unveiled that these follow a power law decay with a unexpectedly small exponent, meaning that every bird may have an effective perception range much larger than the distance with its first neighbors [80]. All these points are still under debate and further simulations and observations are needed.
- Humans can be considered active matter as well. Indeed, when a large number of people are present, self-organization takes place: for instance in the growth of settlements, traffic dynamics or pedestrian movement. At the end of 90s some studies started using collective motion methods to describe human behavior in these cases. Comparisons between models and experiments have been related to the motion of human trail systems [81] and escape panic [82], leading to possible prescriptions on architectural and urban structures to facilitate human motion and prevent accidents.

Further experiments focused on the role of consensus and leadership in human crowds, where a randomly chosen person had the goal of guiding the group towards a random target without explicit communication: providing none or some information about the presence of a leader, the group always reached the target but with a less accurate motion when no information about the leader where given, and with a high accurate motion when the group knew of its presence (even without knowing its identity) [83].

24 1 Introduction

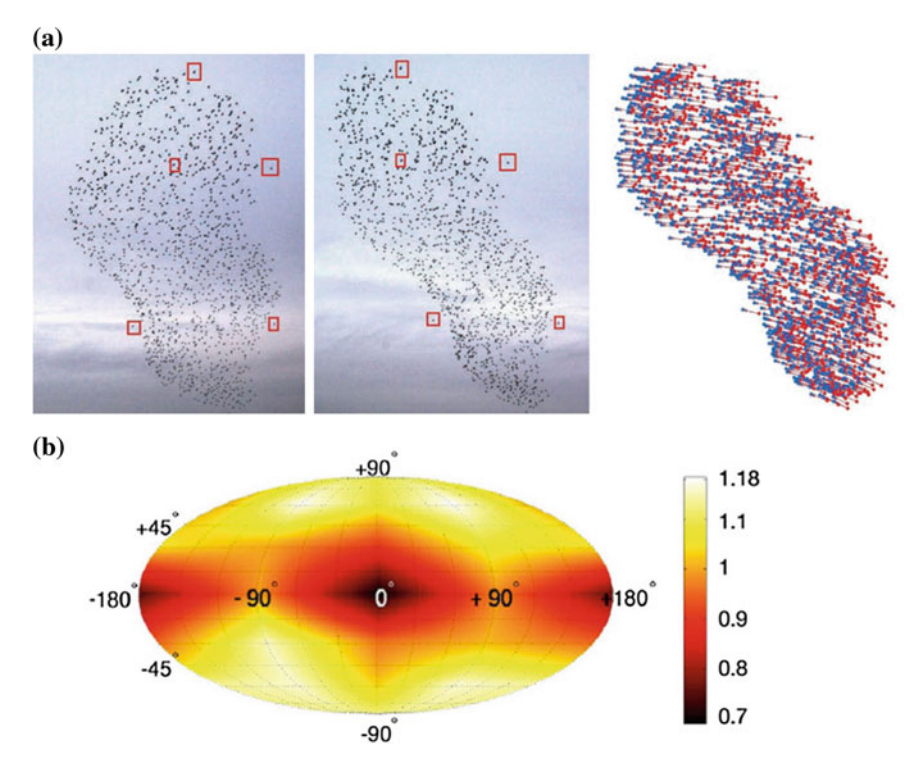


Fig. 1.11 a Bird flocking and the representation of their 3d observed velocities [84]. **b** Angular distribution of the birds' nearest neighbors. The distribution is strongly anisotropic and there is a lack of neighbors in the direction of motion [63, 78]

1.4.3 Non-living Systems

As it has been said before, active systems can be also realized out of biological context. A kind of system extensively studied in the field are **Janus particles**: their name come from the two-faced roman God Janus, because they consist of particles made by two or more parts having different chemical or physical properties. Thus, even a spherical particle can break geometrical rotational invariance and when a particle is at contact with the environment the different reactions on its surface generate a net force acting as a self-propulsion [64]. Spherical Janus particles can be made for instance by a hydrophilic hemisphere separated from a hydrophobic one; the clustering of Janus particles has been shown in Fig. 1.9.

Janus particles are a special kind of non-living active particles called **artificial microswimmers**, i.e. artificially generated particles exploiting some kind of symmetry breaking to self-propel themselves. There are two main categories of propulsion mechanisms: local conversion of energy (such as catalytic processes) or driving by an external field (e.g. electric, magnetic, acoustic); it is important to stress

that there is a deep difference between particles that are internally driven active matter and particles brought out of equilibrium by the action of external fields: though there exist similar effective models describing both categories, they show quite different microscopic details. An extended catalogue of such particles has been reviewed in [64]. A category of artificial active systems made of macroscopic units are collective robotics, namely groups of robots moving on a plane (and sometimes in a 3d region), able to sense obstacles, localize themselves with respect to a static frame and broadcast information with the other units. The very interesting feature of collective robotics is that interaction rules and individual behavior can be externally driven by humans, so they can represent a practical guide to understand how collective behavior stems from individual propulsion and local interactions. Also for collective robotics, several collective motions have been classified, like marching, oscillations, wandering and swarming [86]. There is a huge field of possible applications of collective robotics, such as localization of hazardous emission sources, surveillance in hostile or dangerous places, optimization of telecommunication networks. Last but not least, **driven granulars** have been studied in the framework of active particles in the last decade. Actually, a granular particle moving on a vibrated, rough plate feels the action of a mechanical driving mechanism able to sustain its state of motion: this feature can be correctly interpreted as a self-propulsion mechanism. Experiments on vibrated granular rods showed the presence of collective motion: when considering apolar, symmetric rods, a nematic order and persisting swirling have been observed [85], together with giant number fluctuations; moreover, varying the shape of granular rods several patterns of orientational ordering have been found, see Fig. 1.12. Also vortices can appear, when ordered domains made by nearly vertical granular rods coherently swirl and grow in time (coarsening), depending on the packing fraction and the vibration amplitude [45] (see Fig. 1.13). Conversely, apolar rods (with a head and a tail) have also been studied, displaying local ordering, aggregating at side walls and clustering; when the shaking amplitude is increasing, a collective swirling motion is observed [87]. Collective behavior and pattern formation in granular matter have been reviewed [27]. Many of these features suggested a comparison between driven granular and active matter, at least from a phenomenological point of view because

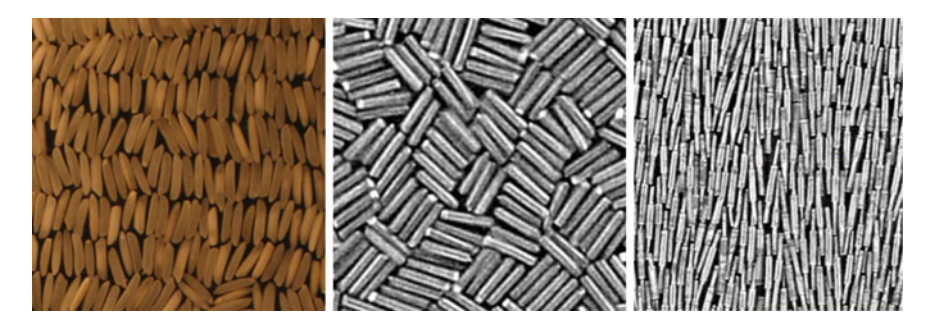


Fig. 1.12 Orientational order in apolar granular rods [85]

26 1 Introduction

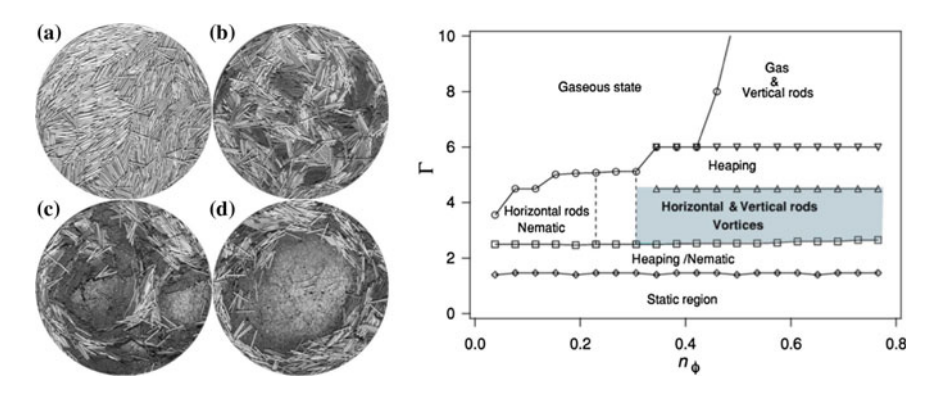


Fig. 1.13 Active phases in vertically vibrated granular rods. Left panel, pattern formation: **a** nematiclike state, **b** moving domains of near vertical rods, **c** multiple vortices and **d** large vortex. See [45] for experimental details. Right panel: phase diagram. All the realizations have frequency f = 50 Hz. Vortices appear for sufficiently high density n and vibration amplitude Γ [45]

of pattern formation, clustering, and so on. Experiments mostly concentrated on the shape of grains, arguing that an oriented shape (like rods instead of disks or spheres) was necessary to create anisotropic relations and thus an aligning mechanism. In Sect. 2.3, it will be shown how this is not necessary and that the inelasticity can play a crucial role in collective dynamics.

References

- 1. H.M. Jaeger, S.R. Nagel, R.P. Behringer, Granular solids, liquids, and gases. Rev. Mod. Phys. 68, 1259–1273 (1996). https://doi.org/10.1103/RevModPhys.68.1259
- 2. T. Pöschel, S. Luding (eds.), in Granular Gases (Springer, Berlin, 2001)
- 3. P.G. de Gennes, Granular matter: a tentative view. Rev. Mod. Phys. **71**, S374–S382 (1999). https://doi.org/10.1103/RevModPhys.71.S374
- L. Landau, E. Lifshitz, in Fluid Mechanics. Course of Theoretical Physics, vol. 6. (Pergamon Press, Oxford, 1987)
- H. Janssen, Versuche über getreidedruck in silozellen. Zeitschr. d. Vereines deutscher Ingenieure 39(35), 1045–1049 (1895)
- T.S. Majmudar, R.P. Behringer, Contact force measurements and stress-induced anisotropy in granular materials. Nature 435(7045), 1079–1082 (2005). https://doi.org/10.1038/nature03805
- 7. R. Brown, J. Richards, in Principles of Powder Mechanics (Pergamon Press, Oxford, 1970)
- 8. D.M. Mueth, H.M. Jaeger, S.R. Nagel, Force distribution in a granular medium. Phys. Rev. E 57(3), 3164 (1998). https://doi.org/10.1103/PhysRevE.57.3164
- C.-H. Liu, S.R. Nagel, Sound in sand. Phys. Rev. Lett. 68(15), 2301 (1992). https://doi.org/10. 1103/PhysRevLett.68.2301
- C.-H. Liu, S.R. Nagel, Sound in a granular material: disorder and nonlinearity. Phys. Rev. B 48(21), 15646 (1993). https://doi.org/10.1103/PhysRevB.48.15646
- J. Tang, Junyao Tang' Home Page, Duke University. http://webhome.phy.duke.edu/~jt41/ research.html#granular
- 12. W. Beverloo, H. Leniger, J. van de Velde, The flow of granular solids through orifices. Chem. Eng. Sci. **15**(3), 260–269 (1961). https://doi.org/10.1016/0009-2509(61)85030-6

References 27

13. K. To, P.-Y. Lai, H.K. Pak, Jamming of granular flow in a two-dimensional hopper. Phys. Rev. Lett. **86**, 71–74 (2001). https://doi.org/10.1103/PhysRevLett.86.71

- J. Tang, R. Behringer, How granular materials jam in a hopper. Chaos-Woodbury 21(4), 041107 (2011). https://doi.org/10.1063/1.3669495
- J. Tang, S. Sagdiphour, R.P. Behringer, Jamming and flow in 2d hoppers. AIP Conf. Proc. 1145(1), 515–518 (2009). https://doi.org/10.1063/1.3179975
- M. Cates, J. Wittmer, J.-P. Bouchaud, Jamming, force chains, and fragile matter. Phys. Rev. Lett. 81(9), 1841 (1998). https://doi.org/10.1103/PhysRevLett.81.1841
- 17. W.T. Kranz, M. Sperl, A. Zippelius, Glass transition for driven granular fluids. Phys. Rev. Lett. 104, 225701 (2010). https://doi.org/10.1103/PhysRevLett.104.225701
- 18. A.J. Liu, S.R. Nagel, Nonlinear dynamics: Jamming is not just cool any more. Nature **396**(6706), 21–22 (1998). https://doi.org/10.1038/23819
- L.E. Silbert, D. Ertaş G.S. Grest, T.C. Halsey, D. Levine, Analogies between granular jamming and the liquid-glass transition. Phys. Rev. E 65, 051307 (2002). https://doi.org/10.1103/PhysRevE.65.051307
- O. Dauchot, G. Marty, G. Biroli, Dynamical heterogeneity close to the jamming transition in a sheared granular material. Phys. Rev. Lett. 95, 265701 (2005). https://doi.org/10.1103/ PhysRevLett.95.265701
- 21. T.S. Majmudar, M. Sperl, S. Luding, R.P. Behringer, Jamming transition in granular systems. Phys. Rev. Lett. **98**, 058001 (2007). https://doi.org/10.1103/PhysRevLett.98.058001
- 22. A. Puglisi, in Transport and Fluctuations in Granular Fluids (Springer, Berlin, 2014)
- D. Howell, R.P. Behringer, C. Veje, Stress fluctuations in a 2d granular Couette experiment: a continuous transition. Phys. Rev. Lett. 82, 5241–5244 (1999). https://doi.org/10.1103/PhysRevLett.82.5241
- R. Khosropour, J. Zirinsky, H.K. Pak, R.P. Behringer, Convection and size segregation in a Couette flow of granular material. Phys. Rev. E 56, 4467–4473 (1997). https://doi.org/10. 1103/PhysRevE.56.4467
- D.A. Huerta, Vibration-induced granular segregation: a phenomenon driven by three mechanisms. Phys. Rev. Lett. 92, 114301 (2004). https://doi.org/10.1103/PhysRevLett.92.114301
- M.E. Möbius, B.E. Lauderdale, S.R. Nagel, H.M. Jaeger, Brazil-nut effect: size separation of granular particles. Nature 414(6861), 270–270 (2001). https://doi.org/10.1038/35104697
- I.S. Aranson, L.S. Tsimring, Patterns and collective behavior in granular media: theoretical concepts. Rev. Mod. Phys. 78, 641–692 (2006). https://doi.org/10.1103/RevModPhys.78.641
- K. Kim, H.K. Pak, Coarsening dynamics of striped patterns in thin granular layers under vertical vibration. Phys. Rev. Lett. 88, 204303 (2002). https://doi.org/10.1103/PhysRevLett.88.204303
- F. Melo, P. Umbanhowar, H.L. Swinney, Transition to parametric wave patterns in a vertically oscillated granular layer. Phys. Rev. Lett. 72, 172–175 (1994). https://doi.org/10.1103/PhysRevLett.72.172
- F. Melo, P.B. Umbanhowar, H.L. Swinney, Hexagons, kinks, and disorder in oscillated granular layers. Phys. Rev. Lett. 75, 3838–3841 (1995). https://doi.org/10.1103/PhysRevLett.75.3838
- 31. P.B. Umbanhowar, F. Melo, H.L. Swinney, Localized excitations in a vertically vibrated granular layer. Nature **382**(6594), 793–796 (1996). https://search.proquest.com/docview/204462031?accountid=13698, https://doi.org/10.1038/382793a0 (29 Aug 1996)
- 32. I. Goldhirsch, G. Zanetti, Clustering instability in dissipative gases. Phys. Rev. Lett. **70**, 1619–1622 (1993). https://doi.org/10.1103/PhysRevLett.70.1619
- 33. E. Falcon, R. Wunenburger, P. Évesque, S. Fauve, C. Chabot, Y. Garrabos, D. Beysens, Cluster formation in a granular medium fluidized by vibrations in low gravity. Phys. Rev. Lett. 83, 440–443 (1999). https://doi.org/10.1103/PhysRevLett.83.440
- 34. E. Falcon, S. Fauve, C. Laroche, Cluster formation, pressure and density measurements in a granular medium fluidized by vibrations. Eur. Phys. J. B Condens. Matter Complex Syst. 9(2), 183–186 (1999). https://doi.org/10.1007/s100510050755
- A. Kudrolli, J. Henry, Non-Gaussian velocity distributions in excited granular matter in the absence of clustering. Phys. Rev. E 62, R1489–R1492 (2000). https://doi.org/10.1103/ PhysRevE.62.R1489

28 1 Introduction

36. A. Kudrolli, M. Wolpert, J.P. Gollub, Cluster formation due to collisions in granular material. Phys. Rev. Lett. **78**, 1383–1386 (1997). https://doi.org/10.1103/PhysRevLett.78.1383

- 37. T.F.F. Farage, P. Krinninger, J.M. Brader, Effective interactions in active Brownian suspensions. Phys. Rev. E **91**, 042310 (2015). https://doi.org/10.1103/PhysRevE.91.042310
- 38. J.S. Olafsen, J.S. Urbach, Clustering, order, and collapse in a driven granular monolayer. Phys. Rev. Lett. 81, 4369–4372 (1998). https://doi.org/10.1103/PhysRevLett.81.4369
- 39. J.S. Olafsen, J.S. Urbach, Velocity distributions and density fluctuations in a granular gas. Phys. Rev. E 60, R2468–R2471 (1999). https://doi.org/10.1103/PhysRevE.60.R2468
- A. Puglisi, V. Loreto, U.M.B. Marconi, A. Petri, A. Vulpiani, Clustering and non-Gaussian behavior in granular matter. Phys. Rev. Lett. 81, 3848–3851 (1998). https://doi.org/10.1103/ PhysRevLett.81.3848
- 41. S. McNamara, W.R. Young, Inelastic collapse and clumping in a one-dimensional granular medium. Phys. Fluids A Fluid Dyn. 4(3), 496–504 (1992). https://doi.org/10.1063/1.858323
- 42. S. McNamara, W.R. Young, Inelastic collapse in two dimensions. Phys. Rev. E **50**, R28–R31 (1994). https://doi.org/10.1103/PhysRevE.50.R28
- 43. W. Losert, D. Cooper, J. Delour, A. Kudrolli, J. Gollub, Velocity statistics in excited granular media. chaos: an interdisciplinary. J. Nonlinear Sci. 9(3), 682–690 (1999). https://doi.org/10. 1063/1.166442
- 44. T. van Noije, M. Ernst, Velocity distributions in homogeneous granular fluids: the free and the heated case. Granul. Matter 1(2), 57–64 (1998). https://doi.org/10.1007/s100350050009
- D.L. Blair, A. Kudrolli, Velocity correlations in dense granular gases. Phys. Rev. E 64, 050301 (2001). https://doi.org/10.1103/PhysRevE.64.050301
- G. Gradenigo, A. Sarracino, D. Villamaina, A. Puglisi, Fluctuating hydrodynamics and correlation lengths in a driven granular fluid. J. Stat. Mech. (Theor. Exp.) 2011(08), P08017 (2011). http://stacks.iop.org/1742-5468/2011/i=08/a=P08017, https://doi.org/10.1088/1742-5468/2011/08/P08017
- A. Puglisi, A. Gnoli, G. Gradenigo, A. Sarracino, D. Villamaina, Structure factors in granular experiments with homogeneous fluidization. J. Chem. Phys. 136(1), 014704 (2012). https://doi.org/10.1063/1.3673876
- 48. G. Pontuale, A. Gnoli, F.V. Reyes, A. Puglisi, Thermal convection in granular gases with dissipative lateral walls. Phys. Rev. Lett. 117, 098006 (2016). https://doi.org/10.1103/PhysRevLett. 117.098006
- S.T. Thoroddsen, A.Q. Shen, Granular jets. Phys. Fluids 13(1), 4–6 (2001). https://doi.org/10. 1063/1.1328359
- A. Baldassarri, F. Dalton, A. Petri, S. Zapperi, G. Pontuale, L. Pietronero, Brownian forces in sheared granular matter. Phys. Rev. Lett. 96, 118002 (2006). https://doi.org/10.1103/ PhysRevLett.96.118002
- J. Krim, P. Yu, R.P. Behringer, Stick-slip and the transition to steady sliding in a 2d granular medium and a fixed particle lattice. Pure Appl. Geophys. 168(12), 2259–2275 (2011). https:// doi.org/10.1007/s00024-011-0364-5
- 52. P. Eshuis, K. van der Weele, D. van der Meer, Granular leidenfrost effect: experiment and theory of floating particle clusters. Phys. Rev. Lett. **95**, 258001 (2005). https://doi.org/10.1103/PhysRevLett.95.258001
- J.J. Brey, A. Prados, Memory effects in vibrated granular systems. J. Phys. Condens. Matter 14(7), 1489 (2002). http://stacks.iop.org/0953-8984/14/i=7/a=307, https://doi.org/10.1088/0953-8984/14/7/307
- 54. C. Josserand, A.V. Tkachenko, D.M. Mueth, H.M. Jaeger, Memory effects in granular materials. Phys. Rev. Lett. 85, 3632–3635 (2000). https://doi.org/10.1103/PhysRevLett.85.3632
- A. Prados, E. Trizac, Kovacs-like memory effect in driven granular gases. Phys. Rev. Lett. 112, 198001 (2014). https://doi.org/10.1103/PhysRevLett.112.198001
- G. Costantini, A. Puglisi, U.B.M. Marconi, Models of granular ratchets. J. Stat. Mech. (Theor. Exp.) 2009(07), P07004 (2009). http://stacks.iop.org/1742-5468/2009/i=07/a=P07004, https://doi.org/10.1088/1742-5468/2009/07/P07004

57. G. Costantini, U.M.B. Marconi, A. Puglisi, Granular Brownian ratchet model. Phys. Rev. E 75, 061124 (2007). https://doi.org/10.1103/PhysRevE.75.061124

- P. Eshuis, K. van der Weele, D. Lohse, D. van der Meer, Experimental realization of a rotational ratchet in a granular gas. Phys. Rev. Lett. 104, 248001 (2010). https://doi.org/10.1103/PhysRevLett.104.248001
- A. Manacorda, A. Puglisi, A. Sarracino, Coulomb friction driving Brownian motors. Commun. Theor. Phys. 62(4), 505 (2014). http://stacks.iop.org/0253-6102/62/i=4/a=08, https://doi.org/10.1088/0253-6102/62/4/08
- S. Luding, E. Clément, A. Blumen, J. Rajchenbach, J. Duran, Studies of columns of beads under external vibrations. Phys. Rev. E 49, 1634–1646 (1994). https://doi.org/10.1103/PhysRevE.49. 1634
- S. Warr, J.M. Huntley, G.T.H. Jacques, Fluidization of a two-dimensional granular system: experimental study and scaling behavior. Phys. Rev. E 52, 5583–5595 (1995). https://doi.org/ 10.1103/PhysRevE.52.5583
- 62. R.D. Wildman, J.M. Huntley, J.-P. Hansen, Self-diffusion of grains in a two-dimensional vibrofluidized bed. Phys. Rev. E **60**, 7066–7075 (1999). https://doi.org/10.1103/PhysRevE. 60.7066
- T. Vicsek, A. Zafeiris, Collective motion. Phys. Rep. 517(3–4), 71–140 (2012). http://www.sciencedirect.com/science/article/pii/S0370157312000968, https://doi.org/10.1016/j.physrep.2012.03.004
- C. Bechinger, R. Di Leonardo, H. Löwen, C. Reichhardt, G. Volpe, G. Volpe, Active particles in complex and crowded environments. Rev. Mod. Phys. 88, 045006 (2016). https://doi.org/ 10.1103/RevModPhys.88.045006
- M.C. Marchetti, J.F. Joanny, S. Ramaswamy, T.B. Liverpool, J. Prost, M. Rao, R.A. Simha, Hydrodynamics of soft active matter. Rev. Mod. Phys. 85, 1143–1189 (2013). https://doi.org/ 10.1103/RevModPhys.85.1143
- 66. S. Ramaswamy, The mechanics and statistics of active matter. Ann. Rev. Condens. Matter Phys. 1(1), 323–345 (2010). https://doi.org/10.1146/annurev-conmatphys-070909-104101
- 67. I. Buttinoni, J. Bialké, F. Kümmel, H. Löwen, C. Bechinger, T. Speck, Dynamical clustering and phase separation in suspensions of self-propelled colloidal particles. Phys. Rev. Lett. 110, 238301 (2013). https://doi.org/10.1103/PhysRevLett.110.238301
- Y. Fily, M.C. Marchetti, Athermal phase separation of self-propelled particles with no alignment. Phys. Rev. Lett. 108, 235702 (2012). https://doi.org/10.1103/PhysRevLett.108.235702
- 69. G.S. Redner, M.F. Hagan, Structure and dynamics of a phase-separating active colloidal fluid. Phys. Rev. Lett. 110, 055701 (2013). https://doi.org/10.1103/PhysRevLett.110.055701
- 70. M.J. Schnitzer, Theory of continuum random walks and application to chemotaxis. Phys. Rev. E 48, 2553–2568 (1993). https://doi.org/10.1103/PhysRevE.48.2553
- 71. M.E. Cates, J. Tailleur, Motility-induced phase separation. Ann. Rev. Condens. Matter Phys. **6**(1), 219–244 (2015). https://doi.org/10.1146/annurev-conmatphys-031214-014710
- 72. E.F. Keller, L.A. Segel, Model for chemotaxis. J. Theor. Biol. **30**(2), 225–234 (1971). http://www.sciencedirect.com/science/article/pii/0022519371900506, https://doi.org/10.1016/0022-5193(71)90050-6
- L.H. Cisneros, R. Cortez, C. Dombrowski, R.E. Goldstein, J.O. Kessler, Fluid dynamics of self-propelled microorganisms, from individuals to concentrated populations. Exp. Fluids 43(5), 737–753 (2007). https://doi.org/10.1007/s00348-007-0387-y
- Y. Wu, A.D. Kaiser, Y. Jiang, M.S. Alber, Periodic reversal of direction allows myxobacteria to swarm. Proc. Natl. Acad. Sci. 106(4), 1222–1227 (2009). http://www.pnas.org/content/106/ 4/1222.abstract, https://doi.org/10.1073/pnas.0811662106
- 75. D. Hoare, I. Couzin, J.-G. Godin, J. Krause, Context-dependent group size choice in fish. Anim. Behav. 67(1), 155–164 (2004). http://www.sciencedirect.com/science/article/pii/S0003347203003580, https://doi.org/10.1016/j.anbehav.2003.04.004
- C. Becco, N. Vandewalle, J. Delcourt, P. Poncin, Experimental evidences of a structural and dynamical transition in fish school. Phys. A Stat. Mech. Appl. 367, 487–493 (2006). http://www.sciencedirect.com/science/article/pii/S0378437105012689, https://doi.org/10.1016/j.physa.2005.11.041

30 1 Introduction

 Y. Katz, K. Tunstrøm, C.C. Ioannou, C. Huepe, I.D. Couzin, Inferring the structure and dynamics of interactions in schooling fish. Proc. Natl. Acad. Sci. 108(46), 18720–18725 (2011). https://doi.org/10.1073/pnas.1107583108

- M. Ballerini, N. Cabibbo, R. Candelier, A. Cavagna, E. Cisbani, I. Giardina, V. Lecomte, A. Orlandi, G. Parisi, A. Procaccini et al., Interaction ruling animal collective behavior depends on topological rather than metric distance: evidence from a field study. Proc. Natl. Acad. Sci. 105(4), 1232–1237 (2008). https://doi.org/10.1073/pnas.0711437105
- 79. J. Buhl, D.J.T. Sumpter, I.D. Couzin, J.J. Hale, E. Despland, E.R. Miller, S.J. Simpson, From disorder to order in marching locusts. Science 312(5778), 1402–1406 (2006). http://science.sciencemag.org/content/312/5778/1402, https://doi.org/10.1126/science.1125142
- A. Cavagna, A. Cimarelli, I. Giardina, G. Parisi, R. Santagati, F. Stefanini, M. Viale, Scale-free correlations in starling flocks. Proc. Natl. Acad. Sci. 107(26), 11865–11870 (2010). https://doi.org/10.1073/pnas.1005766107
- 81. D. Helbing, J. Keltsch, P. Molnar, Modelling the evolution of human trail systems. Nature 388(6637), 47–50 (1997). https://doi.org/10.1038/40353
- 82. D. Helbing, I. Farkas, T. Vicsek, Simulating dynamical features of escape panic. Nature **407**(6803), 487–490 (2000). https://doi.org/10.1038/35035023
- 83. J.J. Faria, J.R. Dyer, C.R. Tosh, Leadership and social information use in human crowds. Anim. Behav. **79**(4), 895–901 (2010). http://www.sciencedirect.com/science/article/pii/S0003347210000047, https://doi.org/10.1016/j.anbehav.2009.12.039
- 84. A. Cavagna, I. Giardina, Bird flocks as condensed matter. Ann. Rev. Condens. Matter Phys. 5(1), 183–207 (2014). https://doi.org/10.1146/annurev-conmatphys-031113-133834
- V. Narayan, N. Menon, S. Ramaswamy, Nonequilibrium steady states in a vibrated-rod monolayer: tetratic, nematic, and smectic correlations. J. Stat. Mech. (Theor. Exp.) 2006(01), P01005 (2006). http://stacks.iop.org/1742-5468/2006/i=01/a=P01005, https://doi.org/10.1088/1742-5468/2006/01/P01005
- 86. K. Sugawara, M. Sano, T. Mizuguchi, Y. Hayakawa, Collective motion of multi-robot system based on simple dynamics, *Human Robot Interaction* (INTECH Open Access Publisher, 2007). https://doi.org/10.5772/5202
- 87. A. Kudrolli, G. Lumay, D. Volfson, L.S. Tsimring, Swarming and swirling in self-propelled polar granular rods. Phys. Rev. Lett. 100, 058001 (2008). https://doi.org/10.1103/PhysRevLett. 100.058001

Chapter 2 Theoretical Models of Granular and Active Matter



Walk on, through the wind
Walk on, through the rain
Though your dreams be tossed and blown
Walk on, walk on
With hope in your heart
And you'll never walk alone

(R. Rodgers, O. Hammerstein)

This chapter introduces the main tehoretical models used to describe and reproduce the behavior of granular and active matter. The first Sect. 2.1 is dedicated to *kinetic theory*: established for the study of elastic gases, its aim is to describe a gas in term of mechanical coordinates of all its particles to derive its macroscopic properties such as pressure, energy and entropy through the statistical properties of the microscopic variables. This method, which was derived for elastic gases, can apply also for granular materials. The second Sect. 2.2 reviews the most important physical models of active matter, focusing on the essential ingredients to produce the typical interactions and self-propulsion discussed in Chap. 1. The last Sect. 2.3 investigates a possible theoretical comparison and symmetry between granular and active matter.

2.1 Kinetic Theory of Rapid Granular Flows

In the present section the classical kinetic theory will be introduced, showing how one can derive the Boltzmann Equation from the Liouville equation for *elastic* smooth hard spheres, moving later to the inelastic case. The kinetic theory will be used to describe the simplest granular regime, the *homogeneous cooling state*, and its instabilities. The last part of this section is an introduction to granular *steady states* and the so-called *steady state representation*. This section is based on the analysis

described in [1, 2] for elastic models, while granular kinetic theory has been deeply studied in [3, 4]. The following section follows the formulation presented in [5].

2.1.1 From Liouville to Boltzmann Equation

A system of N classical particles in a container of volume V is fully determined once the particles' positions and momenta configuration $\mathbf{z}(t)$ at a given time t and their interaction are known, where

$$\mathbf{z}(t) = \{\mathbf{r}_1(t), \mathbf{v}_1(t), \mathbf{r}_2(t), \mathbf{v}_2(t), \dots, \mathbf{r}_N(t), \mathbf{v}_N(t)\} \in V^N \times \mathbb{R}^{3N} = \Gamma, \quad (2.1)$$

introducing Γ as the full phase-space of the system. For an Hamiltonian system, the configuration is given by generalized coordinates and momenta, for which kinetic theory is usually developed. However this is not our case, because granular matter is not Hamiltonian. Since it is impossible to follow the equations of motion of $N\gg 1$ particles, kinetic theory looks at the time-dependent probability density function $\mathcal{P}(\mathbf{z},t)$, representing the probability of finding the system in a configuration \mathbf{z} at time t. This implies that the value of a dynamical observable $A(\mathbf{z})$ at time t is equivalent to

$$\int_{\Gamma} d\mathbf{z} \mathcal{P}(\mathbf{z}, 0) A(\mathbf{z}(t)) = \int_{\Gamma} d\mathbf{z} \mathcal{P}(\mathbf{z}, t) A(\mathbf{z}) , \qquad (2.2)$$

which respectively correspond to the Lagrangian and Eulerian averages. The evolution of A is given by the equations of motions of the configuration \mathbf{z} , but can be resumed into the *streaming operator* S_t , defined by $A(\mathbf{z}(t)) \equiv S_t(\mathbf{z})A(\mathbf{z})$ [5]. Therefore, the equivalence in (2.2) means that

$$\mathcal{P}(\mathbf{z},t) = S_t^{\dagger} \mathcal{P}(\mathbf{z},0) . \tag{2.3}$$

where S_t^{\dagger} is the adjoint operator of S_t . In a general system where particles are subjected to conservative and additive interactions and no external field is present, the streaming operator reads

$$S_t(\mathbf{z}) = \exp[tL(\mathbf{z})] = \exp\left[t\left(\sum_i L_i^0 - \sum_{i < j} \Theta_{ij}\right)\right], \qquad (2.4)$$

where the *Liouville operator* $L(\mathbf{z}) \cdot \equiv \{H(\mathbf{z}), \cdot\}$ is the Poisson bracket with the Hamiltonian function, so that

$$L_i^0 = \mathbf{v}_i \cdot \frac{\partial}{\partial \mathbf{r}_i} \,, \tag{2.5a}$$

$$\Theta_{ij} = \frac{1}{m} \frac{\partial U(r_{ij})}{\partial \mathbf{r}_{ij}} \cdot \left(\frac{\partial}{\partial \mathbf{v}_i} - \frac{\partial}{\partial \mathbf{v}_j} \right), \qquad (2.5b)$$

respectively represent the free streaming operator L_i^0 and the interaction term Θ_{ij} depending from the form of the binary interaction among the particles, $U(r_{ij})$. S_t is a unitary operator, with $S_t^{\dagger} = S_{-t}$ and $L^{\dagger} = -L$. Rewriting Eq. (2.3) in terms of Eq. (2.4) one obtains the *Liouville equation*

$$\frac{\partial}{\partial t} \mathcal{P}(\mathbf{z}, t) = \left(-\sum_{i} L_{i}^{0} + \sum_{i < j} \Theta_{ij} \right) \mathcal{P}(\mathbf{z}, t) , \qquad (2.6)$$

which expresses the incompressibility of the flow in phase space. Some textbooks use to refer to this equation when introducing Liouville's Theorem [2], stating that the distribution function of an Hamiltonian system is constant along any trajectory in the phase space, namely

$$\frac{\mathrm{d}}{\mathrm{d}t}\mathcal{P}(\mathbf{z},t) = 0. \tag{2.7}$$

Let us consider the case of a system made by N identical hard spheres of diameter σ and mass m: the potential U(r) is defined as

$$U(r) = \begin{cases} 0 & r > \sigma \\ +\infty & r < \sigma \end{cases}, \tag{2.8}$$

where r is the distance between two particles. U(r) is a discontinuous potential, which makes the collisions instantaneous: indeed, when particles i and j collide, their precollisional velocities $(\mathbf{v}_i, \mathbf{v}_j)$ abruptly change to postcollisional velocities $(\mathbf{v}_i', \mathbf{v}_j')$. In *elastic* collisions, momentum and energy conservation respectively read

$$m\mathbf{v}_i' + m\mathbf{v}_j' = m\mathbf{v}_i + m\mathbf{v}_j , \qquad (2.9a)$$

$$\frac{1}{2}mv_i^{\prime 2} + \frac{1}{2}mv_j^{\prime 2} = \frac{1}{2}mv_i^2 + \frac{1}{2}mv_j^2.$$
 (2.9b)

Those equations can be easily solved moving to the center of mass frame, considering the total velocity $\mathbf{V} = \frac{1}{2}(\mathbf{v}_1 + \mathbf{v}_2)$ and the relative velocity $\mathbf{v}_{ij} = \mathbf{v}_i - \mathbf{v}_j$; indeed, Eq. (2.9) yield the conservation of the total momentum and of the modulus of the relative velocity. In the smooth hard spheres case, the velocities are reflected after a collision with the rule

$$\mathbf{V}' = \mathbf{V} \,, \tag{2.10a}$$

$$\mathbf{v}'_{ij} = -\mathbf{v}_{ij} \ . \tag{2.10b}$$

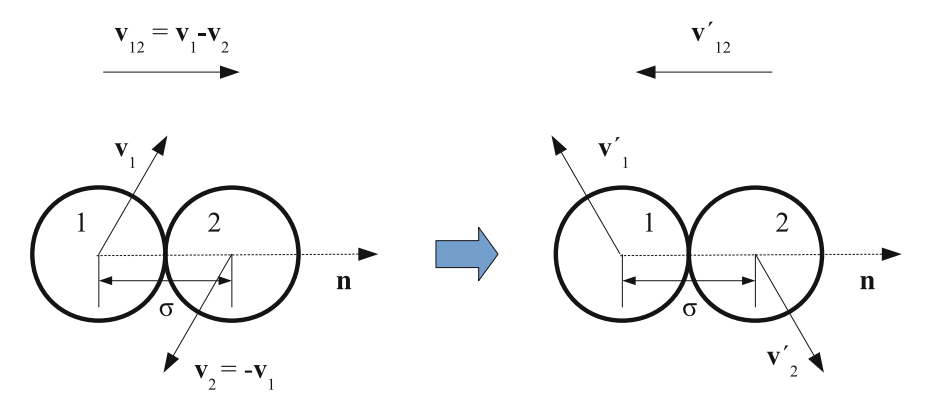


Fig. 2.1 Elastic collision of identical hard spheres in the center of mass frame: pre- and post-collisional velocities have equal modulus and opposite direction. The relative velocity is parallel to the direction of collision, and is reflected after the collision. The velocity components perpendicular to the relative velocity are not affected by the collision

So, in the laboratory frame the postcollisional velocities read

$$\mathbf{v}_{i}' = \mathbf{v}_{i} - \hat{\mathbf{n}} \left[\hat{\mathbf{n}} \cdot \left(\mathbf{v}_{i} - \mathbf{v}_{j} \right) \right], \tag{2.11a}$$

$$\mathbf{v}_{j}' = \mathbf{v}_{j} + \hat{\mathbf{n}} \left[\hat{\mathbf{n}} \cdot \left(\mathbf{v}_{i} - \mathbf{v}_{j} \right) \right] , \qquad (2.11b)$$

being $\hat{\mathbf{n}} = (\mathbf{r}_i - \mathbf{r}_j)/|\mathbf{r}_i - \mathbf{r}_j|$ the unit vector connecting the center of the sphere i with the center of the sphere j, see Fig. 2.1. With the present rule, the collisions can be reintroduced into the Liouville equation by imposing the boundary condition

$$\mathcal{P}(\mathbf{z}',t) = \mathcal{P}(\mathbf{z},t), \qquad (2.12)$$

where \mathbf{z}' is the postcollisional configuration after particles i and j have collided. An instantaneous collision occurs when particles are in contact and the relative velocity \mathbf{v}_{ij} has opposite direction of $\hat{\mathbf{n}}_{ij} = (\mathbf{r}_i - \mathbf{r}_j)/\sigma$: the latter requirement is known as *kinematic constraint*, i.e. the particles must move towards each other to collide. The last requirement is fundamental to guarantee that immediately after a collision the particles do not collide any more. Namely,

$$r_{ij} = \sigma \,, \tag{2.13a}$$

$$\mathbf{v}_{ij} \cdot \hat{\mathbf{n}}_{ij} < 0. \tag{2.13b}$$

In this case, the postcollisional phase space configuration reads

$$\mathbf{z}' = (\mathbf{r}_1, \mathbf{v}_1, \dots, \mathbf{r}'_i, \mathbf{v}'_i, \dots, \mathbf{r}'_j, \mathbf{v}'_j, \dots, \mathbf{r}_N, \mathbf{v}_N), \qquad (2.14a)$$

$$\mathbf{r}_i' = \mathbf{r}_i \,, \tag{2.14b}$$

$$\mathbf{r}_{j}' = \mathbf{r}_{j} , \qquad (2.14c)$$

and \mathbf{v}_i' , \mathbf{v}_i' follow the collisional rule in Eq. (2.11).

Since hard spheres cannot overlap, the effect of excluded volume changes the phase space: there is an excluded region consisting of the occupied volume called Γ_{ov} so that the actual phase space is $\Gamma = V^N \times \mathbb{R}^N - \Gamma_{ov}$, where

$$\Gamma_{ov} = \left\{ \mathbf{z} \in V^N \times \mathbb{R}^N \mid \exists i, j \in \{1, 2, \dots, N\} : |\mathbf{r}_i - \mathbf{r}_j| < \sigma \right\}. \tag{2.15}$$

With the previous condition, the Liouville equation reads

$$\frac{\partial}{\partial t} \mathcal{P}(\mathbf{z}, t) = \left(-\sum_{i} \mathbf{v}_{i} \cdot \frac{\partial}{\partial \mathbf{r}_{i}} \right) \mathcal{P}(\mathbf{z}, t) \quad \text{when } \mathbf{z} \in \Gamma , \quad (2.16a)$$

$$\mathcal{P}(\mathbf{z}, t) = \mathcal{P}(\mathbf{z}', t)$$
 when $\mathbf{z} \in \partial \Gamma$, (2.16b)

where $\partial \Gamma$ is the boundary of the phase space Γ . The interaction term has been resumed in the time-discontinuous boundary condition in the second line, while between two collisions the particles undergo a free motion at constant speed \mathbf{v}_i .

The discontinuity introduced prevents the use of formal perturbation expansion such as the ones usually employed in many-body theory. It can be shown [6] that an alternative expression for the streaming operator can be written in terms of binary collision operators: indeed one can write S_t for two particles labeled 1 and 2 as

$$S_t(1,2) = S_t^0(1,2) + \int_0^t d\tau \, S_\tau^0(1,2) T_+(1,2) S_{t-\tau}^0(1,2) , \qquad (2.17)$$

where S_t^0 is the free flow operator and $T_+(1,2)$ a collisional operator

$$T_{+}(1,2) = \sigma^{2} \int_{\mathbf{v}_{12},\hat{\mathbf{n}} \in 0} d\hat{\mathbf{n}} |\mathbf{v}_{12} \cdot \hat{\mathbf{n}}| \delta \left(\mathbf{r}_{1} - \mathbf{r}_{2} - \sigma \hat{\mathbf{n}}\right) (b_{c} - 1), \qquad (2.18)$$

being $\mathbf{v}_{12} = \mathbf{v}_1 - \mathbf{v}_2$ and b_c a substitution operator which replaces precollisional velocities with postcollisional ones, $(\mathbf{v}_1, \mathbf{v}_2) \to (\mathbf{v}_1', \mathbf{v}_2')$. Equation (2.17) can be interpreted as the evolution of 2-particles dynamics during time t, consisting in a free flow term (no collisions) plus a convolution term considering all eventual collisions at time $0 < \tau < t$. Since two spheres alone cannot collide more than once, one notices that $T_+(1,2)S_0^0(1,2)T_+(1,2) = 0$ and therefore Eq. (2.17) is equivalent to

$$S_t(1,2) = \exp\left\{t\left[L_0(1,2) + T_+(1,2)\right]\right\}.$$
 (2.19)

Generalizing the equation above to the N-particles streaming operator (here in the case of infinite volume) one has

$$S_{\pm t}(\mathbf{z}) = \exp\left\{\pm t \left[L_0(\mathbf{z}) \pm \sum_{i < j} T_{\pm}(i, j) \right] \right\}, \qquad (2.20)$$

where $T_{-}(1, 2)$ represents a backward collisional operator, i.e.

$$T_{-}(1,2) = \sigma^{2} \int_{\mathbf{v}_{12},\hat{\mathbf{n}}>0} d\hat{\mathbf{n}} |\mathbf{v}_{12} \cdot \hat{\mathbf{n}}| \delta \left(\mathbf{r}_{1} - \mathbf{r}_{2} - \sigma \hat{\mathbf{n}}\right) (b_{c} - 1).$$
 (2.21)

 $S_{\pm t}(\mathbf{z})$ is defined as the *pseudo-streaming operator*. Now, a continuous-time Liouville equation can be written by means of the adjoint of $S_{\pm t}$, considering the adjoint operators of $T_{\pm}(1,2)$ which read

$$T_{\pm}^{\dagger}(1,2) = \sigma^{2} \int_{\mathbf{v}_{12} \cdot \hat{\mathbf{n}} \leq 0} d\hat{\mathbf{n}} |\mathbf{v}_{12} \cdot \hat{\mathbf{n}}| \left[\delta \left(\mathbf{r}_{1} - \mathbf{r}_{2} - \sigma \hat{\mathbf{n}} \right) b_{c} - \delta \left(\mathbf{r}_{1} - \mathbf{r}_{2} + \sigma \hat{\mathbf{n}} \right) \right].$$

$$(2.22)$$

At last, the pseudo-Liouville equation can be written

$$\frac{\partial}{\partial t} \mathcal{P}(\mathbf{z}, t) = \left(-\sum_{i} L_{i}^{0} + \sum_{i < j} T_{-}^{\dagger}(i, j) \right) \mathcal{P}(\mathbf{z}, t) , \qquad (2.23)$$

which represents the analogue of Eq. (2.6) for elastic hard spheres. It replaces Eq. (2.16) and will be the starting point to write the granular pseudo-Liouville equation when considering inelastic collisions.

The first step to derive the Boltzmann equation representing the evolution of the one-particle distribution $P(\mathbf{r}, \mathbf{v}, t)$ is to consider the marginalized distribution P_s defined as

$$P_{s}(\mathbf{r}_{1}, \mathbf{v}_{1}, \dots, \mathbf{r}_{s}, \mathbf{v}_{s}; t) = \int_{V^{N-s} \times \mathbb{R}^{3(N-s)}} \left(\prod_{j=s+1}^{N} d\mathbf{r}_{j} d\mathbf{v}_{j} \right) \mathcal{P}(\mathbf{r}_{1}, \mathbf{v}_{1}, \dots, \mathbf{r}_{N}, \mathbf{v}_{N}; t) .$$

$$(2.24)$$

Integrating over $\left(\prod_{j=s+1}^{N} d\mathbf{r}_{j} d\mathbf{v}_{j}\right)$ both sides of Eq. (2.16a) and implementing the boundary condition (2.16b), it can be shown [5] that P_{s} follows the evolution equation

$$\frac{\partial P_s}{\partial t} + \sum_{i=1}^s \mathbf{v}_i \cdot \frac{\partial P_s}{\partial \mathbf{r}_i} = (N - s)\sigma^2 \sum_{i=1}^s \int_{\mathbb{R}^3} \int_{S^+} (P'_{s+1} - P_{s+1}) |\mathbf{V}_i \cdot \hat{\mathbf{n}}| d\hat{\mathbf{n}} d\mathbf{v}_*, \quad (2.25)$$

where $\mathbf{V}_i = \mathbf{v}_i - \mathbf{v}_*$, S_+ is the hemisphere of $\hat{\mathbf{n}}$ having $\mathbf{V}_i \cdot \hat{\mathbf{n}} > 0$ and P'_{s+1} is defined as

$$P'_{s+1} = P'_{s+1}(\mathbf{r}_1, \mathbf{v}_1, \dots, \mathbf{r}_i, \mathbf{v}_i - \hat{\mathbf{n}}(\hat{\mathbf{n}} \cdot \mathbf{V}_i), \dots, \mathbf{r}_s, \mathbf{v}_s, \mathbf{r}_i - \sigma \hat{\mathbf{n}}, \mathbf{v}_* + \hat{\mathbf{n}}(\hat{\mathbf{n}} \cdot \mathbf{V}_i)).$$
(2.26)

The interpretation of Eq. (2.25) is straightforward: its lhs represents the evolution of P_s under the free s-particles flow, while the rhs represents the gain and loss terms of the s-particles configuration due to collisions with one of the remaining N-s particles, which probability is given by the P_{s+1} distribution. The system of Eq. (2.25) is known as BBGKY hierarchy¹: indeed, starting from the one-particle distribution P_1 , its evolution equation contains P_2 , as well as the evolution equation of P_2 contains P_3 and so on... Clearly, this set of equations is closed only if one considers all the marginalized distribution functions up to $P_N \equiv \mathcal{P}(\mathbf{z})$, but this means coming back to the original Liouville equation.

This theoretical limit can be overcome in the case of a rarefied gas, which applies when considering a box of volume 1 cm³ at atmospheric pressure and room temperature, for which one has $N \sim 10^{20}$, $\sigma \sim 10^{-8}$ cm, hence for small s $(N-s)\sigma^2 \sim N\sigma^2 \sim 1\text{m}^2$; furthermore, the difference between \mathbf{r}_i and $\mathbf{r}_i + \sigma \hat{\mathbf{n}}$ can be neglected compared with system size, as well as the occupied volume $N\sigma^3 \sim 10^{-4}$ cm³, so that the collision between two *selected* particles can be considered a rare event. These considerations lead to the so-called *Boltzmann–Grad limit*, which consists in taking $N \to \infty$ and $\sigma \to 0$ while $N\sigma^2$ remains finite. It is remarkable that the scattering cross section for two hard spheres is $\pi\sigma^2$, so that in a system with volume and typical velocities of order 1 the total cross section multiplied by N reads $N\pi\sigma^2$: the Boltzmann–Grad limit states that the single particle collision probability must vanish while the total number of collisions remains of order 1. So, Eq. (2.25) can be modified changing $(N-s)\sigma^2 \to N\sigma^2$ and putting $\sigma = 0$ into (2.26).

The last but crucial assumption to obtain the Boltzmann equation is the *Molecular Chaos assumption*, namely

$$P_2(\mathbf{r}_1, \mathbf{v}_1, \mathbf{r}_2, \mathbf{v}_2; t) = P_1(\mathbf{r}_1, \mathbf{v}_1, t) P_1(\mathbf{r}_2, \mathbf{v}_2, t),$$
 (2.27)

for particles that are about to collide, i.e. when $\mathbf{r}_2 = \mathbf{r}_1 - \sigma \hat{\mathbf{n}}$ and $\mathbf{v}_{12} \cdot \hat{\mathbf{n}} < 0$. The Molecular Chaos assumption states that the *pre*collisional velocities of the colliding particles are uncorrelated: it relies on the Boltzmann–Grad limit, for which we already axid that a collision between two selected particles i, j is a rare event, hence between two collisions of the same particles they will have collided many times with other particles of the system, "forgetting" the possible correlation induced by the precedent collision. It is important to stress that Molecular Chaos states that *pre*collisional velocities are uncorrelated, but doesn't say anything about the *post*collisional velocities distribution. This assumption can be clearly justified only in dilute gases and will be heavily used in Part II of this Thesis.

The Molecular Chaos assumption in (2.27) immediately closes the BBGKY hierarchy at s = 1: the first equation of the hierarchy then reads (writing $P = P_1$ and omitting time dependence)

¹From Bogoliubov, Born, Green, Kirkwood and Yvon [2].

$$\frac{\partial P(\mathbf{r}, \mathbf{v})}{\partial t} + \mathbf{v} \cdot \frac{\partial P(\mathbf{r}, \mathbf{v})}{\partial \mathbf{r}} = N\sigma^2 \int_{\mathbb{R}^3} \int_{S^+} \left[P(\mathbf{r}, \mathbf{v}') P(\mathbf{r}, \mathbf{v}'_*) - P(\mathbf{r}, \mathbf{v}) P(\mathbf{r}, \mathbf{v}_*) \right] |\mathbf{V} \cdot \hat{\mathbf{n}}| d\mathbf{v}_* d\hat{\mathbf{n}},$$
(2.28)

with $\mathbf{v}' = \mathbf{v} - \hat{\mathbf{n}}(\mathbf{V} \cdot \hat{\mathbf{n}})$, $\mathbf{v}'_* = \mathbf{v}_* + \hat{\mathbf{n}}(\mathbf{V} \cdot \hat{\mathbf{n}})$ and $\mathbf{V} = \mathbf{v} - \mathbf{v}_*$. Equation (2.28) is the *Boltzmann equation* for hard spheres. Its lhs contains the time evolution given by the free flow in phase space coordinates and its rhs the instantaneous evolution given by collisions. It is here evident that the first (positive) term into the integral is accounting for all the collisions where one particle has the postcollisional velocity \mathbf{v} and therefore comes into phase space region around (\mathbf{r}, \mathbf{v}) , whereas the second (negative) term is accounting for all the collisions where one of the particles has the precollisional velocity \mathbf{v} , and therefore after a collision it escapes from the phase space region measured by $P(\mathbf{r}, \mathbf{v})$.

Actually, it is not unusual to find the evolution equation for the single-particle distribution P directly written without considering the full phase space distribution \mathcal{P} but rather computing the gain/loss terms through probabilistic considerations, see for instance [2]. Although this alternative derivation is well-based and legitimate, the full information about the physical system considered is given by $\mathcal{P}(\mathbf{z},t)$, while $P(\mathbf{r},\mathbf{v},t)$ contains less information and its derivation from the Liouville equation (2.6) has shown the assumptions needed. However, for many practical purposes, P is the main quantity of interest, as it will be seen in Part II.

2.1.2 Inelastic Collisions and Granular Boltzmann Equation

The aim of the present paragraph is to derive a Boltzmann equation for inelastic smooth hard spheres, which are a fundamental modelization of granular particles. Before doing that, the inelastic collisions need to be well-defined: conversely from elastic collisions, the former conserve momentum but dissipate energy, namely Eq. (2.9) become

$$m\mathbf{v}_i' + m\mathbf{v}_j' = m\mathbf{v}_i + m\mathbf{v}_j , \qquad (2.29a)$$

$$\frac{1}{2}mv_i^{\prime 2} + \frac{1}{2}mv_j^{\prime 2} < \frac{1}{2}mv_i^2 + \frac{1}{2}mv_j^2.$$
 (2.29b)

In order to quantify the energy loss during a collision, it is common to introduce the restitution coefficient $0 \le \alpha < 1$; after a collision, the relative velocity in the center of mass frame reads

$$\mathbf{v}'_{ij} = -\alpha \mathbf{v}_{ij} \ . \tag{2.30}$$

The last equation defines α and states that after a collision the relative velocity along the collision direction is reflected *and rescaled* by a factor α : when $\alpha=0$, the postcollisional velocity vanishes and the colliding particles get stuck together, as when a ripe tomato crushes falling on the ground (sticky collision); conversely when

 $\alpha=1$ the collision is elastic, and the previous paragraph's theory with Eqs. (2.9)–(2.11) is recovered. The energy dissipation is absent when $\alpha=1$ and increases as α decreases towards its minimum $\alpha=0$, where the dissipation is maximal.

Setting a restitution coefficient equivalent for each particle and collision event is clearly an idealization, as well as considering all particles as spheres having the same diameter: indeed, during a collision, the kinetic energy of particles is mainly dissipated into work deforming the particles themselves - which cannot be exactly spherical anymore -, and in real collisions the dissipation ratio $\Delta E/E$ depends on the shape of the particles and the collision point on their surfaces as well as their relative velocity. Actually, there are granular models considering velocity-dependent restitution coefficient $\alpha(v)$ [7, 8], but their description is beyond the aim of this thesis. Furthermore, there are no tangential frictional forces (smooth grains) which may be taken into account considering also the rotational degree of freedom of particles: the simplest model satisfying this condition is the rough hard spheres gas [9]. For our purpose, a constant restitution coefficient is a good approximation.

The collisional rule for identical inelastic smooth hard spheres now reads

$$\mathbf{v}_{i}' = \mathbf{v}_{i} - \frac{1+\alpha}{2}\hat{\mathbf{n}}\left[\hat{\mathbf{n}}\cdot\left(\mathbf{v}_{i} - \mathbf{v}_{j}\right)\right], \qquad (2.31a)$$

$$\mathbf{v}_{j}' = \mathbf{v}_{j} + \frac{1+\alpha}{2}\hat{\mathbf{n}}\left[\hat{\mathbf{n}}\cdot\left(\mathbf{v}_{i} - \mathbf{v}_{j}\right)\right], \qquad (2.31b)$$

and the energy dissipation is

$$\Delta E = E' - E = -\frac{1 - \alpha^2}{4} \left| \hat{\mathbf{n}} \cdot (\mathbf{v}_i - \mathbf{v}_j) \right|^2. \tag{2.32}$$

Some fundamental features of inelastic collisions deserve to be underlined.

1. *Inelastic collisions are not invariant under time-reversal.* Equation (2.23) is invariant under time-reversal: indeed, the elastic collision rule (2.11) states that $(\mathbf{v}_i, \mathbf{v}_j) \to (\mathbf{v}_i', \mathbf{v}_j')$ as well as $(-\mathbf{v}_i', -\mathbf{v}_j') \to (-\mathbf{v}_i, -\mathbf{v}_j)$. On the contrary, in inelastic collisions there is energy dissipation and the reversed collision should increase the energy to recover the original precollisional state: indeed, precollisional velocities can be obtained from postcollisional ones with the rule

$$\mathbf{v}_{i} = \mathbf{v}_{i} - \frac{1+\alpha}{2\alpha} \hat{\mathbf{n}} \left[\hat{\mathbf{n}} \cdot \left(\mathbf{v}_{i}' - \mathbf{v}_{j}' \right) \right], \qquad (2.33a)$$

$$\mathbf{v}_{j} = \mathbf{v}_{j} + \frac{1+\alpha}{2\alpha} \hat{\mathbf{n}} \left[\hat{\mathbf{n}} \cdot \left(\mathbf{v}_{i}' - \mathbf{v}_{j}' \right) \right], \qquad (2.33b)$$

which corresponds to the original collisional rule (2.31) when transforming $\alpha \to 1/\alpha$: the only invariant case is the elastic collision with $\alpha = 1$. Figure 2.2 compares the outcomes of elastic and inelastic collisions.

2. *Velocities align after a collision*. The inelastic collisional rule shrinks the velocity component parallel to the relative velocity, $\mathbf{v}^{\parallel} = \hat{\mathbf{n}} \cdot \mathbf{v}$ but conserves the transverse

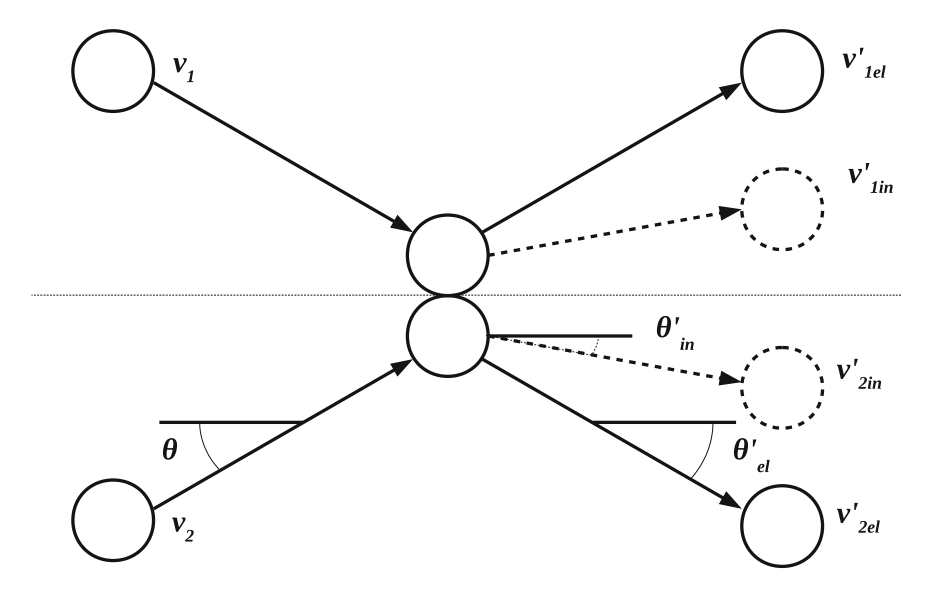


Fig. 2.2 Elastic versus inelastic collision: elastic trajectories (continuous lines) are reflected with a postcollisional angle $\theta'_{el} = \theta$ equivalent to the precollisional one - time reversal invariance -, while in the inelastic collision (dashed lines) the velocities get more aligned because $\theta'_{in} < \theta$

component $\mathbf{v}^\perp = \mathbf{v} - \mathbf{v}^\parallel$. Therefore, after a collision the transverse component weight is increased with respect to the parallel one: the relative angle between particles' velocities reduces and their velocities get more aligned, see Fig. 2.2 for geometrical visualization. This feature has a great importance in momentum transfer, because the velocities tend to get correlated at a microscopic level. In granular flows, the velocity alignment creates groups of particles collectively moving with almost the same velocities.

3. *Inelastic collapse*. It has already been mentioned in Sect. 1.3.1 that clustering is connected with inelastic collapse: the simplest example is the case of three particles on a line [10], see top left panel of Fig. 2.3a. When outer particles move monotonically toward each other, the central one bounces with them from both sides. In the elastic case at least one of the outer particles would be rejected from the collision and no more collisions occur unless a wall redirects the particles toward each other. In the inelastic case, if the dissipation is strong enough the outer particles don't change their direction and they ceaselessly collide with the central one with geometrically smaller space and time scales at each successive cycle. The critical value of the dissipation is $\alpha < \alpha_c = 7 - 4\sqrt{3} \sim 0.0718$ [10]. When $\alpha > \alpha_c$, the inelastic collapse can occur in presence of an inelastic wall, see Fig. 2.3a, if the number of particles is sufficiently high. In more than 1 dimension, inelastic collapse can be realized in a large cluster, see Fig. 2.3b. This phenomenon has dramatical consequences on inelastic hard spheres simulations: indeed, since time and space scales between two collisions geometrically decrease, the

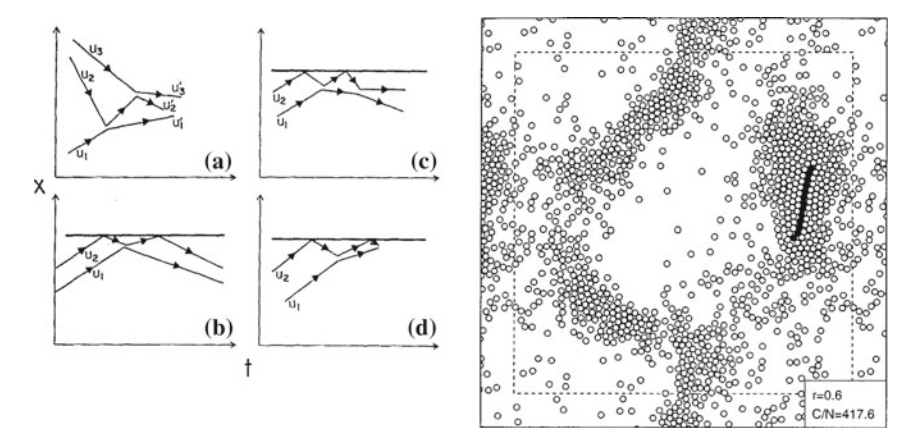


Fig. 2.3 Inelastic collapse: a schematic trajectories showing inelastic collapse. (a) Three particle collapse: without surrounding walls, collapse occurs when $\alpha < \alpha_c = 7 - 4\sqrt{3} \sim 0.0718$. (b) Two particles collide between themselves and a wall, but do not collapse since $\alpha > 0.346015$. (c) At critical $\alpha = 0.346015$, the inner particle is stationary after two collisions with the outer one. (d) For $\alpha < 3 - 2\sqrt{2} \sim 0.17157$ there is inelastic collapse [10]. **b** a snapshot from a MD simulation of inelastic hard spheres cooling in a square box with periodic boundary conditions, with $\alpha = 0.6$ and N = 1024 particles. C/N = 417.6 is the total number of collisions per particle at the time the simulation is stopped. Black particles are involved in the last two hundred collision: the linear arrangement characteristic of inelastic collapse is evident [11]

assumption of binary collisions will fail. Furthermore, the time between two collisions will become exponentially small and event-driven simulation time steps will dramatically slow down, until at a certain time the simulation stops running as an infinite number of collisions occur in finite time. A snapshot of this situation in 2d is plotted in Fig. 2.3b, where collapsed particles are highlighted. To avoid the inelastic collapse, some models consider a velocity-dependent restitution coefficient, becoming more and more elastic as the relative velocity tends to zero, in agreement with experimental observations. This description is generally known as *viscoelastic model*. Simulations of such models have shown that the inelastic collapse is removed, suggesting that it is an artificial consequence of fixing a constant restitution coefficient [4].

Having considered the deep qualitative differences between elastic and inelastic collisions, now the Boltzmann equation for granular gases can be derived. The pseudo-Liouville equation (2.23) holds, provided that the binary collision operator $T_{-}^{\dagger}(1,2)$ is now written in terms of inelastic collision rules, Eqs. (2.31) and (2.33). Since direct and inverse transformation do not coincide anymore in the $\alpha < 1$ case, the operator b_c in T_{-} and T_{-}^{\dagger} which exchanges precollisional velocities withpostcollisional ones must be exchanged with its inverse b_c^{-1} . The adjoint of the

inverse binary inelastic collision operator therefore reads

$$T_{-}^{\dagger}(1,2) = \sigma^{2} \int_{\mathbf{v}_{12} \cdot \hat{\mathbf{n}} > 0} d\hat{\mathbf{n}} |\mathbf{v}_{12} \cdot \hat{\mathbf{n}}| \left[\frac{1}{\alpha^{2}} \delta \left(\mathbf{r}_{1} - \mathbf{r}_{2} - \sigma \hat{\mathbf{n}} \right) - \delta \left(\mathbf{r}_{1} - \mathbf{r}_{2} + \sigma \hat{\mathbf{n}} \right) \right].$$
(2.34)

Deriving the BBGKY hierarchy and considering the first equation for one-particle distribution, the Molecular Chaos assumption gives the Boltzmann equation for granular gases

$$\left(\frac{\partial}{\partial t} + L_1^0\right) P(\mathbf{r}_1, \mathbf{v}_1, t) = N\sigma^2 Q(P, P), \qquad (2.35a)$$

$$Q(P, P) = \int d\mathbf{v}_2 \int_{\mathbf{v}_{12} \cdot \hat{\mathbf{n}} > 0} d\hat{\mathbf{n}} |\mathbf{v}_{12} \cdot \hat{\mathbf{n}}| \left[\frac{1}{\alpha^2} P(\mathbf{r}_1, \mathbf{v}_1^*, t) P(\mathbf{r}_1, \mathbf{v}_2^*, t) \right]$$
(2.35b)

$$-P(\mathbf{r}_1,\mathbf{v}_1,t)P(\mathbf{r}_1,\mathbf{v}_2,t)],$$

where \mathbf{v}_1^* and \mathbf{v}_2^* indicate the precollisional velocities required to have \mathbf{v}_1 and \mathbf{v}_2 as postcollisional ones, see Eq. (2.33).

As a first approach, this equation can be studied in the spatially homogeneous case (therefore $L_1^0 = 0$), including the Enskog correction $\Xi(\sigma, n)$, which has been introduced to account for velocity correlations under some assumptions, and acts as a multiplicative factor correcting Molecular Chaos approximation [5]. The homogeneous equation reads

$$\frac{\partial}{\partial t}P(\mathbf{v}_1,t) = \Xi(\sigma,n)n\sigma^2Q(P,P), \qquad (2.36)$$

where *n* is the average number density; the last equation has been studied by Goldshtein and Shapiro [9] and by Ernst and van Noije [12]. This is the first step to derive dynamical equations of granular quantities, as it will be done in the next paragraph.

2.1.3 The Homogeneous Cooling State and Haff's Law

From now on only the spatially homogeneous case is considered.

The granular cooling has no stationary state, since the energy keeps dissipating because of the collisions all along the trajectory. Therefore, it is useful to define the rescaled velocity distribution \tilde{f} as

$$NP(\mathbf{v},t) = \frac{n}{v_T^3(t)}\tilde{f}(\mathbf{v}/v_T(t)), \qquad (2.37)$$

where the temperature $T(t) = m\langle v^2 \rangle/3 = mv_T^2(t)/2$ defines the thermal velocity $v_T(t)$. It can be shown that $N^2Q \to n^2v_T^2\tilde{Q}$, with

$$\tilde{Q} = \int d\mathbf{c}_2 \int_{\mathbf{c}_{12} \cdot \hat{\mathbf{n}} > 0} d\hat{\mathbf{n}} |\mathbf{c}_{12} \cdot \hat{\mathbf{n}}| \left[\frac{1}{\alpha^2} \tilde{f}(\mathbf{c}_1^*, t) \tilde{f}(\mathbf{c}_2^*, t) - \tilde{f}(\mathbf{c}_1, t) \tilde{f}(\mathbf{c}_2, t) \right], \quad (2.38)$$

defining a rescaled velocity $\mathbf{c} = \mathbf{v}/v_T$. The collisions cause the temperature decay: from Eq. (2.32), one expects that they reduce the energy by a quantity proportional to the kinetic energy itself. The temperature evolution equation reads

$$\frac{\mathrm{d}}{\mathrm{d}t} \left(\frac{3}{2} nT \right) \bigg|_{coll} = \int \mathrm{d}\mathbf{v} \, \frac{mv^2}{2} \sigma^2 N^2 Q(P, P) \,, \tag{2.39}$$

$$= \sigma^2 n^2 v_T \frac{m v_T^2}{2} \int d\mathbf{c}_1 c_1^2 \tilde{Q} = -\sigma^2 n^2 v_T T \mu_2 , \qquad (2.40)$$

being

$$\mu_p = -\int d\mathbf{c}_1 c_1^p \tilde{Q} . \tag{2.41}$$

Therefore

$$\frac{\mathrm{d}T}{\mathrm{d}t}\bigg|_{\mathrm{cell}} = -\zeta(t)T(t) , \qquad (2.42)$$

where

$$\zeta(t) = \frac{2\sqrt{2}}{3}n\sigma^2\mu_2\sqrt{\frac{T(t)}{m}}.$$
 (2.43)

Equation (2.42) rules the Homogeneous Cooling State (HCS). Since the density is constant and any global velocity can be put to 0 by means of a Galilean transformation, the temperature field is the only hydrodynamic relevant field in the HCS. Because of these simplifications, the HCS is usually the starting point to study granular flows and instabilities, see Sect. 3.1.2 and Chap. 4.

Throughout homogeneous cooling all the particles continuously lose energy by means on inelastic collisions with uniform distribution in space, which makes the granular temperature homogeneously decreasing after having initialized the system with some non-trivial velocity distribution. This is the reason why \tilde{f} has been introduced: indeed $P(\mathbf{v})$ necessarily tends to a Dirac delta $\delta(\mathbf{v})$. The dissipation coefficient $\zeta(t)$ is time-dependent, i.e. $\zeta(t) \propto \sqrt{T(t)}$: this is the effect of a hard-core potential, which makes the collision frequency proportional to the thermal velocity,

$$\omega_c \sim v_T \sim \sqrt{T} \,,$$
 (2.44)

where $\omega_c dt$ is the probability that a given particle undergoes a collision between t and t + dt.

When computing the time-derivative of the rescaled distribution, additional contributions appear

$$\frac{\partial NP}{\partial t} = \frac{n}{v_T^3} \frac{\partial \tilde{f}}{\partial t} + \left(-\frac{3n}{v_T^4} \tilde{f} + \frac{n}{v_T^3} \frac{\partial \tilde{f}}{\partial c_1} \frac{\partial c_1}{\partial v_T} \right) \frac{\mathrm{d}v_T}{\mathrm{d}t} , \qquad (2.45)$$

leading to the following evolution equation

$$\frac{1}{v_T} \frac{\partial \tilde{f}}{\partial t} - \frac{1}{v_T^2} \frac{\partial (\mathbf{c}_1 \tilde{f})}{\partial \mathbf{c}_1} \frac{\mathrm{d}v_T}{\mathrm{d}t} = \sigma^2 n \tilde{Q} . \tag{2.46}$$

The second term in the lhs can be computed through Eqs. (2.42) and (2.41),

$$\frac{1}{v_T^2} \frac{dv_T}{dt} = \sqrt{\frac{m}{2T}} \frac{1}{2T} \frac{dT}{dt} = -\frac{1}{3} \sigma^2 n \mu_2 , \qquad (2.47)$$

which prove it to be time-independent.

Assuming the existence of a scaling stationary solution, namely \tilde{f}_{HCS} such that $\partial \tilde{f}_{HCS}/\partial t = 0$, this must satisfy

$$\frac{\mu_2}{3} \frac{\partial (\mathbf{c}_1 \tilde{f}_{HCS})}{\partial \mathbf{c}_1} = \tilde{Q} . \tag{2.48}$$

The latter equation defines the Homogeneous Cooling State. Finally, in the HCS the temperature evolution reads

$$T_{HCS}(t) = \frac{T(0)}{\left(1 + \frac{\zeta(0)t}{2}\right)^2},$$
 (2.49)

which is known as the Haff's law [13] and has the remarkable property of being independent of the initial temperature in the long time limit, namely

$$T(t) \sim 4(\overline{\zeta}t)^{-2} \,, \tag{2.50}$$

with

$$\bar{\zeta} = \frac{\zeta(T_{HCS}(t))}{T_{HCS}^{1/2}(t)} = \frac{\zeta_0 v_T(t)}{l T_{HCS}^{1/2}(t)} , \qquad (2.51)$$

where $l \propto 1/(n\sigma^2)$ is the mean free path and ζ_0 is the dimensionless cooling rate, a physical parameter of the system.

2.1.4 Steady State Representation

Equation (2.43) and Haff's law in (2.50) says that for long times

$$\omega_c(t) \sim \frac{2}{\overline{\zeta}t} \quad \Rightarrow \quad N_c(t) \sim \ln(\overline{\zeta}t/2) \,, \tag{2.52}$$

where $N_c(t)$ is the number of cumulated collisions after a time t. A new time-scale can now be introduced

$$\tau(t) = \tau_0 \ln \frac{t}{t_0} \,, \tag{2.53}$$

with arbitrary τ_0 and t_0 ; Eq. (2.53) gives the trend of the mean intercollisional time τ at time t. In this new time scale, the number of collisions in a time interval $d\tau$ is constant. This yields

$$\frac{\partial}{\partial t} = \frac{\tau_0}{t} \frac{\partial}{\partial \tau} \,, \tag{2.54}$$

therefore for long times one has

$$\frac{1}{v_T(t)}\frac{\partial}{\partial t} \sim \frac{\overline{\zeta}\tau_0}{2}\frac{\partial}{\partial \tau}.$$
 (2.55)

Finally, the evolution equation of the one particle distribution in the new time scale τ reads

$$\frac{\partial \tilde{f}}{\partial \tau} + \frac{n\sigma^2 \mu_2}{3} \frac{\partial (\mathbf{c}_1 \tilde{f})}{\partial \mathbf{c}_1} = \sigma^2 n \tilde{Q} , \qquad (2.56)$$

which is equivalent to the Boltzmann equation of particles subjected to an external force

$$\mathbf{F} = \frac{n\sigma^2 \mu_2}{3} \mathbf{c} \,, \tag{2.57}$$

acting like a *positive* viscosity. Actually, this equivalence makes sense as long as the state remains homogeneous; in Sect. 3.1.2 it will be shown how the HCS is unstable for long wavelengths perturbations [14].

Equation (2.56) is the Boltzmann equation in the *steady state representation* [15]: indeed, it has been seen how looking at the system in terms of the rescaled velocity \mathbf{c} is equivalent to adding a *propulsive* continuous force, increasing the energy of the system. The meaning is evident: the velocity rescales and as the new time scale τ slows down when t increases, the new velocity reads

$$\mathbf{w}(\tau) = \frac{\mathrm{d}\mathbf{x}}{\mathrm{d}\tau} = \frac{\mathrm{d}\mathbf{x}}{\mathrm{d}t} \frac{\mathrm{d}t}{\mathrm{d}\tau} = \frac{t}{\tau_0} \mathbf{v}(t) , \qquad (2.58)$$

so the effect of the propelling force is to inject back in the particles the same average quantity of energy lostby collisions, which follow the same rule (2.31) because they are instantaneous and not affected by time rescaling.

In this representation, Eq. (2.56) provides a new evolution equation for the rescaled homogeneous temperature $\tilde{T}_H(\tau) = m \langle w^2 \rangle / 3$ [15],

$$\left(\frac{\mathrm{d}}{\mathrm{d}\tau} - \frac{2}{\tau_0}\right)\tilde{T}_H(\tau) = -\overline{\zeta}\tilde{T}_H^{3/2}(\tau), \qquad (2.59)$$

whose solution reads

$$\tilde{T}_{H}(\tau) = \left(\frac{2}{\tau_{0}\overline{\zeta}}\right)^{2} \left[1 + \left(\frac{2}{\tau_{0}\overline{\zeta}\tilde{T}_{H}^{1/2}(0)} - \right)e^{-\tau/\tau_{0}}\right].$$
(2.60)

Consequently, the rescaled temperature tends to a stationary value given by

$$\tilde{T}_{st} = \left(\frac{2}{\tau_0 \overline{\zeta}}\right)^2 \,. \tag{2.61}$$

From Eq. (2.51), it can be shown that $\tau_0 \tilde{v}_{T,st}$ is independent from τ_0 and proportional to the dimensionless cooling rate ζ_0 , an intrinsic property of the system.

So, when considering rescaled variables, the steady state representation shows how the HCS forgets its initial condition after sufficiently long times and tends to a value determined by the parameters of the system, regardless of the initial velocity distribution. The steady state representation provides a mapping between a granular cooling, where no stationary state is possible, to a system where the energy is dissipated and injected at the same rate, leading to the stationary values described above.

2.1.5 Driven Granular Systems

A granular fluid can reach a stationary state when power is supplied in order to balance the energy lost because of collisions. There are two main theoretical description of driven granulars:

- 1. imposing boundary conditions like in a sheared or shaken granular, which is typically done in the hydrodynamic description see Sect. 3.1.2 and implemented in numerical simulations see Sect. 4;
- 2. driving the granular in the bulk, i.e. supplying energy to all the particles in their microscopic dynamics. This is the case discussed in this section.

I report the randomly driven granular gas model [16, 17], consisting of a gas made by N identical hard objects of mass m and diameter D moving inside a d-dimensional

box of volume $V=L^d$, being L the side of the box. The dynamics of the gas is ruled by the interplay between two physical phenomena: a continuous interaction with the environment (Langevin process) and the inelastic collisions among the grains. The equations of motion read

$$\frac{\mathrm{d}}{\mathrm{d}t}\mathbf{x}_{i}(t) = \mathbf{v}_{i}(t) , \qquad (2.62a)$$

$$m\frac{\mathrm{d}}{\mathrm{d}t}\mathbf{v}_{i}(t) = -\gamma_{b}\mathbf{v}_{i}(t) + \sqrt{2\gamma_{b}T_{b}}\boldsymbol{\xi}_{i}(t) + \mathbf{F}_{i}(t). \qquad (2.62b)$$

So, the grains are coupled with a thermal bath, calling $\tau_b = m/\gamma_b$ and T_b respectively the characteristic time and temperature of the bath. The function $\boldsymbol{\xi}_i(t)$ is a standard Wiener process, i.e. $\langle \boldsymbol{\xi}_i(t) \rangle = 0$ and $\langle \boldsymbol{\xi}_i^{\alpha}(t) \boldsymbol{\xi}_j^{\beta}(t') \rangle = \delta(t-t')\delta_{ij}\delta_{\alpha\beta}$. The noise coefficient $\sqrt{2\gamma_bT_b}$ satisfies the Einstein fluctuation-dissipation relation. Inelastic collisions are taken into account by $\mathbf{F}_i(t)$: they occur instantaneously with a mean intercollisional time τ_c .

Therefore, the parameters defining the dynamics are the restitution coefficient α and the ratio between the characteristic time scales, $\rho = \tau_b/\tau_c$. Depending on these (adimensional) parameters, one can define three limit cases of the dynamics

- the elastic limit $\alpha \to 1^-$;
- the collisionless limit $\rho \to 0 \quad (\tau_c \gg \tau_b)$;
- the cooling limit $\rho \to \infty$ $(\tau_c \ll \tau_b)$.

In d > 1, the elastic limit is smooth and one can take $\alpha = 1$: this is equivalent to consider an elastic gas, where the collisions contribute to the relaxation towards an homogeneous particle distribution in space and a Maxwellian distribution of velocities, with temperature T_b . In d = 1 the situation is different because in elastic collisions the particles exchange their velocities *exactly*, so there is no mixing because a collision is equivalent to an exchange of labels, namely $(v_i, v_j) \rightarrow (v_j, v_i)$ and the initial set of velocities is conserved in time.

In the collisionless limit $\tau_c \gg \tau_b$, therefore collisions are very rare and the gas can be considered as a gas of non-interacting random Brownian walkers, which sometimes collide between them but then relax toward a Maxwellian distribution with temperature T_b and homogeneous density.

Finally, in the cooling limit $\tau_c \ll \tau_b$ and collisions dominate: between two collisions the particles move almost ballistically. The bath is heating the granular but this effect can be seen only for time scales greater than τ_b : for intermediate observation times $\tau_c \ll t \ll \tau_b$ the gas behaves like a cooling granular gas.

2.1.6 Inelastic Maxwell Molecules

Finally, we conclude this review of granular kinetic theory focusing on *inelastic Maxwell molecules*: this is a category of particles whose collision integral *does*

not depend on the flux term $|\mathbf{v}_{12} \cdot \hat{\mathbf{n}}|$ [18]. The kinetic theory has shown that this is approximately the case for particles in d dimensions subject to a power law repulsive interaction potential $U(r) \sim r^{-2(d-1)}$, being r the distance between the particles [5]. The Boltzmann Equation for Maxwell molecules is greatly simplified, and in the inelastic 1d case reads

$$\frac{\partial}{\partial \tau}P(v,\tau) + P(v,\tau) = \beta \int du P(u,\tau)P(\beta v + (1-\beta)u,\tau), \qquad (2.63)$$

where $\beta=2/(1+\alpha)$ and τ is the number of collisions per particle. For Maxwell molecules the collision frequency ω_c is constant, i.e. it doesn't depend from the thermal velocity as for hard spheres, hence τ is linear with t and they can be used alternatively. Otherwise, one can take the flux term |v-v'| in 1d hard rods to be proportional to the thermal velocity, \sqrt{T} ; by means of a time reparametrization $\tau(t)$, the latter factor can be eliminated and the Boltzmann equation reduces to Eq. (2.63). This description is called *pseudo-Maxwell* model [19].

Equation (2.63) implies that at each time step an arbitrary couple of particles is selected and their velocities are transformed following the collisional rule (2.31) in d=1. This model was applied by in 1999 [20] as a traffic flow model, and further analyzed in [21]: essentially, it analyzes the dynamics of Maxwell molecules in the mean field case, i.e. disregarding spatial structure. In the homogeneous case of zero total momentum (i.e. in the center of mass frame) the authors obtained an exponential decay of velocity moments, namely

$$\langle v^n \rangle \sim e^{-a_n \tau} \,, \tag{2.64}$$

but with decay rates $a_n \neq na_2/2$, arguing the presence of a *multiscaling* behavior, namely that higher-order moments cannot be written as functions of the second moment. The authors in [21] consequently exclude the existence of a rescaled asymptotic distribution $P(v, \tau) \rightarrow f(v/v_T(\tau))/v_T(\tau)$ in the long time limit. On the contrary, it has been shown [22] that the rescaled distribution function

$$f(v/v_0(\tau)) = \frac{2}{\pi \left[1 + (v/v_0(\tau))^2\right]^2},$$
 (2.65)

is a physical asymptotic solution of Eq. (2.63) when considering inelastic hard rods on a lattice. Since it has the form of a power law with $f(c) \sim c^{-4}$ for high c, moments $\langle v^n \rangle$ with $n \geq 3$ diverge and therefore do not scale with the second moment.

Remarkably, the scaling velocity distribution form in (2.65) does not depend on the restitution coefficient α : the dynamics is completely contained in the thermal velocity $v_0(\tau)$. Furthermore, Eq. (2.64) leads to a new version of Haff's law (2.49) for Maxwell molecules, namely

$$T(t) \sim e^{-a_2\tau} \,, \tag{2.66}$$

so that the temperature exponentially decays in function of the collisional clock τ . Further studies have shown that the multiscaling behavior yields non-stationary total energy fluctuations [23]

$$\frac{\langle E^2(\tau) \rangle - \langle E(\tau) \rangle^2}{\langle E(\tau) \rangle^2} = \frac{1}{N} \left[A + B \exp(2\zeta^2 t) \right], \qquad (2.67)$$

where $E(\tau) = \sum_{i=1}^N v_i^2(\tau)$ is the total energy, $2\zeta^2 = 2a_2 - a_4$ and A and B depend on the initial velocity distribution. The energy fluctuations vanish in the large-size limit since they scale as $1/\sqrt{N}$ and so a thermal capacity can always be defined, but it grows with time. This property will be discussed in Sect. 5.3 for the granular lattice model introduced in Chap. 4.

A great deal of attention has been focused on Maxwell molecules over the last years, because the simplification of Maxwell particles allows the derivation of several analytical results. Models of Maswell Molecules on a lattice will be described in more detail in Sect. 3.3.2, and will be one of the subject of this thesis analyzed in Chap. 4.

2.2 Active Models

The collective phenomenology of active matter introduced in Chap. 1 raises many questions about its theoretical description: as we saw, there are many kind of collective motion exhibited by several living and non-living systems. Hence, a good modelization of active matter is very difficult if one wants to replicate *all* the observed features in a single, universal model, and it is rather preferable to seek for the essential ingredients of motion leading to the emergence of collective behavior. Statistical mechanics is a powerful tool to develop a theoretical representation of active matter: many models start from Brownian motion and add some prescriptions about interactions and self-propulsion. These are the main ingredients of active matter models and, before introducing the most established, it is useful to give a short classification of active systems.

Active systems can be **dense or dilute**: in human made systems the density is a control parameter which can be easily tuned, but biological, self-organized systems show that the properties of their motion can strongly depend on density. The latter affects interactions and observed phases: indeed at higher densities the effect of the excluded volume gets more important, and self-trapping becomes more probable. Also, in dense systems the particles are more likely to interact continuously between the same ones, and the Molecular Chaos assumption - stated in Eq. (2.27) - does not often give a good approximation.

The **Interactions** can also be produced by several different mechanisms, as it has been described before, and have various physical features. Vicsek and Zafeiris classified them as [24]

- physical, chemical, visual or medium-mediated;
- isotropic or anisotropic, polar or apolar;
- metrical or topological;
- short-range or long-range.

For instance, in driven granulars the grains collide between themselves (physical interaction) while birds in flocks almost never do it, probably interacting through a visual mechanism. Generally speaking, the shape and symmetries of the units affect the typology of the interactions: for instance, granular rods are nematic and apolar particles, while Janus spheres are isotropic and polar. Any combination of these properties is possible, accounting for several possible interactions. It has been shown that the notion of distance in collective motion is ambiguous: birds in a flock seem to interact through a topological rather than metrical distance, as said in Sect. 1.4.2.

The case of medium-mediated or long-range interactions deserves a specific consideration: until now, a self-propulsion mechanism has always been considered as a momentum and energy injection in a unity able to convert internal energy into kinetic energy, or to generate a non-trivial motion in presence of external fields. However, the role of the surrounding medium (excluding external fields) has generally been disregarded. Actually, neglecting external forces such as gravity, active particles can change their motion only by interacting with the surrounding fluid: the total momentum of the fluid and the active unit *does not change* in the self-propulsion reaction, because a particle moving in a given direction pushes the fluid in the opposite one, as we do when we swim or we row on a boat. The particles typically creates a force dipole, which can have various shapes depending on the self-propulsion mechanism and propagates across the fluid, see Fig. 2.4, and reaches other units at long-range distances [26, 27]. These are called *hydrodynamic interactions* and motivate two kinds of active models: **dry or wet active matter**. In the latter, it is not always

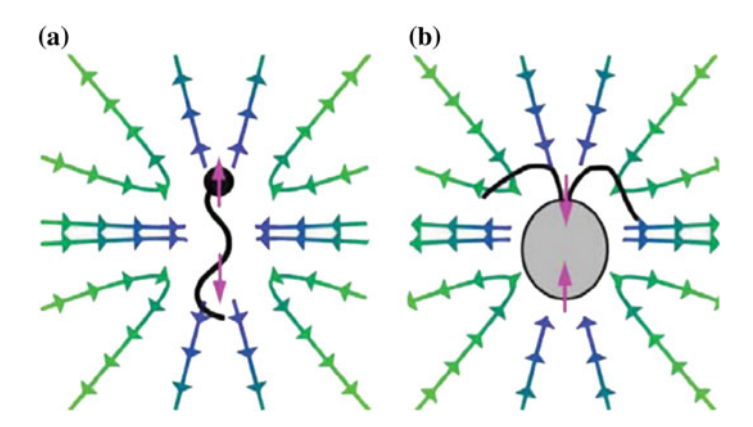


Fig. 2.4 Force dipoles in a fluid medium generated by microswimmers, namely called **a** *pushers* or **b** *pullers*, depending on the polarity of their swimming mechanism: purple arrows display the self-propelling forces [25]

2.2 Active Models 51

necessary to consider the coupled evolution of the swimmers and the surrounding fluid, but one can consider the fluid as a mediator of interactions between active particles, transmitted for instance by means of hydrodynamic waves. These particles are called *microswimmers* and have been reviewed in [25, 28]. It can be summarized that in dry models the self-propulsion is an individual force, which any particle feels independently and momentum is not conserved; conversely, in wet models the self-propulsion is always coupled with a momentum transport, which propagates in the medium and is transmitted to surrounding particles, and the *total* momentum is always conserved.

The role of **equilibrium** in the description and modelization of active matter is very important and currently under debate: it is physically clear that active matter is out of equilibrium because of the continuous energy dissipation and injection occurring in the single active units, and that non-conservative interactions are acting. However, many studies on active matter use an equilibrium description, defining an effective Hamiltonian, temperature and free energy, yielding the existence of equilibrium phase transitions [29–32]. For instance, aligning interactions inspired a modeling of birds flock as ferromagnetic models, inspired from the Ising, Heisenberg or XY models [33–37]. This approach is clearly motivated by the wide and self-consistent progresses made by equilibrium statistical physics and the theory of critical phenomena through the last century. However, its application needs some justifications: these have been studied in the very last years and related to the characteristic time scales of the system. Indeed, if a scale separation is present between equilibrium and out-of equilibrium mechanisms, a local equilibrium approximation can be made to consider the local time behavior of the system as an equilibrium process. In 2016, Mora et al. [37] introduced a ferromagnetic model to study the behavior of bird flocks, which are driven out of equilibrium by the continuous rearrangement of their interaction network, typically occurring in active matter. The experimental comparison between the alignment relaxation time τ_r and the network rearrangement time τ_n showed that $\tau_r \ll \tau_n$, therefore interactions occur at almost fixed network: this result justifies a local equilibrium approximation for the model purposed. Furthermore, few weeks before Fodor et al. [38] published a study with the aim of quantifying the non-equilibrium properties of an active matter model, namely the Active Ornstein-Uhlenbeck Particles model (see Sect. 2.2.4). In this model, the active particles feel a self-propelling persistent velocity with a correlation time τ : the authors have shown that the entropy production is of order $\mathcal{O}(\tau^2)$ for small τ , and therefore argued that there exists a regime where direct and reversed trajectories have the same probabilities, entropy production vanishes and the system relaxes towards an effective Boltzmann distribution. In both studies, some specific models have been used to give a quantitative analysis of non-equilibrium properties and justify the local equilibrium approximations made; a general response about the limits of the equilibrium properties in active matter is still under investigation [39].

It is now evident that an active model is composed by two ingredients: a **self-propulsion** mechanism and an **interaction** rule. Their qualitative properties, especially for interactions, have been overviewed in this paragraph; the following paragraphs are dedicated to successful models that headed the study of active matter

in the last decades. It has to be stressed that self-propulsion and interactions can be considered separately, and that the self-propulsion mechanism of a model can be combined with the interaction rule of another model. So, two models of interactions will be introduced: the Kuramoto model and the Vicsek model, respectively in Sects. 2.2.1 and 2.2.2. Models of self-propulsion will be introduced in further sections. Any realistic model of active particles requires an implementation of both ingredients.

2.2.1 The Kuramoto Model

The Kuramoto model, introduced in 1975 [40, 41], is one of the most successful models describing the collective *synchronization* of coupled rotators. Its success consisted in an essential description of a transition to order by means of "aligning" interactions, tuned by the coupling strength acting as the control parameter of the transition. A complete review of the model can be foundin [42]; for the need of this thesis, also the analysis in [43, 44] is sufficient.

Consider a set of N coupled rotators of phase θ_j , with quenched random frequencies ω_i : the standard Kuramoto model dynamics is given by

$$\dot{\theta_j} = \omega_j + \frac{K}{N} \sum_{k=1}^{N} \sin(\theta_k - \theta_j) . \qquad (2.68)$$

This evolution equation describes a system of overdamped rotators moving at a fixed and random individual frequency ω_j modified by a sort of elastic interaction among all of them, with fixed intensity K/N: each rotator feels the phase difference with other rotators as an attractive force to the synchronized state where $\theta_k = \theta_j$ for all j, k. The transition to synchronization can be analyzed in few steps: first, one sees that the global motion of phases evolves through the deterministic equation

$$\frac{1}{N} \sum_{j=1}^{N} \dot{\theta_j} = \frac{1}{N} \sum_{j=1}^{N} \omega_j = \Omega , \qquad (2.69)$$

where the last equivalence defines the global frequency Ω . It is convenient to define a sort of "center of mass" frame, where $\theta \to \theta - \Omega t$ and $\omega \to \omega - \Omega$: the evolution Eq. (2.68) is invariant under this translation and the new global frequency of the system vanishes, i.e. $\sum_i \omega_i = 0$.

The synchronization can be observed through the complex order parameter

$$re^{i\psi} = \frac{1}{N} \sum_{i=1}^{N} e^{i\theta_i},$$
 (2.70)

2.2 Active Models 53

which is finite in the large size limit, defining the *coherence* r and the *global phase* ψ . Their meaning is evident if one considers the swarming phase described in Sect. 1.4.1: when $r \approx 0$, the rotators move with random, disordered phases and no global order is observed; conversely, when $r \approx 1$, the rotators are locked to the same phase, oscillating with the same frequency and acting as a unique, giant rotator. By means of the complex order parameter, the evolution equation of the single rotator can be written as

$$\dot{\theta_i} = \omega_i + Kr\sin(\psi - \theta_i), \qquad (2.71)$$

where r and ψ generally depend on time.

In the large size limit, let's call $g(\omega)$ the density of natural frequencies ω_j , normalized to one and assumed even for simplicity and symmetry reasons. The probability distribution of the phase θ for a rotator of given frequency ω is called $\rho(\theta|\omega,t)$, and evolves according to

$$\frac{\partial \rho}{\partial t} + \frac{\partial}{\partial \theta} \left[(\omega + Kr \sin(\psi - \theta)) \rho \right] = 0, \qquad (2.72)$$

which stems from Eq. (2.71) and must be completed by the initial condition $\rho(\theta|\omega, 0)$. In the infinite N limit, the complex order parameter can be computed as

$$re^{i\psi} = \langle e^{i\theta} \rangle = \int_{-\pi}^{\pi} d\theta \int_{-\infty}^{+\infty} d\omega \, e^{i\theta} \rho(\theta|\omega, t) g(\omega) \,. \tag{2.73}$$

The last equation has a stationary uniform solution $\rho(\theta|\omega)=1/(2\pi)$ for any coupling constant K: the solution yields r=0 and uniform distribution of phases, i.e. no synchronization. Synchronized solutions can be found looking at fixed points of Eq. (2.71): assuming r>0 and $\psi=0$ without loss of generality, if $|\omega|< Kr$ one has a stable fixed point $\theta_0=\sin^{-1}(\omega/Kr)$; otherwise, for $|\omega|>Kr$ there are no fixed points. Therefore a stationary distribution of rotator's phases can be piecewise defined as

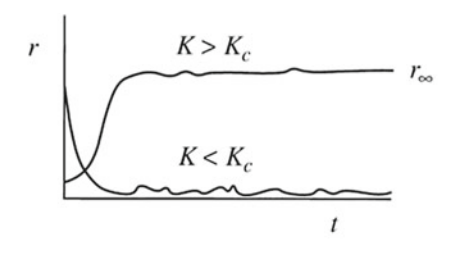
$$\rho(\theta|\omega) = \begin{cases} \delta \left[\theta - \sin^{-1}(\omega/Kr)\right] |\omega| < Kr \\ \frac{1}{2\pi} \frac{\sqrt{\omega^2 - (Kr)^2}}{|\omega - Kr \sin \theta|} & |\omega| > Kr \end{cases}, \tag{2.74}$$

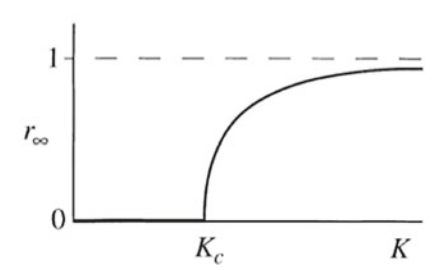
where the second line is given by Eq. (2.72) with $\partial_t = 0$. The coherence r can be computed through Eq. (2.73), and the only non-vanishing term is the one for $|\omega| < Kr$ [45]. So,

$$r = \int_{-\pi}^{\pi} d\theta \int_{-Kr}^{Kr} d\omega \, e^{i\theta} \delta[\theta - \sin^{-1}(\omega/Kr)]g(\omega) \,. \tag{2.75}$$

The latter has a consistent solution only if

$$K > K_c = \frac{2}{\pi g(0)} \,, \tag{2.76}$$





- (a) Coherence in function of time for trajectories above and below the critical coupling K_c .
- **(b)** Steady-state coherence in function of critical coupling *K*.

Fig. 2.5 Synchronization in Kuramoto model [45]

having assumed that the frequency distribution $g(\omega)$ has a maximum in 0. Therefore, K_c is the critical value of the coupling strength above which synchronization occurs, see Fig. 2.5. If $g(\omega)$ is regular up to ω^2 terms around $\omega = 0$, the coherence parameter scales as $r \sim (K - K_c)^{1/2}$.

The Kuramoto model has been studied and generalized including the inertia of rotators, a friction force, non-uniform couplings K_{kj} and noise terms; the latter is generally introduced adding a Gaussian White Noise (GWN) term $\eta_j(t)$ to the evolution Eq. (2.68), with $\langle \eta_j(t) \rangle = 0$ and $\langle \eta_k(t) \eta_j(t') \rangle = 2D\delta_{kj}\delta(t-t')$. The noise introduces a second control parameter competing with the coupling strength K, because the former leads the system away from order while the latter is accounting for synchronization: a more detailed discussion on oscillators' phases and their linear stability can be found in [42].

2.2.2 The Vicsek Model

The Vicsek model is a milestone in the theoretical description of self-propelled particles. Introduced in 1995 by Vicsek et al. [46], it aims at reproducing the self-ordering of active systems. The original model consists of N point particles moving on a periodic square cell of linear size L, with positions $\mathbf{x}_j(t)$ and velocities $\mathbf{v}_j(t)$ of constant modulus v. The velocities are described only by their orientation $\theta_j(t)$ and their equations of motion in discrete time read

$$\mathbf{x}_{i}(t + \Delta t) = \mathbf{x}_{i}(t) + \mathbf{v}_{i}(t)\Delta t, \qquad (2.77a)$$

$$\theta_i(t + \Delta t) = \langle \theta(t) \rangle_R + \xi_i(t),$$
 (2.77b)

with $\Delta t = 1$, being $\langle \theta(t) \rangle_R$ the average direction of particles' velocities within a circle of radius R from the focusal particle j, which is included in the average, namely

2.2 Active Models 55

$$\langle \theta(t) \rangle_R = \tan^{-1} \left(\frac{\langle \sin \theta(t) \rangle_R}{\langle \cos \theta(t) \rangle_R} \right).$$
 (2.78)

The term $\xi_j(t)$ is a random number drawn with uniform distribution in the interval $[-\eta/2,\eta/2]$. Since the particles have no extension, without loss of generality the interaction radius can be taken R=1. The free parameters of the system are then η (noise), $\rho=N/L^2$ (number density) and v (speed, i.e. the distance run by a particle between two updates); the self-propulsion is guaranteed by the constant speed v. Varying the parameters η and ρ several phases can be observed - see Fig. 2.6. Especially, at high density and small noise a global ordered swarming state arises. Fixing the speed at v=0.03, the authors looked at the swarming order parameter

$$v_a = \frac{1}{Nv} \left| \sum_{j=1}^N \mathbf{v}_j \right| , \qquad (2.79)$$

and observed a non-equilibrium transition when the noise is reduced below a critical value $\eta_c(\rho)$, or alternatively when the density is increased above $\rho_c(\eta)$. The transition is studied for several number of particles and gets sharper for large N, see Fig. 2.7. Thus, even in a non-equilibrium system as the one studied a phase transition occurs which is quite similar to an equilibrium transition.

From previous results the authors argued that in the thermodynamic limit the swarming parameter scales as

$$v_a \sim [\eta_c(\rho) - \eta]^{\beta}$$
, $v_a \sim [\rho - \rho_c(\eta)]^{\delta}$, (2.80)

defining the critical exponents β and δ . Numerical fits gave $\beta = 0.45 \pm 0.07$ and $\delta = 0.35 \pm 0.06$. Combined results are the basis to build a phase diagram in the plane $\eta - \rho$: the critical line has been numerically found as

$$\eta_c(\rho) \sim \rho^{\kappa}$$
(2.81)

with $\kappa = 0.45 \pm 0.05$ [47].

A first application of the Vicsek model has been the description of hydrodynamics and vortex formation in bacteria colonies for the case of *Bacillus subtilis* [48]. Further analysis on the Vicsek model showed the presence of moving clusters, a strong connection with the XY model especially at low speed $v \ll 1$, and a similar behavior when considering different shapes of the surface [33]; the Vicsek model has been enhanced and modified considering nematic (apolar) particles, adding cohesion and introducing the role of surrounding fluid [34]. Moreover, a strong connection between Kuramoto and Vicsek model has been found, because the two models show a similar bifurcation behavior under variation of the control parameters [49]: indeed, te synchronization in Kuramoto model is equivalent to the swarming in Vicsek model. The success of the Vicsek model is basically resumed in the sentence

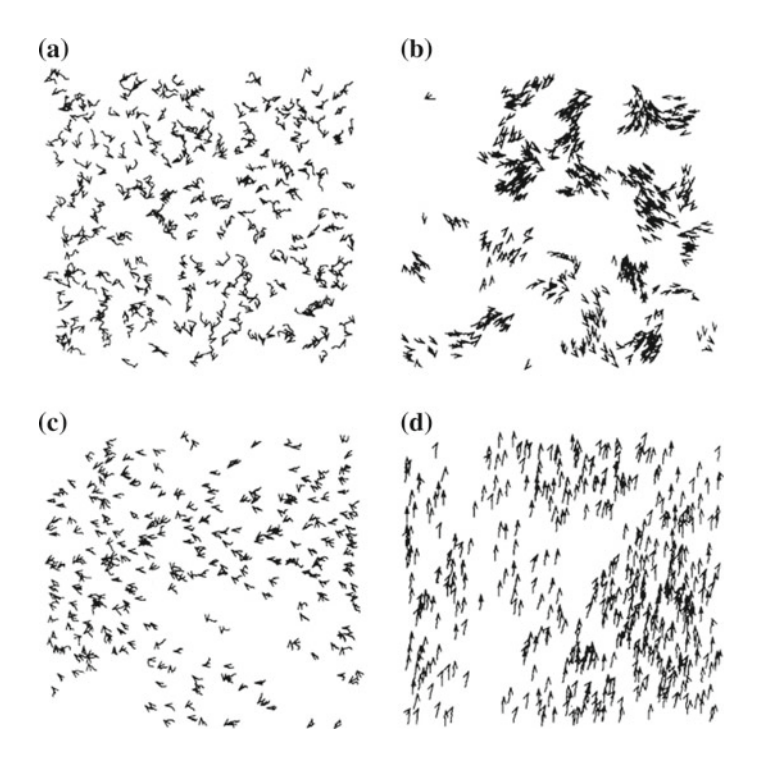


Fig. 2.6 Snapshots of the Vicsek model with N=300 particles: velocities are indicated by a small arrow and the last 20 time steps of the trajectories are shown by a short continuous curve. Panels show **a** initial disordered configuration at L=7 and $\eta=2.0$, **b** formation of coherent motion groups for small densities and noise, L=25 and $\eta=0.1$, **c** randomly moving particles with some correlation for high density and noise, L=7 and $\eta=2.0$ and **d** collective swarming for high densities and small noise, L=5 and $\eta=0.1$ [46]

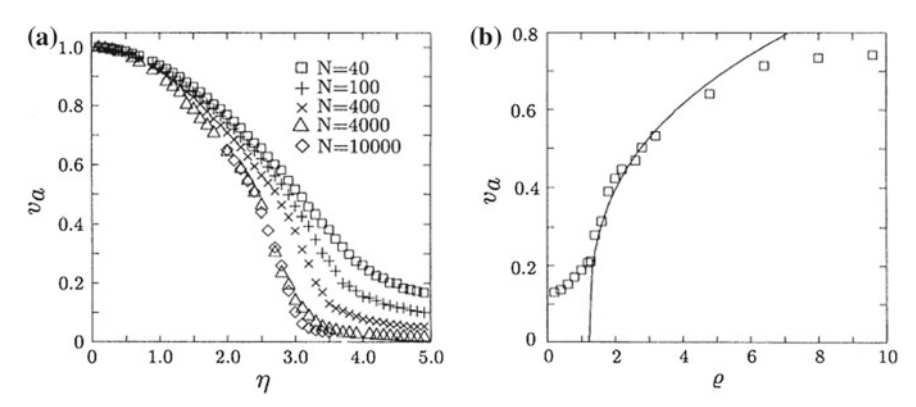


Fig. 2.7 Swarming parameter v_a in function of noise η (left) and density ρ (right). In left panel, the density is kept constant and the cell size is varied according to legend; in right panel, the noise is constant and the cell size is L=20 [46]

2.2 Active Models 57

We have chosen this realization because of its simplicity, however, there may be several more interesting alternatives of implementing the main rules of the model. In particular, the absolute value of the velocities does not have to be fixed, one can introduce further kind of particle interactions and or consider lattice alternatives of the model [46].

Actually, the Vicsek model is a very commonly used starting point to observe collective motion from microscopic behavior of self-propelled interacting particles, and many subsequent models are variations of this one [24].

2.2.3 Active Brownian Particles and Run-and-Tumble Dynamics

Having considered Kuramoto and Vicsek models as a starting point to introduce ordering interactions in a system of active particles, the most used models of self-propelled particles will be now introduced. The goal of all the following descriptions is to introduce a self-propulsion mechanism accounting for two properties:

- keep the particles in a constant state of motion, avoiding cooling because of dissipative collisions or interactions with the environment;
- describe the changes of direction in particles' motion.

In this section only *dry* particles are considered, which means that self-propulsion does not conserve momentum as it has been discussed above.

Active Brownian particles (ABP) are one of the most general model of active particles [28]: each unit is a Brownian particle performing active motion, generated by internal energy storing or nonlinear velocity-dependent friction [50]. ABPs equations of motion for a particle of unit mass m=1 generally read

$$\dot{\mathbf{r}} = \mathbf{v} \,, \tag{2.82a}$$

$$\dot{\mathbf{v}} = \mathbf{F}_d(\mathbf{r}, \mathbf{v}) - \nabla U(\mathbf{r}) + \boldsymbol{\xi}(t) , \qquad (2.82b)$$

being $\mathbf{F}_d(\mathbf{r}, \mathbf{v})$ a position and velocity-dependent dissipation force, $U(\mathbf{r})$ an external potential and $\boldsymbol{\xi}(t)$ a stochastic force acting on the particle. For $F_d = -\gamma \mathbf{v}$ and a GWN $\boldsymbol{\xi}(t)$ satisfying the Einstein relation $\langle \xi_\alpha(t)\xi_\beta(t')\rangle = 2\gamma T\,\delta_{\alpha\beta}\delta(t-t')$, one recovers the classical Brownian motion at equilibrium. On the contrary, a different choice of the dissipation is sufficient to have a self-propulsion force: a suitable choice is to define a velocity dependent friction $\mathbf{F}_d = -\gamma(\mathbf{v})\mathbf{v}$, for instance

$$\gamma(\mathbf{v}) = -a + bv^2 = a\left(\frac{v^2}{v_0^2} - 1\right),$$
 (2.83)

leading the particles to the stable fixed point $v_0 = \sqrt{a/b}$: the nonlinear friction accelerates the particle in its direction of motion for $v < v_0$ and slows it down

for high speed $v > v_0$. The viscosity in Eq. (2.83) is called *Rayleigh–Helmoltz friction*. An exact solution of Eq. (2.82b) without noise or external potential is given in Appendix B.1. Without noise or interactions, no changing of orientation is possible. When the noise is Gaussian and white with variance 2D, the probability density $P(\mathbf{r}, \mathbf{v}, t | \mathbf{r}_0, \mathbf{v}_0, t_0)$ of this process follows the Kramers Equation [51]

$$\frac{\partial P}{\partial t} + \mathbf{v} \cdot \nabla P - \nabla U(\mathbf{r}) \cdot \frac{\partial P}{\partial \mathbf{v}} = \frac{\partial}{\partial \mathbf{v}} \left[\gamma(\mathbf{v}) \mathbf{v} P + D \frac{\partial P}{\partial \mathbf{v}} \right], \qquad (2.84)$$

which in the homogeneous case $\nabla = 0$ (no spatial gradients) has a stationary solution

$$P_0(\mathbf{v}) = \mathcal{N} \exp[-\Phi(\mathbf{v})/D], \qquad (2.85)$$

where $\Phi(\mathbf{v})$ is a velocity-dependent effective potential, namely $\Phi(\mathbf{v}) = \int^{\mathbf{v}} d\mathbf{v}' \gamma(\mathbf{v}') \mathbf{v}'$, holding for a general choice of $\gamma(\mathbf{v})$; for the Rayleigh-Helmoltz viscosity, one has $\Phi(\mathbf{v}) = -\frac{a}{2}v^2 + \frac{b}{4}v^4$. Depending on the sign of a the motion of particles can be passive (a < 0) or active a > 0; active particles potential has the typical mexican hat shape, leading to a continuous set of minima with speed $|\mathbf{v}| = v_0$, see Fig. 2.8; there is spontaneous symmetry breaking in each trajectory where particles travel along a given direction, which is what one observes when looking at experiments and simulation on swarming particles.

The stationary distribution in Eq. (2.85) has a limit value for the high dissipation regime: if $b/D \to \infty$ while $v_0 = \sqrt{a/b}$ remains finite, the distribution converges to a delta function

$$P_0(\mathbf{v}) = \delta(|\mathbf{v}| - v_0). \tag{2.86}$$

The latter applies when the relaxation time towards the fixed point v_0 is extremely small compared to the characteristic time of rotational diffusion. Therefore, particles can be considered at constant speed $\mathbf{v} = v_0$ and their motion is described by the

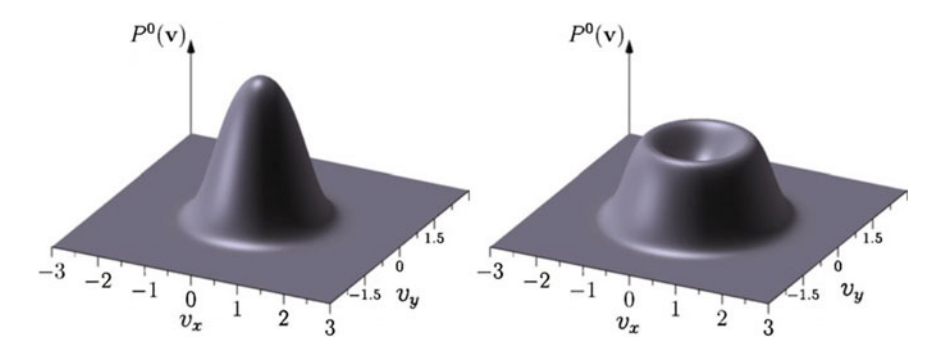


Fig. 2.8 Stationary velocity distribution $P_0(\mathbf{v})$ (2.85) in the Cartesian plane for Rayleigh–Helmoltz friction. Left panel: passive regime with a=-0.1. Right panel: active regime with a=1.0. In both cases b=1.0 and D=0.5 [50]

2.2 Active Models 59

angular orientation $\theta(t)$. Two possible dynamics of the orientation are the **angular diffusion** [44] or the **run-and-tumble dynamics** [29, 52], which are frequently used to describe active systems, especially for crowded environments such as bacteria colonies [28]. In the former, the orientation evolves gradually, following a Wiener process with diffusion coefficient D_R , namely

$$\dot{\theta} = \sqrt{2D_R}\xi(t) \,, \tag{2.87}$$

where now $\xi(t)$ is a GWN of unit variance; on the other side, run-and-tumble dynamics consists of particles following a ballistic, straight motion and undergoing instantaneous scattering events $\theta \to \theta + \eta$ at a rate λ per unit time, where η is a random angular variable with distribution $p(\eta)$. Both dynamics can be expressed by the Fokker–Planck equation

$$\frac{\partial P}{\partial t} + v_0 \mathbf{e}(\theta) \cdot \nabla P = I[P], \qquad (2.88)$$

where $\mathbf{e}(\theta)$ is the unit vector in the direction θ and the functional I[P] accounts for diffusion rule, which for angular diffusion reads

$$I[P] = D_R \frac{\partial^2 P}{\partial \theta^2} \,, \tag{2.89}$$

while for run-and-tumble dynamics one has [44]

$$I[P] = -\lambda P(\mathbf{r}, \theta, t) + \lambda \int_{-\infty}^{+\infty} d\eta p(\eta) P(\mathbf{r}, \theta - \eta, t) , \qquad (2.90)$$

Both angular diffusion and run-and-tumble dynamics reproduce the tendency of active particles to explore space by changing their orientation, for instance when seeking nutrients. It is usual to read of active Brownian particles as a synonym of angular diffusion motion. The angular diffusion is often used to describe the motion of self-propelling Janus colloids, while run-and-tumble dynamics has been introduced to describe the motion of *E. coli* bacteria [28]. It has been shown that, despite the two models follow quite different microscopic dynamics, their diffusion properties for long times are equivalent [53]; an effective equilibrium regime has been found and can be applied for both models if angular diffusion and tumbles act on the same time scale [31].

2.2.4 Active Ornstein-Uhlenbeck Particles

Another interesting modelization of self-propelling particles is the **Active Ornstein–Uhlenbeck Particles** model (AOUPs), introduced in the last years [54–57]. Its

simplest version consists of particles following the overdamped motion equation

$$\dot{\mathbf{r}} = -\mu \nabla U(\mathbf{r}) + \mathbf{v}(t) , \qquad (2.91)$$

where μ is the mobility, $U(\mathbf{r})$ an external or interaction potential, and $\mathbf{v}(t)$ a noise term persistent in time, namely

$$\langle \mathbf{v}(t) \rangle = 0 \,, \tag{2.92a}$$

$$\langle v_{\alpha}(t)v_{\beta}(t')\rangle = \delta_{\alpha\beta}\Gamma(t-t')$$
. (2.92b)

The memory term is often taken as $\Gamma(t) = \frac{D}{\tau} e^{-|t|/\tau}$. In this case, the noise $\mathbf{v}(t)$ is an Ornstein–Uhlenbeck process [51], and the equation of motion (2.91) can be written as

$$\dot{\mathbf{r}}(t) = -\mu \nabla U(\mathbf{r}) + \mathbf{v}(t) , \qquad (2.93a)$$

$$\tau \dot{\mathbf{v}}(t) = -\mathbf{v}(t) + \sqrt{2D}\boldsymbol{\xi}(t) \,, \tag{2.93b}$$

where $\xi(t)$ is GWN of unit variance. The AOUPs model is often called *Gaussian Colored Noise* model (GCN). The persistence of motion produces a self-propulsion mechanism; in the limit $\tau \to 0$, memory effects vanish and Eq. (2.93) reduce to overdamped Brownian motion equations. The persistence is driving the system out of equilibrium, and its characteristic time τ can be considered as a *distance* from the latter [38]. An effective equilibrium description can be developed also for AOUPs [54, 57]. The model has been used to describe the behavior of active colloids [54] and the motility-induced phase separation [55]; moreover, it turned to be a useful approach to describe the accumulation of active particles around obstacles, and a good approximation for the pressure generated by active matter [56].

Looking at Eq. (2.91), it is fundamental to clarify that in this case $\dot{\mathbf{r}} \neq \mathbf{v}$: the variable \mathbf{v} is *not* the actual velocity of the units, feeling the action of potential $U(\mathbf{r})$ because of the overdamping, but rather an *active velocity* representing an internal stochastic mechanism driving the particles to a certain speed and energy. Actually, the active velocity becomes the physical velocity of the unit when no external potential or interactions are present, i.e. the unit is free to move with velocity $\dot{\mathbf{r}} = \mathbf{v}$, so one may interpret the velocity \mathbf{v} as an "intentional" velocity.

Although the discussed models have been developed to describe systems showing different behaviors at a microscopic scale, it is tempting to find a unified description of their behavior at a mesoscopic or macroscopic scale (see Fig. 2.9); while angular diffusion and run-and-tumble dynamics have shown an equivalent behavior at a macroscopic scale, it is still under debate if AOUPs model shares the same macroscopic properties [28].

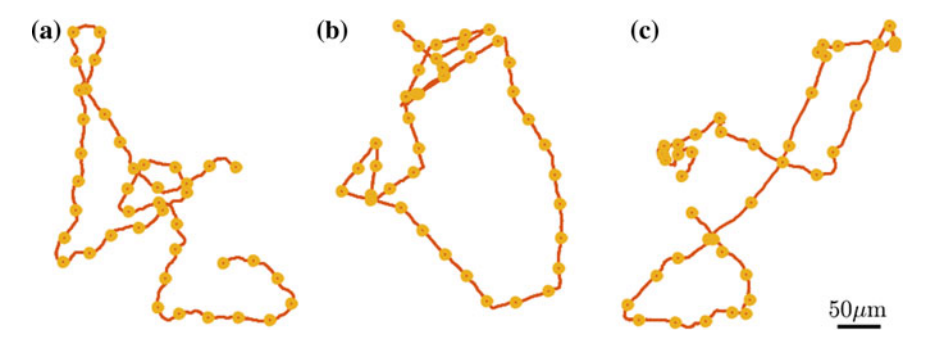


Fig. 2.9 Sample trajectories illustrating three kinds of active motion of a single particle: **a** angular diffusion dynamics, **b** run-and-tumble dynamics, **c** active Ornstein–Uhlenbeck particle. The position of the particle (dots) is sampled every 5 s [28]

2.3 Grains and Active Particles

In Sect. 1.4.3 it has been shown how granular matter has been used to produce systems of active particles, when energy dissipation is balanced through some driving mechanism. Some questions arise: can active particles and driven granulars be considered two manifestations of the same physical phenomena? Is it possible to build a unified theory describing both of them?

Experiments on polar or anisotropic vibrated granular particles have shown the collective behavior illustrated in Sect. 1.4.3. A key model to understand how granular collisions can lead to collective motion even for apolar and isotropic particleshas been introduced by Grossman, Aranson and Ben Jacob [58]. The authors examined a model of self-propelled smooth disks of unit mass moving on a 2d frictionless surface. Interactions between particles are inelastic and passive: they actually are a variation of granular collision rule (2.11), allowing an overlap between particles. The degree of inelasticity is measured by the restitution coefficient α . At each time step, the units also undergo a self-propulsion force compensating the energy lost during collisions; the self-propelling force is constant in the direction of motion if v < 1, and vanishes for v > 1.

The model has been numerically studied under many conditions, varying the number of particles, the number density and the restitution coefficient. Also, both reflecting and periodic boundary conditions have been implemented, and the model has been simulated with different confined geometries (circular, squared and elliptic). The main observation is the formation of vortices and collective migration - swarming - depending on boundary conditions and physical parameters of the system. In Fig. 2.10 the evolution of the swarming order parameter and snapshots of the system displaying swarming formation are shown. Furthermore, when a stochastic angular noise is added in the motion equations - analogously to Vicsek angular noise - the competition between noise and density yields an apparent first-order transition from disorder to swarming, as it had been observed by Vicsek et al. [46].

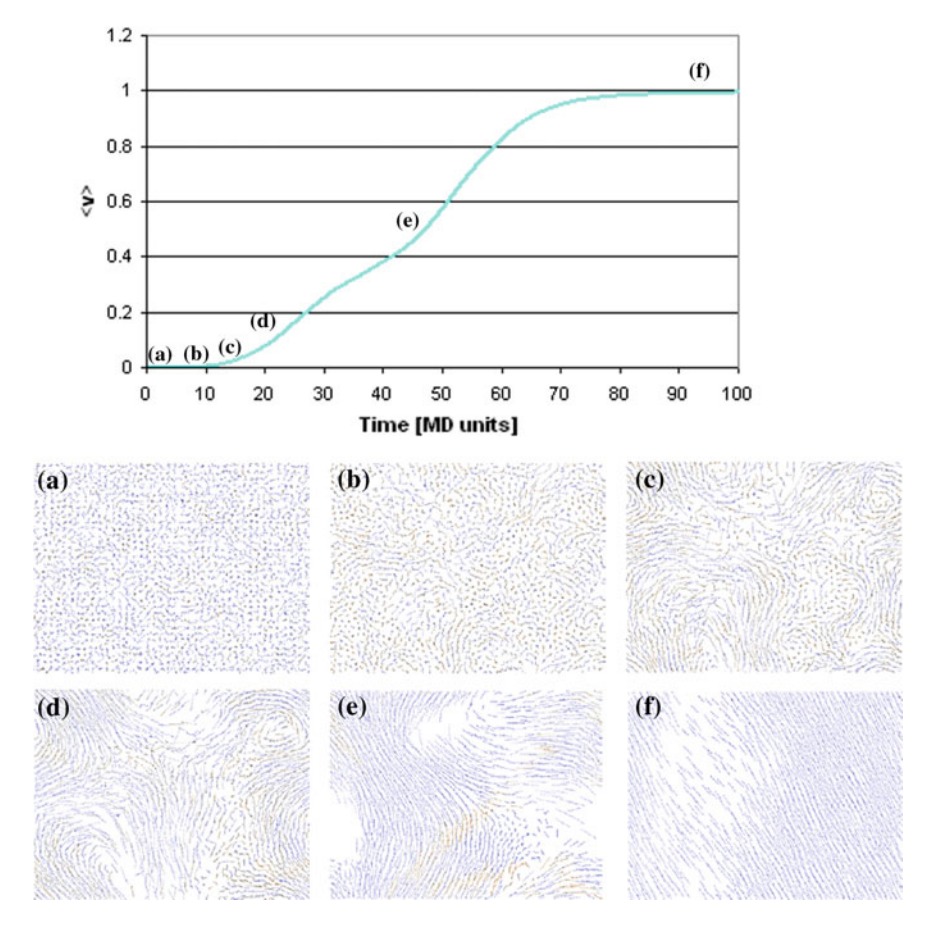


Fig. 2.10 Evolution of Grossman et al. model with periodic boundary conditions, N=1600 particles, number density n=0.6 and restitution coefficient $\alpha=0.93$. Top panel: time evolution of swarming order parameter $\langle v \rangle = \frac{1}{N} \left| \sum_j \mathbf{v}_j \right|$. Bottom panel: snapshots of the system showing swarming formation. The letter of each snapshot corresponds to the time indicated in top panel [58]

So, even a system of isotropic and apolar particles without steering or sensing capabilities has shown the presence of collective, ordered motion. The authors claim that

[...] the results can be interpreted as if the inelastic interaction coupled with the self-propagation serves the equivalent role of the traditional velocity alignment force in the biologically inspired agent models. [...]

The underlying reason why coherent motion is attained in our model is that simple inelastic collisions between isotropic particles create an increase in velocity correlation each time two particles collide [58].

Therefore the *inelasticity*, increasing the correlations between the particles, is playing the role of an effective aligning force, because after an inelastic collisions the velocities tend to increase their alignment (see Fig. 2.2). Active matter studies often distinguish between interactions with *explicit* or *implicit alignment rule* [24], where repulsion - like in the above-examined model - is considered a non-aligning force. This is true when considering elastic repulsion, but in the granular case the inelastic collisions have the same effect of aligning interactions: once the self-propelling force is increased enough to consider the speed v as a constant, the model of Grossman et al. is in every aspect a granular version of the Vicsek model. In the last years, experiments on vibrated granular layers confirmed and studied the presence of collective motion for polar disks [59, 60] and a binary mixture of polar rods and spherical beads [61].

Granular and active matter have been frequently associated and studied together. Indeed, the continuous energy injection and dissipation mechanisms underlying their dynamics are quite similar, especially when considering bulk driven granular matter - see Sect. 2.1.5. Granular and active matter share similar practical applications, one of the most interesting being *Brownian motors* or *ratchets* [5, 28], namely the possibility of building devices where the random motion of granular or active particles is converted into directed, drifting motion of a bigger unit called the motor, thanks to the asymmetry under time reversal characteristic of out of equilibrium systems. However, while on one hand the kinetic theory of granular matter has been developed in a systematic way in the last decades, on the other hand a systematic and general kinetic theory of active matter is missing. A framework where comparisons between granular and active matter can be done is the *hydrodynamic description*, which will be analyzed in the next chapter.

References

- C. Cercignani, R. Illner, M. Pulvirenti, in The Mathematical Theory of Dilute Gases (Springer Science & Business Media, Berlin, 2013)
- 2. K. Huang, in Statistical Mechanics, 2nd edn. (Wiley, New York, 1987)
- 3. T. Pöschel, N.V. Brilliantov, in Granular Gas Dynamics (Springer, Berlin, 2003)
- 4. N. Brilliantov, T. Pöschel (eds.), in Kinetic Theory of Granular Gases (Oxford University Press, Oxford, 2004)
- 5. A. Puglisi, in Transport and Fluctuations in Granular Fluids (Springer, Berlin, 2014)
- M. Ernst, J. Dorfman, W. Hoegy, J.V. Leeuwen, Hard-sphere dynamics and binary-collision operators. Physica 45(1), 127–146 (1969). http://www.sciencedirect.com/science/article/pii/ 0031891469900676, https://doi.org/10.1016/0031-8914(69)90067-6
- 7. J.-M. Hertzsch, F. Spahn, N.V. Brilliantov, On low-velocity collisions of viscoelastic particles. J. Phys. II Fr. 5(11), 1725–1738 (1995). https://doi.org/10.1051/jp2:1995210
- 8. N.V. Brilliantov, F. Spahn, J.-M. Hertzsch, T. Pöschel, Model for collisions in granular gases. Phys. Rev. E **53**, 5382–5392 (1996). https://doi.org/10.1103/PhysRevE.53.5382
- A. Goldshtein, M. Shapiro, Mechanics of collisional motion of granular materials. part 1. general hydrodynamic equations. J. Fluid Mech. 282, 75–114 (1995). https://doi.org/10.1017/ S0022112095000048

- S. McNamara, W.R. Young, Inelastic collapse and clumping in a one-dimensional granular medium. Phys. Fluids A Fluid Dyn. 4(3), 496–504 (1992). https://doi.org/10.1063/1.858323
- 11. S. McNamara, W.R. Young, Dynamics of a freely evolving, two-dimensional granular medium. Phys. Rev. E 53, 5089–5100 (1996). https://doi.org/10.1103/PhysRevE.53.5089
- 12. T. van Noije, M. Ernst, Velocity distributions in homogeneous granular fluids: the free and the heated case. Granul. Matter 1(2), 57–64 (1998). https://doi.org/10.1007/s100350050009
- P.K. Haff, Grain flow as a fluid-mechanical phenomenon. J. Fluid Mech. 134, 401–430 (1983). https://doi.org/10.1017/S0022112083003419
- I. Goldhirsch, G. Zanetti, Clustering instability in dissipative gases. Phys. Rev. Lett. 70, 1619– 1622 (1993). https://doi.org/10.1103/PhysRevLett.70.1619
- J.J. Brey, M.J. Ruiz-Montero, F. Moreno, Steady-state representation of the homogeneous cooling state of a granular gas. Phys. Rev. E 69, 051303 (2004). https://doi.org/10.1103/PhysRevE. 69.051303
- A. Puglisi, V. Loreto, U.M.B. Marconi, A. Petri, A. Vulpiani, Clustering and non-Gaussian behavior in granular matter. Phys. Rev. Lett. 81, 3848–3851 (1998). https://doi.org/10.1103/ PhysRevLett.81.3848
- A. Puglisi, V. Loreto, U.M.B. Marconi, A. Vulpiani, Kinetic approach to granular gases. Phys. Rev. E 59, 5582–5595 (1999). https://doi.org/10.1103/PhysRevE.59.5582
- M. Ernst, Nonlinear model-Boltzmann equations and exact solutions. Phys. Rep. 78, 1–171 (1981). https://doi.org/10.1016/0370-1573(81)90002-8
- 19. D. Blackwell, R.D. Mauldin, Ulam's redistribution of energy problem: collision transformations. Lett. Math. Phys. 10(2), 149–153 (1985). https://doi.org/10.1007/BF00398151
- E. Ben-Naim, P.L. Krapivsky, Maxwell model of traffic flows. Phys. Rev. E 59, 88–97 (1999). https://doi.org/10.1103/PhysRevE.59.88
- E. Ben-Naim, P.L. Krapivsky, Multiscaling in inelastic collisions. Phys. Rev. E 61, R5–R8 (2000). https://doi.org/10.1103/PhysRevE.61.R5
- A. Baldassarri, U.M.B. Marconi, A. Puglisi, Influence of correlations on the velocity statistics of scalar granular gases. EPL (Europhys. Lett.) 58(1), 14 (2002). https://doi.org/10.1209/epl/ i2002-00600-6
- G. Costantini, U.M.B. Marconi, A. Puglisi, Velocity fluctuations in a one-dimensional inelastic Maxwell model. J. Stat. Mech. Theory Exp. 2007(08), P08031 (2007). http://stacks.iop.org/ 1742-5468/2007/i=08/a=P08031, https://doi.org/10.1088/1742-5468/2007/08/P08031
- T. Vicsek, A. Zafeiris, Collective motion. Phys. Rep. 517(3–4), 71–140 (2012). http://www.sciencedirect.com/science/article/pii/S0370157312000968, https://doi.org/10.1016/j.physrep.2012.03.004
- J. Elgeti, R.G. Winkler, G. Gompper, Physics of microswimmers–single particle motion and collective behavior: a review. Rep. Prog. Phys. 78(5), 056601 (2015). https://doi.org/10.1088/ 0034-4885/78/5/056601
- A. Baskaran, M.C. Marchetti, Statistical mechanics and hydrodynamics of bacterial suspensions. Proc. Natl. Acad. Sci. 106(37), 15567–15572 (2009). https://doi.org/10.1073/pnas. 0906586106
- M.C. Marchetti, J.F. Joanny, S. Ramaswamy, T.B. Liverpool, J. Prost, M. Rao, R.A. Simha, Hydrodynamics of soft active matter. Rev. Mod. Phys. 85, 1143–1189 (2013). https://doi.org/ 10.1103/RevModPhys.85.1143
- C. Bechinger, R. Di Leonardo, H. Löwen, C. Reichhardt, G. Volpe, G. Volpe, Active particles in complex and crowded environments. Rev. Mod. Phys. 88, 045006 (2016). https://doi.org/ 10.1103/RevModPhys.88.045006
- J. Tailleur, M.E. Cates, Statistical mechanics of interacting run-and-tumble bacteria. Phys. Rev. Lett. 100, 218103 (2008). https://doi.org/10.1103/PhysRevLett.100.218103
- W. Bialek, A. Cavagna, I. Giardina, T. Mora, E. Silvestri, M. Viale, A.M. Walczak, Statistical mechanics for natural flocks of birds. Proc. Natl. Acad. Sci. 4791(13), 109–4786 (2012). http://www.pnas.org/content/109/13/4786.abstract, arXiv:http://www.pnas.org/content/109/13/4786.full.pdf, https://doi.org/10.1073/pnas. 1118633109

References 65

31. A.P. Solon, M.E. Cates, J. Tailleur, Active Brownian particles and run-and-tumble particles: a comparative study. Eur. Phys. J. Spec. Top. **224**(7), 1231–1262 (2015). https://doi.org/10.1140/epjst/e2015-02457-0

- 32. M. Paoluzzi, C. Maggi, U.M.B. Marconi, N. Gnan, Critical phenomena in active matter. Phys. Rev. E 94, 052602 (2016). https://doi.org/10.1103/PhysRevE.94.052602
- 33. A. Czirók, T. Vicsek, Collective behavior of interacting self-propelled particles. Phys. A Stat. Mech. Appl. **281**(1–4), 17–29 (2000). https://doi.org/10.1016/S0378-4371(00)00013-3
- 34. H. Chaté, F. Ginelli, G. Grégoire, F. Peruani, F. Raynaud, Modeling collective motion: variations on the Vicsek model. Eur. Phys. J. B **64**, 451–456 (2008). https://doi.org/10.1140/epjb/e2008-00275-9
- 35. F. Ginelli, H. Chaté, Relevance of metric-free interactions in flocking phenomena. **105**, 168103 (2010). https://doi.org/10.1103/PhysRevLett.105.168103
- 36. A.P. Solon, J. Tailleur, Revisiting the flocking transition using active spins. Phys. Rev. Lett. 111, 078101 (2013). https://doi.org/10.1103/PhysRevLett.111.078101
- T. Mora, A.M. Walczak, L. Del Castello, F. Ginelli, S. Melillo, L. Parisi, M. Viale, A. Cavagna, I. Giardina, Local equilibrium in bird flocks. Nat. Phys. 12(12), 1153–1157 (2016). https://doi. org/10.1038/nphys3846
- 38. E. Fodor, C. Nardini, M.E. Cates, J. Tailleur, P. Visco, F. van Wijland, How far from equilibrium is active matter? Phys. Rev. Lett. 117, 038103 (2016). https://doi.org/10.1103/PhysRevLett. 117.038103
- 39. U.M.B. Marconi, A. Puglisi, C. Maggi, Heat, temperature and clausius inequality in a model for active Brownian particles. Sci. Rep. 7 (2017). https://doi.org/10.1038/srep46496
- 40. Y. Kuramoto, Self-entrainment of a population of coupled non-linear oscillators (Springer, Berlin, 1975), pp. 420–422. https://doi.org/10.1007/BFb0013365
- 41. Y. Kuramoto, in Chemical Oscillations, Waves, and Turbulence (Springer, Berlin, 1984)
- J.A. Acebrón, L.L. Bonilla, C.J. Pérez Vicente, F. Ritort, R. Spigler, The Kuramoto model: a simple paradigm for synchronization phenomena. Rev. Mod. Phys. 77, 137–185 (2005). https://doi.org/10.1103/RevModPhys.77.137
- 43. E. Bertin, in Statistical Physics of Complex Systems (Springer, Berlin, 2016)
- 44. E. Bertin, Theoretical approaches to the steady-state statistical physics of interacting dissipative units. J. Phys. A Math. Theory **50**(8), 083001 (2017). http://stacks.iop.org/1751-8121/50/i=8/a=083001, https://doi.org/10.1088/1751-8121/aa546b
- 45. S.H. Strogatz, From Kuramoto to Crawford: exploring the onset of synchronization in populations of coupled oscillators. Phys. D Nonlinear Phenom. 143(1), 1–20 (2000). http://www.sciencedirect.com/science/article/pii/S0167278900000944, https://doi.org/10.1016/S0167-2789(00)00094-4
- T. Vicsek, A. Czirók, E. Ben-Jacob, I. Cohen, O. Shochet, Novel type of phase transition in a system of self-driven particles. Phys. Rev. Lett. 75, 1226–1229 (1995). https://doi.org/10. 1103/PhysRevLett.75.1226
- 47. A. Czirók, H.E. Stanley, T. Vicsek, Spontaneously ordered motion of self-propelled particles. J. Phys. A Math. Gen. 30(5), 1375 (1997). https://doi.org/10.1088/0305-4470/30/5/009
- A. Czirók, E. Ben-Jacob, I. Cohen, T. Vicsek, Formation of complex bacterial colonies via self-generated vortices. Phys. Rev. E 54, 1791–1801 (1996). https://doi.org/10.1103/PhysRevE.54. 1791
- 49. A. Chepizhko, V. Kulinskii, On the relation between Vicsek and Kuramoto models of spontaneous synchronization. Phys. A Stat. Mech. Appl. **389**(23), 5347–5352 (2010). https://doi.org/10.1016/j.physa.2010.08.016
- P. Romanczuk, M. Bär, W. Ebeling, B. Lindner, L. Schimansky-Geier, Active Brownian particles. Eur. Phys. J. Spec. Top. 202(1), 1–162 (2012). https://doi.org/10.1140/epjst/e2012-01529-y
- 51. C. Gardiner, Stochastic Methods. A Handbook for the Natural and Social Sciences., 4th edn. (Springer, Berlin, 2009)
- 52. Phys. Rev. E Theory of continuum random walks and application to chemotaxis. 48, 2553–2568 (1993). https://doi.org/10.1103/PhysRevE.48.2553

- 53. M.E. Cates, J. Tailleur, When are active Brownian particles and run-and-tumble particles equivalent? consequences for motility-induced phase separation. EPL (Europhys. Lett.) **101**(2), 20010 (2013). https://doi.org/10.1209/0295-5075/101/20010
- N. Koumakis, C. Maggi, R. Di Leonardo, Directed transport of active particles over asymmetric energy barriers. Soft Matter 10, 5695–5701 (2014). https://doi.org/10.1039/C4SM00665H
- 55. T.F.F. Farage, P. Krinninger, J.M. Brader, Effective interactions in active Brownian suspensions. Phys. Rev. E **91**, 042310 (2015). https://doi.org/10.1103/PhysRevE.91.042310
- C. Maggi, U.M.B. Marconi, N. Gnan, R. Di Leonardo, Multidimensional stationary probability distribution for interacting active particles. Sci. Rep. 5, 10742 (2015). https://doi.org/10.1038/ srep10742
- U.M.B. Marconi, C. Maggi, Towards a statistical mechanical theory of active fluids. Soft Matter 11, 8768–8781 (2015). https://doi.org/10.1039/C5SM01718A
- 58. D. Grossman, I.S. Aranson, E.B. Jacob, Emergence of agent swarm migration and vortex formation through inelastic collisions. New J. Phys. **10**(2), 023036 (2008). http://stacks.iop.org/1367-2630/10/i=2/a=023036, https://doi.org/10.1088/1367-2630/10/2/023036
- C.A. Weber, T. Hanke, J. Deseigne, S. Léonard, O. Dauchot, E. Frey, H. Chaté, Long-range ordering of vibrated polar disks. Phys. Rev. Lett. 110, 208001 (2013). https://doi.org/10.1103/ PhysRevLett.110.208001
- J. Deseigne, O. Dauchot, H. Chaté, Collective motion of vibrated polar disks. Phys. Rev. Lett. 105, 098001 (2010). https://doi.org/10.1103/PhysRevLett.105.098001
- 61. N. Kumar, H. Soni, S. Ramaswamy, A. Sood, Flocking at a distance in active granular matter. Nat. Commun. 5 (2014). https://doi.org/10.1038/ncomms5688

Chapter 3 Hydrodynamic Description and Lattice Models



Quei giorni perduti a rincorrere il vento

(F. de André)

When a fluid is flowing, for instance under the action of gravity or a pressure gradient, its motion can be described introducing the continuous *hydrodynamic fields* such as density $\rho(\mathbf{x},t)$, velocity $\mathbf{u}(\mathbf{x},t)$ and temperature $T(\mathbf{x},t)$, which measure the *local* mechanical and thermodynamical properties of the fluid at the position \mathbf{x} and time t. Hydrodynamic fields generally depend on time and space, and hydrodynamic equations aim at describing their time evolution, affected by spatial gradients and external forces.

The hydrodynamic description of a fluid relies on kinetic theory. Although Euler and Navier–Stokes hydrodynamic equations were derived through continuum mechanics arguments, the kinetic theory allows a derivation based on a clear separation of time and space scales: indeed, hydrodynamics is well-defined if the typical length of variation of the fields is much bigger than the mean free path of the particles between two collisions. In this chapter, the classical derivation of elastic hydrodynamics will be given in the first Sect. 3.1.1; then, the hydrodynamic descriptions of granular matter - Sect. 3.1.2 - and active matter - Sect. 3.1.4 - will be overviewed. Section 3.2 will be devoted to *fluctuating hydrodynamics*, namely a hydrodynamic theory where the role of statistical fluctuations cannot be neglected as in classical hydrodynamics.

The second part of this chapter, Sect. 3.3, will be dedicated to the study of *lattice models*. Actually, the formulation of hydrodynamics presents many technical difficulties and needs many physical assumptions and approximations to derive a consistent set of equations. On the contrary, lattice models developed in the last decades can describe hydrodynamic behavior and at the same time yield exact results also on

fluctuating hydrodynamics. For this reason, they have become a powerful tool in nonequilibrium statistical mechanics, and have been a guide for the development of this thesis.

3.1 Hydrodynamics

3.1.1 Conservative Interactions

Our starting point is the Boltzmann Equation (2.28), which in presence of external forces \mathbf{F} reads

$$\frac{\partial f}{\partial t} + \mathbf{v} \cdot \frac{\partial f}{\partial \mathbf{r}} + \frac{\mathbf{F}}{m} \cdot \frac{\partial f}{\partial \mathbf{v}} = Q(f, f), \qquad (3.1a)$$

$$Q(f, f) = C \int_{\mathbb{R}^3} \int_{S^+} (f' f'_* - f f_*) \left| \mathbf{V} \cdot \hat{\mathbf{n}} \right| d\mathbf{v}_* d\hat{\mathbf{n}}, \qquad (3.1b)$$

where the Enskog correction in (2.36) has been neglected and the probability density $P(\mathbf{r}, \mathbf{v}, t)$ has been rescaled to give $f(\mathbf{r}, \mathbf{v}, t)$ so that

$$n(\mathbf{r},t) = \int_{\mathbb{R}^3} f(\mathbf{r}, \mathbf{v}, t) d\mathbf{v}, \qquad (3.2a)$$

$$N = \int_{V} \int_{\mathbb{R}^{3}} f(\mathbf{r}, \mathbf{v}, t) d\mathbf{r} d\mathbf{v}, \qquad (3.2b)$$

where N is the number of particles in volume V, and $n(\mathbf{r}, t) = \frac{1}{m}\rho(\mathbf{r}, t)$ is the number density with particles of mass m. The collisional term Q(f, f) is equivalent to the one introduced in Eq. (2.36), where the C factor includes $N\sigma^2$ and other factors coming from the rescaling from P to f.

When considering a fluid flow on a macroscopic volume, the possibility of a continuum description relies on the smoothness of the hydrodynamic fields, i.e. the fields and their gradients must not diverge. This is possible thanks to the fact that the total density, momentum and energy of two particles are conserved during collisions. Indeed, it can be proven [1] that if a generic observable $\chi(\mathbf{r}, \mathbf{v})$ satisfies the relation

$$\chi_1 + \chi_2 = \chi_1' + \chi_2' \,, \tag{3.3}$$

where the primed variables indicate as usual the postcollisional observable, then one has

$$\int_{\mathbb{R}^3} d\mathbf{v} \chi(\mathbf{r}, \mathbf{v}) Q(f, f) = 0.$$
 (3.4)

Thus, multiplying equation (3.1a) by $\chi(\mathbf{r}, \mathbf{v})$ and integrating by dv one gets

$$\int_{\mathbb{R}^3} d\mathbf{v} \chi(\mathbf{r}, \mathbf{v}) \left[\frac{\partial f}{\partial t} + \mathbf{v} \cdot \frac{\partial f}{\partial \mathbf{r}} + \frac{\mathbf{F}}{m} \cdot \frac{\partial f}{\partial \mathbf{v}} \right] = 0.$$
 (3.5)

Integrating by parts and assuming that $f(\mathbf{r}, \mathbf{v}, t) \underset{v \to \infty}{\longrightarrow} 0$ and that external forces do not depend on velocity, one gets the conservation theorem

$$\frac{\partial}{\partial t} \langle n\chi \rangle + \frac{\partial}{\partial \mathbf{r}} \cdot \langle n\mathbf{v}\chi \rangle - n \left\langle \mathbf{v} \cdot \frac{\partial \chi}{\partial \mathbf{r}} \right\rangle - n \left\langle \mathbf{f} \cdot \frac{\partial \chi}{\partial \mathbf{v}} \right\rangle = 0 \tag{3.6}$$

where the average is performed over the velocities and is local in space and time, namely $\langle A \rangle(\mathbf{r},t) = \int d\mathbf{v} A(\mathbf{r},\mathbf{v}) f(\mathbf{r},\mathbf{v},t)$ and $\mathbf{f} = \mathbf{F}/m$ is the external force per mass unit.

Elastic collisions conserve density, momentum and energy, so one can take respectively $\chi = m$, $m\mathbf{v}$, $\frac{1}{2}mv^2$ or, equivalently, a combination of them. Introducing the average velocity

$$\mathbf{u}(\mathbf{r},t) = \langle \mathbf{v} \rangle \tag{3.7}$$

and the temperature as (being always in d = 3)

$$k_B T(\mathbf{r}, t) = \frac{1}{3} m \langle |\mathbf{v} - \mathbf{u}|^2 \rangle$$
 (3.8)

the conservation theorem (3.6) leads to

$$\frac{\partial \rho}{\partial t} + \nabla \cdot (\rho \mathbf{u}) = 0$$
 (mass conservation) (3.9a)

$$\rho \left(\frac{\partial}{\partial t} + \mathbf{u} \cdot \nabla \right) \mathbf{u} = \rho \mathbf{f} - \nabla \cdot \mathsf{P}$$
 (momentum conservation) (3.9b)

$$\rho \left(\frac{\partial}{\partial t} + \mathbf{u} \cdot \nabla \right) T = -\frac{2m}{3} \left(\nabla \cdot \mathbf{q} + \mathsf{P} : \nabla \mathbf{u} \right)$$
 (energy conservation) (3.9c)

where the following quantities have been defined

$$\mathbf{q}(\mathbf{r},t) = \frac{1}{2} \rho \langle (\mathbf{v} - \mathbf{u}) | \mathbf{v} - \mathbf{u} |^2 \rangle$$
 (heat flux) (3.10)

$$P_{ij} \equiv \rho \langle (v_i - u_i)(v_j - u_j) \rangle$$
 (pressure tensor) (3.11)

and it has been taken $k_B = 1$. The term $\nabla \mathbf{u}$ is the velocity gradient tensor of components $\partial u_i/\partial x_j$, and the : operator in Eq. (3.9c) is the scalar product between tensors, namely $\mathsf{P}: \nabla u \equiv \sum_{i,j} P_{ij} \partial u_i/\partial x_j$.

The Hydrodynamic equations (3.9) have only a formal value because the heat flux and pressure tensor are determined by the distribution function $f(\mathbf{r}, \mathbf{v}, t)$ solving the Boltzmann equation. Since f is generally unknown, we need to make some assumptions about its behavior.

As it has been stated above, we expect the hydrodynamic fields to be almost constant over microscopic length scales, which correspond to the *mean free path* λ . Therefore, if L is a characteristic length of the macroscopic system, one expects that there is a scale separation whether

$$Kn = \frac{\lambda}{L} \ll 1, \tag{3.12}$$

having defined the *Knudsen number* Kn, an adimensional parameter indicating the validity of a hydrodynamic approach. In this limit, the hydrodynamic equations (3.9) can be closed assuming that the heat flux and pressure tensor can be expressed in terms of the uniform fields and their gradients, so [2]

$$\mathbf{q} = -\kappa \nabla T,\tag{3.13a}$$

$$P_{ij} = p\delta_{ij} - \eta \left(\frac{\partial u_i}{\partial x_j} + \frac{\partial u_j}{\partial x_i} - \frac{2}{3} \delta_{ij} \nabla \cdot \mathbf{u} \right). \tag{3.13b}$$

The last expressions define the *hydrostatic pressure p* and the transport coefficients η and κ , respectively the *shear viscosity* and the *thermal conductivity*. Their values are unknown until we find a way to derive them from the Boltzmann Equation. The pressure tensor P is the sum of a diagonal, isotropic part $p\delta_{ij}$ and a symmetric and traceless part, to the first order in the velocity gradients.

The pressure tensor and heat flux obtained can be placed back in Eq. (3.9); however, since we are introducing linearized terms with respect to the gradients into exact equations, the perturbative approach must be carried out carefully. This is done by the *Chapman–Enskog* procedure [3, 4]: the separation of spatial scales when $\epsilon \ll 1^1$ physically means that a particle in a volume of macroscopic size $\sim L^d$ will undergo an enormous number of collisions with other particles on the region, thermalizing to some *local* velocity distribution: the fundamental assumption of the Chapman–Enskog procedure is that the macroscopic gradients scale with the Knudsen parameter, i.e. $\nabla \sim \epsilon$, $\nabla^2 \sim \epsilon^2$, Therefore, the distribution function can be expanded as

$$f = f^{(0)} + \epsilon f^{(1)} + \epsilon^2 f^{(2)} + \cdots,$$
 (3.14)

where $f^{(0)}$ denotes the homogeneous unperturbed solution (no gradients), $f^{(1)}$ the linear approximation with respect to the field gradients, and so on. Obviously, the zeroth order solution $f^{(0)}$ is the Maxwell–Boltzmann distribution, as it will be proved below.

¹From now on we call ϵ the Knudsen number to be consistent with literature.

Furthermore, the collisional invariants introduce a separation of *fast* variables from *slow* variables: while the particles' velocities abruptly change during a collision, conserved variables should change only over long scales of space and time. Therefore, one assumes that the Boltzmann Equation admits a *normal solution*

$$f(\mathbf{r}, \mathbf{v}, t) = f[\mathbf{v}|n(\mathbf{r}, t), \mathbf{u}(\mathbf{r}, t), T(\mathbf{r}, t))]$$
(3.15)

where the dependence in time and space comes from the hydrodynamic (slow) fields, and the only fast variable is the velocity \mathbf{v} . The normal assumption (3.15) yields the time derivative

 $\frac{\partial f}{\partial t} = \frac{\partial f}{\partial n} \frac{\partial n}{\partial t} + \frac{\partial f}{\partial \mathbf{u}} \cdot \frac{\partial \mathbf{u}}{\partial t} + \frac{\partial f}{\partial T} \frac{\partial T}{\partial t}.$ (3.16)

The last equation can be approached because the time derivatives of $n = \rho/m$, **u** and T can be evaluated through Eq. (3.9). Substituting the expression of pressure and heat flux from (3.13) and marking the gradients with the corresponding power of ϵ , one gets

$$\frac{\partial \rho}{\partial t} = -\epsilon \nabla \cdot (\rho \mathbf{u}) \tag{3.17a}$$

$$\frac{\partial \mathbf{u}}{\partial t} = -\epsilon \left(\mathbf{u} \cdot \nabla \mathbf{u} - \mathbf{f} + \frac{1}{\rho} \nabla p \right) + \epsilon^2 \frac{\eta}{\rho} \left(\nabla^2 \mathbf{u} + \frac{1}{3} \nabla \left(\nabla \cdot \mathbf{u} \right) \right)$$
(3.17b)

$$\frac{\partial T}{\partial t} = -\epsilon \left(\mathbf{u} \cdot \nabla T + \frac{2}{3n} p(\nabla \cdot \mathbf{u}) \right) + \epsilon^2 G \tag{3.17c}$$

where the external force has been assumed to be of first order in ϵ , consistently with a conservative force, $\mathbf{F} = -\nabla \phi$. The second order term G reads

$$G = \frac{2\eta}{3n} \left[\frac{\partial u_i}{\partial x_j} \frac{\partial u_j}{\partial x_i} + \frac{\partial u_i}{\partial x_j} \frac{\partial u_i}{\partial x_j} - \frac{2}{3} \left(\nabla \cdot \mathbf{u} \right)^2 \right] + \frac{2\kappa}{3n} \nabla^2 T$$
 (3.18)

where the usual sum over repeated indices is implied.

When writing Eq. (3.17), only the first two orders in ϵ have been retained: this is the so-called *Navier–Stokes* order of the hydrodynamic description. Adding the ϵ^3 terms, one gets a next order description named *Burnett* order. Substituting Eq. (3.17) into (3.16), the time derivative of the distribution function is given as a series of terms at several powers of ϵ . This behavior suggests the need for a *multiple-scale analysis*, a procedure well described in [5]: assuming a scale separation also when considering characteristic times of the system, the time derivative can be expanded as

$$\frac{\partial}{\partial t} = \frac{\partial^{(0)}}{\partial t} + \epsilon \frac{\partial^{(1)}}{\partial t} + \epsilon^2 \frac{\partial^{(2)}}{\partial t} + \cdots$$
 (3.19)

A rigorous derivation of the procedure can be found in [4]. The physical meaning of multiple-scale analysis in this context is the requirement that the higher the order of the space gradient, the slower the time variation it causes [2].

Thus, the Boltzmann Equation (3.1) can be perturbatively solved at each order, writing a *local* Boltzmann equation (where the time and space dependence occurs only through the slow fields, Eq. (3.15) supplemented by the hydrodynamic equations (3.9). At first order, they read

$$\frac{\partial^{(0)}}{\partial t}f^{(0)} = Q(f^{(0)}, f^{(0)}), \qquad (3.20a)$$

$$\frac{\partial^{(0)}n}{\partial t} = 0, (3.20b)$$

$$\frac{\partial^{(0)}\mathbf{u}}{\partial t} = 0, \tag{3.20c}$$

$$\frac{\partial^{(0)}T}{\partial t} = 0. ag{3.20d}$$

Since all the fields are constant at this order, from Eq. (3.16) one has $Q(f^{(0)}, f^{(0)}) = 0$; therefore, the homogeneous solution $f^{(0)}$ is the Maxwell–Boltzmann distribution

$$f^{(0)} = n^{(0)} [m/(2\pi m T^{(0)})]^{3/2} \exp\left[-\frac{m}{2T^{(0)}} |\mathbf{v} - \mathbf{u}^{(0)}|^2\right], \tag{3.21}$$

where $n^{(0)}$, $\mathbf{u}^{(0)}$ and $T^{(0)}$ are in principle arbitrary functions of space and time, satisfying the self-consistency equations

$$n^{(0)} = \int d\mathbf{v} f^{(0)}, \tag{3.22a}$$

$$\mathbf{u}^{(0)} = \int d\mathbf{v} \mathbf{v} f^{(0)}, \tag{3.22b}$$

$$T^{(0)} = \int d\mathbf{v} \frac{1}{3} |\mathbf{v} - \mathbf{u}|^2 f^{(0)}.$$
 (3.22c)

which can be taken as the *actual* local hydrodynamic fields $n(\mathbf{r}, t)$, $\mathbf{u}(\mathbf{r}, t)$ and $T(\mathbf{r}, t)$ [4].

Going to the next order in the expansion, one finds

$$\frac{\partial^{(0)}}{\partial t}f^{(1)} + \left(\frac{\partial^{(1)}}{\partial t} + \mathbf{u} \cdot \nabla\right)f^{(0)} = Q(f^{(0)}, f^{(1)}) + Q(f^{(1)}, f^{(0)}), \quad (3.23a)$$

$$\frac{\partial^{(1)}\rho}{\partial t} = -\nabla \cdot (\rho \mathbf{u}), \qquad (3.23b)$$

$$\left(\frac{\partial^{(1)}}{\partial t} + \mathbf{u} \cdot \nabla\right) \mathbf{u} = \mathbf{f} - \frac{1}{\rho} \nabla p , \qquad (3.23c)$$

$$\left(\frac{\partial^{(1)}}{\partial t} + \mathbf{u} \cdot \nabla\right) T = -\frac{2}{3} (\nabla \cdot \mathbf{u}) T. \tag{3.23d}$$

The third equation is known as the Euler equation and for this reason this is called the *Euler order* of hydrodynamics. Some remarks have to be done: first, Eq. (3.23b) accounts for mass conservation at the first order. This is called the *continuity equation*, and it holds at *any* order. The Euler equation for the velocity is the equation for a flow induced by external acceleration $\bf f$ and pressure field p in absence of viscosity. The pressure can be derived at this order using the Maxwell–Boltzmann distribution, and for dilute systems reads p = nT [1]. Finally, the fourth equation describes the evolution of the temperature, and substituting $\nabla \cdot \bf u$ from Eq. (3.23b) one gets

$$\left(\frac{\partial^{(1)}}{\partial t} + \mathbf{u} \cdot \nabla\right) \left(\rho T^{-3/2}\right) = 0, \qquad (3.24)$$

which is the equation of state for an adiabatic transformation; indeed, at the Euler order the heat flux vanishes and the local evolution of the fluid is adiabatic. Finally, when $\mathbf{F} = -\nabla \phi$ is a conservative force, the Euler equation gives the *Bernoulli Equation* which holds for an inviscid flow [1]

$$\nabla \left(\frac{1}{2}u^2 + \frac{1}{\rho}p + \frac{1}{m}\phi \right) = 0.$$
 (3.25)

The viscosity and heat flux can be recovered in the hydrodynamic equations moving to the next order of the expansion; the first step is to derive the form of $f^{(1)}$ from Eq. (3.23a) knowing $f^{(0)}$; the former accounts for spatial gradients and through a quite long procedure leads to a closed expression for the transport coefficients in function of the hydrodynamic fields [4]. For elastic hard spheres of mass m and diameter σ , one finds [2]

$$\eta = \frac{5}{16\sigma^2} \sqrt{\frac{mT}{\pi}} \,, \tag{3.26}$$

$$\kappa = \frac{75}{64\sigma^2} \sqrt{\frac{T}{\pi m}} \,. \tag{3.27}$$

A remarkable result of the hydrodynamic derivation of viscosity is that it doesn't depend on the density of the fluid, contrarily to our physical intuition.

The ϵ dependence in Eq. (3.17) can now be reabsorbed into the gradients taking $\epsilon=1$ and recovering the Navier–Stokes order of hydrodynamic equations, which finally read

$$\left(\frac{\partial}{\partial t} + \mathbf{u} \cdot \nabla\right) \rho = 0, \tag{3.28a}$$

$$\left(\frac{\partial}{\partial t} + \mathbf{u} \cdot \nabla\right) \mathbf{u} = \mathbf{f} - \frac{1}{\rho} \nabla p + \nu \left[\nabla^2 \mathbf{u} + \frac{1}{3} \nabla \left(\nabla \cdot \mathbf{u} \right) \right], \qquad (3.28b)$$

$$\left(\frac{\partial}{\partial t} + \mathbf{u} \cdot \nabla\right) \mathbf{u} T = -\frac{2}{3n} p(\nabla \cdot \mathbf{u}) + \frac{2\kappa}{3n} \nabla^2 T + \frac{4\eta}{3n} \left[\mathbf{D} : \mathbf{D} - \frac{1}{3} \left(\nabla \cdot \mathbf{u} \right)^2 \right], \qquad (3.28c)$$

where D is the symmetrized velocity gradient tensor $D_{ij} \equiv (\partial_{x_i} u_j + \partial_{x_j} u_i)/2$ and $\nu \equiv \eta/\rho$ is the kinematic viscosity.

The equations display the fundamental features of hydrodynamic behavior. In the lhs it always appears the *material derivative* $\partial_t + \mathbf{u} \cdot \nabla$, representing the time variation of hydrodynamic fields in a frame comoving with the local fluid stream \mathbf{u} . Therefore, Eq. (3.28a) implies that the density is conserved along the streaming lines because of the incompressibility, i.e. $\nabla \cdot \mathbf{u} = 0$. The velocity equation (3.28b) is the balance equation for velocity, corresponding to Newton's law $\mathbf{F} = m\mathbf{a}$ for a volume element of fluid; the Laplacian of the velocity on the rhs is given by the viscosity and leads to a *velocity diffusion*. In the temperature evolution equation (3.28c), the first term of the rhs is responsible for *temperature diffusion*, and the equation actually gets back to the heat equation when the fluid is at rest, i.e. $\mathbf{u} = 0$. The last term is increasing the temperature when a shear (namely a velocity gradient) is present in a viscous fluid: this phenomenon is called *viscous heating* and it is the consequence of frictional effects dissipating kinetic energy into heat when the fluid is sheared.

3.1.2 Granular Hydrodynamics

The successful results obtained on conservative hydrodynamics inspired the formulation of granular hydrodynamics. Since a kinetic theory has been consistently defined for granular matter, the same approach can be implemented in the case of inelastic collisions. The main difference consists in energy dissipation: mass and momentum are still conserved by collisions while the energy is not, therefore the conservation theorem (3.6) cannot be rigorously applied to the latter. However, one can always derive the continuity equations (3.9) simply by integrating over 1, \mathbf{v} , \mathbf{v}^2 ; while the equations for the mass density and average velocity do not change, the temperature evolution equation now reads [2]

$$\rho \left(\frac{\partial}{\partial t} + \mathbf{u} \cdot \nabla \right) T = -\zeta T - \frac{2m}{3} \left(\nabla \cdot \mathbf{q} + \mathsf{P} : \nabla \mathbf{u} \right) . \tag{3.29}$$

The appearance of the term ζT , known as *sink term*, is given by the energy dissipation which is acting at the *microscopic level* during each collision. The parameter ζ is the *cooling coefficient* already encountered in Sect. 2.1.3, which stems from the rhs of Boltzmann Equation (2.1.3) multiplied by $mv^2/2$ and integrated over \mathbf{v} , i.e.

$$\int d\mathbf{v} \frac{mv^2}{2} Q(f, f) \equiv -\frac{3}{2} nT\zeta, \qquad (3.30)$$

75

yielding [2]

$$\zeta(\mathbf{r},t) = \frac{\pi m \sigma^2}{24nT} (1 - \alpha^2) \int d\mathbf{v} d\mathbf{v}_* V^3 f(\mathbf{r}, \mathbf{v}, t) f(\mathbf{r}, \mathbf{v}_*, t) . \tag{3.31}$$

The zeroth order of the Chapman–Enskog equations now reads

$$\frac{\partial^{(0)}}{\partial t}f^{(0)} = Q(f^{(0)}, f^{(0)}), \qquad (3.32a)$$

$$\frac{\partial^{(0)}n}{\partial t} = 0, \qquad (3.32b)$$

$$\frac{\partial^{(0)}\mathbf{u}}{\partial t} = 0, \qquad (3.32c)$$

$$\frac{\partial^{(0)}T}{\partial t} = -\zeta^{(0)}T, \qquad (3.32d)$$

where the zeroth order cooling coefficient $\zeta^{(0)}$ can be calculated through Eq. (3.31) with the homogeneous distribution function $f^{(0)}$, which for a constant restitution coefficient α reads

$$f^{(0)} = \frac{n}{v_T^3} \tilde{f}^{(0)} \left(\frac{\mathbf{v} - \mathbf{u}}{v_T} \right) , \tag{3.33}$$

as in Eq. (2.37), yielding

$$\zeta^{(0)} = \frac{2\sqrt{2}}{3}n\sigma^2\mu_2\sqrt{\frac{T}{m}}\,,\tag{3.34}$$

where μ_2 has been defined in Eq. (2.41), and the zeroth order of ζ naturally coincides with the HCS result of Eq. (2.43). The Chapman–Enskog procedure can be carried on exactly as before: the only difference from the elastic case of Sect. 3.1.1 is the presence of the sink term and that the heat flux expressed in function of the linear gradients now reads

$$\mathbf{q} = -\kappa \nabla T - \mu \nabla n \,, \tag{3.35}$$

where the coefficient μ relates the heat flux with the density gradient and is non vanishing only for $\alpha < 1$, as well as the cooling coefficient ζ [6]. All the transport coefficients can be analogously computed for granular hydrodynamics: their explicit expressions, which can be found in [2], show that in the elastic limit $\alpha \to 1$ the conservative hydrodynamics values are recovered.

The last feature is the qualitative difference between granular and elastic particles. Actually, energy dissipation occurs from the zeroth order of expansion, therefore one cannot assume a local equilibrium behavior of the system as stated above. However,

if the dissipation is small enough so that the cooling coefficient can be compared with the gradients in Chapman–Enskog procedure, the local equilibrium can be recovered. This is known as the *quasielastic limit* and will be widely used in Chap. 4. Finally, the Navier–Stokes hydrodynamic equations can be written substituting Eqs. (3.29) and (3.35) in Eq. (3.17), obtaining for a compressible fluid ($\nabla \cdot \mathbf{u} \neq 0$)

$$\left(\frac{\partial}{\partial t} + \mathbf{u} \cdot \nabla\right) n = -n\nabla \cdot \mathbf{u} \,,\tag{3.36a}$$

$$\left(\frac{\partial}{\partial t} + \mathbf{u} \cdot \nabla\right) \mathbf{u} = -\frac{1}{nm} \nabla p + \frac{\eta}{nm} \left(\nabla^2 \mathbf{u} + \frac{1}{3} \nabla \left(\nabla \cdot \mathbf{u}\right)\right), \tag{3.36b}$$

$$\left(\frac{\partial}{\partial t} + \mathbf{u} \cdot \nabla\right) T = -\zeta T - \frac{2}{3n} p(\nabla \cdot \mathbf{u}) + \frac{2}{3n} \left[\kappa \nabla^2 T + \mu \nabla^2 n + \eta \left(2\mathsf{D} : \mathsf{D} - \frac{2}{3} \left(\nabla \cdot \mathbf{u} \right)^2 \right) \right]. \tag{3.36c}$$

3.1.3 Hydrodynamic Instabilities and the HCS

As for conservative hydrodynamics, the Eq. (3.36) for n, \mathbf{u} and T are coupled and nonlinear, therefore a solution can be found only under suitable conditions. When a stationary solution is present, one can look at its *linear stability*. Linear stability analysis is widely used in dynamical systems [7]: when a dynamical observable is evolving under the evolution equation x(t) = F(x(t)), the dynamics can be linearized around a fixed point x^* such that $F(x^*) = 0$, so that a perturbation near x^* initially evolves as

$$\frac{\mathrm{d}}{\mathrm{d}t}\delta x(t) = \lambda \delta x \,, \tag{3.37}$$

where $x(t) = x^* + \delta x(t)$ and $\lambda = dF/dx|_{x^*}$. Thus, the perturbation diverges for $\lambda > 0$ (unstable fixed point) and vice versa vanishes for $\lambda < 0$ (stable fixed point). For d > 1 case, Eq. (3.37) is a vectorial relation

$$\frac{\mathrm{d}}{\mathrm{d}t}\delta x_i(t) = \sum_{j=1}^d L_{ij}\delta x_j(t) , \qquad (3.38)$$

so one has to find the eigenvalues of the stability matrix $L_{ij} \equiv \partial F_i/\partial x_j|_{\mathbf{x}^*}$. The fixed point \mathbf{x}^* is now stable if the real part of its eigenvalues is always negative [7].

The same linearization can be carried out for hydrodynamic equations (3.17): hydrodynamic instabilities are an important research field in fluid dynamics, as they have been introduced to describe the departure of hydrodynamics from a stationary state [8, 9]. In Appendix C the reader will find some links to videos describing the most studied. Looking at the granular case, one starts from Eq. (3.36). One of the basic granular states is, again, the HCS, which is known to be linearly unstable [10]. A spatially dependent perturbation of the HCS reads

$$n(\mathbf{r}, t) = n + \delta n(\mathbf{r}, t), \quad \mathbf{u}(\mathbf{r}, t) = \delta \mathbf{u}(\mathbf{r}, t), \quad T(\mathbf{r}, t) = T_{HCS}(t) + \delta T(\mathbf{r}, t),$$
(3.39)

where n = N/V is the constant and homogeneous number density, and $T_{HCS}(t)$ is the homogeneous Haff's law from Eq. (2.49). As discussed in Sect. 2.1.3, the HCS has no stationary state because of the continuous energy dissipation, so one looks at the rescaled hydrodynamic fields

$$\tilde{n} \equiv \frac{\delta n}{n} \ll 1 \; ; \quad \tilde{\mathbf{u}} \equiv \frac{\delta \mathbf{u}}{\sqrt{T_{HCS}(t)}} \; , \; |\tilde{\mathbf{u}}| \ll 1 \; ; \quad \tilde{T} \equiv \frac{\delta T}{T_{HCS}(t)} \ll 1 \; .$$
 (3.40)

The mechanism of cluster formation, qualitatively explained in Sect. 1.3.1, is the cause of the instability of the homogeneous state. Furthermore, inelastic collisions are correlating the particles, reducing the outgoing angle with respect to the incoming angle of collision and yielding an aligning mechanism - see Sect. 2.3. This mechanism accounts for vortex formation, which will be explained below.

The linear stability of hydrodynamic equations can be better analyzed in Fourier space, defining the Fourier transform of a generic observable $\mathbf{a}(\mathbf{r}, t)$ and its inverse as

$$\mathbf{a}_{\mathbf{k}}(t) = \frac{1}{\sqrt{V}} \int d\mathbf{r} \, e^{-i\mathbf{k}\cdot\mathbf{r}} \mathbf{a}(\mathbf{r}, t) ,$$

$$\mathbf{a}(\mathbf{r}, t) = \frac{1}{\sqrt{V}} \sum_{\mathbf{k}} e^{i\mathbf{k}\cdot\mathbf{r}} \mathbf{a}_{\mathbf{k}}(t) ,$$
(3.41)

where $V = L^3$ is the volume of the system, and **k** are the discrete wave vectors $\mathbf{k} = \frac{2\pi}{L}(n_x, n_y, n_z)$, with $n_i \in \mathbb{Z}$. With these transformations and changing the time t into the mean collisional time $\tau(t)$ defined in (2.53), one gets the linearized equations [2]

$$\frac{\partial \tilde{n}_{\mathbf{k}}}{\partial \tau} = -i\mathbf{k} \cdot \tilde{\mathbf{u}}_{\mathbf{k}} \,, \tag{3.42a}$$

$$\frac{\partial \tilde{\mathbf{u}}_{\mathbf{k}}}{\partial \tau} = \frac{1}{4} \zeta^* \tilde{\mathbf{u}}_{\mathbf{k}} - \frac{1}{2} i \mathbf{k} \left(\tilde{n}_{\mathbf{k}} + \tilde{T}_{\mathbf{k}} \right) - \eta^* \left[k^2 \tilde{\mathbf{u}}_{\mathbf{k}} + \frac{1}{3} \mathbf{k} \left(\mathbf{k} \cdot \tilde{\mathbf{u}}_{\mathbf{k}} \right) \right], \quad (3.42b)$$

$$\frac{\partial \tilde{T}_{\mathbf{k}}}{\partial \tau} = -\frac{1}{4} \zeta^* (\tilde{T}_{\mathbf{k}} + 2\tilde{n}_{\mathbf{k}}) - \frac{5}{2} k^2 (\kappa^* \tilde{T}_{\mathbf{k}} + \mu^* \tilde{n}_{\mathbf{k}}) - \frac{2}{3} (i \mathbf{k} \cdot \tilde{\mathbf{u}}_{\mathbf{k}}) , \qquad (3.42c)$$

where the coefficients ζ^* , η^* , κ^* and μ^* are the transport coefficients computed in the HCS. Equation (3.42) can be written in a compact form as

$$\frac{\partial \Psi}{\partial \tau} = \mathsf{L}\Psi \,, \tag{3.43}$$

where L is the stability matrix defined in Eq. (3.38) and $\Psi = (\tilde{n}_k, \tilde{\mathbf{u}}_k, \tilde{T}_k)$ is a five-dimensional vector containing all the hydrodynamic fields. The eigenvectors Ψ_l of the stability matrix are called *hydrodynamic modes*, where $l = 1, \ldots, 5$: if their

corresponding eigenvalues $\lambda_l(\mathbf{k})$ satisfy Re $[\lambda_l(\mathbf{k})] < 0$, the hydrodynamic mode is stable, otherwise it is not. This analysis can be applied to any hydrodynamic state.

Looking at the HCS linearized equations (3.42), it is convenient to separate the rescaled velocity into a longitudinal component $\tilde{\mathbf{u}}_{\mathbf{k}}^{\parallel} = \tilde{\mathbf{u}}_{\mathbf{k}} \cdot \mathbf{k}/k$ and a transverse component $\tilde{\mathbf{u}}_{\mathbf{k}}^{\perp} = \tilde{\mathbf{u}}_{\mathbf{k}} - \tilde{\mathbf{u}}_{\mathbf{k}}^{\parallel}$. Since

$$i\mathbf{k} \cdot \tilde{\mathbf{u}}_{\mathbf{k}}^{\perp} = 0, \quad i\mathbf{k} \cdot \tilde{\mathbf{u}}_{\mathbf{k}}^{\parallel} = ik\tilde{u}_{\mathbf{k}}^{\parallel},$$
 (3.44)

Equation (3.42b) gives a decoupled equation for the transverse component

$$\frac{\partial \tilde{\mathbf{u}}_{\mathbf{k}}^{\perp}}{\partial \tau} = \left(\frac{1}{4} \zeta^* - \eta^* k^2\right) \tilde{\mathbf{u}}_{\mathbf{k}}^{\perp} , \qquad (3.45)$$

so the transverse velocity is a hydrodynamic mode with the eigenvalue

$$\lambda_{\perp}(\mathbf{k}) = \frac{1}{4}\zeta^* - \eta^* k^2 \,.$$
 (3.46)

The last equation gives the *shear instability* criterion in the HCS, revealing the existence of a threshold wavelength

$$k_{\perp}^{*}(\alpha) = \frac{1}{2} \sqrt{\frac{\zeta^{*}(\alpha)}{\eta^{*}(\alpha)}} \propto \sqrt{1 - \alpha^{2}}.$$
 (3.47)

Thus, for short-wave perturbations (large k) shear modes are stable and decay rapidly, while long-wave modes (low k) grow exponentially. The critical equation (3.47) leads to a critical value of the size $L^*(\alpha)$: indeed, since $k \ge 2\pi/L$, the instability arises only when the size of the system exceeds a critical value

$$L^*(\alpha) = \frac{2\pi}{k_\perp^*(\alpha)} \propto \frac{1}{\sqrt{1 - \alpha^2}}$$
 (3.48)

depending on the restitution coefficient α , accounting for dissipation. Actually, when the system size increases over $L^*(\alpha)$ the wavelengths of unstable modes are smaller than the system size and the modes can be amplified by the dynamics of the system. The critical values of k and L are coupled to α , and as expected the instability is absent for $\alpha=1$; at fixed size of the system, one may recover unstable modes also increasing the dissipation over a critical value α^* .

The shear instability is responsible for vortex formation: indeed, the shear creates long-ranged waves of transversally aligned particles. When two shear waves cross each other, the particles on the *x* direction wave are moving in the *y* direction, where they encounter the flux of the perpendicular shear wave and therefore they start rotating their velocity. A clear representation of the phenomenon is given in [2]. It must be stressed that the vortex formation is observed in the *rescaled* variables,

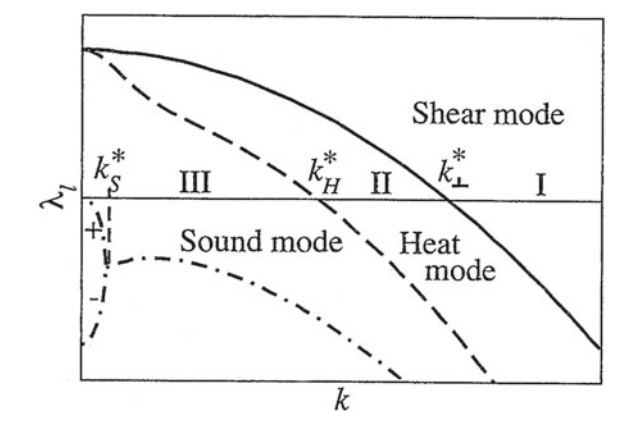
i.e. vortices are growing when compared with the thermal velocity $v_T(t)$, which is decreasing with Haff's law; they act on rapidly decreasing velocity scales, because the total energy is decreasing by means of collisions. Finally, the meaning of the minimal size allowing the formation of structures is controversial and still object of debate [2].

The cluster formation can be analyzed analogously, underlining that the rescaled density \tilde{n} has a different physical meaning with respect to rescaled velocity and temperature, because the homogeneous density is not decaying in time. From the stability analysis of Eq. (3.42), excluding shear modes which are independent from the rest of the system, one finds three eigenstates corresponding to the *heat mode* with real eigenvalue $\lambda_H(\mathbf{k})$ and two *sound modes* of complex eigenvalues $\lambda_{S1/2}(\mathbf{k})$; their behavior is shown in Fig. 3.1. The heat eigenvalue λ_H changes sign at $k_H^*(\alpha)$, a new critical value below which a combination of density, temperature and longitudinal velocity grow exponentially; therefore the density grows exponentially and clustering occurs. The critical value $k_H^*(\alpha)$ yields another critical size of the system. However, one has $k_H^*(\alpha) < k_\perp^*(\alpha)$, so three scenarios are possible depending on the size of the system

- $L < 2\pi/k_{\perp}^{*}(\alpha)$: no vortex or cluster formation. The HCS is stable.
- $2\pi/k_{\perp}^*(\alpha) < L < 2\pi/k_H^*(\alpha)$: vortices are present, but no clusters. The shear mode of maximum wavelength dominates the system. The HCS linearized equations are no longer valid.
- $L > 2\pi/k_H^*(\alpha)$: vortices (sooner) and clusters (later) form. The final state is strongly inhomogeneous.

As it can be seen, the first instability observed when increasing the system size is the shear instability: this observation will motivate the first model purposed in this thesis, which will be analysed in Chap. 4.

Fig. 3.1 Plot of the real part of the eigenvalues of the hydrodynamic modes in function of the wave vector k. The marginal values k_{\perp}^* , k_H^* and k_S^* are shown, respectively indicating the regions of stability of the shear mode, of the heat mode and of the propagating sound modes [2]



3.1.4 Active Hydrodynamics

Active hydrodynamics has not yet reached the same level of systematic development of conservative and granular hydrodynamics. The main reason is that an active kinetic theory is still under development, because of the relevant differences between active particles and passive molecules. The interactions between active particles and the surrounding fluid can be very complex and strongly dependent on the considered system [11]. Furthermore, as shown in Sect. 2.2, dry active systems do not conserve their total momentum, and thus both energy and momentum do not obey the conservation law (3.5). In the last years some studies derived a Boltzmann Equation for particular models of active particles, leading to a hydrodynamic description as discussed above for the elastic and granular case [12–14].

The first attempts to derive an active hydrodynamics have been strictly connected with the development of microscopic models such as Vicsek model. A milestone of active hydrodynamics is the continuum field description of orientation density in an active fluid, introduced by Toner and Tu in 1995 [15, 16]. The model is based on the continuum equations

$$\frac{\partial \rho}{\partial t} + \nabla \cdot (\rho \mathbf{u}) = 0, \qquad (3.49a)$$

$$\frac{\partial \mathbf{u}}{\partial t} + \lambda_1 (\mathbf{u} \cdot \nabla) \mathbf{u} + \lambda_2 (\nabla \cdot \mathbf{u}) \mathbf{u} + \lambda_3 \nabla (|\mathbf{u}|^2) =$$
(3.49b)

$$\alpha \mathbf{u} - \beta |\mathbf{u}|^2 \mathbf{u} - \nabla P + D_B \nabla (\nabla \cdot \mathbf{u}) + D_T \nabla^2 \mathbf{u} + D_2 (\mathbf{u} \cdot \nabla)^2 \mathbf{u} + \mathbf{f},$$

$$P = P(\rho) = \sum_{n=1}^{\infty} \sigma_n (\rho - \rho_0)^n$$
, (3.49c)

where β , D_B , D_T and D_2 are all positive, and **f** is a GWN force. A transition from disorder to order is present when α becomes positive: indeed the first two terms of the rhs are equivalent to the Rayleigh-Helmoltz friction described in Sect. 2.2.3, and the equations have an homogeneous fixed point at density ρ_0 and velocity $u = \sqrt{\alpha/\beta}$. The equations are *not* derived through a coarse-graining procedure from a Boltzmann Equation as in previous sections, but rather wrote down as the most general continuum equations of motion for velocity and density consistent with the symmetries ad conservation laws of the system, namely rotation invariance and number of particles conservation [17]. On the contrary, Galilean invariance doesn't hold because of lack of momentum conservation: for these reason, in principle all the convective coefficients λ in lhs are present, while in the Galilean case one has $\lambda_2 = \lambda_3 = 0$ and $\lambda_1 = 1$. The pressure P is expanded around the uniform density ρ_0 , forcing the system to the uniform density case. The symmetry arguments used to derive Eq. (3.49) are very powerful; however, within this approach the transport coefficients cannot be derived from microscopic dynamics as we have seen in previous sections, and one must derive them from other arguments.

The authors concentrated on the broken symmetry ordered phase with $\alpha > 0$, looking at the velocity component \mathbf{u}_{\perp} perpendicular to the direction of collective motion and at the density fluctuations $\delta \rho = \rho - \rho_0$. By means of renormalization group methods they performed a scaling analysis leading to the scaling exponents of the model. The analysis of the model is strongly supported by a comparison with ferromagnetic models, especially the XY model, with the big difference that the swarming transition breaks the rotational *continuous* symmetry also in 2d, which is forbidden in short-range equilibrium systems [18].

Recently, a derivation of active hydrodynamics from kinetic theory has been carried out by Bertin et al. [12, 13]. The authors derived a Boltzmann Equation for a system of N pointlike particles, combining binary collisions mimicking Vicsek interactions with run-and-tumble dynamics: when two particles are closer than a given distance d_0 , their orientations change as $\theta_i \to \theta_i' = \bar{\theta} + \eta_i$, where $\bar{\theta} = \text{Arg}[e^{i\theta_i} + e^{i\theta_j}]$ is the average orientation of the two particles, and η_i are identically distributed and independent GWN with variance σ^2 . The Boltzmann Equation for this model reads

$$\frac{\partial f}{\partial t}(\mathbf{r}, \theta, t) + \mathbf{e}(\theta) \cdot \nabla f(\mathbf{r}, \theta, t) = I_{dif}[f] + I_{col}[f, f], \qquad (3.50)$$

which is the extension of Eq. (2.88) to the interacting case, where in the rhs the diffusion functional $I_{dif}[f]$ and the collision functional $I_{col}[f, f]$ account for run-and-tumble dynamics and interactions, respectively. Following a coarse-graining and scale separation procedure, the authors find the hydrodynamic equation for the momentum $\mathbf{w} \equiv \rho \mathbf{v}$

$$\frac{\partial \mathbf{w}}{\partial t} + \gamma (\mathbf{w} \cdot \nabla) \mathbf{w} = -\frac{1}{2} \nabla (\rho - \kappa \mathbf{w}^2) + (\mu - \xi) |\mathbf{w}|^2) \mathbf{w} + \nu \nabla^2 \mathbf{w} - \kappa (\nabla \cdot \mathbf{w}) \mathbf{w},$$
(3.51)

recovering several features observed in Toner and Tu Eq. (3.49b). The kinetic model allows the computation of transport coefficients from microscopic parameters. Again, the homogeneous disordered and ordered phase are present, respectively when $\mu < 0$ and $\mu > 0$; the authors recover a noise-dependent threshold density $\rho^*(\sigma)$ above which the ordered phase becomes stable under homogeneous perturbations, showing the transition to collective motion. Taking into account space-dependent perturbations, the homogeneous disordered state is found to be stable for any $\rho < \rho^*$. On the other hand, the homogeneous flow state is unstable for long-wave longitudinal fluctuations near the transition line, while it gets stable at high densities $\rho \gg \rho^*$: this phenomenon is called *restabilization*, a delicate result because in this region the system is far from the validity domain of the hydrodynamic description. The linear stability must be analyzed through the Boltzmann Equation, which confirms the stability for high densities, an interesting result because it shows how hydrodynamic equations are predictive beyond their validity domain. An agreement with numerical simulations of agent-based models has been found [13]. This model was further analysed and modified in [19], where multibody interactions have been reintroduced following a Vicsek-like approach: this correction allowed to recover the phase diagram of Vicsek et al. in the continuum mode. Finally, these studies proved that the Toner and Tu theory is actually the continuum limit of the Vicsek model under a suitable choice of the transport coefficients, confirming the generality claim in the formulation of the model.

In the last years, active hydrodynamics models have been developed also from overdamped, microscopic Langevin equations leading to Smoluchowski dynamics for the density function and then to hydrodynamic equations in the coarse-grained case. Studying the density ρ , momentum \mathbf{w} and alignment tensor $\mathbf{Q} = \hat{\mathbf{u}}\hat{\mathbf{u}} - \frac{1}{d}\mathbf{I}$ [11, 20–22], similar results have been found with respect to the above-mentioned models, typically differing in the transport coefficients because of the microscopic rules defining the model. A rich variety of models is still under development and debate; in Chap. 6, it will be shown how an hydrodynamic description of active matter can be derived from microscopic rules, reproducing on a lattice the kinetic behavior of active particles in the case of a dilute system with short-range interactions.

3.2 Fluctuating Hydrodynamics

The hydrodynamic theory described in the last section is *deterministic*: hydrodynamic fields are averaged quantities and fluctuations are not observable when the number of particles in a fluid volume element is very large (for instance of the order of Avogadro's number). However, we know that granular and active matter are *small* systems, and the number of active units or grains typically is in the range $10^2 \div 10^4$. This means that fluctuations become measurable: their description is the goal of fluctuating hydrodynamics. To do this, one can generally write deterministic hydrodynamic equations as in the previous section and add a noise source directly in the equations.

In general, noise can be thought as the result of a coarse-graining of the system. For instance, for a conservative system with Hamiltonian $H(\mathbf{p}, \mathbf{q})$ one can include the effect of an external reservoir adding a noise and dissipation term, i.e.

$$\dot{\mathbf{q}} = \frac{\partial H}{\partial \mathbf{p}},$$

$$\dot{\mathbf{p}} = -\frac{\partial H}{\partial \mathbf{q}} - \gamma \mathbf{p} + \boldsymbol{\xi}(t),$$
(3.52)

where $\xi(t)$ is a GWN satisfying $\langle \xi_{\alpha}(t)\xi_{\beta}(t')\rangle = D\delta_{\alpha\beta}\delta(t-t')$. For a canonical Hamiltonian $H=p^2/2m+V(\mathbf{q})$, the probability distribution $f(\mathbf{q},\mathbf{p};t)$ follows the Fokker–Planck equation

$$\frac{\partial f}{\partial t} = -\frac{\partial}{\partial \mathbf{q}} \cdot \left(\frac{\mathbf{p}}{m}f\right) + \frac{\partial}{\partial \mathbf{p}} \cdot \left[\left(\nabla V(\mathbf{q}) + \gamma \mathbf{p}\right)f\right] + \frac{D}{2} \frac{\partial^2 f}{\partial p^2}, \tag{3.53}$$

which under a change of variables leads to the Kramers' Equation [23]. The noise and friction term generally stem from the average of fast variables with respect to the Hamiltonian coordinates $\bf p$ and $\bf q$. So, dissipation and noise come from the same coarse-graining mechanism, and *at equilibrium* they are related by the Einstein relation, namely $D=2m\gamma k_BT$. This crucial relation between diffusivity and mobility provides that the Boltzmann distribution $f(\bf p, q) \sim \exp[-H(\bf p, q)/k_BT]$ is a stationary solution of Eq. (3.53). Therefore, if the Einstein relation is satisfied the fluctuations can be reintroduced into Hamiltonian dynamics leaving the equilibrium Boltzmann distribution unchanged.

The procedure described above relies on the *fluctuation-dissipation relations* between the linear response of an observable to a perturbation and its autocorrelation in time [24]. It must be stressed that the particular relation depends on the coarse-graining applied: indeed, the viscous friction $-\gamma \mathbf{p}$ instantaneously acts on the particle without any memory effect of its trajectory; when memory effects are present, the noise $\boldsymbol{\xi}$ must be modified as well to recover the equilibrium Boltzmann distribution [25]. The main idea of *Landau-Lifschitz* fluctuating hydrodynamics is the following [8]: given the deterministic hydrodynamic equations $\partial_t \Psi = \mathcal{F}[\Psi]$, being $\Psi(\mathbf{x},t)$ the vectorial field of density, momentum and temperature, and \mathcal{F} the deterministic average hydrodynamic evolution operator, the fluctuating equations should be written

$$\partial_t \Psi(\mathbf{x}, t) = \mathcal{F}[\Psi(\mathbf{x}, t)] + \xi(\mathbf{x}, t), \qquad (3.54)$$

where the deterministic hydrodynamic operator \mathcal{F} is taking into account only the average, deterministic terms and all the fluctuations are contained in $\boldsymbol{\xi}$. Now, \mathcal{F} already defines dissipative terms such as viscosity and heat diffusion: therefore, in the case of conservative interactions one may directly introduce a Gaussian noise $\boldsymbol{\xi}$ which correlation properties are determined by equilibrium fluctuation-dissipation relations, avoiding the ambiguity of the coarse-graining described above.

For out of equilibrium systems, the situation is more complicated because the distribution function is generally unknown and differs from Boltzmann distribution. This lack of information removes the constraint on noise definition. Thus, nonequilibrium methods are necessary to derive the correct fluctuations at a mesoscopic scale.

In 1969, a seminal paper of Bixon and Zwanzig [26] introduced the *Boltzmann–Langevin* Equation: the one-particle distribution function is written as

$$f(\mathbf{x}, \mathbf{v}; t) = \sum_{j=1}^{N} \delta(\mathbf{x}_{j}(t) - \mathbf{x}) \delta(\mathbf{v}_{j}(t) - \mathbf{v}), \qquad (3.55)$$

where $\mathbf{x}_j(t)$ and $\mathbf{v}_j(t)$ are the position and velocity of the j-th particle in the system, with $j=1,\ldots,N$. The field f is a dynamical, *fluctuating* observable, which averaged over initial conditions gives the one-particle marginalized distribution defined in Eq. (2.24), which we here call \overline{f} . Thus, the distribution deviation $\phi = (f - \overline{f})/\overline{f}$ in linear approximation evolves through a Boltzmann–Langevin Equation, namely a

Boltzmann Equation modified by some noise term, i.e.

$$\frac{\partial \phi}{\partial t} + \mathbf{v} \cdot \nabla \phi - J\phi = F(\mathbf{r}, \mathbf{v}, t), \qquad (3.56)$$

where J is the linearized collision operator and F a random noise term, whose average over initial conditions must vanish. The noise term is an *effective* term coming from the contribution of 2-particles distribution $F_2(\mathbf{x}_1, \mathbf{v}_1, \mathbf{x}_2, \mathbf{v}_2; t)$: its contribution is an effect of the second equation of the Boltzmann hierarchy. Equation (3.56) leads to hydrodynamic equations through the usual Chapman–Enskog procedure, but the pressure tensor and heat flux are now written as a sum of a deterministic and a fluctuating component. At equilibrium, the averaged distribution is the Maxwell–Boltzmann distribution $\overline{f} = f_{MB}$ and the Einstein relations are recovered, validating Landau-Lifschitz theory.

The work of Bixon and Zwanzig inspired the study of fluctuating hydrodynamics in inelastic materials. Indeed, when equilibrium doesn't hold, the kinetic theory is the starting point to obtain macroscopic predictions from microscopic features. Fluctuating hydrodynamics has been applied to the case of granular materials [27, 28]. Generally speaking, the fluctuations of the microscopic density leads to fluctuations of any general hydrodynamic field $\psi(\mathbf{x},t)$, which can be written as $\psi^{\mathrm{av}}(\mathbf{x},t) + \delta \psi(\mathbf{x},t)$, separating the average term $\psi^{\mathrm{av}}(\mathbf{x},t)$ from the zero-average fluctuations $\delta \psi(\mathbf{x},t)$. The latter follow a generalized Langevin equation: its solution leads to the correlation properties of hydrodynamic fluctuations, namely $\langle \delta \psi(\mathbf{x},t) \delta \psi(\mathbf{x}',t') \rangle$.

To see a real example, let's focus on the shear mode, a particular hydrodynamic mode [28]. The fluctuating transverse velocity field in Fourier space is defined as

$$u_{\perp}(k,t) \equiv \sum_{j=1}^{N} v_{y,j}(t)e^{-ikx_{j}(t)}$$
, (3.57)

where k is the wave number of the mode, $x_j(t)$ is the x-coordinate and $v_{y,j}(t)$ is the y-velocity of the j-th particle at time t. The shear mode is the analytically simplest mode, as it has been shown to decouple from other modes in linearized hydrodynamics. We aim at describing the rescaled autocorrelation function

$$C_{\perp}(k,t) \equiv \frac{\langle u_{\perp}(k,0)u_{\perp}^{*}(k,t)\rangle}{2T}, \qquad (3.58)$$

where u_{\perp}^* is the complex conjugate of u_{\perp} and T is the (isotropic) temperature of the system, corresponding to the room temperature for elastic fluids or to the granular temperature for granular materials. Both the equilibrium case and the HCS can be studied. In the former, the Landau–Lifschitz fluctuating hydrodynamics predicts the stochastic equation

$$\frac{\partial}{\partial t}u_{\perp}(k,t) = -\nu k^2 u_{\perp}(k,t) + \xi(k,t), \qquad (3.59)$$

where ν is the kinematic viscosity. The Einstein relation corresponds to

$$\langle \xi(k,t)\xi(k',t')\rangle = \delta_{k,-k'}\delta(t-t')2TN\nu k^2, \qquad (3.60)$$

being of order N because u_{\perp} is an extensive field, so the noise associated to the intensive field u_{\perp}/N is scaling as 1/N. Eq. (3.59) leads to the correlation function

$$C_{\perp}(k,t) = \frac{N}{2}e^{-\nu k^2 t} \,. \tag{3.61}$$

In the inelastic case, the evolution equation for the transverse velocity can be written as

$$\frac{\partial}{\partial t} u_{\perp}(k,t) = -\nu(T(t))u_{\perp}(k,t) + \xi(k,t). \tag{3.62}$$

Here, the temperature is decaying following the Haff's law, therefore noise correlations must be time-dependent as well. A first approximation can be derived using the granular temperature instead of the room temperature, and writing an Einstein relation in the granular case [29]. The evolution equation for the rescaled velocity, Eq. (3.45), can be written as

$$\frac{\partial}{\partial \tau} \tilde{u}_{\perp}(k,\tau) = -z(k)\tilde{u}_{\perp}(k,\tau) + \tilde{\xi}(k,\tau) , \qquad (3.63)$$

with $z(k) = qk^2 - \zeta/2$, where $q = \nu(T(t))/\omega_c(T(t))$ is the time-independent ratio between kinematic viscosity and collision rate, and ζ is the cooling coefficient, from $T(\tau) \sim \exp(-\zeta\tau)$. The coefficient z(k) is now constant and so are the noise correlations. Analogously with the equilibrium case, one can now write

$$\langle \xi(k,t)\xi(k',t')\rangle = \delta_{k,-k'}\delta(t-t')2TNqk^2, \qquad (3.64)$$

where T is the granular temperature. The HCS is stable for z(k) > 0: for stable modes, the stationary autocorrelation reads

$$C_{\perp}(k,\tau) = \frac{N}{2} \frac{qk^2}{z(k)} e^{-z(k)\tau},$$
 (3.65)

which in the elastic case $\zeta = 0$ is equivalent to the equilibrium correlation in (3.61).

This result has been obtained following the physical intuitive analogy between granular temperature in granular fluids and physical temperature in molecular fluids, and assuming the validity of a local Einstein relation. However, a rigorous derivation of noise correlations must follow the Boltzmann–Langevin derivation described above. In this case, noise correlations can be computed and give [27]

$$\left\langle \tilde{\xi}(k,\tau)\tilde{\xi}(k',\tau') \right\rangle = \delta_{k,-k'} 2Nk^2 G(|\tau-\tau'|) \tag{3.66}$$

where $G(s) \neq \delta(s)$. So, memory terms are present and confirmed by numerical simulations. The stationary autocorrelation is no longer a simple exponential, but it has an exponential tail for long times: Eq. (3.63) in this case leads to

$$C_{\perp}(k,0) = \frac{N}{2} \frac{q_1 k^2}{z(k)} \,, \tag{3.67a}$$

$$C_{\perp}(k,\tau) = \frac{N}{2} \frac{(q_1 + q_2)k^2}{z(k)} e^{-z(k)\tau} \qquad \tau \gg 1,$$
 (3.67b)

where q_1 and q_2 have been computed in [27]. The time-dependent expression is valid after a transient, indeed the value of Eq. (3.67b) at $\tau=0$ does not coincide with Eq. (3.67a). In the elastic limit $\zeta\to 0$, $q_1\to q$ and $q_2\to 0$, so the equilibrium result of Eq. (3.61) is recovered. While the initial value and the transient are different, for long times the correlations derived from kinetic theory get the same temperature decay of correlations derived with the Einstein-Landau prescription in Eq. (3.64). This result confirms that the latter is a good approximation for long times correlations, while memory terms observables for short times can be obtained b means of kinetic theory. The Einstein-Landau prescription is predictive also in the case of driven granular gases, both for bulk [30] or boundary driving [31]. Numerical results are in fair agreement with the theory, and again the Einstein-Landau approach has been recovered as a limit of kinetic derivation. The case of a bulk driven granular medium including external viscosity has been analyzed theoretically [32, 33] and experimentally: it has been shown that this is a good description of a quasi-2d vibrated granular on a horizontal plate [34].

The shear mode is one of the simplest cases of fluctuating hydrodynamics, because it is decoupled from the others, therefore it can be treated individually; nevertheless, this "simplicity" leads to complicated analytical calculations. Heat and sound modes are coupled and the derivation of fluctuating hydrodynamics from kinetic theory is a very hard challenge. For this reasons, further methods to describe fluctuating hydrodynamics are an important goal in current research.

Hydrodynamic fluctuations have been studied in the last years also in the framework of *Macroscopic Fluctuation Theory* (MFT), which has been derived to describe macroscopic fluctuations of hydrodynamic quantities in non-equilibrium steady states (NESS) [35, 36]. The general procedure considers a hydrodynamic density field $\rho(\mathbf{x}, t)$ and its associated current $\mathbf{j}(\mathbf{x}, t)$, satisfying

$$\partial_t \rho + \nabla \cdot \mathbf{j} = 0 \,, \tag{3.68a}$$

$$\mathbf{j}(\mathbf{x},t) = \mathbf{J}([\rho]; \mathbf{x}, t), \qquad (3.68b)$$

respectively the continuity equation and the constitutive relation for the current **j** depending on the field ρ and eventually on time and space through the functional **J**. For driven diffusive systems, the latter generally reads

$$\mathbf{J}([\rho]; \mathbf{x}, t) = -D(\rho)\nabla\rho + \chi(\rho)E(\mathbf{x}, t) \tag{3.69}$$

defining the diffusivity $D(\rho)$ and the mobility $\chi(\rho)$ under the action of an external field $E(\mathbf{x}, t)$. Under these assumptions, one can compute the probability of a trajectory (ρ, j) between time t_0 and t_1 as

$$\mathbb{P}_{\rho_0} \approx \exp[-\epsilon^{-d} \mathcal{I}_{[t_0,t_1]}(\rho,j)]$$

$$\mathcal{I}_{[t_0,t_1]}(\rho,j) = \frac{1}{4} \int_{t_0}^{t_1} \mathrm{d}t \int \mathrm{d}\mathbf{x} \left[\mathbf{j} - \mathbf{J}([\rho];\mathbf{x},t)\right] \cdot \chi^{-1}(\rho) \cdot \left[\mathbf{j} - \mathbf{J}([\rho];\mathbf{x},t)\right]$$
(3.70)

where $\epsilon \ll 1$ is an adimensional parameter such that $\epsilon \to 0$ when $N \to \infty$, where N is the number of particles of the system, and the trajectories are constrained to satisfy the continuity equation (3.68a) and the initial condition $\rho(t_0) = \rho_0$. The rate functional $\mathcal{I}_{[t_0,t_1]}(\rho,j)$ acts as a *large deviation functional* [37], and the average hydrodynamic field and current correspond to the optimal path $\rho_{\rm av}(\mathbf{x},t)$, $\mathbf{j}_{\rm av}(\mathbf{x},t)$ defined by

$$\min_{(\rho,j)} \mathcal{I}_{[t_0,t_1]}(\rho,j) = \mathcal{I}_{[t_0,t_1]}(\rho_{\text{av}},j_{\text{av}}). \tag{3.71}$$

The theory derives back the deterministic hydrodynamic equations and obtains the hydrodynamic fluctuations beyond the linear approximation which has been used in the previous part of the section, which always leads to Gaussian fluctuations. The theory represents also a bridge between nonequilibrium fluctuation relations [24, 38–40], stochastic thermodynamics [41] and hydrodynamic theory.

MFT ha been recently applied to study fluctuating hydrodynamics of active systems, when comparing ABP and Run-and-Tumble dynamics [21] or investigating lattice models of interacting bacteria [42]. MFT found a successful field of application in *lattice models*, where a derivation of macroscopic hydrodynamic equations (3.68) from microscopic dynamics can be done in a transparent and rigorous way [43]. Lattice models have been developed in the last 40 years as a tool to investigate several out-of-equilibrium processes, deriving their essential macroscopic features from minimal microscopic dynamics. The most important lattice models for our purpose will be reviewed in the following of this chapter, as they have been a guide to introduce the lattice models of granular and active matter in Part II which are the fundamental result of this thesis.

3.3 Lattice Models

Lattice models have been widely used in statistical physics in the last century because of the great simplifications that they introduce and consequently the possibility of many analytical calculations. The most famous lattice models have been developed for equilibrium systems, especially describing ferromagnetic behavior as in the Ising, Heisenberg or XY model. Nevertheless, these models introduce an universal behavior and they can be adopted to describe several physical systems, such as lattice gases and binary alloys [1]. The reason of their success is the capability to reproduce

complex physical behavior such as phase transitions by means of few essential, microscopic rules, yielding at the same time new theoretical predictions; furthermore, the investigation on lattice models usually doesn't need equilibrium assumptions but rather relies on the microscopic dynamics of the system. Therefore, the analysis is generally developed out of equilibrium, recovering the equilibrium case by a suitable choice of boundary conditions [44].

A plethora of lattice models have been developed in the last years, and a single model can lead to many others simply through a slight variation of its rules. Here a selection of the most significant models is presented, starting in Sect. 3.3.1 from the Kipnis–Marchioro–Presutti (KMP) model describing heat conduction in a chain of harmonic oscillators, and the simple exclusion processes (SEP) describing the diffusion of hopping particles on a linear chain. Both these models have *conservative* interactions and can be either in or out of equilibrium, depending on the boundary conditions. Subsequently, in Sect. 3.3.2 the case of dissipative models will be introduced, for which *inelastic* interactions necessarily drive the system out of equilibrium.

3.3.1 Conservative Models

In 1982, Kipnis, Marchioro and Presutti introduced a lattice model to describe the time evolution and heat flux of a linear chain of L mechanically uncoupled oscillators coupled with two thermal reservoir at both extremities [45]. A configuration of the system is given by $\{q_i, p_i\}$, i.e. the set of coordinates and momenta of all the sites, with $i = -L, \ldots, L$. The energy at each site reads $\varepsilon_i = q_i^2 + p_i^2$. The system undergoes a stochastic evolution: at each discrete time step, two nearest-neighbors sites are chosen and exchange their energy redistributing it randomly, namely

$$\varepsilon_i' = p(\varepsilon_i' - \varepsilon_{i+1}'), \quad \varepsilon_{i+1}', = (1 - p)(\varepsilon_i' - \varepsilon_{i+1}'), \tag{3.72}$$

so that the microscopic evolution conserves the total energy. At sites $i = \pm L$ the oscillators thermalize with the reservoirs at temperatures T_+ (+L) and T_- (-L), i.e. they exchange energy with oscillators whose random energy follows the Boltzmann distribution.

The authors derive a mathematically rigorous expression for the evolution equation of the energy distribution $P(\{\varepsilon\}, t)$, and prove that in the stationary limit it converges to the local equilibrium distribution

$$f(\varepsilon; x, t) = \frac{1}{k_B T(x)} e^{-\varepsilon/k_B T(x)}, \qquad (3.73)$$

where f is the one-site distribution and $P(\{\varepsilon\}, t) = \prod_x f(\varepsilon; x, t)$, x is the site index $x = i/L \in [-1, 1]$ which is continuous in the hydrodynamic limit $L \to \infty$, and T(x) the temperature profile

3.3 Lattice Models 89

$$T(x) = T_{-}\frac{1-x}{2} + T_{+}\frac{1+x}{2}.$$
 (3.74)

So, after a transient time the oscillators thermalize and develop a temperature profile depending on the temperatures at the boundaries. Although the system is out of equilibrium for $T_+ \neq T_-$, the local equilibrium holds *exactly* for the system.

The heat flux q can be defined as the energy transferred from the i-th to the i+1-th oscillator, and therefore it is a stochastic quantity. Its average behavior can be written as

$$q_i(t) = \int_0^\infty d^L \varepsilon P(\{\varepsilon\}, t) \int_0^1 dp \left[\varepsilon_i(t) - p(\varepsilon_i(t) + \varepsilon_{i+1}) \right], \qquad (3.75)$$

and since in the steady state local equilibrium holds one has

$$q(x) = -\frac{k_B}{2} \frac{\mathrm{d}T}{\mathrm{d}x} \,, \tag{3.76}$$

which is the Fourier's law with diffusion coefficient $D = k_B/2$. The stochastic energy current can be generally defined as $J(x,t) = q(x,t) + \xi(x,t)$, and the evolution equation of the local energies can be written as

$$\partial_t \varepsilon = -\partial_x J(x) = -\partial_x \left(-\frac{k_B}{2} \partial_x \varepsilon + \xi \right) ,$$
 (3.77)

which is the fluctuating hydrodynamics equation for the energy field $\varepsilon(x, t)$, namely a stochastic diffusion equation. Now, the noise amplitude and correlations can be directly computed through the local equilibrium distribution in (3.73); moreover, a noise term appears in the current of Eq. (3.77), which is a continuity equation also at a stochastic level, because energy conservation exactly holds in microscopic interactions, and the mesoscopic equation (3.77) must respect it.

The model has been a milestone for lattice models of nonequilibrium statistical physics, since it shows how fundamental features such as heat diffusion can be rigorously recovered from lattice models, and the nonequilibrium probability distribution can be derived through the dynamics of the system. There is no need to define an effective Hamiltonian, or an equilibrium distribution, or to assume an Einstein relation: the local equilibrium approximation is the asymptotic limit of a nonequilibrium process. The local equilibrium found allows to derive the current fluctuations without the need to guess them from equilibrium dynamics.

The KMP model can be interpreted as well as the diffusion of particles on a chain, or diffusion of excitations on a linear system. Lattice models have indeed been applied from the beginning to describe density diffusion, magnetic models, fermionic systems, vibrations on a harmonic chain or electrical lines [46]. Among them, we will concentrate on models of *hopping* particles on a lattice. Random walk on a lattice is very well known, leading to the diffusion equation for the average density $\partial_t \rho = D \partial_x^2 \rho$ and the diffusive relation $\overline{x^2(t)} \sim t$. It has been shown that, when a

particle jumps on an heterogeneous medium (where the hopping rates depend on the position and they can be asymmetric), several regimes of motion arise depending on the statistical properties of the hopping rates [47, 48]. The simple exclusion processes (SEP) aim, at describing the motion of particles moving on a linear chain with excluded volume interactions. The system is made by a random number of particles placed on L sites: each site i = 1, ..., L is occupied or not depending on the occupation number $n_i = 1, 0$. The hops are a Poissonian process: at each continuous time interval of length $d\tau$, a particle on i can jump either to site i-1 or i+1 only if the site is empty and with probability $d\tau$ for both directions (symmetric process, SSEP). The chain is coupled with two reservoirs of particles at the extremities, analogous to the thermal baths of KMP model: if the site i = 0 (L) is empty, a particle can enter the system with probability $\alpha d\tau$ ($\delta d\tau$); otherwise, if the site i (L) is occupied, the particle can leave the chain with probability $\gamma d\tau$ ($\beta d\tau$); the full dynamics of the SSEP is represented in Fig. 3.2. Thus, the system is Markovian and it is possible to write the evolution equations for the average density $\langle n_i(t) \rangle$ in the limit $d\tau \to 0$, which read [43]

$$\frac{\mathrm{d}\langle n_1 \rangle}{\mathrm{d}\tau} = -\langle n_1 \left[\gamma + (1 - n_2) \right] \rangle + \langle (1 - n_1)(\alpha + n_2) \rangle
= \alpha - (\alpha + \gamma + 1)\langle n_1 \rangle + \langle n_2 \rangle ,$$

$$\frac{\mathrm{d}\langle n_i \rangle}{\mathrm{d}\tau} = -\langle n_1 \left[(1 - n_{i-1}) + (1 - n_{i+1}) \right] \rangle + \langle (1 - n_1)(n_{i-1} + n_{i+1}) \rangle
= \langle n_{i-1} \rangle - 2\langle n_i \rangle + \langle n_{i+1} \rangle \quad \text{for } i = 2, \dots, L ,$$

$$\frac{\mathrm{d}\langle n_L \rangle}{\mathrm{d}\tau} = -\langle n_L \left[\beta + (1 - n_{L-1}) \right] \rangle + \langle (1 - n_L)(\delta + n_{L-1}) \rangle
= \langle n_{L-1} \rangle - (\beta + \delta + 1)\langle n_L \rangle + \delta .$$
(3.78a)

Equation (3.78a) and (3.78c) are the boundary conditions of the system, while the evolution of the bulk is given by Eq. (3.78b). The derivation of a *closed* set of equations for the density has been made possible by the *exact* cancellation of two-point correlations $\langle n_i n_{i+1} \rangle$, which vanish in Eq. (3.78) regardless of their value. The stationary solution can be found imposing $d\langle n_i \rangle/d\tau = 0$, yielding

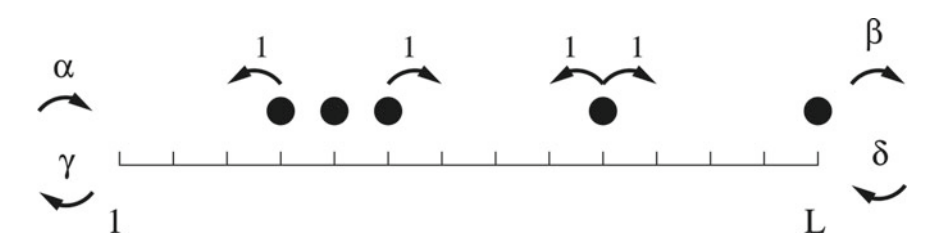


Fig. 3.2 A sketch of the SSEP model [43]

3.3 Lattice Models 91

$$\langle n_i \rangle = \frac{\rho_a(L + 1/(\beta + \delta) - i) + \rho_b(i - 1 + 1/(\alpha + \gamma))}{L + 1/(\alpha + \gamma) + 1/(\beta + \delta) - 1}, \qquad (3.79)$$

with $\rho_a = \alpha/(\alpha + \gamma)$ and $\rho_b = \delta/(\beta + \delta)$. In the hydrodynamic limit $L \to \infty$, it is natural to introduce once again the continuum position x = i/L, for which the stationary density reads

$$\langle n_i \rangle \equiv \rho_s(x) = \rho_a(1-x) + \rho_b x , \qquad (3.80)$$

which has the same form of the KMP equation for the temperature profile, except that here $x \in [0, 1]$ whereas for KMP $x \in [-1, 1]$ (keeping the original choice of the authors). So, ρ_a and ρ_b are the densities of the reservoirs, and if the particles carry an energy ε the reservoirs become heat baths with temperatures T_a and T_b , satisfying

$$\exp\left[\frac{\varepsilon}{k_B T_a}\right] = \frac{\alpha}{\gamma} \quad , \quad \exp\left[\frac{\varepsilon}{k_B T_b}\right] = \frac{\delta}{\beta} \, . \tag{3.81}$$

As for Eq. (3.78), the evolution equation of the average current and two-points correlations can be computed; their steady state reads

$$\langle J \rangle \equiv \langle n_i (1 - n_{i+1}) - n_{i+1} (1 - n_i) \rangle \simeq \frac{\rho_a - \rho_b}{I} , \qquad (3.82)$$

$$\langle n_i n_j \rangle_c \equiv \langle n_i n_j \rangle - \langle n_i \rangle \langle n_j \rangle = -\frac{x(1-y)}{L} (\rho_a - \rho_b)^2,$$
 (3.83)

where x = i/L and y = j/L. Equation (3.82) gives the Fick's law for the SSEP model. These results show that currents and correlations are nonvanishing only when a density gradient $\rho_a \neq \rho_b$ is applied, and they are both finite-size effects of order 1/L. One may say that these can therefore be easily neglected when $L \to \infty$, however this can be done only in first approximation as it will be shown in Chap. 4. Moreover, when considering macroscopic quantities such as the fluctuations of the total number of particles N in the system, one sees that

$$\langle N^2 \rangle - \langle N \rangle^2 = \sum_{i} \left[\langle n_i \rangle - \langle n_i \rangle^2 \right] + 2 \sum_{i < j} \langle n_i n_j \rangle_c$$

$$\simeq L \left[\int_0^1 \mathrm{d}x \rho_s(x) (1 - \rho_s(x)) - 2(\rho_a - \rho_b)^2 \int_0^1 \mathrm{d}x \int_0^1 \mathrm{d}y x (1 - y) \right],$$
(3.84)

so the correlations contribute at the leading order to the macroscopic fluctuations of the system.

The above-mentioned results have been derived for the discrete set of microscopic configurations $\{n_i\}$; however, from Eq. (3.78) it is tempting to move to a continuum description in the hydrodynamic limit $L \to \infty$. This is possible if one assumes that averaged fields slowly vary with position, i.e. making the smoothness ansatz

$$\langle n_{i\pm 1}\rangle \equiv \rho(x \pm \Delta x, \tau) = \rho(x, \tau) \pm \Delta x \left. \frac{\partial \rho}{\partial x} \right|_{x,t} + \frac{1}{2} (\Delta x)^2 \left. \frac{\partial^2 \rho}{\partial x^2} \right|_{x,\tau} + \mathcal{O}((\Delta x)^3),$$
(3.85)

so the $\langle n_{i+1} \rangle$ terms in Eq. (3.78) can be expanded and one has

$$\partial_{\tau}\rho(x=0,t) = \alpha - (\alpha + \gamma)\rho(0,t) + \Delta x \,\partial_{x}\rho(x=0) ,$$

$$\partial_{\tau}\rho(x,t) = (\Delta x)^{2}\partial_{x}^{2}\rho(x,t) ,$$

$$\partial_{\tau}\rho(x=1,t) = \beta - (\beta + \delta)\rho(0,t) + \Delta x \,\partial_{x}\rho(x=1) .$$
(3.86)

Now, the lattice spacing $\Delta x = 1/L$ explicitly appears in the equations in the continuum limit $L \to \infty$: this implies that a macroscopic, *hydrodynamic time* must be defined as

$$t = (\Delta x)^2 \tau \tag{3.87}$$

for this model, yielding $\partial_{\tau} = (\Delta x)^2 \partial_t$ and canceling the explicit Δx dependence. By matching the equations at the leading orders in Δx , one has the evolution equation

$$\partial_t \rho(x,t) = \partial_x^2 \rho(x,t) ,$$

$$\rho(0) = \rho_a , \quad \rho(1) = \rho_b ,$$
(3.88)

which has the stationary solution of Eq. (3.80). The time rescaling defined in Eq. (3.87) is called *hydrodynamic scaling*, and will be widely used in Part II: its physical meaning is that hydrodynamic phenomena are evolving with characteristic times L^2 times bigger than the characteristic time of the microscopic evolution, namely the mean time between two hops. This is related with the scale separation introduced in the Chapman–Enskog procedure, and the ratio between microscopic and hydrodynamic times is equivalent to the Knudsen number for this model. The scaling $t = (\Delta x)^2 \tau$ is called a *diffusive* scaling: indeed, in this case a diffusive behavior has been derived, see Eq. (3.88). On the contrary, when $t = (\Delta x) \tau$ the scaling is said to be *ballistic*, because a tracer in the system follows a ballistic motion $\overline{x^2(t)} \sim t^2$. A fluctuating hydrodynamic description of the model has been made possible, mainly applying the Macroscopic Fluctuation Theory described in Sect. 3.2 [43].

The SSEP model can be modified by changing one of the hopping rates in the bulk from 1 to q: this case is known as the asymmetric simple exclusion process (ASEP). This asymmetry typically represents the effect of a driving force applied to the system, which can be gravity acceleration, electrical field, and so on. The ASEP model reproduces the essential features of driven diffusive models, and has been used as a model of traffic, growth and polymer dynamics. Equations for the mean density evolution can be derived as in (3.78), but now the correlation terms do not vanish and must be treated carefully. The large scale ASEP behavior presents shock waves whereas the SSEP is purely diffusive.

Those two models have been both investigated in the framework of MFT to derive fluctuating hydrodynamics predictions. Their great utility is the possibility to derive several theoretical results far from equilibrium, and coming back to the equilibrium

3.3 Lattice Models 93

case when no gradient is applied at the boundaries. Their generalization to arbitrary dimensions is straightforward [43].

3.3.2 Dissipative Models

The last models have been a useful guide to study the fluctuating hydrodynamics of driven and diffusive conservative systems. However, this is not the case of granular or active matter systems, where dissipation is present in the bulk dynamics because of inelastic collisions and/or self-propulsion. Granular models have been often developed on a lattice; especially, granular models in one dimension have been used to develop a rigorous hydrodynamic description [49, 50]. A granular lattice model can be introduced as a linear chain of L grains with velocities v_i , with $i = 1, \ldots, L$; at each discrete time step $p \in \mathbb{N}$, a pair i, i+1 of nearest-neighbors is drawn and collides according to the inelastic collision rule in Eq. (2.31), which in 1d reads

$$v'_{i} = v_{i} - \frac{1+\alpha}{2}(v_{i} - v_{i+1}),$$

$$v'_{i+1} = v_{i+1} + \frac{1+\alpha}{2}(v_{i} - v_{i+1}).$$
(3.89)

Similar models have been studied to find the asymptotic scaling distribution in the HCS or investigate the multiscaling properties described in Sect. 2.16. The collision probability P_i of the pair i, i + 1 plays a crucial role: indeed this can be chosen uniformly, $P_i = 1/L$, corresponding to Maxwell molecules dynamics; or it can contain a kinematic constraint $P_i \propto \Theta(v_i - v_i + 1)$, which implies that particles collide only when their velocities are directed towards each other; or there can be a flux term $P_i \propto |v_i - v_{i+1}|$, analogous with the flux term in the collisional operator of Boltzmann Equation for hard spheres (2.35b), increasing the collision probability with the magnitude of the relative velocity. When the last two terms are taken together, the system behaves as a 1d channel of inelastic hard rods, exchanging their velocities by means of collisions, with a perfect exchange when $\alpha = 1$ (elastic case) and a slight reduction of speeds for $\alpha < 1$. It is worth stressing that in the elastic case $\alpha = 1$ the system is not really evolving in time: once given the set of initial velocities $\{v\}_{t=0}$ the collisions only exchange labels, say $v'_i = v_{i+1}$ and $v'_{i+1} = v_i$, so the empirical velocity distribution is invariant in time. The model leads to a hydrodynamic description and several regimes of temperature decay are found, especially in the case of high dissipation $\alpha \approx 0$: indeed, when $\alpha = 0$, after a collision two particles move with the same velocities and don't collide any more until a third particle change their velocity once again. Shock waves have been observed when the kinematic constraint is included, both in molecular dynamics (MD) of inelastic hard rods and in simulations of the lattice model; similarly, a 2d model has shown the presence of vortices spontaneously arising in the dynamics of the system [50]. It must be underlined that in this model the particles are *not* moving: indeed, all the sites are occupied, there are

no hops and their velocities do not represent their motion but rather the dynamical observable involved in collisions, more or less like in the KMP model where we disregarded the physical meaning of position q_i and momentum p_i to concentrate only on the energy ε_i , which could be taken as the energy level of the site.

The first attempt to derive a fluctuating hydrodynamics theory of dissipative lattice models has been done in 2011 by Prados, Lasanta and Hurtado [51, 52]: inspired from the KMP model, they introduced a model of driven dissipative media, made by a chain on L particles each carrying an energy ρ_i , and coupled with two heat baths at the boundaries. The dynamics is equivalent to the KMP model, but with a slightly modified interaction rule

$$\rho'_{i} = z_{p}\alpha(\rho_{i} + \rho_{i+1}), \quad \rho'_{i+1} = (1 - z_{p})\alpha(\rho_{i} + \rho_{i+1}),$$
 (3.90)

where z_p is a random uniform number drawn at ecach time step between 0 and 1, and $\alpha \in [0, 1)$ is the inelasticity coefficient analogous to the restitution coefficient in granular collisions; the particles can be extracted uniformly or according to a distribution which typically depends on the total energy of the pair, i.e.

$$P_i(\{\rho\}) = \frac{f(\Sigma_i)}{L\Omega(L)}, \quad \Omega(L) = \sum_{i=1}^{L}, f(\Sigma_i)$$
(3.91)

being $\{\rho\}$ the configuration of the system, $\Sigma_i \equiv \rho_i + \rho_{i+1}$ the total energy of the colliding particles and $f(\Sigma)$ a projection function which, together with the collisional rule (3.90), determines the dynamics of the system. The time dependence of variables ρ_i has been omitted for simplicity. Without the need of specifying the collisional probability $f(\Sigma)$, the authors derived the hydrodynamic equations in the large-size limit

$$\partial_t \rho_{\text{av}}(x,t) = -\partial_x J_{\text{av}}(x,t) + d_{\text{av}}(x,t) , \qquad (3.92)$$

where the "av" fields are averaged fields such $\langle \rho \rangle = \rho_{\rm av}$. The energy current J and dissipation rate d can be computed through the local equilibrium approximation, i.e. taking a Gaussian energy distribution on a site i and assuming that $F_2(\rho_i, \rho_{i+1}; t) \approx F_1(\rho_i, t)F_1(\rho_{i+1}, t)$. So, one can write

$$J_{\rm av}(x,t) = -D(\rho_{\rm av})\partial_x \rho_{\rm av} \,, \tag{3.93}$$

$$d_{\rm av}(x,t) = \nu R(\rho_{\rm av}), \qquad (3.94)$$

defining a diffusion coefficient $D(\rho)$, a transport coefficient $R(\rho)$ related to dissipation and a mesoscopic dissipation coefficient $\nu = (1 - \alpha^2)/2L^2$. The latter is non-vanishing in the large size limit only if $\alpha = 1 - \mathcal{O}(L^{-2})$ for large L: this is called *quasielastic limit* and will be assumed as well in Chap. 4, being strictly connected with the local equilibrium assumption. While the scaling of $1 - \alpha$ is needed to match the current and dissipation terms in Eq. (3.92), we have already seen that for the KMP model ($\alpha = 1$) the asymptotic distribution was the Boltzmann distribu-

3.3 Lattice Models 95

tion, so we expect that the asymptotic distribution in the quasielastic limit may be a perturbation of the equilibrium one.

The transport coefficients can be computed for a general f and read

$$D(\rho) = \frac{1}{6} \int_0^{+\infty} dr \, r^7 \, f(\rho r^2) e^{-r^2} \,, \tag{3.95a}$$

$$R(\rho) = \rho \int_0^{+\infty} dr \, r^5 \, f(\rho r^2) e^{-r^2} \,, \tag{3.95b}$$

under the local equilibrium assumption. Hydrodynamic equation (3.92) can be written in the fluctuating form

$$\partial_t \rho(x,t) = -\partial_x J(x,t) + d(x,t) , \qquad (3.96)$$

with $J(x,t) = \widetilde{J}(x,t) + \xi(x,t)$ and $d(x,t) = \widetilde{d}(x,t) + \eta(x,t)$. The idea is to split the fluctuating current and dissipation in two contributions: one from the average terms $\langle \widetilde{J} \rangle = J_{\rm av}, \, \langle \widetilde{d} \rangle = d_{\rm av}$, and the other from the noises taken as zero-average fluctuations, ξ and η . Microscopic dynamics allows to compute the noise correlations, yielding at the leading order in 1/L

$$\langle \xi(x,t)\xi(x',t')\rangle \sim \frac{1}{L}\sigma(\rho_{\rm av})\delta(x-x')\delta(t-t'),$$
 (3.97a)

$$\langle \eta(x,t)\eta(x',t')\rangle \sim \frac{1}{L^3}\nu^2\kappa(\rho)\delta(x-x')\delta(t-t')$$
, (3.97b)

so, the dissipation fluctuations are much smaller than the current fluctuations and therefore are neglected in the following. The noises have been proved to be Gaussian. The amplitude of the current noise is given by

$$\sigma(\rho) = 2\rho^2 D(\rho) \,, \tag{3.98}$$

relating the mobility $\sigma(\rho)$ to the diffusivity $D(\rho)$. This is a kind of *fluctuation-dissipation* relation, which is connected with the quasielastic limit introduced above. Again, this relation has not been assumed from some equilibrium relation, but derived from the microscopic dynamics. Finally, for a specific choice of $f(\Sigma)$, the time evolution of the energy in the HCS can be found, recovering the Haff's law in the hard spheres case, $f(\Sigma) \propto \sqrt{\Sigma}$; in the heated case, the stationary profiles of energy, current and dissipation can be derived as well. The model has been analyzed in the framework of MFT, confirming previous results and leading to new theoretical prediction on his fluctuating hydrodynamics.

The model of Prados, Lasanta and Hurtado introduced above has been a key guide to develop this thesis. I did not report the technical calculations, because many of them will be explained for the granular sheared model of Chap. 4; a rigorous derivation can be found in [53]. Finally, lattice models have been developed also to describe active matter: in 1995, Csahók and Vicsek developed a lattice model of active particles,

interlacing the Vicsek model of collective motion with lattice gas methods [54]. More recently, in 2011 Thompson et al. introduced a 1*d* model of run-and-tumble bacteria, hopping on a lattice without excluded volume, aiming at reproducing the observed features in off lattice run-and-tumble dynamics and deriving the fluctuating hydrodynamics of the system [42]. As it has been shown, lattice models lead to a huge number of theoretical predictions, especially on fluctuating quantities. The analytical power together with the phenomenological realism inspired us to derive the models in Part II.

References

- 1. K. Huang, Statistical Mechanics, 2nd edn. (Wiley, USA, 1987)
- N. Brilliantov, T. Pöschel (eds.), Kinetic Theory of Granular Gases (Oxford University Press, Oxford, 2004)
- 3. S. Chapman, T.G. Cowling, *The Mathematical Theory of Non-Uniform Gases*, 3rd edn. (Cambridge University Press, Cambridge, 1990)
- 4. J.H. Ferziger, H.G. Kaper, *Mathematical Theory of Transport Processes in Gases* (North Holland, 1972)
- 5. C.M. Bender, S.A. Orszag, Advanced Mathematical Methods for Scientists and Engineers (Springer, Berlin, 1999)
- J.J. Brey, J.W. Dufty, C.S. Kim, A. Santos, Hydrodynamics for granular flow at low density. Phys. Rev. E 58, 4638–4653 (1998). https://doi.org/10.1103/PhysRevE.58.4638
- M. Cencini, F. Cecconi, A. Vulpiani. Chaos: From Simple Models to Complex Systems (World Scientific, 2010)
- 8. L. Landau, E. Lifshitz, *Fluid Mechanics*. Course of Theoretical Physics, vol. 6 (Pergamon Press, 1987)
- P.G. Drazin, W.H. Reid, Hydrodynamic Stability (Cambridge University Press, Cambridge, 2004)
- I. Goldhirsch, G. Zanetti, Clustering instability in dissipative gases. Phys. Rev. Lett. 70, 1619– 1622 (1993). https://doi.org/10.1103/PhysRevLett.70.1619
- M.C. Marchetti, J.E. Joanny, S. Ramaswamy, T.B. Liverpool, J. Prost, M. Rao, R.A. Simha, Hydrodynamics of soft active matter. Rev. Mod. Phys. 85, 1143–1189 (2013). https://doi.org/ 10.1103/RevModPhys.85.1143
- 12. E. Bertin, M. Droz, G. Grégoire, Boltzmann and hydrodynamic description for self-propelled particles. Phys. Rev. E **74**, 022101 (2006). https://doi.org/10.1103/PhysRevE.74.022101
- E. Bertin, M. Droz, G. Grégoire, Hydrodynamic equations for self-propelled particles: microscopic derivation and stability analysis. J. Phys. A. Math. Theor. 42(44), 445001 (2009). https://doi.org/10.1088/1751-8113/42/44/445001
- A. Peshkov, E. Bertin, F. Ginelli, H. Chaté, Boltzmann-Ginzburg-Landau approach for continuous descriptions of generic Vicsek-like models. Eur. Phys. J. Spec. Top. 223(7), 1315–1344 (2014). https://doi.org/10.1140/epjst/e2014-02193-y
- J. Toner, Y. Tu, Long-range order in a two-dimensional dynamical XY model: how birds fly together. Phys. Rev. Lett. 75, 4326–4329 (1995). https://doi.org/10.1103/PhysRevLett.75.4326
- J. Toner, Y. Tu, Flocks, herds, and schools: a quantitative theory of flocking. Phys. Rev. E 58, 4828–4858 (1998). https://doi.org/10.1103/PhysRevE.58.4828
- T. Vicsek, A. Zafeiris, Collective motion. Phys. Rep. 517(3–4):71–140 (2012). http://www.sciencedirect.com/science/article/pii/S0370157312000968, https://doi.org/10.1016/j.physrep.2012.03.004

References 97

 J. Toner, Y. Tu, S. Ramaswamy, Hydrodynamics and phases of flocks. Adv. Phys. 318(1):170–244 (2005) [Special Issue]. http://www.sciencedirect.com/science/article/pii/S0003491605000540, https://doi.org/10.1016/j.aop.2005.04.011

- T. Ihle, Kinetic theory of flocking: derivation of hydrodynamic equations. Phys. Rev. E 83, 030901 (2011). https://doi.org/10.1103/PhysRevE.83.030901
- A. Baskaran, M.C. Marchetti, Hydrodynamics of self-propelled hard rods. Phys. Rev. E 77, 011920 (2008). https://doi.org/10.1103/PhysRevE.77.011920
- A.P. Solon, M.E. Cates, J. Tailleur, Active Brownian particles and run-and-tumble particles: a comparative study. Eur. Phys. J. Spec. Top. 224(7), 1231–1262 (2015). https://doi.org/10. 1140/epjst/e2015-02457-0
- B. Hancock, A. Baskaran, Statistical mechanics and hydrodynamics of self-propelled hard spheres. J. Stat. Mech. (Theor. Exp.) 2017(3), 033205 (2017). http://stacks.iop.org/1742-5468/ 2017/i=3/a=033205, https://doi.org/10.1088/1742-5468/aa5ed1
- 23. C. Gardiner, Stochastic Methods. A Handbook for the Natural and Social Sciences, 4th edn. (Springer, Berlin, 2009)
- U. Marini Bettolo Marconi, A. Puglisi, L. Rondoni, A. Vulpiani, Fluctuation–dissipation: response theory in statistical physics. Phys. Rep. 461(4–6), 111 195 (2008). http://www.sciencedirect.com/science/article/pii/S0370157308000768, https://doi.org/10.1016/j.physrep.2008.02.002
- 25. R. Kubo, M. Toda, N. Hashitsume, *Statistical Physics Ii: Nonequilibrium Statistical Mechanics* (Springer Science & Business Media, Berlin, 2012)
- M. Bixon, R. Zwanzig, Boltzmann-Langevin equation and hydrodynamic fluctuations. Phys. Rev. 187, 267–272 (1969). https://doi.org/10.1103/PhysRev.187.267
- J.J. Brey, P. Maynar, M.I. García de Soria, Fluctuating hydrodynamics for dilute granular gases. Phys. Rev. E 79, 051305 (2009). https://doi.org/10.1103/PhysRevE.79.051305
- 28. A. Puglisi, Transport and Fluctuations in Granular Fluids (Springer, Berlin, 2014)
- T.P.C. van Noije, M.H. Ernst, R. Brito, J.A.C. Orza, Mesoscopic theory of granular fluids. Phys. Rev. Lett. 79, 411–414 (1997). https://doi.org/10.1103/PhysRevLett.79.411
- T.P.C. van Noije, M.H. Ernst, E. Trizac, I. Pagonabarraga, Randomly driven granular fluids: large-scale structure. Phys. Rev. E 59, 4326–4341 (1999). https://doi.org/10.1103/PhysRevE. 59,4326
- G. Costantini, A. Puglisi, Fluctuating hydrodynamics in a vertically vibrated granular fluid with gravity. Phys. Rev. E 84, 031307 (2011). https://doi.org/10.1103/PhysRevE.84.031307
- A. Puglisi, V. Loreto, U. Marini, Bettolo Marconi, A. Petri, A. Vulpiani, Clustering and nongaussian behavior in granular matter. Phys. Rev. Lett. 81, 3848–3851 (1998). https://doi.org/ 10.1103/PhysRevLett.81.3848
- G. Gradenigo, A. Sarracino, D. Villamaina, A. Puglisi, Fluctuating hydrodynamics and correlation lengths in a driven granular fluid. J. Stat. Mech. (Theor. Exp.) 2011(08), P08017 (2011). https://doi.org/10.1088/1742-5468/2011/08/P08017
- G. Gradenigo, A. Sarracino, D. Villamaina, A. Puglisi, Non-equilibrium length in granular fluids: From experiment to fluctuating hydrodynamics. EPL (Europhys. Lett.) 96(1), 14004 (2011). https://doi.org/10.1209/0295-5075/96/14004
- L. Bertini, A. De Sole, D. Gabrielli, G. Jona-Lasinio, C. Landim, Macroscopic fluctuation theory for stationary non-equilibrium states. J. Stat. Phys. 107(3), 635–675 (2002). https://doi. org/10.1023/A:1014525911391
- L. Bertini, A. De Sole, D. Gabrielli, G. Jona-Lasinio, C. Landim, Macroscopic fluctuation theory. Rev. Mod. Phys. 87, 593–636 (2015). https://doi.org/10.1103/RevModPhys.87.593
- 37. A. Vulpiani, F. Cecconi, M. Cencini, A. Puglisi, D. Vergni, *Large Deviations in Physics* (Springer, Berlin, 2014)
- 38. G. Gallavotti, E.G.D. Cohen, Dynamical ensembles in nonequilibrium statistical mechanics. Phys. Rev. Lett. **74**, 2694–2697 (1995). https://doi.org/10.1103/PhysRevLett.74.2694
- C. Jarzynski, Nonequilibrium equality for free energy differences. Phys. Rev. Lett. 78, 2690–2693 (1997). https://doi.org/10.1103/PhysRevLett.78.2690

- J.L. Lebowitz, H. Spohn, A Gallavotti-cohen-type symmetry in the large deviation functional for stochastic dynamics. J. Stat. Phys. 95(1), 333–365 (1999). https://doi.org/10.1023/A:1004589714161
- U. Seifert, Stochastic thermodynamics, fluctuation theorems and molecular machines. Rep. Prog. Phys. 75(12), 126001 (2012). https://doi.org/10.1088/0034-4885/75/12/126001
- A.G. Thompson, J. Tailleur, M.E. Cates, R.A. Blythe, Lattice models of nonequilibrium bacterial dynamics. J. Stat. Mech. (Theor. Exp.) 2011(02), P02029 (2011). https://doi.org/10.1088/1742-5468/2011/02/P02029
- 43. B. Derrida, Non-equilibrium steady states: fluctuations and large deviations of the density and of the current. J. Stat. Mech. (Theor. Exp.) **2007**(07), P07023 (2007). https://doi.org/10.1088/1742-5468/2007/07/P07023
- 44. J. Marro, R. Dickman, *Nonequilibrium Phase Transitions in Lattice Models* (Cambridge University Press, Cambridge, 2005)
- 45. C. Kipnis, C. Marchioro, E. Presutti, Heat flow in an exactly solvable model. J. Stat. Phys. 27(1), 65–74 (1982). https://doi.org/10.1007/BF01011740
- S. Alexander, J. Bernasconi, W.R. Schneider, R. Orbach, Excitation dynamics in random one-dimensional systems. Rev. Mod. Phys. 53, 175–198 (1981). https://doi.org/10.1103/ RevModPhys.53.175
- 47. B. Derrida, Y. Pomeau, Classical diffusion on a random chain. Phys. Rev. Lett. 48, 627–630 (1982). https://doi.org/10.1103/PhysRevLett.48.627
- 48. B. Derrida, Velocity and diffusion constant of a periodic one-dimensional hopping model. J. Stat. Phys. **31**(3), 433–450 (1983). https://doi.org/10.1007/BF01019492
- A. Baldassarri, U. Marini, Bettolo Marconi, A. Puglisi, Cooling of a lattice granular fluid as an ordering process. Phys. Rev. E 65, 051301 (2002). https://doi.org/10.1103/PhysRevE.65. 051301
- A. Baldassarri, A. Puglisi, U. Marini, Bettolo Marconi, Kinetic models of inelastic gases. Math. Models Methods Appl. Sci. 12(07), 965–983 (2002). https://doi.org/10.1142/ S0218202502001982
- 51. A. Prados, A. Lasanta, P.I. Hurtado, Large fluctuations in driven dissipative media. Phys. Rev. Lett. 107, 140601 (2011). https://doi.org/10.1103/PhysRevLett.107.140601
- A. Prados, A. Lasanta, P.I. Hurtado, Nonlinear driven diffusive systems with dissipation: fluctuating hydrodynamics. Phys. Rev. E 86, 031134 (2012). https://doi.org/10.1103/PhysRevE. 86.031134
- A. Lasanta, Algunas propiedades de los estados estacionarios de sistemas disipativos sencillos,
 Ph.D. thesis, Universidad de Granada, 2014
- Z. Csahók, T. Vicsek, Lattice-gas model for collective biological motion. Phys. Rev. E 52, 5297–5303 (1995). https://doi.org/10.1103/PhysRevE.52.5297

Part II Fluctuating Hydrodynamics of Granular and Active Matter: Lattice Models

Chapter 4 Granular Lattice: Fluctuating Hvdrodynamics



Jusqu'ici tout va bien

(La Haine)

Inspired from the works of Baldassarri et al. [1] and Prados et al. [2], we formulated a granular lattice model to derive fluctuating hydrodynamics from microscopic ingredients under controlled assumptions, considering only shear modes on a granular linear chain [3]. The evolution of the system conserves momentum and dissipates energy, as in granular collisions. The new model is different from the previous proposals in a few crucial aspects. In [1], the velocity field evolved under the enforcement of the so-called kinematic constraint, which is disregarded here. In [2], only the energy field was considered, therefore momentum conservation was absent. The results I present especially focus on the hydrodynamic behavior of the model; the analysis of velocity distribution evolution and a detailed approach to a mesoscopic fluctuation theory of our model can be found respectively in [4–6].

The aim of the model is reproducing the shear hydrodynamics of a granular system and deriving its fluctuating behavior starting from microscopic rules. As it has been shown in Sect. 3.1.2, there is a range of sizes of granular systems such as the only linearly unstable mode in the HCS is the shear mode: this implies that the velocity field is incompressible and the density does not evolve from its initial uniform configuration. Such a regime may be observed for a certain amount of time (longer and longer as the elastic limit is approached). In two dimensions, granular

The material in this chapter is mostly directed adapted from the following Springer publication and is reproduced here with permission: Alessandro Manacorda, Carlos A. Plata, Antonio Lasanta, Andrea Puglisi, and Antonio Prados. Lattice models for granular-like velocity fields: Hydrodynamic description. *J. Stat. Phys.*, 164(4):810–841, Aug 2016.

hydrodynamic equations (3.36) are obeyed with constant density and, for instance, $u_x = 0$ whereas the hydrodynamic fields u_y and T only depend on x, leading to

$$\partial_t u_{\nu}(x,t) = (nm)^{-1} \partial_x [\eta \partial_x u_{\nu}(x,t)], \tag{4.1a}$$

$$\partial_t T(x,t) = \frac{1}{n} \eta [\partial_x u_y(x,t)]^2 + \frac{1}{n} \partial_x [\kappa \partial_x T(x,t)] - \zeta T. \tag{4.1b}$$

In Sect. 4.2 we will see that our lattice model is well described, in the continuum limit, by the same equations.

It is interesting to put in evidence that Eq. (4.1) also sustain also particular stationary solutions. Seeking time-independent solutions thereof, one finds

$$\partial_x [\eta \partial_x u_y^{(s)}(x)] = 0 , \quad \eta [\partial_x u_y^{(s)}(x)]^2 = -\partial_x [\kappa \partial_x T^{(s)}(x)] + n \zeta T^{(s)}(x) . \quad (4.2)$$

The general situation is that both the average velocity and temperature profiles are inhomogeneous: this is the so-called Couette flow state, which also exists in molecular fluids. Yet, in granular fluids, there appears a new steady state in which the temperature is homogeneous throughout the system, $T^{(s)}(x) \equiv T$, and the average velocity has a constant gradient, $\partial_x u_y \equiv a$: this is the Uniform Shear Flow (USF) state, characterized by the equations

$$\partial_x^2 u_y^{(s)}(x) = 0, \quad \eta[\partial_x u_y^{(s)}(x)]^2 = nk_B \zeta T^{(s)}. \tag{4.3}$$

Such a steady state is peculiar of granular gases where the viscous heating term is locally compensated by the energy sink term. In a molecular fluid, this compensation is lacking and viscous heating must be balanced by a continuous heat flow toward the boundaries, which entails a gradient in the temperature field, typical of the Couette flow.

The formal definition of the model is given in Sect. 4.1. In Sect. 4.2 the hydrodynamic equations are derived as the continuum limit of the microscopic balance equations. Section 4.3 is devoted to the analysis of some relevant physical states such as the Homogeneous Cooling State (HCS), the Uniform Shear Flow (USF) and the Couette flow. In Sect. 4.4 the fluctuating currents are defined and their correlations are derived. Section 4.5 contains the numerical analysis of hydrodynamic states and fluctuating currents discussed in previous sections.

4.1 Definition of the Model

In this section, the granular model is introduced by means of a Markovian process, defining an evolution equation of the phase-space probability distribution P_N and later deriving the evolution equation of the single particle distribution P_1 . In the rest of the chapter, these quantities will not be part of the analysis, as we will focus on

hydrodynamic fields. Nevertheless, the present section shows that a "kinetic" derivation of hydrodynamic equations is possible, following the approach of Sect. 2.1. Furthermore, the Markovian description is transparent and without ambiguities, illustrating also the residence-time algorithm which will actually be used in simulations. In our work, the derivation of hydrodynamics from microscopic balance equations preceded in time the Markovian description; since the two procedures have shown to be equivalent, the microscopic balance equations are contained in Appendix A.1 for the sake of completeness.

4.1.1 Master Equation for the Lattice Model

The model is defined on a 1d lattice with N sites, but it can be generalized to higher dimensions. In each site there is a scalar velocity v_i , so that the state of the system is determined by the vector $\mathbf{v} \in \mathbb{R}^N$. The evolution is a Markov jump process which - in general - takes place in continuous time τ , each jump representing a collision. The latter are counted by the integer $p \in \{0, 1, 2...\}$. The random time increment $\delta \tau_p$ between two collisions $p \to p+1$ is given by

$$\delta \tau_p = \Omega_p(L)^{-1} |\ln \chi|, \quad \Omega_p(L) = \omega \sum_{l=1}^L |v_{l,p} - v_{l+1,p}|^{\beta},$$
 (4.4)

in which χ is a stochastic variable homogeneously distributed in the interval (0,1), ω is a constant frequency that determines the time scale, and L is the number of pairs that can collide (i.e. L=N when periodic boundary conditions are considered, or L=N+1 when thermostatted boundaries are taken into account). The physical meaning of Eq. (4.4) is clear: $\Omega_p(L)$ is the total exit rate from the state of the system, as given by its velocity configuration ${\bf v}$, at time p, and the time increment $\delta \tau$ follows the distribution $P(\delta \tau) = \Omega_p(L) \exp[-\Omega_p(L)\delta \tau]$ as in a Poissonian process. The parameter $\beta \geq 0$ affects the collision rate: for $\beta = 0$, the collision rate is independent of the relative velocity, similarly to the case of pseudo-Maxwell molecules [1]. For this reason, we refer to $\beta = 0$ as the MM case, while $\beta = 1$ and $\beta = 2$ are analogous to the hard spheres (HS) [7] and "very hard-core" [8, 9] collisions, respectively.

It is convenient to define $\Delta_l = v_l - v_{l+1}$, and to introduce the operator b_l , which evolves the vector **v** by colliding the pair (l, l+1) according to the granular collision rule (2.31), i.e.

$$\hat{b}_{l}(v_{1},...,v_{l},v_{l+1},...,v_{N}) = \left(v_{1},...,v_{l} - \frac{1+\alpha}{2}\Delta_{l},v_{l+1} + \frac{1+\alpha}{2}\Delta_{l},...,v_{N}\right),$$
(4.5)

where $\alpha \in [0, 1]$ is the restitution coefficient. After the *p*-th collision the momentum is conserved, $v_{l,p} + v_{l+1,p} = v_{l,p+1} + v_{l+1,p+1}$, while the energy, if $\alpha < 1$, is not:

$$v_{l,p+1}^2 + v_{l+1,p+1}^2 - v_{l,p}^2 - v_{l+1,p}^2 = (\alpha^2 - 1)\Delta_{l,p}^2/2 < 0.$$
 (4.6)

Also, note that for a generic function of the velocities $f(\mathbf{v})$ one has

$$\int d\mathbf{v}' |v_l' - v_{l+1}'|^{\beta} \delta(\mathbf{v} - \hat{b}_l \mathbf{v}') f(\mathbf{v}') = \frac{|\Delta_l|^{\beta}}{\alpha^{\beta+1}} f(\hat{b}_l^{-1} \mathbf{v}).$$
 (4.7)

The operator \hat{b}_l^{-1} is the inverse of \hat{b}_l , that is, it changes the post-collisional velocities into the pre-collisional ones when the colliding pair is (l, l+1).

The continuous time Markov process is fully described by the two-time conditional probability $P_N(\mathbf{v}, \tau | \mathbf{v}_0, \tau_0)$ with $\tau \ge \tau_0$, which evolves according to the following forward Master Equation,

$$\partial_{\tau} P_{N}(\mathbf{v}, \tau | \mathbf{v}_{0}, \tau_{0}) = \int d\mathbf{v}' W(\mathbf{v} | \mathbf{v}') P_{N}(\mathbf{v}', \tau | \mathbf{v}_{0}, \tau_{0}) - \Omega(\mathbf{v}) P_{N}(\mathbf{v}, \tau | \mathbf{v}_{0}, \tau_{0}), \quad (4.8)$$

where the transition rates $W(\mathbf{v}'|\mathbf{v})$ and the total exit rate $\Omega(\mathbf{v})$ are given by

$$W(\mathbf{v}'|\mathbf{v}) = \omega \sum_{l=1}^{N} |\Delta_l|^{\beta} \delta(\mathbf{v}' - \hat{b}_l \mathbf{v}), \quad \Omega(\mathbf{v}) = \int d\mathbf{v}' W(\mathbf{v}'|\mathbf{v}) = \omega \sum_{l=1}^{N} |\Delta_l|^{\beta}.$$
(4.9)

The Master Equation can be simplified by making use of (4.7), with the final result

$$\partial_{\tau} P_{N}(\mathbf{v}, \tau | \mathbf{v}_{0}, \tau_{0}) = \omega \sum_{l=1}^{L} |\Delta_{l}|^{\beta} \left[\frac{P_{N}(\hat{b}_{l}^{-1}\mathbf{v}, \tau | \mathbf{v}_{0}, \tau_{0})}{\alpha^{\beta+1}} - P_{N}(\mathbf{v}, \tau | \mathbf{v}_{0}, \tau_{0}) \right]. \tag{4.10}$$

The conditional probability distribution $P_N(\mathbf{v}, \tau | \mathbf{v}_0, \tau_0)$ is the solution of the above equation with the initial condition $P_N(\mathbf{v}, \tau_0 | \mathbf{v}_0, \tau_0) = \delta(\mathbf{v} - \mathbf{v}_0)$. On the other hand, the one-time probability distribution $P_N(\mathbf{v}, \tau)$ verifies the same equation but with an arbitrary (normalized) initial condition $P_N(\mathbf{v}, \tau)$.

Residence time algorithms that give a numerical integration of the master equation in the limit of infinite trajectories [10, 11] show that either Eqs. (4.8) or (4.10) is the Master equation for a continuous time jump Markov process consisting in the following chain of events:

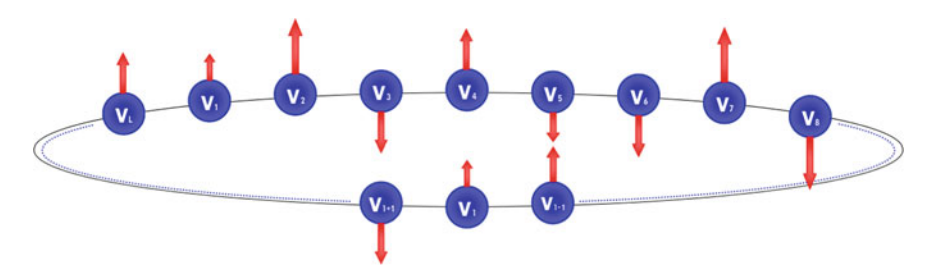
- 1. at time τ , a random "free time" $\tau_f \ge 0$ is extracted with a probability density $\Omega(\mathbf{v})\exp[-\Omega(\mathbf{v})\tau_f]$ which depends upon the state of the system \mathbf{v} ;
- 2. time is advanced by such a free time $\tau \to \tau + \tau_f$;
- 3. the pair (l, l + 1) is chosen to collide with probability $\omega |\Delta_l|^{\beta} / \Omega(\mathbf{v})$;
- 4. the process is repeated from step 1.

The Master equation derived above can be considered our "Liouville equation", that is, it evolves the probability in full phase-space. It is tempting, from such equation, to derive a Lyapunov (or "H") functional which is minimized by the dynamics, as it is customary for Markov processes [12]. However, in the general case our system

does not admit an asymptotic steady state, apart from the trivial zero, and therefore the usual H function (which relies upon the existence of the steady state) cannot be built. However, this programme can be carried on in the presence of appropriate boundary conditions, e.g. thermostats, which allow the system to reach a steady state [13, 14]. Recently, an *H*-theorem for the driven system has been formulated and proven to hold under certain mathematical assumptions on the initial distribution [15].

4.1.2 Physical Interpretation

The model, if taken literally, implies that there is no mass transport, particles are at fixed positions and they only exchange momentum and kinetic energy. As discussed above, this can be a valid assumption in an incompressible regime which is expected when the velocity field is divergence free, for instance during the first stage of the development of the shear instability, or in the so-called Uniform Shear Flow. We are also disregarding the so-called kinematic constraint, which is fully considered in [1]: indeed a colliding pair is chosen independently of the sign of its relative velocity, while in a real collision only approaching particles can collide. Even without the kinematic constraint, the model has a straightforward physical interpretation: the dynamics occurs inside an elongated 2d or 3d channel, the lattice sites represent the positions on the long axis, while the transverse (shorter) directions are ignored; the velocity of the particles do not represent their motion along the lattice axis but rather along a perpendicular one, see Fig. 4.1. One may easily imagine that the (hidden) component along the lattice axis is of the order of the perpendicular component, but with random direction. On the one hand, this justifies the choice of disregarding the kinematic constraint, while on the other, the collision rate may still be considered proportional to some power β of the velocity difference (in absolute value). A fair confirmation of this interpretation comes from the average hydrodynamics equations derived in Sect. 4.2, which, as anticipated in the introduction, replicate the transport equations (4.1) for granular gases in d > 1 restricted to the shear (transverse) velocity field.



 $\textbf{Fig. 4.1} \quad \text{A sketch of the granular lattice model with periodic boundaries. The velocities are represented by red arrows}$

4.1.3 Evolution Equation for the One-Particle Distribution

Let us now apply the usual procedure of kinetic theory and map the Master equation into a BBGKY hierarchy. In particular, we focus on the evolution equation for the one-particle distribution function at site l and at time τ , which we denote by $P_1(v; l, \tau)$. The behavior of the one-particle distribution P_1 will be deeply analyzed in [6]. By definition,

$$P_1(v; l, \tau) = \int d\mathbf{v} P_N(\mathbf{v}, \tau) \delta(v_l - v). \tag{4.11}$$

It is easy to show that none of the terms in the sum (4.10) contribute to the time evolution of P_1 except those corresponding to l-1 and l, because the collisions involving the pairs (l-1, l) and (l, l+1) are the only ones which change the velocity at site l. Therefore,

$$\partial_{\tau} P_{1}(v; l, \tau) = \omega \times \left\{ \int_{-\infty}^{+\infty} dv_{l-1} |\Delta_{l-1}|^{\beta} \left[\frac{P_{2}(\hat{b}_{l-1}^{-1}\{v_{l-1}, v\}; l-1, l, \tau)}{\alpha^{\beta+1}} - P_{2}(v_{l-1}, v; l-1, l, \tau) \right] + \int_{-\infty}^{+\infty} dv_{l+1} |\Delta_{l}|^{\beta} \left[\frac{P_{2}(\hat{b}_{l}^{-1}\{v, v_{l+1}\}; l, l+1, \tau)}{\alpha^{\beta+1}} - P_{2}(v, v_{l+1}; l, l+1, \tau) \right] \right\},$$
(4.12)

where, for the sake of simplicity, we also denote by \hat{b}_l^{-1} the backward collisional operator acting only on the velocities of the colliding particles. In the equation above, we have the two-particles probability distribution $P_2(v,v';l,l+1,\tau)$ for finding the particles at the l-th and (l+1)-th sites with velocities v and v', respectively. For the special case $\beta=0$, the evolution equation for P_1 can be further simplified, because the terms on the rhs of (4.12) coming from the loss (negative) terms of the master equation can be integrated. We get

$$\partial_{\tau} P_{1}(v; l, \tau) = \omega \left[-2P_{1}(v; l, \tau) + \frac{1}{\alpha} \int_{-\infty}^{+\infty} dv_{l-1} P_{2}(\hat{b}_{l-1}^{-1} \{v_{l-1}, v\}; l-1, l, \tau) + \frac{1}{\alpha} \int_{-\infty}^{+\infty} dv_{l+1} P_{2}(\hat{b}_{l}^{-1} \{v, v_{l+1}\}; l, l+1, \tau) \right].$$

$$(4.13)$$

The equation for P_1 , either (4.12) for a generic β or (4.13) for $\beta = 0$, could be converted to a closed equation for P_1 by introducing the *Molecular Chaos* assumption, which in our present context means that

$$P_2(v, v'; l, l+1, \tau) = P_1(v; l, \tau) P_1(v'; l+1, \tau) + O(L^{-1}).$$
(4.14)

By neglecting the $O(L^{-1})$ terms in (4.14), we obtain a pseudo-Boltzmann or kinetic equation for P_1 , which determines the evolution of the one-time and one-particle averages under the assumption of $O(L^{-1})$ correlations. Note that since $L/N \to 1$ for a large system, independently of the boundary conditions, orders of inverse powers of N and L are utterly equivalent. It is important to stress that the range of validity of assumption (4.14) is assessed in numerical simulations, see Sect. 4.5. In Chap. 5 the conjecture that two-particle correlations scale with L^{-1} will be proven analytically. Note that this "smallness" of two-particle correlations do not prevent them from being long-ranged.

The structure of the kinetic equation for P_1 is thus much simpler for the MM case. In particular, we see along the next sections that the evolution equations for the moments are closed under the molecular chaos assumption, without further knowledge of the probability distribution P_1 . This is the reason why, from now on, we restrict ourselves to the MM case $\beta = 0$, since the mathematical treatment needed for the $\beta \neq 0$ case is much more complicated and then is deferred to further studies.

4.2 Hydrodynamics

In the following section, we derive the hydrodynamic behavior for $\beta=0$, in which the evolution equations for the averages are closed. Moreover, the MM case makes it possible to grasp the essential points.

4.2.1 Microscopic Balance Equations

From Eq. (4.8) it is straightforward to get the evolution rule for $v_{l,p}$ (for any site l) at collision index p:

$$v_{l,p+1} - v_{l,p} = -j_{l,p} + j_{l-1,p} , (4.15)$$

where the momentum current, that is, the flux of momentum from site l to site l+1 at the p-th collision reads

$$j_{l,p} = \frac{1+\alpha}{2} \Delta_{l,p} \delta_{y_p,l} , \qquad (4.16)$$

Here $\delta_{y_p,l}$ is Kronecker's δ and $y_p \in [1, L]$ is a random integer which selects the colliding pair.

The corresponding equation for the energy, obtained by squaring (4.15), reads

$$v_{l,p+1}^2 - v_{l,p}^2 = -J_{l,p} + J_{l-1,p} + d_{l,p}. (4.17)$$

Again, the energy current from site l to site l + 1 is defined as

$$J_{l,p} = (v_{l,p} + v_{l+1,p})j_{l,p}. (4.18)$$

In addition, the energy dissipation at site l is

$$d_{l,p} = (\alpha^2 - 1)[\delta_{y_p,l} \Delta_{l,p}^2 + \delta_{y_p,l-1} \Delta_{l-1,p}^2]/4 < 0.$$
 (4.19)

The total energy of the system at the *p*-th collision is $E_p = \sum_{l=1}^{N} v_{l,p}^2$.

It is customary to define, as relevant fields for hydrodynamics, the following local averages, at a given collision number p, over initial conditions and noise realizations:

$$u_{l,p} = \langle v_{l,p} \rangle, \qquad E_{l,p} = \langle v_{l,p}^2 \rangle, \qquad T_{l,p} = E_{l,p} - u_{l,p}^2.$$
 (4.20)

A few words should be spent for commenting the choice of the relevant fields: in the usual conservative kinetic theory, the velocity and energy fields are naturally "slow" because of their global conservation (recall that there is no density transport in the model, as discussed before in Sect. 4.1.2). For a granular gas, the energy is not necessarily slow: however, when α approaches 1, as it is in many physical situations, the total energy evolves quite slowly and can be thought of as a *quasi-slow* variable. In the following, we show that the continuum limit necessary to get a hydrodynamic description requires $\alpha \to 1$ if dissipation of energy and diffusion take place over the same time scale. It is important to realize, however, that such an elastic limit is singular here: in 1d, when $\alpha = 1$ the dynamics corresponds to a pure relabelling without mixing or ergodicity.

The microscopic equations for the evolution of averages at time (number of collisions) p at site l are obtained by averaging equations (4.15) and (4.17):

$$u_{l,p+1} - u_{l,p} = -\langle j_{l,p} \rangle + \langle j_{l-1,p} \rangle,$$
 (4.21)

$$E_{l,p+1} - E_{l,p} = -\langle J_{l,p} \rangle + \langle J_{l-1,p} \rangle + \langle d_{l,p} \rangle. \tag{4.22}$$

For the case of MM ($\beta=0$, i.e. all sites collide with the same probability) we have that $\langle \delta_{y_p,l} f(\mathbf{v}_p) \rangle = L^{-1} \langle f(\mathbf{v}_p) \rangle$ and therefore we can write the averages as

$$\langle j_{l,p} \rangle = \frac{1+\alpha}{2L} \langle \Delta_{l,p} \rangle ,$$
 (4.23a)

$$\langle J_{l,p} \rangle = \frac{1+\alpha}{2L} \langle \Delta_{l,p} (v_{l,p} + v_{l+1,p}) \rangle , \qquad (4.23b)$$

$$\langle d_{l,p} \rangle = \frac{\alpha^2 - 1}{4L} \langle \Delta_{l,p}^2 + \Delta_{l-1,p}^2 \rangle. \tag{4.23c}$$

From these equations, it is readily obtained that

$$\langle j_{l,p} \rangle = \frac{1+\alpha}{2L} \left(u_{l,p} - u_{l+1,p} \right) , \qquad (4.24a)$$

$$\langle J_{l,p} \rangle = \frac{1+\alpha}{2L} \left(T_{l,p} - T_{l+1,p} + u_{l,p}^2 - u_{l+1,p}^2 \right)$$
 (4.24b)

$$\langle d_{l,p} \rangle = \frac{\alpha^2 - 1}{4L} \left[2T_{l,p} + T_{l+1,p} + T_{l-1,p} \right] ,$$

$$+2\left(u_{l,p}-\frac{u_{l+1,p}+u_{l-1,p}}{2}\right)^{2}+\frac{1}{2}(u_{l+1,p}-u_{l-1,p})^{2}$$
 (4.24c)

In order to write the average dissipation, we have neglected $O(L^{-1})$ terms, since we have made use of the molecular chaos approximation, more specifically of the equality $\langle v_{l,p}v_{l\pm 1,p}\rangle = u_{l,p}u_{l\pm 1,p} + O(L^{-1})$.

Had we considered $\beta \neq 0$, we would have had an extra factor $|\Delta_{l,p}|^{\beta}$ in the averages on the rhs of (4.23). This extra factor would have made it necessary, apart from the "molecular chaos" hypothesis, to use further assumptions about the one-particle distribution function. More specifically, we would have needed to know its shape, at least in some approximation scheme, to calculate the moments in the average currents and dissipation in terms of the hydrodynamic fields u and T, that is, the so-called constitutive relations.

4.2.2 Balance Equations in the Continuum Limit

We now assume that $u_{l,p}$ and $E_{l,p}$ are smooth functions of space and time and introduce a continuum, "hydrodynamic", limit (CL). First, the macroscopic space and time variables (x,t) are defined which are related to the microscopic ones (l,p) through size-dependent factors:

$$x = l/L, \quad t = p/L^3.$$
 (4.25)

Note that both x and t are dimensionless variables. The choice of the above scalings is dictated by the aim of: (i) working with a "reduced" unit size to prevent L factors enter into the solutions through the boundary conditions, and (ii) matching the dominant L dependence on the right hand side and left hand side of the balance equations. With the identification $f_{l,p} = f(l/L, p/L^3)$, we say that f(x, t) is a smooth function if

$$f_{l\pm 1,p} - f_{l,p} = \pm L^{-1} \partial_x f(x,t) + O(L^{-2}),$$
 (4.26)

$$f_{l,p\pm 1} - f_{l,p} = \pm L^{-3} \partial_t f(x,t) + O(L^{-6})$$
 (4.27)

It is natural, on the scales defined by the CL, to define the mesoscopic fields u(x, t), E(x, t) and T(x, t) such that

$$u_{l,p} = u(l/L, p/L^3), \quad E_{l,p} = E(l/L, p/L^3), \quad T_{l,p} = T(l/L, p/L^3).$$
 (4.28)

and assume them to be smooth.

Using these definitions and the smoothness assumption, one finds that each discrete spatial derivative in Eqs. (4.21) and (4.22) introduces a L^{-1} leading factor. Then, the difference between the current terms in the balance equations is of the order of L^{-3} , because the average currents $\langle j_{l,p} \rangle$ and $\langle J_{l,p} \rangle$ are of the order of L^{-2} , as we have discrete derivatives of the currents therein. Those terms, therefore, perfectly balance the $1/L^3$ dominant scaling on the left-hand side, i.e. the time-derivative. Since $\langle d_{l,p} \rangle$ is of the order of $(1-\alpha^2)/L$, to match the scaling $1/L^3$ of the other terms, we define the *macroscopic inelasticity*

$$\nu = (1 - \alpha^2)L^2 \,, \tag{4.29}$$

and assume it to be order 1 when the limit is taken. This choice implies that when $L \to \infty$ one has $\alpha \to 1$, that is, microscopic collisions are quasi-elastic.

From a mathematical point of view, the following results for the average hydrodynamic behavior become exact in the double limit $\alpha \to 1$, $L \to \infty$ but finite $\nu = (1-\alpha^2)L^2$, provided that the initial conditions are smooth in the sense given by Eq. (4.26). Nonetheless, for a large-size system, the following results will hold over a certain time window, which is expected to increase as its size L increases. An analysis of the limits of validity of our hydrodynamic equations is carried out in Sect. 4.3.4.

By defining the average mesoscopic currents

$$j_{\text{av}}(x,t) = \lim_{L \to \infty} L^2 \langle j_{l,p} \rangle , \quad J_{\text{av}}(x,t) = \lim_{L \to \infty} L^2 \langle J_{l,p} \rangle ,$$
 (4.30)

and the average mesoscopic dissipation of energy

$$d_{\rm av}(x,t) = \lim_{L \to \infty} L^3 \langle d_{l,p} \rangle , \qquad (4.31)$$

one gets the CL of (4.21) and (4.22), which are

$$\partial_t u(x,t) = -\partial_x j_{av}(x,t) , \qquad (4.32a)$$

$$\partial_t E(x,t) = -\partial_x J_{\text{av}}(x,t) + d_{\text{av}}(x,t). \tag{4.32b}$$

Therein, the average currents and dissipation follow from (4.30), (4.31) and (4.24), with the result

$$j_{\rm av}(x,t) = -\partial_x u(x,t) \,, \tag{4.33a}$$

111

$$J_{\text{av}}(x,t) = -\partial_x \left[u^2(x,t) + T(x,t) \right], \qquad (4.33b)$$

$$d_{\rm av}(x,t) = -\nu T \ . \tag{4.33c}$$

Note that (i) $1 + \alpha$ has been replaced by 2, because $\alpha^2 = 1 - \nu L^{-2}$, and we have already neglected L^{-1} terms and (ii) $J_{av}(x,t) = -\partial_x E(x,t)$, with $E(x,t) = u^2(x,t) + T(x,t)$, consistently with (4.20).

Taking into account the above expressions, the following average hydrodynamic equations are obtained,

$$\partial_t u(x,t) = \partial_{xx} u(x,t) \,, \tag{4.34a}$$

$$\partial_t T(x,t) = -\nu T(x,t) + \partial_{xx} T(x,t) + 2\left[\partial_x u(x,t)\right]^2. \tag{4.34b}$$

These equations must be supplemented with boundary conditions for the situation of interest. The identification with the granular Navier–Stokes hydrodynamic equations (4.1) in the shear mode regime is immediate, particularized for the case of constant (time and space-independent) κ and η .

Additionally, the time evolution of higher central moments of the one-particle distribution function, such as

$$\mu_3 = \langle (v - u)^3 \rangle, \quad \mu_4 = \langle (v - u)^4 \rangle, \tag{4.35}$$

can be derived. These moments are particularly relevant to check deviations from the Gaussian behavior, since for a Gaussian distribution with variance T one has that $\mu_3 = 0$ and $\mu_4 = 3T^2$. Their evolution equations are

$$\partial_t \mu_3 = -\frac{3}{2} \nu \mu_3 + \partial_{xx} \mu_3 + 6 \left(\partial_x u \right) \left(\partial_x T \right), \tag{4.36a}$$

$$\partial_t \mu_4 = -2 \nu \mu_4 + \partial_{xx} \mu_4 + 8 (\partial_x \mu_3) (\partial_x u) + 12T (\partial_x u)^2$$
. (4.36b)

Again, these evolution equations must be supplemented with appropriate boundary conditions, which also depend on the physical situation of interest. It is important to stress that μ_3 and μ_4 are *not* hydrodynamic fields because $(v-u)^n$ with $n \ge 3$ is not conserved during collisions, not even in the quasielastic limit as considered in Sect. 4.2.1. The derivation of equation (4.36b) is given in Appendix A.2.

4.3 Physically Relevant States

In this section, always under the assumption $\beta=0$, we analyze some physically relevant states that are typical of dissipative systems such as granular fluids. Specifically, we investigate the Homogeneous Cooling State (HCS), the Uniform Shear Flow

(USF) state and the Couette Flow state. The theoretical results obtained throughout are compared to numerical results in Sect. 4.5.

4.3.1 The Homogeneous Cooling State

We now focus our attention on the case of spatial periodic boundary conditions, with an initial "thermal condition": $v_{l,0}$ is a random Gaussian variable with zero average and unit variance, that is, $T_{l,0} \equiv T(x,0) = 1$. Starting from this condition, the system typically falls into the so-called Homogeneous Cooling State (HCS), where the total energy decays in time and the velocity and temperature fields remain spatially uniform. In this case, the solution of the average hydrodynamic equations (4.34) reads

$$u(x,t) = 0$$
, $T_{HCS}(x,t) = T(t=0)e^{-\nu t}$. (4.37)

The exponential decrease of the granular temperature is typical of MM, where the collision frequency is velocity-independent. It replaces the so-called Haff's law which was originally derived in the HS case, where $T_{\rm HCS} \sim t^{-2}$ because $\dot{T} \propto -T^{3/2}$ [16].

The HCS is known to be unstable: as discussed in Sect. 3.1.2, it breaks down in too large or too inelastic systems. In our model and in the hydrodynamic limit, this condition is expected to be replaced by a condition of large ν . The stability is studied by introducing rescaled fields $\tilde{u}(x,t) = u(x,t)/\sqrt{T_{HCS}(t)}$ and $\tilde{T}(x,t) = T(x,t)/T_{HCS}(t)$ and by linearizing the hydrodynamic equations near the HCS, i.e. $\tilde{T}(x,t) = 1 + \delta \tilde{T}(x,t)$ and $\tilde{u}(x,t) = \delta \tilde{u}(x,t)$. The analysis of linear equations becomes straightforward by space-Fourier-transforming, which gives

$$\partial_t \delta \tilde{u}(k,t) = \frac{\nu - 2k^2}{2} \delta \tilde{u}(k,t) , \qquad \partial_t \delta \tilde{T}(k,t) = -k^2 \delta \tilde{T}(k,t) . \tag{4.38}$$

Therefore, $\delta \tilde{u}$ is unstable for wave numbers that verify $\nu - 2k^2 > 0$. In continuous space, the system size is 1, so that the minimum available wavenumber is $k_{min} = 2\pi$. Thus, recalling that $\nu = (1 - \alpha^2)L^2$ there is no unstable mode for ν (lengths) below a certain threshold ν_c (L_c), with

$$\nu_c = 8\pi^2, \qquad L_c = 2\pi\sqrt{2}\left(1 - \alpha^2\right)^{-1/2}.$$
 (4.39)

On the contrary, for $\nu > \nu_c$ ($L > L_c$), the HCS is unstable and the rescaled modes with wave numbers verifying $k < \sqrt{\nu/2}$ amplify with time. This instability mechanism is identical to the one found in granular gases for shear modes and described in Sect. 3.1.2. Theoretical predictions and simulated results perfectly agree, as shown in Fig. 4.2. It is important to stress that the amplification appears in the rescaled velocity $\tilde{u}(x,t)$ and not in the velocity u(x,t). The same result is found and compares well with simulations in the HS case. The numerical analysis of the HCS instability and the existence of a critical dissipation (length) ν_c (L_c) will be carried out in Sect. 4.5.

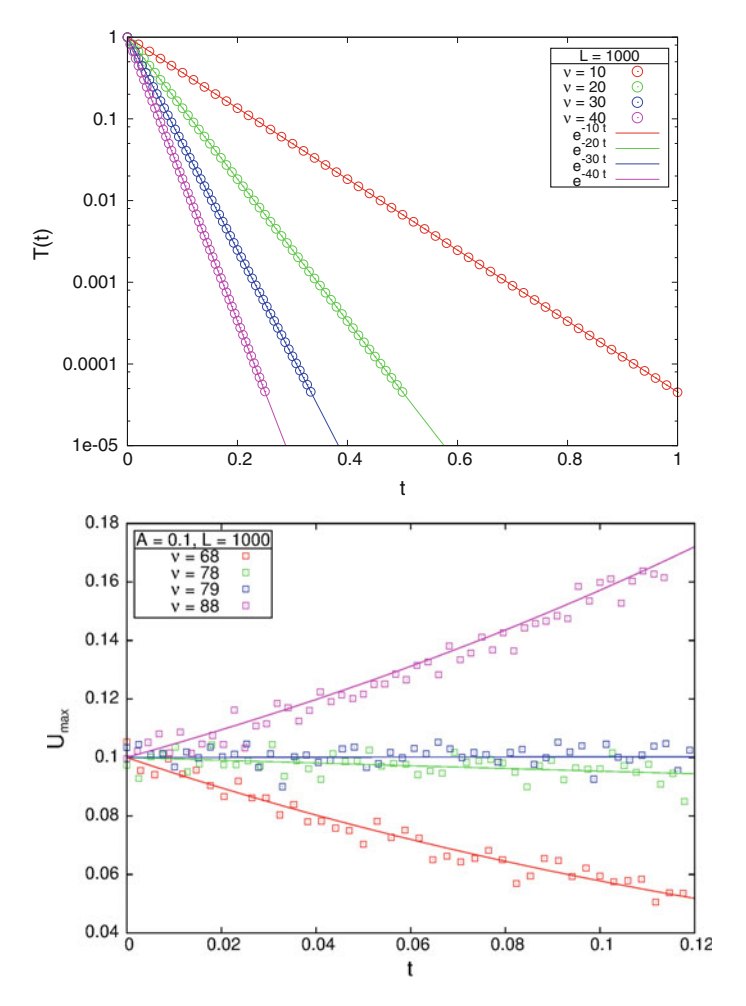


Fig. 4.2 Top: numerical results (circles) and theoretical predictions (lines) for HCS average temperature, $T(t) = \int \mathrm{d}x T(x,t)$, with $\nu=10,20,30,40$. and N=1000. Bottom: rescaled velocity profile maximum $U_{\mathrm{max}} = \tilde{u}(x_M,t)$ as a function of time, where $x_M=1/4$. Trajectories start from a sinusoidal average velocity profile $u(x,0)=u_0\sin(2\pi x)$ (here $u_0=0.1$), which gives hydrodynamic predictions $\tilde{u}(x,t)=u_0\sin(2\pi x)e^{(\nu-\nu_c)t/2}$ (drawn as solid lines). The averages have been taken over $M=10^5$ trajectories

The one-particle velocity distribution has been derived; although of course $p(v) \to \delta(v)$ because of the cooling, when looking at rescaled variables it has been found that the shape of the initial distribution is not altered in the HCS: it only "shrinks" with the thermal velocity [4].

Perturbation of the HCS: Non-homogeneous Cooling

The average hydrodynamic equations (4.34) are non-linear, but for the MM case we are considering they can be solved for general periodic initial conditions u(x, 0) and

T(x,0): the evolution of the velocity profile u(x,t) is decoupled from the evolution of the temperature profile T(x,t) and then u(x,t) can be readily obtained. Afterwards, the evolution equation for T(x,t) can be integrated, with the non-linear viscous heating term $(\partial_x u)^2$ playing the role of a inhomogeneity. Going to Fourier space, it is easily shown that

$$u(x,t) = \sum_{n=-\infty}^{+\infty} e^{-n^2 \nu_c t/2} e^{ik_n x} \hat{u}(k_n,0) , \qquad (4.40)$$

being $\hat{u}(k,0)$ the Fourier-transform of the velocity at the initial time, and $k_n=2\pi n$. This general result shows that the damping coefficient of the n-th shear mode is $\nu_c n^2/2$; therefore, the slowest decaying mode is the first mode n=1, which yields the instability of the HCS for $\nu>\nu_c$. Note that $\hat{u}(k_0,0)=0$, since in the center-of-mass frame we have that $\int_0^1 dx u(x,0)=0$ and total momentum is conserved for periodic boundary conditions.

To be concrete, let's consider an initial perturbation that only excites one Fourier mode in the velocity field, whereas the temperature remains homogeneous. The general solution for an arbitrary initial perturbation will be derived in Sect. 4.3.2. Thus,

$$u(x, 0) = u_0 \sin(2\pi m x), \quad T(x, 0) = T_0,$$
 (4.41)

being m an integer number. Then, on the one hand the velocity profile can be immediately written by making use of Eq. (4.40) and, on the other, the viscous heating term $(\partial_x u)^2$ gives rise to two Fourier modes in the evolution of the temperature, corresponding to n = 2m and n = 0. Namely, we have

$$u(x,t) = e^{-m^2 \nu_c t/2} u_0 \sin(2\pi m x) , \qquad (4.42a)$$

$$T(x,t) = T_0 e^{-\nu t} + e^{-m^2 \nu_c t} \frac{u_0^2}{2} m^2 \nu_c \times \left[\frac{1 - e^{-(\nu - m^2 \nu_c)t}}{\nu - m^2 \nu_c} + \cos(4\pi m x) \frac{1 - e^{-(\nu + m^2 \nu_c)t}}{\nu + m^2 \nu_c} \right] . \quad (4.42b)$$

The presence of a velocity gradient induces the development of a non-homogeneous temperature profile, through the local mechanism of viscous heating.

4.3.2 The Uniform Shear Flow Steady State

Here we consider that our system is sheared at the boundaries: we impose a velocity difference *a* (shear rate) between the velocities at the left and right ends of the system. This is done by considering the Lees-Edwards boundary conditions [17]

$$u(1,t) - u(0,t) = a, \ u'(1,t) = u'(0,t), \ T(1,t) = T(0,t), \ T'(1,t) = T'(0,t),$$

$$(4.43)$$

in which the prime stands for the spatial derivative ∂_x .

With the above conditions, there is a steady solution of the hydrodynamic equations (4.34) characterized by a linear velocity profile and a homogeneous temperature:

$$u_s(x) = a(x - 1/2), \quad T_s = 2a^2/\nu.$$
 (4.44)

This steady state is called Uniform Shear Flow and it is peculiar of dissipative systems, in which the continuous energy loss in collisions may compensate the viscous heating.

The USF state is expected to be globally stable, in the sense that the system tends to it from any initial condition compatible with the Lees-Edwards boundary conditions. This stems from the energy injection allowing the system to fully explore its phase space, which entails that the H-theorem for the master equation holds [12–14]. Therefore, the N-particles distribution $P_N(\mathbf{v}; x, t)$ approaches the steady solution of the master equation $P_N^{(s)}(\mathbf{v}; x)$ corresponding to the USF monotonically as time increases.

Contrarily from the HCS, where the initial shape of the rescaled velocity distribution was conserved in time, the velocity distribution of the USF tends to a Gaussian stationary distribution with average local velocity $u_s(x)$ and homogeneous temperature T_s [4]. In a recent paper, Plata and Prados showed that in the USF the one-particle velocity distribution follows an H-theorem under some mathematical assumptions, which can be generalized to the bulk driven case [15].

Transient Evolution Towards the USF

We here consider the hydrodynamic equations (4.34) with the Lees-Edwards boundary conditions (4.43), and look for the general time-dependent solution thereof.

To start with, we consider the deviations of the average velocity and temperature with respect to their USF values, namely

$$\delta u(x,t) = u(x,t) - u_s(x), \quad \delta T(x,t) = T(x,t) - T_s.$$
 (4.45)

The Lees-Edwards boundary conditions for (u, T) are changed into periodic boundary conditions for $(\delta u, \delta T)$. The latter satisfy the equations

$$\partial_t \delta u = \partial_{xx} \delta u, \quad \partial_t \delta T = -\nu \delta T + \partial_{xx} \delta T + 4a \partial_x \delta u + 2(\partial_x \delta u)^2.$$
 (4.46)

Since no linearization has been done when deriving the above equations from Eq. (4.34), they exactly describe the approach of the system to the USF state. Note that if we set a=0 in Eq. (4.46), we reobtain the exact evolution equations for the deviations from the HCS. Therefore, the general solution for the hydrodynamic fields in the HCS correspond to putting a=0 in the expressions derived below. Now, we go to Fourier space by defining

$$\delta u(x,t) = \sum_{n=-\infty}^{+\infty} \hat{u}(k_n,t)e^{ik_nx} , \quad \delta T(x,t) = \sum_{n=-\infty}^{+\infty} \hat{T}(k_n,t)e^{ik_nx} . \tag{4.47}$$

The initial values for the Fourier components (\hat{u}, \hat{T}) are given by

$$\hat{u}(k_n, 0) = \int_0^1 dx \, \delta u(x, 0) e^{-ik_n x} \,, \quad \hat{T}(k_n, 0) = \int_0^1 dx \, \delta T(x, 0) e^{-ik_n x} \,. \tag{4.48}$$

Recall that (i) $k_n = 2n\pi$ and (ii) $\hat{u}(k_0, t) = 0$ in the centre of mass frame.

The quadratic term in Eq. (4.46) that stems from viscous heating couples different Fourier modes. More specifically, the evolution equations in Fourier space read

$$\partial_{t}\hat{u}(k_{n},t) = -k_{n}^{2}\hat{u}(k_{n},t),$$

$$\partial_{t}\hat{T}(k_{n},t) = -(\nu + k_{n}^{2})\hat{T}(k_{n},t) + 4iak_{n}\hat{u}(k_{n},t)$$

$$+ \sum_{m=-\infty}^{+\infty} k_{m}(k_{m} - k_{n})\hat{u}(k_{m},t)\hat{u}^{*}(k_{m} - k_{n},t).$$
(4.49a)
$$(4.49a)$$

The solution of the equation for $\hat{u}(k_n, t)$ can be written straight away; afterwards, this solution is inserted into the equation for $\hat{T}(k_n, t)$ that is thus transformed into a closed non-homogeneous linear equation. Hence, we get

$$\hat{u}(k_n, t) = \hat{u}(k_n, 0)e^{-k_n^2 t}, \qquad (4.50a)$$

$$\hat{T}(k_n, t) = \hat{T}(k_n, 0)e^{-(\nu + k_n^2)t} + 4iak_n\hat{u}(k_n, 0)e^{-k_n^2 t} \frac{1 - e^{-\nu t}}{\nu} + 2e^{-k_n^2 t} \sum_{m = -\infty}^{+\infty} k_m (k_m - k_n)\hat{u}(k_m, 0)\hat{u}^*(k_m - k_n, 0) \frac{e^{-\nu t} - e^{-2k_m (k_m - k_n)t}}{2k_m (k_m - k_n) - \nu}. \qquad (4.50b)$$

Note that there are no unstable modes in the USF of our model: when the denominators in (4.50) are zero, the numerators also vanish and the corresponding fractions remain finite. This is consistent with the (linear) stability of the USF state of a dilute granular gas of hard spheres described by the Boltzmann equation with respect to perturbations in the velocity gradient (the only possible ones in our model) [18]. Nevertheless, here the analysis is not restricted to small perturbations, at the level of the hydrodynamic equations the USF is globally stable.

4.3.3 The Couette Flow Steady State

As introduced in Sect. 4.2.2, Eq. (4.34) yields a steady state solution when the system is coupled to reservoirs at its boundaries, e.g. when at sites 0 (L) and N+1 (R) we have two particles with independent normal velocity distributions, with average

 $u_{L/R}$ and variance $T_{L/R}$. Thus the system is no longer periodic, there are L=N+1 colliding pairs and the boundary conditions for the mesoscopic fields read $u(0)=u_L$, $u(1)=u_R$, $T(0)=T_L$ and $T(1)=T_R$. It must be stressed that momentum is no longer conserved for this choice of boundary conditions, since in general $u'(1,t) \neq u'(0,t)$.

The stationary solution for hydrodynamic equations (4.34), setting symmetric conditions

$$T_R = T_L = T_R$$
, $u_R = -u_L = a/2$, (4.51)

is

$$u(x) = a\left(x - \frac{1}{2}\right), \quad T(x) = \frac{2a^2}{\nu} + \left(T_B - \frac{2a^2}{\nu}\right) \frac{\cosh\left[\sqrt{\nu}(x - 1/2)\right]}{\cosh\left(\sqrt{\nu}/2\right)}.$$
(4.52)

Here, we have put ourselves in the centre of mass frame by considering that $u_R = -u_L$, and we see that when $T_B = 2a^2/\nu$ the USF state described in Sect. 4.3.2 is recovered. On the other hand, when $T_B \neq 2a^2/\nu$, the average velocity profile remains linear but the temperature develops a gradient, because the viscous heating that stems from the velocity gradient is not *locally* compensated by the energy sink, which is proportional to the temperature. In other words, when $T_B = 2a^2/\nu$, the velocity gradient a is exactly the one needed to satisfy (4.34) with an homogeneous temperature throughout the system. Otherwise, if the velocity gradient is smaller, the bulk temperature will be lower than that at the boundaries, and vice versa when the velocity gradient is steeper.

These results satisfy the energy balance (4.32b) required to have a stationary state, namely

$$J_{\text{av}}(x=0) - J_{\text{av}}(x=1) = \nu \int_0^1 dx \, T(x) ,$$
 (4.53)

where the lhs is the energy flow entering the system at the boundaries and the rhs is the energy loss in collisions.

The one-particle distribution function is not Gaussian in this steady state, except in the case $T_B=2a^2/\nu$ for which we recover the USF. This can be readily seen by taking into account the time evolution of higher-order-than-two central moments of the velocity, whose evolution is governed by Eq. (4.36). In the Couette case, we have Gaussian distributions at the boundaries and the appropriate boundary conditions are $\mu_3(0,t)=\mu_3(1,t)=0, \,\mu_4(0,t)=\mu_4(1,t)=3T_B^2$. Equation (4.36a) clearly shows the point: if the term $\partial_x u \, \partial_x T \neq 0$, the third central moment μ_3 cannot be identically zero in the steady state and the one-particle distribution is non-Gaussian.

Therefore, the only steady state with a Gaussian probability distribution in the present model is the USF. We recall that the HCS is not a steady state, although the probability distribution for the rescaled velocity is a time-independent Gaussian if it starts from a Gaussian shape. The theoretical expressions for μ_3 and μ_4 are not particularly illuminating and will be disregarded here.

We do not write down the theoretical expressions for μ_3 and μ_4 in Couette's steady state because they are not particularly illuminating.

4.3.4 Validity of the Hydrodynamic Description

There are some analogies between our expansion in terms of L^{-1} and the Chapman-Enskog expansion of the Boltzmann equation. In both cases, terms up to the second order in the gradients (of the order of k^2 , being k the wave vector, in Fourier space) are kept. On the one hand, and from a purely mathematical point of view, in our model Eq. (4.34) becomes exact in the limit $L \to \infty$, with $\nu = (1 - \alpha^2)L^2$ of the order of unity, as previously stated. On the other hand, on a physical basis, the hydrodynamic equations are approximately valid whenever the terms omitted upon writing them are negligible against the ones we have kept.

Following the discussion in the preceding paragraph, we must impose that $L\gg 1$. Moreover, we have also to impose that $t\ll L$ in order to have an approximate hydrodynamic description, which stems from the correlations $\langle v_i v_{i\pm 1} \rangle$ being of the order of L^{-1} as compared to the granular temperature, see Sect. 5.1. For example, in the elastic case at equilibrium, the correlations $\langle v_i v_{i+j} \rangle$ do not depend on the distance j, and therefore $\langle v_i v_{i+j} \rangle = -T(L-1)^{-1}, \forall j\neq 0$. More specifically, the term proportional to the correlations in the evolution equation for the granular temperature over the microscopic time scale τ is of the order of $(1-\alpha^2)L^{-1}$, which must also be negligible against the second spatial derivative terms, of the order of L^{-2} . Then, $(1-\alpha^2)L\ll 1$ must be further imposed when the correlations are neglected in Eq. (4.34). This condition, although less restrictive that $1-\alpha^2=O(L^{-2})$, also implies that the microscopic dynamics is quasi-elastic. In Chap. 5 it will be shown how to relax these conditions and take into account spatial correlations in the system.

4.4 Fluctuating Hydrodynamics

4.4.1 Definition of Fluctuating Currents

The size of granular systems is limited both in real experiments and in numerical or theoretical studies, as discussed before, particularly when the instability of the HCS was analysed in Sect. 4.3.1. Therefore, it is important to investigate finite size effects and the first way to take into account such effects is to develop a fluctuating hydrodynamic description, as introduced in Sect. 3.2: the microscopic currents are split in two terms, their "main" contribution that depends only on the hydrodynamic variables, and their corresponding "noises", with zero average.

The main physical idea under the fluctuating hydrodynamics approach is to calculate the averages that lead from the microscopic dynamics to the hydrodynamic equations in two steps. First, the average over the "fast" variables (namely y_p) is taken, conditioned to given values of the hydrodynamic fields. This defines the "main" contribution to the current, which is still a function of the "slow" hydrodynamic variables. The difference between the microscopic current and its main contribution is the noise of the current, which by definition has zero average: it is clear that the

average value of the microscopic current (both over the "fast" and "slow" variables) coincides with the average of the main contribution (only over the "slow" variables). Specifically, each physical magnitude is written as $x = \overline{x} + \xi^{(x)}$, where \overline{x} is its main contribution and $\xi^{(x)}$ is its noise.

Following the above discussion we start by splitting the microscopic currents in their main parts and their noises, namely

$$j_{l,p} = \overline{j}_{l,p} + \xi_{l,p}^{(j)}, \quad J_{l,p} = \overline{J}_{l,p} + \xi_{l,p}^{(J)}, \quad d_{l,p} = \overline{d}_{l,p} + \xi_{l,p}^{(d)}.$$
 (4.54)

As stated above, overlined variables correspond to partial averages over the fast variables $y_{l,p}$ conditioned to given values of the slow ones $v_{l,p}$. We are considering the particular case of MM, that is, $\beta = 0$. Consequently,

$$\overline{j}_{l,p} = \frac{1+\alpha}{2L} \Delta_{l,p} , \qquad (4.55a)$$

$$\overline{J}_{l,p} = \frac{1+\alpha}{2L} \Delta_{l,p} (v_{l,p} + v_{l+1,p}), \qquad (4.55b)$$

$$\overline{d}_{l,p} = \frac{\alpha^2 - 1}{4L} (\Delta_{l,p}^2 + \Delta_{l-1,p}^2) . \tag{4.55c}$$

It is clear that such choices guarantee that all noises $\xi^{(j)}$, $\xi^{(J)}$ and $\xi^{(d)}$ have zero average.

4.4.2 Noise Correlations

Noise Correlations: Momentum Current

We start by studying the properties of the current noise correlation function $\xi_{l,p}^{(j)} = j_{l,p} - \overline{j}_{l,p}$, namely the moment $\langle \xi_{l,p}^{(j)} \xi_{l',p'}^{(j)} \rangle$, which reads

$$\langle \xi_{l,p}^{(j)} \xi_{l',p'}^{(j)} \rangle = \langle j_{l,p} j_{l',p'} \rangle - \langle \overline{j}_{l,p} \overline{j}_{l',p'} \rangle. \tag{4.56}$$

In order to obtain the noise correlations, we exploit a series of conditions. First, it is straightforward that $\langle \xi_{l',p}^{(j)} \xi_{l',p'}^{(j)} \rangle = 0$ for $p \neq p'$, because y_p and $y_{p'}$ are independent random numbers. For equal times, p = p', the second term on the right hand of (4.56) is negligible because it is $O(L^{-2})$, while the leading behavior of the first term will be shown to be $O(L^{-1})$. Using now the definition (4.16) of the microscopic momentum current, we get

$$j_{l,p}j_{l',p'} = \frac{(1+\alpha)^2}{4} \Delta_{l,p} \delta_{y_p,l} \Delta_{l',p'} \delta_{y'_p,l'}.$$
 (4.57)

Second, we take into account, setting again $\beta = 0$, that $\langle \delta_{y_p,l} \delta_{y_p,l'} \rangle = \delta_{l,l'} \langle \delta_{y_p,l} \rangle = L^{-1} \delta_{l,l'}$. Thus, for p = p', we have

$$\langle \xi_{l,p}^{(j)} \xi_{l',p}^{(j)} \rangle = \frac{(1+\alpha)^2}{4L} \langle \Delta_{l,p}^2 \rangle \delta_{l,l'} + O(L^{-2}). \tag{4.58}$$

At this point, we can make use of (i) the quasi-elasticity of the microscopic dynamics to substitute $(1+\alpha)/2$ by 1 (neglecting terms of order L^{-2}) and (ii) the molecular chaos assumption to obtain $\langle \Delta_{l,p}^2 \rangle$, with the result

$$\langle \Delta_{l,p}^2 \rangle = T_{l,p} + T_{l+1,p} + (u_{l,p} - u_{l+1,p})^2 + O(L^{-1}) \sim 2T_{l,p},$$
 (4.59)

because both $u_{l+1,p} - u_{l,p}$ and $T_{l+1,p} - T_{l,p}$ are of the order of L^{-1} . Therefore,

$$\langle \xi_{l,p}^{(j)} \xi_{l',p'}^{(j)} \rangle \sim 2L^{-1} T_{l,p} \, \delta_{l,l'} \, \delta_{p,p'} \,.$$
 (4.60)

In the large size system, $j_{l,p}$ scales as L^{-2} , as given by Eq. (4.30) (an analogous scaling has been found in other simple dissipative models, see [19]). Therefore, the mesoscopic noise of the momentum current is defined as

$$\xi^{(j)}(x,t) = \lim_{L \to \infty} L^2 \xi_{l,p} , \quad j(x,t) = \overline{j}(x,t) + \xi^{(j)}(x,t) , \qquad (4.61)$$

in which, again, $\overline{j}(x,t) = \lim_{L \to \infty} L^2 \overline{j}_{l,p}$. Going to the continuous limit and remembering the scaling (4.25), which implies that $\delta_{l,l'}/\Delta x \sim \delta(x-x')$ and $\delta_{p,p'}/\Delta t \sim \delta(t-t')$, the noise amplitude of the momentum current reads

$$\langle \xi^{(j)}(x,t)\xi^{(j)}(x',t')\rangle \sim 2L^{-1}T(x,t)\,\delta(x-x')\delta(t-t')$$
. (4.62)

Noise Correlations: Energy Current

We are here interested in the correlation properties of the noise $\xi_{l,p}^{(J)} = J_{l,p} - \overline{J}_{l,p}$

$$\langle \xi_{l,p}^{(J)} \xi_{l',p'}^{(J)} \rangle = \langle J_{l,p} J_{l',p'} \rangle - \langle \overline{J}_{l,p} \overline{J}_{l',p'} \rangle. \tag{4.63}$$

Similarly to the case of the current noise, we have that (i) $\langle \xi_{l,p}^{(J)} \xi_{l',p'}^{(J)} \rangle = 0$ for $p \neq p'$, (ii) the second term on the right-hand side is $O(L^{-2})$ and thus subdominant in the limit $L \to \infty$ and (iii) the noise correlation is dominated by the contribution that stems from the first term on the rhs. Therefore, making use of Eq. (4.18), and again of the relation (for $\beta=0$) $\langle \delta_{y_p,l}\delta_{y_p,l'}\rangle = \delta_{l,l'}\langle \delta_{y_p,l}\rangle = \frac{\delta_{l,l'}}{L}$, we obtain

$$\langle \xi_{l,p}^{(J)} \xi_{l',p'}^{(J)} \rangle \sim L^{-1} \left(\left(v_{l,p}^2 - v_{l+1,p}^2 \right)^2 \right) \delta_{l,l'} \delta_{p,p'} .$$
 (4.64)

In general, the moment $\left(\left(v_{l,p}^2-v_{l+1,p}^2\right)^2\right)$ is not a function of the hydrodynamic variables u and T, unless the one-particle distribution is Gaussian.

In order to obtain a closed fluctuating hydrodynamic description, we need to write $\langle (v_{l,p}^2 - v_{l+1,p}^2)^2 \rangle$ in terms of the hydrodynamic variables. Then, on top of the Molecular Chaos assumption (i.e. the factorization of the moments involving several sites), we introduce the so-called local equilibrium approximation (LEA): the one-particle distribution function P_1 is assumed to be the equilibrium distribution corresponding to the local values of the hydrodynamic variables, which in our case corresponds to a Gaussian distribution of the velocities. There is strong numerical evidence that the LEA gives a good quantitative description of the noise amplitudes in some dissipative models without momentum conservation [2, 19–21], as a consequence of the quasi-elasticity of the underlying microscopic dynamics. In our model, we know that the LEA is not an approximation but an exact result for some physical states, such as the HCS¹ or the USF. For other states like the Couette flow, its range of validity is a priori unknown.

In the large system size limit, $J_{l,p}$ scales as L^{-2} and it is expected that the noise does too. Along the same lines as in the preceding section, after using the LEA and neglecting terms of the order of L^{-2} , we obtain the autocorrelation of the energy current noise,

$$\langle \xi^{(J)}(x,t)\xi^{(J)}(x',t')\rangle \sim 4L^{-1}T(x,t)[T(x,t)+2u^2(x,t)]\delta(x-x')\delta(t-t')$$
. (4.65)

Thus, the energy current noise is also white and its amplitude scales as L^{-1} with the system size L, accordingly with the physical intuition.

Noise Correlations: Dissipation Field

Now we deal with the third "current" in the system, the dissipation field $d_{l,p}$ by repeating the same procedure as before. We are interested in the correlation properties of the noise $\xi_{l,p}^{(d)} = d_{l,p} - \overline{d}_{l,p}$.

Once more, $\langle \xi_{l,p}^{(d)} \xi_{l',p'}^{(d)} \rangle = 0$ for $p \neq p'$ and the dominant contribution for p = p' comes from the dissipation correlation $\langle d_{l,p} d_{l',p} \rangle$. Making use of the definition of Eq. (4.19),

$$\langle d_{l,p}d_{l',p}\rangle = \frac{(\alpha^2 - 1)^2}{16L} \left[\delta_{l,l'} \langle (v_{l,p} - v_{l+1,p})^4 + (v_{l-1,p} - v_{l,p})^4 \rangle + \delta_{l,l'-1} \langle (v_{l,p} - v_{l+1,p})^4 \rangle + \delta_{l,l'+1} \langle (v_{l-1,p} - v_{l,p})^4 \rangle \right].$$
(4.66)

Therefore, by taking into account the LEA and neglecting $O(L^{-2})$ terms,

$$\langle \xi_{l,p}^{(d)} \xi_{l',p'}^{(d)} \rangle \sim \frac{3(\alpha^2 - 1)^2}{4L} T_{l,p}^2 [2\delta_{l,l'} + \delta_{l,l'-1} + \delta_{l,l'+1}] \delta_{p,p'} .$$
 (4.67)

¹For the usual choice of an initial Gaussian distribution, see Sect. 4.3.1.

In the large size system $d_{l,p}$ scales as L^{-3} and we expect the same scaling for the noise. Going to the continuous limit, we get

$$\langle \xi^{(d)}(x,t)\xi^{(d)}(x',t')\rangle \sim L^{-3} 3\nu^2 T(x,t)^2 \delta(x-x')\delta(t-t')$$
. (4.68)

In summary, the noise of the dissipation is subdominant with respect to the moment and energy currents, its amplitude being proportional to L^{-3} , and therefore it is usually negligible.

4.4.3 Cross-Correlations of the Noises and Gaussianity

Interestingly, being in the presence of two fluctuating fields, correlations between different noises appear. The cross correlations between different noises are straightforwardly obtained, along similar lines:

$$\langle \xi^{(j)}(x,t)\xi^{(J)}(x',t')\rangle = 4L^{-1}T(x,t)u(x,t)\delta(x-x')\delta(t-t'), \qquad (4.69)$$

$$\langle \xi^{(j)}(x,t)\xi^{(d)}(x',t')\rangle = 0, \qquad \langle \xi^{(J)}(x,t)\xi^{(d)}(x',t')\rangle = 0,$$

up to and including $O(L^{-1})$. Theoretical predictions for noise correlations, amplitudes and Gaussianity have been successfully tested in simulations, see Sect. 4.5.

In the large system size limit $L \gg 1$, the current noise introduced in the Sect. 4.4.1 is Gaussian and white. We can introduce a new noise field $\tilde{\xi}(x,t)$ by

$$\xi^{(j)}(x,t) = L^{-1/2}\tilde{\xi}(x,t), \qquad (4.70)$$

and $\tilde{\xi}(x,t)$ remains finite in the large system size limit $L \to \infty$,

$$\langle \tilde{\xi}(x,t) \rangle = 0, \qquad \langle \tilde{\xi}(x,t)\tilde{\xi}(x',t') \rangle \sim 2T(x,t)\delta(x-x')\delta(t-t').$$
 (4.71)

It will be here shown that all the higher-order cumulants of $\tilde{\xi}(x,t)$ vanish in the thermodynamic limit as $L\to\infty$. Let us consider a cumulant of order n of the microscopic noise $\xi_{l,p}$ that is equal to the n-th order moment of the ξ plus a sum of nonlinear products of lower moments of ξ . A calculation analogous to the one carried out for the correlation $\langle \xi_{l,p}^{(j)} \xi_{l',p'}^{(j)} \rangle$ shows that the leading behavior of any moment is of the order of L^{-1} , which is obtained when all the times are the same. Therefore, the moment $\langle j_{l,p} j_{l',p'}...j_{l^{(n)},p^{(n)}} \rangle$ gives the leading behavior of the considered cumulant, which is thus of the order of L^{-1} for $p=p'=...=p^{(n)}$; any other contribution to the cumulant is at least of the order of L^{-2} . We have that

$$\langle j_{l,p}j_{l',p'}\cdots j_{l^{(n)},p^{(n)}}\rangle \sim L^{-1}\langle C_{l,p}\rangle \delta_{l,l'}\delta_{l',l''}\delta_{l^{(n-1)},l^{(n)}}\cdots \delta_{p,p'}\delta_{p',p''}\delta_{p^{(n-1)},p^{(n)}},$$
 (4.72)

where $\langle C_{l,p} \rangle$ is certain average that remains finite in the large system size limit as $L \to \infty$. In the continuous limit, each current introduces a factor L^2 due to the scaling introduced in Sect. 4.4. Moreover, we take into account the relationship between Kronecker and Dirac δ 's in the continuum limit to write the cumulants $\langle \langle \cdots \rangle \rangle$ of the rescaled noise introduced in Eq. (4.70) as

$$\langle \langle \tilde{\xi}(x,t)\tilde{\xi}(x',t')\cdots\tilde{\xi}(x^{(n)},t^{(n)})\rangle \rangle \sim L^{3(1-\frac{n}{2})}\langle C(x,t)\rangle \times \\ \delta(x-x')\delta(x'-x'')\delta(x^{(n-1)}-x^{(n)})\cdots\delta(t-t')\delta(t'-t'')\delta(t^{(n-1)}-t^{(n)}).$$
(4.73)

Thus, in the limit as $L \to \infty$,

$$\langle \tilde{\xi}(x,t)\tilde{\xi}(x',t')\cdots\tilde{\xi}(x^{(n)},t^{(n)})\rangle = 0, \quad \text{for all } n > 2,$$
(4.74)

and the vanishing of all the cumulants for n > 2 means that the momentum current noise is Gaussian in the infinite size limit.

The same procedure can be repeated for the energy current noise, by defining $\xi^{(J)}(x,t) = L^{-1/2}\tilde{\eta}(x,t)$, with the result

$$\langle \langle \tilde{\eta}(x,t)\tilde{\eta}(x',t')\cdots\tilde{\eta}(x^{(n)},t^{(n)})\rangle \rangle \sim L^{3(1-\frac{n}{2})}\langle D(x,t)\rangle \times \\ \delta(x-x')\delta(x'-x'')\delta(x^{(n-1)}-x^{(n)})\cdots\delta(t-t')\delta(t'-t'')\delta(t^{(n-1)}-t^{(n)}) .$$
(4.75)

In the equation above, $\langle D(x,t) \rangle$ is a certain average, different from $\langle C(x,t) \rangle$, but also finite in the large system size limit. Thus, we have that

$$\langle \tilde{\eta}(x,t)\tilde{\eta}(x',t')\cdots\tilde{\eta}(x^n,t^n)\rangle = 0, \text{ for all } n > 2,$$
 (4.76)

and the energy current noise also becomes Gaussian in the continuum limit.

Note that the Gaussianity of the noises is independent of the validity of the local equilibrium approximation, which is only needed to write $\langle C(x,t) \rangle$ and $\langle D(x,t) \rangle$ in terms of the hydrodynamic fields u(x,t) and T(x,t). Besides, a similar procedure for the dissipation noise gives that the corresponding scaled noise vanishes in the continuum limit, since the power of L in the dominant contribution to the n-th order cumulant is 3-5n/2 instead of 3-3n/2. This means that the dissipation noise is subdominant as compared to the currents noises in the continuum limit, and can be neglected.

We conclude this section mentioning that, in general, our noise amplitudes do not seem to satisfy any "equilibrium-like" Fluctuation-Dissipation relation of the 2nd kind (see for instance [22]). This is however not surprising, considered that it is a non-conservative model.

4.5 Numerical Results

4.5.1 General Simulation Strategy

Simulations have been made reproducing M times the phase-space trajectory of a system of N particles, each one carrying a velocity v_l and being at a definite position $l=1,\ldots,L$, with L=N for periodic or Lees-Edwards boundaries and L=N+1 for a thermostatted system. For each trajectory, the system starts with a random extraction of velocities v_l normally distributed with $\langle v_l \rangle = 0$ and $\langle v_l^2 \rangle = T_0$, unless otherwise specified. Afterwards, we move to the centre of mass frame making the transformation $v_l \Rightarrow v_l' = v_l - \frac{1}{L} \sum_{l=1}^L v_l$, so that the total momentum of the system is zero.

Monte Carlo simulations of the system dynamics have been carried out through the residence time algorithm described in Sect. 4.1.1 [10, 11]. This procedure allows us to compute the time-evolution of our model for every collision rate β , although we focus here only on the case $\beta = 0$ (MM).

4.5.2 Homogeneous and Non-homogeneous Cooling

Following the above-mentioned procedure, we have simulated the homogeneous cooling state described in Sect. 4.3.1 a system made of 10^3 particles, with periodic boundaries and starting from a flat velocity profile $u(x, 0) \equiv 0$ with unit variance $T(x, 0) \equiv T_0 = 1$. Theoretical predictions for average velocity and temperature decay in Eq. (4.37) perfectly agree with simulations. The instability of the HCS has been investigated through the rescaled velocity field for a perturbed initial condition

$$u(x,0) = A\sin(2\pi x)$$
, (4.77)

introducing a small sinusoidal perturbation and measuring the time evolution of its rescaled amplitude \tilde{u} . Theory and simulations are compared in Fig. 4.2, where the existence of a threshold value of the dissipation around $\nu_c = 8\pi^2$ is evident. Also, simulations of non-homogeneous cooling have been performed, starting as in Sect. 4.3.1 from a sinusoidal periodic average velocity profile $u(x,0) = u_0 \sin(2\pi mx)$, with m integer, and a homogeneous temperature $T(x,0) = T_0 = 1$ as before. The simulations show the cooling of the system, as expected from Eq. (4.42), with the development of a temperature profile given by viscous heating. Comparisons between numerical results and theoretical predictions for the non-homogeneous case are displayed in Fig. 4.3.

4.5 Numerical Results 125

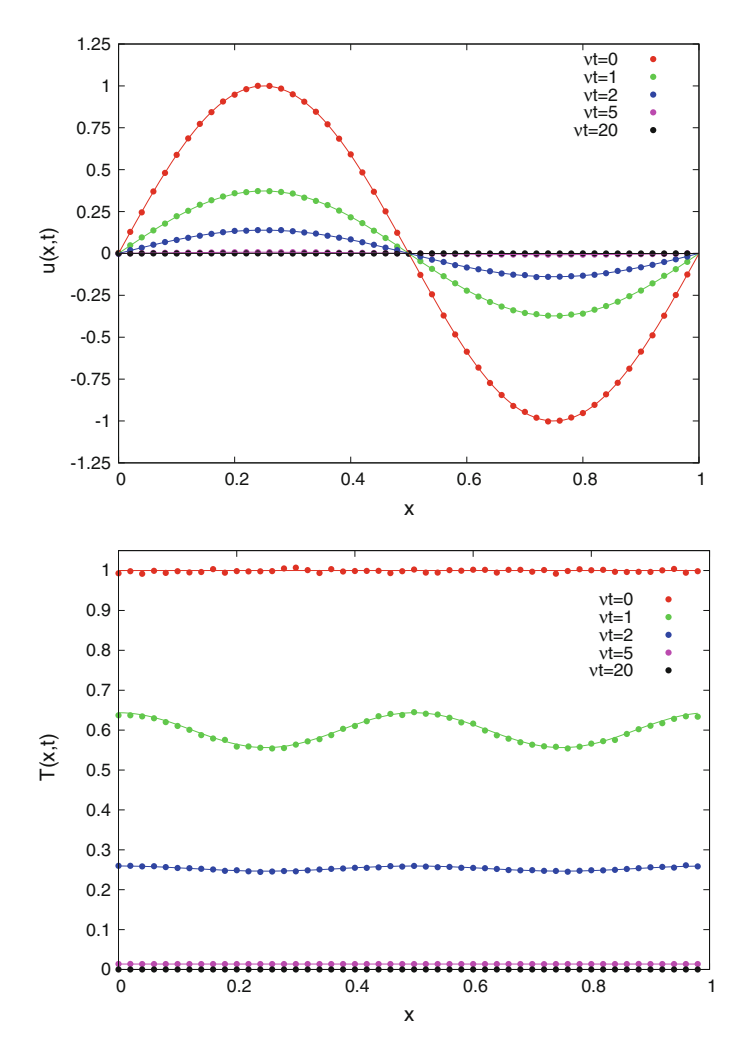


Fig. 4.3 Top: numerical results (points) and theoretical values (solid lines) for the average sinusoidal velocity profile u(x,t) in the HCS, with $u_0=1,\ \nu=40,\ N=500,\ T_0=1$ and m=1 for $\nu t=0,1,2,5,20$. Bottom: same plot for the temperature profile T(x,t) of the system. Here, the averages have been taken over $M=10^5$ trajectories

4.5.3 Uniform Shear Flow State

The Uniform Shear Flow described in Sect. 4.3.2 can be simulated by introducing appropriate boundary conditions in the simulations. When the pair (1, N) is chosen to collide at time p, there are two separate collisions: particle 1 (N) undergoes a collision with a particle with velocity $v_{N,p} - a(v_{1,p} + a)$. These boundary collision rules introduce a shear rate a between the left and right ends of the system, and at

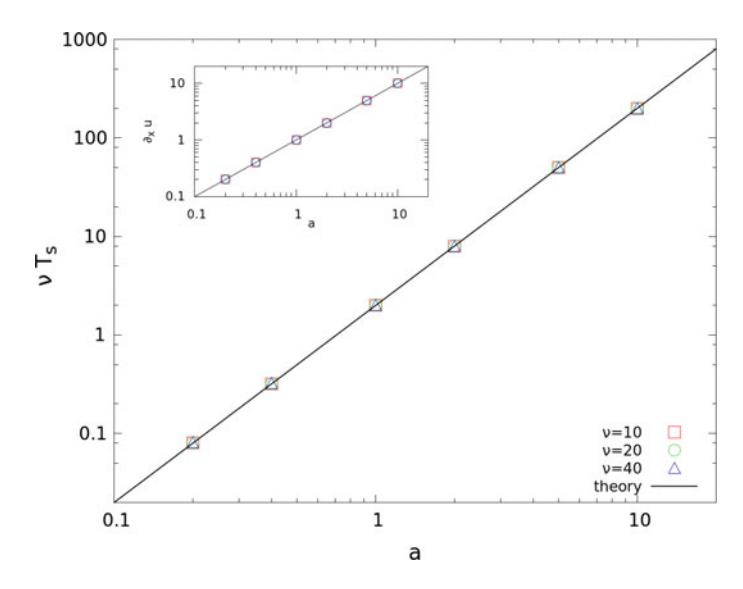


Fig. 4.4 Steady temperature in the USF state as a function of the shear rate a. We consider three different values of ν in a system of size N=500, with averages over $M=10^5$ realizations. In the vertical axis the numerical and theoretical values of νT_s are plotted, the latter being given by Eq. (4.44). In the inset, the numerical value of the velocity gradient $\partial_x u_s(x)$ as a function of the shear rate is shown. Note the logarithmic scale in both axes

the hydrodynamic level they are represented by the Lees-Edwards conditions (4.43). This can be readily shown by considering the special evolution equations for $v_{1,p}$ and $v_{N,p}$ with the above boundary collision rules in the continuum limit.

Theoretical predictions in the USF state, given by (4.44), have been tested for the steady (i) profile of the average velocity and (ii) value of the temperature. Simulations have been performed in a system with N=500 particles and three different values of ν , namely $\nu=10$, 20 and 40. As seen in Fig. 4.4, the agreement is excellent in all cases.

Furthermore, Figs. 4.5 and 4.6 show the tendency of the hydrodynamic variables u and T towards their USF values, as predicted in Sect. 4.3.2. In both figures the evolution of the velocity and temperature profiles towards its steady value has been plotted, starting from an initial state such that (i) $T(x, t = 0) = T_0 = 1$ and (ii)

$$u(x, t = 0) = u_s(x) + A\sin(2\pi x), \quad A = 1,$$
 (4.78)

$$u(x, t = 0) = u_s(x) + A\sin(2\pi x) + B\cos(2\pi x), \quad A = B = 1,$$
 (4.79)

respectively. In both cases, only the n=1 Fourier mode is present. However, an important physical difference should be stressed: the temperature profile is always horizontal at the boundaries in Fig. 4.5, which is not in Fig. 4.6. Therefore, there is heat flux at the system boundaries in the latter case but not in the former. Anyhow, the agreement between simulation and theory is excellent in both situations.

4.5 Numerical Results 127

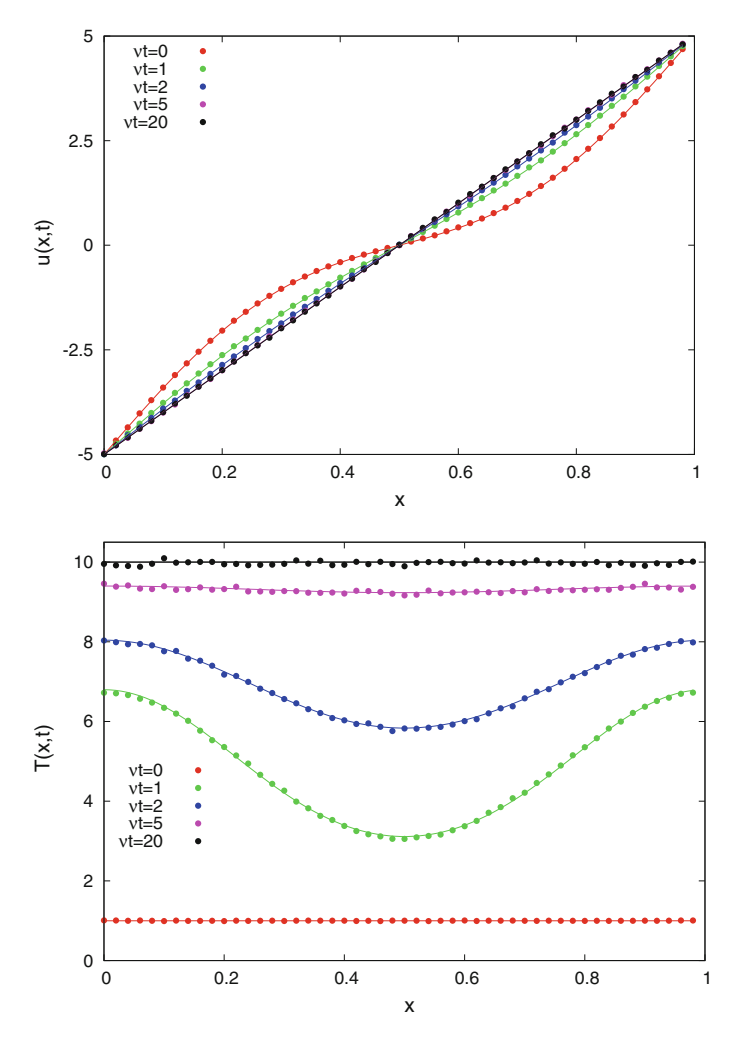


Fig. 4.5 Transient evolution of the velocity (top) and the temperature (bottom) to their steady profiles in the USF state, for a=10. The numerical curves are plotted with points, whereas the solid lines correspond to the theoretical expression (4.50). The agreement between simulation and theory is excellent in both cases. The system size is N=500, the dissipation coefficient is $\nu=20$, and the number of trajectories is $M=10^5$. In this case, initial conditions correspond to Eq. (4.78), namely A=1 and B=0

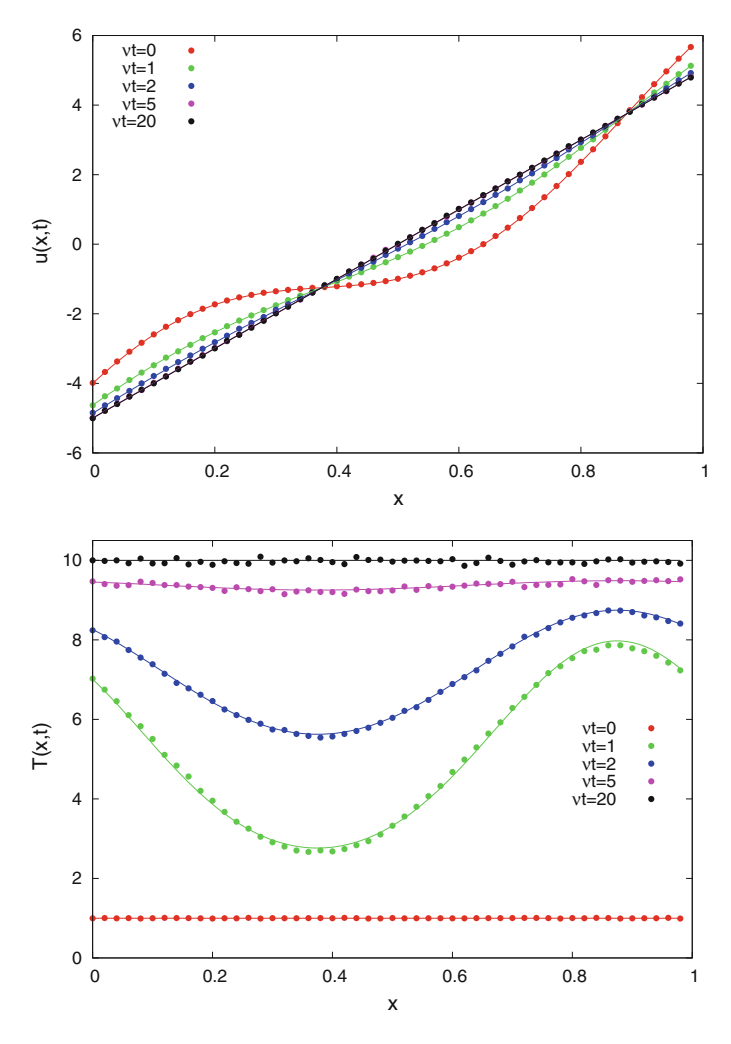


Fig. 4.6 Same as in Fig. 4.5, but for initial conditions defined in Eq. (4.79), namely A = B = 1

4.5.4 The Couette Flow State

We now consider a system coupled to two reservoirs at both ends, as described in Sect. 4.3.3. In the simulations, two "extra" sites 0 and N+1 are introduced, so that the number of colliding pairs is L=N+1. When the colliding pair involves one boundary particle (that is, pairs (0,1) or (N,N+1)), the same collision rule for the bulk pairs $(1,2),\ldots,(N-1,N)$ is applied but the velocity of the "wall" particles is drawn from a Gaussian distribution with fixed average velocities $u_{L/R}$ and temperatures $T_{L/R}$. This is the only change in the simulations, which no longer correspond to periodic boundary conditions either in u or T. In particular, the

4.5 Numerical Results 129

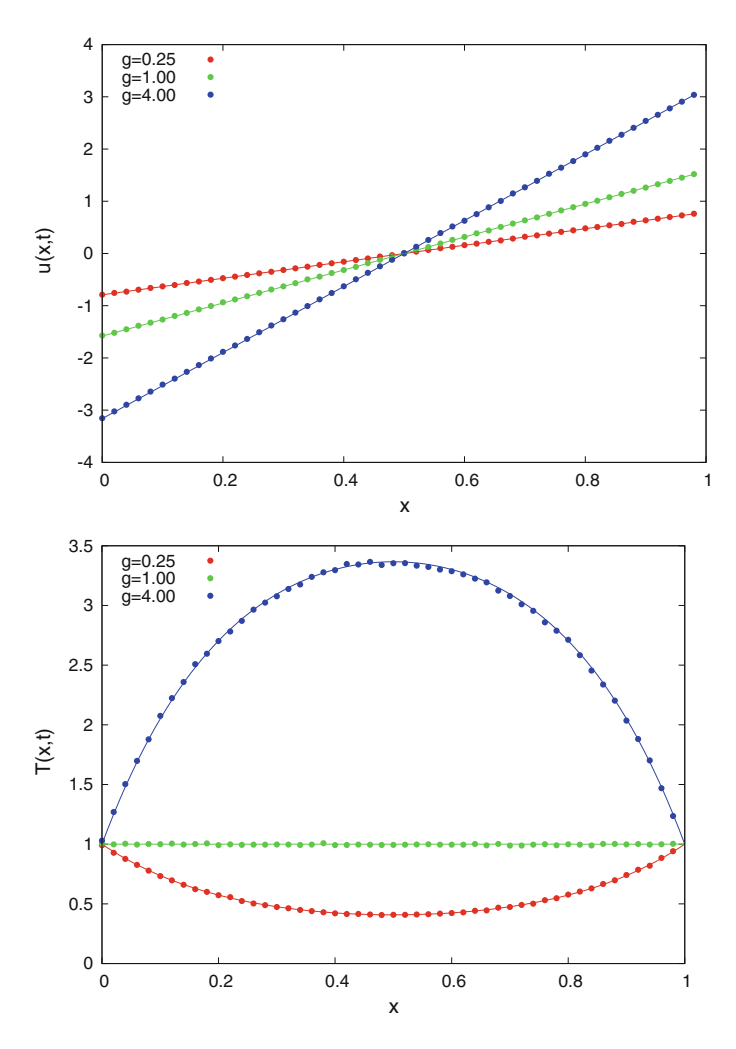


Fig. 4.7 Numerical results (symbols) and theoretical values (solid lines) for the stationary velocity profile u(x) (top) and the stationary temperature profile T(x) (bottom) in the Couette state. The parameter values are $\nu = 20$, N = 500, $M = 10^5$, for g = 0.25, 1, 4. The profiles have been plotted at the final time $\nu t = 20$.

non-periodicity of u' implies that momentum is not conserved in the time evolution of the system, conversely to the case of the HCS and USF states.

Figure 4.7 shows the comparison between simulations and theoretical predictions from Eq. (4.52), for different values of the parameter $g = 2a^2/(\nu T_B)$. The boundary conditions are chosen as $T_{L/R} = T_B = 1$, $u_R = -u_L = a/2$. It should be recalled that g = 1 corresponds to the case in which the Couette steady state coincides with the USF state and there is no heat current in the system. For g > 1 (g < 1), viscous heating is stronger (weaker) than that of the USF, and the steady temperature profile is concave (convex), that is, T'' < 0 (T'' > 0) and displays a maximum (minimum) at the centre of the system x = 1/2. Simulations start from a non-stationary profile,

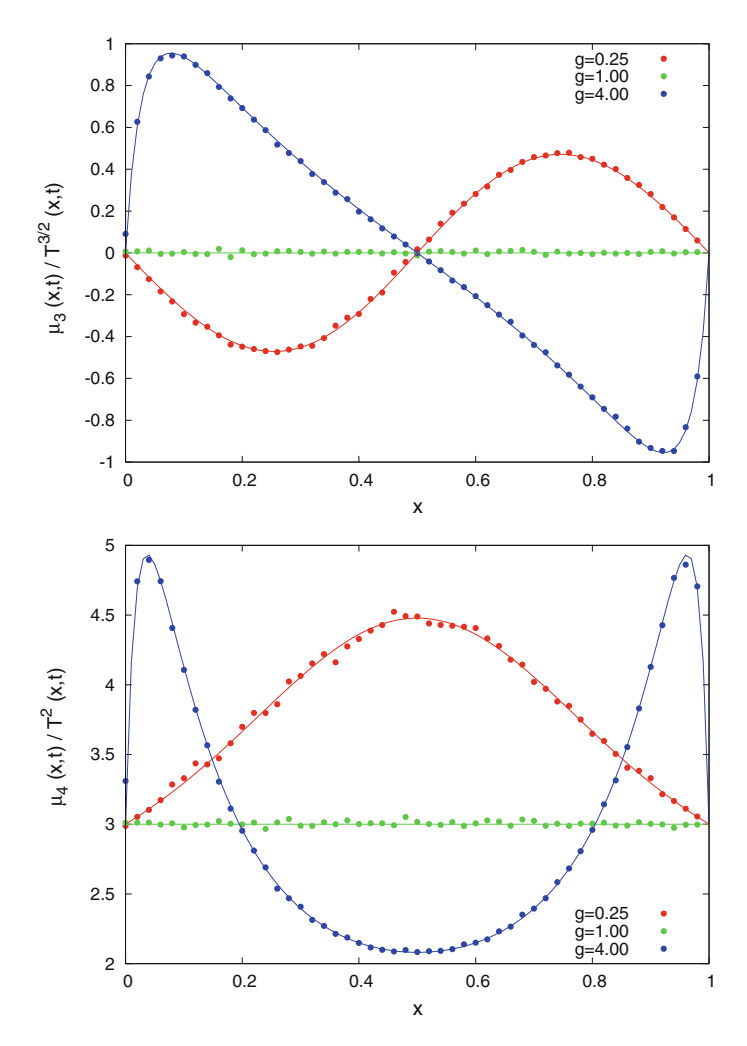


Fig. 4.8 Third and fourth central moments μ_3 (top) and μ_4 (bottom) in the Couette steady state for the same simulation as in Fig. 4.7. Numerical results are shown with symbols whereas the lines stand for the theoretical prediction, i.e. the solutions of Eq. (4.36). It is evident that, excluding the case q = 1, the one particle distribution is far from Gaussian in most of the spatial domain

initial particle velocities are drawn from a Gaussian distribution with local average velocity u(x, 0) = 0 and temperature T(x, 0) = 1. An excellent agreement is found in all the cases.

Figure 4.8 depicts the third and fourth central moments of the one-particle velocity distribution, scaled with their corresponding powers of the temperature, namely $\mu_3/T^{3/2}$ and μ_4/T^2 . Both moments display a non-trivial structure. In particular, the non-vanishing third moment clearly shows that the one-particle distribution is not symmetric with respect to the average velocity u. It is evident that the distribution is non-Gaussian, except for the case $T_B = 2a^2/\nu$, which corresponds to the USF state.

4.5 Numerical Results 131

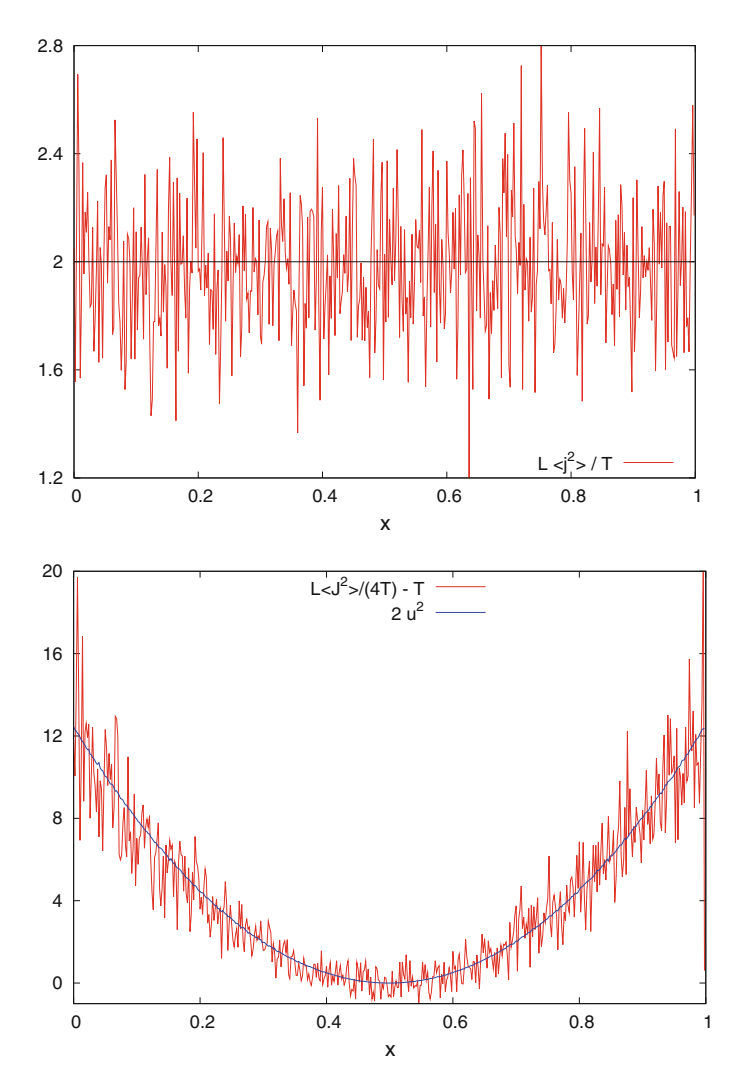


Fig. 4.9 Top: amplitude of the momentum current as a function of x in the USF state. Specifically, the rescaled amplitude $L\langle j^2(x,t)\rangle/T_s$ in the simulations (red line) and the theoretical constant value (black line) are plotted. Bottom: amplitude of the energy current as a function of x in the USF state. The numerical values of $L\langle J^2(x,t)\rangle/4T(x,t)-T(x,t)$ (red line) and $2u_s^2(x)$ (blue line) are here plotted. All the simulations have been done in a system with N=500, $\nu=20$, a=5, and $M=10^5$

4.5.5 Fluctuating Currents

A comparison for the amplitudes of noise for the velocity and energy currents is shown in Fig. 4.9. We carry it out in the USF state, in which the steady distribution

is Gaussian but the average velocity is not homogeneous. This allows us to make a more exigent test of the theoretical result for the amplitude of the energy current, as given by Eq. (4.65), which contains a term proportional to u^2 . The agreement is excellent for the amplitudes of both noises.

References

- A. Baldassarri, U. Marini Bettolo Marconi, A. Puglisi, Influence of correlations on the velocity statistics of scalar granular gases. EPL Europhys. Lett. 58(1),14 (2002). http://stacks.iop.org/ 0295-5075/58/i=1/a=014, https://doi.org/10.1209/epl/i2002-00600-6
- A. Prados, A. Lasanta, P.I. Hurtado, Large fluctuations in driven dissipative media. Phys. Rev. Lett. 107, 140601 (2011). https://link.aps.org/doi/10.1103/PhysRevLett.107.140601
- A. Lasanta, A. Manacorda, A. Prados, A. Puglisi, Fluctuating hydrodynamics and mesoscopic effects of spatial correlations in dissipative systems with conserved momentum. New J. Phys. 17, 083039 (2015). https://doi.org/10.1088/1367-2630/17/8/083039
- A. Manacorda, C.A. Plata, A. Lasanta, A. Puglisi, A. Prados, Lattice models for granular-like velocity fields: hydrodynamic description. J. Stat. Phys. 164(4), 810–841 (2016). https://doi. org/10.1007/s10955-016-1575-z
- C.A. Plata, A. Manacorda, A. Lasanta, A. Puglisi, A. Prados, Lattice models for granular-like velocity fields: finite-size effects. J. Stat. Mech. (Theor. Exp.) 2016(9), 093203 (2016). http:// stacks.iop.org/1742-5468/2016/i=9/a=093203
- 6. C.A. Plata, Ph.D. thesis, To be defended
- J.J. Brey, M.J. Ruiz-Montero, D. Cubero, Homogeneous cooling state of a low-density granular flow. Phys. Rev. E 54, 3664–3671 (1996). https://link.aps.org/doi/10.1103/PhysRevE.54.3664
- 8. M. Ernst, Nonlinear model-Boltzmann equations and exact solutions. Phys. Rep. **78**(1), 1–171 (1981). http://www.sciencedirect.com/science/article/pii/0370157381900028
- 9. M.H. Ernst, E. Trizac, A. Barrat, The rich behavior of the Boltzmann equation for dissipative gases. EPL (Europhys. Lett.) **76**(1), 56 (2006). http://stacks.iop.org/0295-5075/76/i=1/a=056, https://doi.org/10.1209/epl/i2006-10225-3
- A. Bortz, M. Kalos, J. Lebowitz, A new algorithm for Monte Carlo simulation of Ising spin systems. J. Comput. Phys. 17(1, 10–18 (1975). http://www.sciencedirect.com/science/article/ pii/0021999175900601
- A. Prados, J.J. Brey, B. Sánchez-Rey, A dynamical Monte Carlo algorithm for master equations with time-dependent transition rates. J. Stat. Phys. 89(3), 709–734 (1997). http://dx.doi.org/ 10.1007/BF02765541
- 12. N.G.V. Kampen. Stochastic Processes in Physics and Chemistry (North-Holland, 1992)
- U. Marini Bettolo Marconi, A. Puglisi, A. Vulpiani, About an H-theorem for systems with non-conservative interactions. J. Stat. Mech. (Theor. Exp.) 2013(08), P08003 (2013). http:// stacks.iop.org/1742-5468/2013/i=08/a=P08003
- M.I.G. de Soria, P. Maynar, S. Mischler, C. Mouhot, T. Rey, E. Trizac, Towards an H-theorem for granular gases. J. Stat. Mech. (Theor. Exp.) 2015(11), P11009 (2015). http://stacks.iop.org/ 1742-5468/2015/i=11/a=P11009
- C.A. Plata, A. Prados, Global stability and H theorem in lattice models with nonconservative interactions. Phys. Rev. E 95, 052121 (2017). https://link.aps.org/doi/10.1103/PhysRevE.95. 052121
- P.K. Haff, Grain flow as a fluid-mechanical phenomenon. J. Fluid Mech. 134, 401–430 (1983). https://doi.org/10.1017/S0022112083003419
- 17. A.W. Lees, S.F. Edwards, The computer study of transport processes under extreme conditions. J. Phys. C Solid State Phys. 5(15), 1921 (1972). http://stacks.iop.org/0022-3719/5/i=15/a=006

References 133

V. Garzó, Transport coefficients for an inelastic gas around uniform shear flow: linear stability analysis. Phys. Rev. E 73, 021304 (2006). https://link.aps.org/doi/10.1103/PhysRevE.73.021304

- A. Prados, A. Lasanta, P.I. Hurtado, Nonlinear driven diffusive systems with dissipation: fluctuating hydrodynamics. Phys. Rev. E 86, 031134 (2012). https://link.aps.org/doi/10.1103/ PhysRevE.86.031134
- P.I. Hurtado, A. Lasanta, A. Prados, Typical and rare fluctuations in nonlinear driven diffusive systems with dissipation. Phys. Rev. E 88, 022110 (2013). https://link.aps.org/doi/10.1103/ PhysRevE.88.022110
- 21. A. Lasanta, P.I. Hurtado, A. Prados, Statistics of the dissipated energy in driven diffusive systems. Eur. Phys. J. E **39**(3), 35 (2016), http://dx.doi.org/10.1140/epie/i2016-16035-4
- 22. R. Kubo, M. Toda, N. Hashitsume, *Statistical Physics II: Nonequilibrium Statistical Mechanics* (Springer Science & Business Media, Berlin, 2012)

Chapter 5 Granular Lattice: Beyond Molecular Chaos



I'm looking for a complication Looking cause I'm tired of trying Make my way back home when I learn to fly high

(Foo Fighters)

The hydrodynamic behavior derived in Chap. 4 and numerically analyzed in Sect. 4.5 has been obtained through the Molecular Chaos ansatz (4.14), mathematically equivalent to the factorization of velocity correlations

$$\langle v_{l,p}v_{l',p}\rangle = \langle v_{l,p}\rangle\langle v_{l',p}\rangle. \tag{5.1}$$

This approximation has been found acceptable when comparing the numerical data with the theoretical results. However, when looking at the time behavior of the rescaled temperature $\tilde{T}(t) = T(t)/T_{\text{HCS}}(t)$, numerical analysis has shown a divergence from the stationary solution $\tilde{T}=1$ which is expected in the region of stability of the HCS, so the Haff's law is violated as can be seen in Fig. 5.1. The main reason of this violation is the presence of velocity correlations between next-neighbor particles: in this section, we will analyze the effect of the correlations on the free cooling of the system. Interestingly, for the case of Maxwell molecules the effect of the correlations in the cooling can be determined in quite a detailed way. It will be shown that long-range correlations arise in the system, and tend to a stationary value. A multiple scales analysis of the temperature decay yields a "renormalised" mesoscopic dissipation coefficient ν^r , equivalent to ν in the limit $L \to \infty$. Finally, rescaled fluctuations of the total energy (expected to be stationary in the HCS) also have a divergent behavior in time: their time evolution is again derived from microscopic balance equations, showing the fact that two-particles energy corre-

lations are not scaling with the square of the temperature and therefore produce an increase of energy fluctuations with time. Numerical observations are shown together with analytical results.

5.1 Perturbative Solution for Temperature and Correlations

The system is assumed to be invariant under spatial translations, such as in the HCS case, see Sect. 4.3.1. The correlation of the velocity at time τ between two particles at distance k is

$$C_k(\tau) = \langle v_i(\tau)v_{i+k}(\tau) \rangle. \tag{5.2}$$

Throughout this section, the microscopic *continuous* time τ will be used, being equivalent to the collisional discrete time p with $\langle \delta \tau_p \rangle = (\omega \Omega_p(L))^{-1}$, see Sect. 4.1.1. For k=0, the correlations reduce to the average temperature

$$T(\tau) \equiv C_0(\tau) = \langle v_i^2(\tau) \rangle. \tag{5.3}$$

From the Master Equation 4.10 one can derive the evolution equations of the velocity correlations, namely

$$\omega^{-1}\partial_{\tau}C_0 = (\alpha^2 - 1)(C_0 - C_1), \tag{5.4a}$$

$$\omega^{-1}\partial_{\tau}C_{1} = \frac{1-\alpha^{2}}{2}(C_{0}-C_{1}) + (1+\alpha)(C_{2}-C_{1}), \tag{5.4b}$$

$$\omega^{-1}\partial_{\tau}C_{k} = (1+\alpha)(C_{k+1} + C_{k-1} - 2C_{k}), \quad 2 \le k \le (L-1)/2, \quad (5.4c)$$

$$C_{\frac{L+1}{2}} = C_{\frac{L-1}{2}}, \quad \forall \tau. \tag{5.4d}$$

The τ -dependence of the correlations has been omitted in the above equations to keep the notation simple. Here we have taken an odd L, because the boundary condition (5.4d) is simpler to write, and obviously this choice is irrelevant in the large size limit $L \to \infty$. The same equations can be derived in discrete time p by averaging Eq. (4.17).

The momentum conservation yields the "sum rule"

$$C_0(\tau) + 2\sum_{k=1}^{\frac{L-1}{2}} C_k(\tau) = 0, \quad \forall \tau,$$
 (5.5)

holding in the center of mass frame. In the equilibrium case with conservative interactions and $\alpha=1$, the correlations do not depend on the sites' distance k and they read $C_k^{\rm eq}=-T(L-1)^{-1}, \forall k>0$, see Appendix A.4.1, therefore being of order $O(L^{-1})$. In a non-equilibrium state, correlations may be non-uniform in space, but we still

assume them to be of order $O(L^{-1})$. Then, we introduce the rescaled correlation $D_k(\tau)$ as

$$D_k(\tau) = LC_k(\tau),\tag{5.6}$$

which is assumed to be finite in the infinite size limit.

In the large system size limit we expect $D_k(\tau)$ to be a smooth function of space, in the sense that $D_{k+1}(\tau) - D_k(\tau) = O(L^{-1})$. Then, introducing again the typical hydrodynamic length and time scales defined in Eq. (4.25), i.e.

$$x = \frac{k-1}{L}, \quad t = \frac{\omega\tau}{L^2} = \frac{p}{L^3},$$
 (5.7)

we can now write Eq. (5.4) in the large size limit. Keeping solely terms up to $O(L^{-1})$, we arrive at

$$\frac{dT(t)}{dt} = -\nu \left[T(t) - L^{-1} \psi(t) \right],\tag{5.8a}$$

$$\nu T(t) + 4\partial_x D(x,t)|_{x=0} = L^{-1} \left(\frac{d\psi(t)}{dt} + \nu \psi(t) \right), \tag{5.8b}$$

$$\partial_t D(x,t) = 2 \, \partial_{xx} D(x,t),$$
 (5.8c)

$$\partial_x D(x,t)|_{x=1/2} = \frac{1}{2} L^{-1} \frac{d\chi(t)}{dt},$$
 (5.8d)

having defined

$$\psi(t) = \lim_{x \to 0} D(x, t), \quad \chi(t) = \lim_{x \to \frac{1}{2}} D(x, t). \tag{5.9}$$

These equations hold exactly up to times $t \ll L^2$, since the $O(L^{-2})$ terms are the lower order terms neglected; those would lead to the appearance of fourth derivatives in space in Eq. (5.8b). Equation (5.8a) shows the presence of a $O(L^{-1})$ correction of the cooling rate, given by the non-vanishing nearest-neighbor velocity correlation.

The derived equations are - and must be - consistent with the sum rule (5.5). Retaining only terms up to $O(L^{-1})$ included, we find (see Appendix A.3 for details)

$$T(t) + 2 \int_0^1 dx \, D(x, t) + L^{-1} \left[\psi(t) - 2\chi(t) \right] = O(L^{-2}). \tag{5.10}$$

The lhs of the above equation is a constant of motion, as can be readily shown from the evolution equations (5.8).

The solution of the above system can be made easier defining the scaled (tilde) fields with their corresponding power of $T_{HCS}(t)$, analogously with Sect. 4.3.1. Introducing

$$\widetilde{T}(t) = \frac{T(t)}{T_{\text{HCS}}(t)}, \quad \widetilde{D}(x,t) = \frac{D(x,t)}{T_{\text{HCS}}(t)}, \tag{5.11}$$

the rescaled fields obey the equations

$$\frac{d\tilde{T}(t)}{dt} = \nu L^{-1}\tilde{\psi}(t),\tag{5.12a}$$

$$\nu \tilde{T}(t) + 4\partial_x \tilde{D}(x,t)|_{x=0} = L^{-1} \frac{d\tilde{\psi}(t)}{dt},$$
(5.12b)

$$\partial_t \widetilde{D}(x,t) = \nu \widetilde{D}(x,t) + 2 \,\partial_{xx} \widetilde{D}(x,t),$$
 (5.12c)

$$\partial_x \widetilde{D}(x,t)|_{x=1/2} = \frac{1}{2} L^{-1} \left(\frac{d\widetilde{\chi}(t)}{dt} - \nu \widetilde{\chi}(t) \right). \tag{5.12d}$$

The system above is linear in (\tilde{T}, \tilde{D}) , so it is possible to look for its exact solution: this has been done in [1, 2]. We are here interested in the cooling rate correction introduced by the velocity correlations, so we look for a solution of Eq. (5.12) by means of a perturbative approach. We define the expansion of all functions of time in powers of L^{-1} as

$$\tilde{T}(t) = \tilde{T}_0(t) + L^{-1}\tilde{T}_1(t) + O(L^{-2}),$$
 (5.13a)

$$\widetilde{D}(x,t) = \widetilde{D}_0(x,t) + L^{-1}\widetilde{D}_1(x,t) + O(L^{-2}),$$
 (5.13b)

with analogous expansions for $\widetilde{\psi}(t)$ and $\widetilde{\chi}(t)$.

To the lowest order, one gets

$$\frac{\mathrm{d}}{\mathrm{d}t}\tilde{T}_0 = 0,\tag{5.14a}$$

$$\nu \tilde{T}_0 + 4\partial_x \tilde{D}_0|_{x=0} = 0, \tag{5.14b}$$

$$\partial_t \widetilde{D}_0 = \nu \widetilde{D}_0 + 2 \,\partial_{xx} \widetilde{D}_0, \tag{5.14c}$$

$$\partial_x \widetilde{D}_0|_{x=1/2} = 0. (5.14d)$$

The first equation yields the constant solution $T_0 = 1$. Furthermore, the scaled correlations tend to a stationary value for long times, given by

$$\widetilde{D}_0(x) = -A\cos\left[\pi\sqrt{\frac{\nu}{\nu_c}}(1-2x)\right], \quad A = \pi\sqrt{\frac{\nu}{\nu_c}}\csc\left(\pi\sqrt{\frac{\nu}{\nu_c}}\right). \tag{5.15}$$

Looking for the first order corrections, the correction to the dissipation coefficient is given by the equation for $\tilde{T}_1(t)$, namely

$$\frac{\mathrm{d}}{\mathrm{d}t}\tilde{T}_1(t) = \nu \tilde{\psi}_0(t). \tag{5.16}$$

When the correlations reached the stationary profile (5.15), we can write

$$\frac{\mathrm{d}}{\mathrm{d}t}\tilde{T}_1(t) = \nu\psi_{\mathrm{HCS}},\tag{5.17}$$

defining ψ_{HCS} as

$$\psi_{\text{\tiny HCS}} \equiv -\pi \sqrt{\frac{\nu}{\nu_c}} \cot \left(\pi \sqrt{\frac{\nu}{\nu_c}} \right). \tag{5.18}$$

Therefore, for $t \gg 1$ the rescaled temperature is linearly diverging as

$$\tilde{T}(t) \sim 1 + \frac{\nu \psi_{\text{HCS}}}{L} t + O(L^{-2}),$$
 (5.19)

neglecting the transient terms for \tilde{T}_1 . The last result explains the divergence of the rescaled temperature in time, and it has been compared with simulations in Fig. 5.1. Equation (5.19) also yields the presence of a transition at $\nu = \nu_{\psi} = 2\pi^2$, where $\psi_{\text{HCS}} = 0$ and first-order corrections to Haff's law vanish.

The theoretical prediction (5.15) for the velocity correlations in the HCS has been numerically checked in Fig. 5.2. The nearest-neighbors rescaled correlation $\widetilde{\psi}(t)$ and the amplitude A are there plotted in function of time t and dissipation ν respectively, and compared with Eq. (5.15). Trajectories start from a random configuration of velocities with uniform distribution and zero average, i.e. $u(x, 0) \equiv 0$. A very good agreement is found once more.

It has been already observed that the solution of Eq. (5.19) is valid only for $\psi_{\text{HCS}}\nu t/L\ll 1$, while in this section the stationary value of the correlations has been used supposing $t\gg 1$. These conditions may be consistent or not depending on the value of ν and L: actually, simulated data in Fig. 5.2 clearly agree with the theoretical prediction of Eq. (5.19) for $\nu<60$, while for higher values of the dissipation the nearest-neighbor correlations do not seem to have reached their stationary value. Therefore, longer trajectories should be observed and this leads to the divergence of the first order perturbation O(t/L), breaking the validity of the perturbative expansion introduced.

5.2 Temperature and Correlations Evolution: Multiple-Scale Analysis

In order to build up a consistent theory over long times, we now introduce a multiple-scale perturbative solution of Eq. (5.12). Following the approach in [3], from Eq. (5.12a) two distinct time scales can be defined: the usual time t and a slow time scale σ , namely

$$s = t, \ \sigma = L^{-1}t, \ \partial_t = \partial_s + L^{-1}\partial_\sigma.$$
 (5.20)

This notation allows a distinction between ∂_t (with constant x) and ∂_s (with constant x and σ). All functions of time are expanded in powers of L^{-1} as before and considered as functions of two *independent* times (s, σ) . So, to the lowest order we have

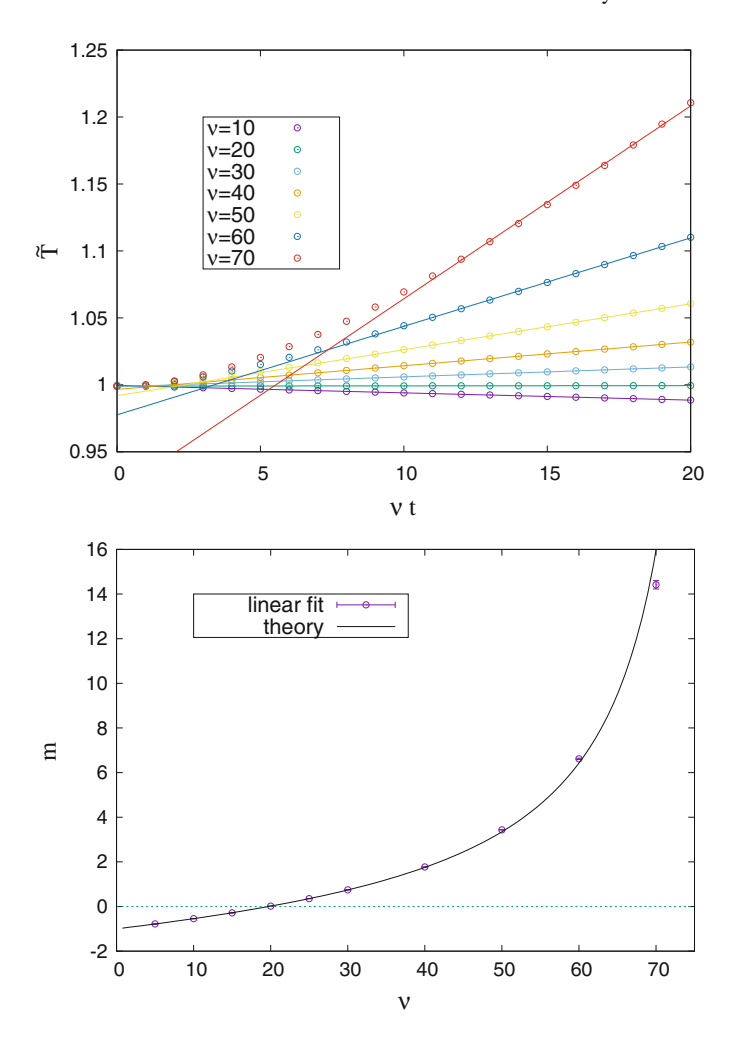


Fig. 5.1 Top panel: rescaled temperature \tilde{T} as a function of time. The numerical values of \tilde{T} (circles) and the linear fits (lines) in the second part of the trajectory are compared, for several values of ν (see legend). Bottom panel: the slope $m = L d\tilde{T}/d(\nu t)$ as a function of ν . Comparison between the fitted slopes in the top panel (circles) and their theoretical values, given by $\psi_{ ext{HCS}}$ in Eq. (5.16) (blue line). The horizontal dashed line marks the transition at $\nu_{\psi} = 2\pi^2$. Simulations are made with L = 1000 sites

$$\partial_s \tilde{T}_0(s, \sigma) = 0, \tag{5.21a}$$

$$\nu \tilde{T}_0 + 4 \partial_x \tilde{D}_0|_{x=0} = 0,$$

$$\partial_s \tilde{D}_0 = \nu \tilde{D}_0 + 2 \partial_{xx} \tilde{D}_0,$$
(5.21b)
(5.21c)

$$\partial_s \widetilde{D}_0 = \nu \widetilde{D}_0 + 2 \, \partial_{xx} \widetilde{D}_0, \tag{5.21c}$$

$$\partial_x \widetilde{D}_0|_{x=1/2} = 0. \tag{5.21d}$$

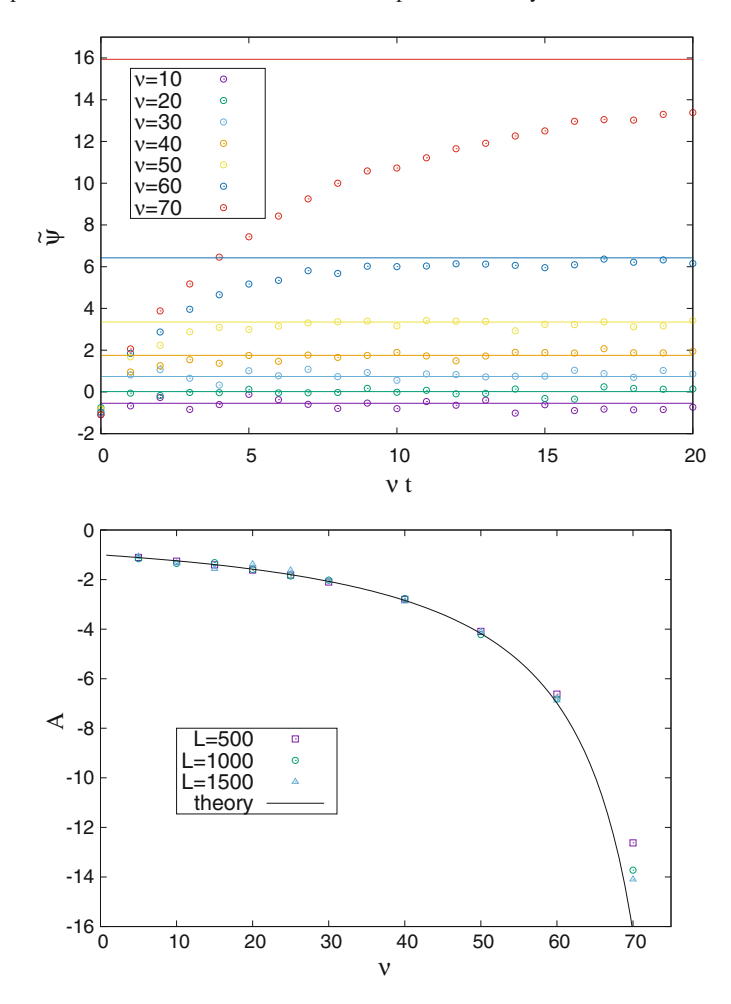


Fig. 5.2 Top panel: time evolution of nearest-neighbor rescaled correlations $\psi(t)$. Numerical values (circles) for several ν (see legend) are plotted as a function of the dimensionless time νt , together with their theoretical stationary values given by Eq. (5.18) (lines). The correlations reach their stationary value for all $\nu \leq 60$ in the plotted time window, while they do not for $\nu = 70$. This discrepancy will be analyzed in Fig. 5.3. Simulations made with L = 1000. Bottom panel: correlation amplitude A, defined in Eq. (5.15), as a function of ν . The numerical value (symbols) and its theoretical expectation (black line) are plotted. Simulations with L = 250, 500, 1000. A very good agreement is found for all $\nu < 70$

having the same form of Eq. (5.14), but now \tilde{T}_0 depends also on the slow time scale σ ; more precisely, Eq. (5.21a) prove that it depends only on σ , $\tilde{T}_0(s,\sigma) = \tilde{T}_0(\sigma)$. Also, a pseudo-stationary solution for $\tilde{D}_0(x,s,\sigma)$ can be found from Eq. (5.21), for long time scales $s \gg 1$ but finite σ , namely

¹Note that $\tilde{T}_0(\sigma)$ remains undetermined at the lowest order.

$$\widetilde{D}_0(x,\sigma) = -\widetilde{T}_0(\sigma)A\cos\left[\pi\sqrt{\frac{\nu}{\nu_c}}(1-2x)\right],\tag{5.22}$$

differing from (5.15) because of the σ dependence of $\tilde{T}_0(\sigma)$. The latter can be obtained by writing down the equations for the first order corrections. In fact, for the present purposes, it suffices to write the evolution equation for $T_1(s, \sigma)$,

$$\partial_s \tilde{T}_1 + \frac{d}{d\sigma} \tilde{T}_0 = \nu \tilde{\psi}_0, \qquad \tilde{\psi}_0 = \tilde{T}_0 \psi_{\text{HCS}}.$$
 (5.23)

Since the rescaled energy should not contain linear terms in time (see [1, 2] for a rigorous proof), the first lhs term of (5.23) must vanish, and

$$\nu \psi_{\text{HCS}} \tilde{T}_0(\sigma) - \frac{\mathrm{d}}{\mathrm{d}\sigma} \tilde{T}_0 = 0 \implies \tilde{T}_0(\sigma) = e^{\nu \psi_{\text{HCS}}\sigma},$$
 (5.24)

taking into account that $\tilde{T}_0(t=0)=1$. Going back to the unscaled variables, Eq. (5.24) can be rewritten as

$$T(t) = T(0) \exp\left[-\nu_{\text{HCS}}^{r}t\right] + O(L^{-1}), \qquad \nu_{\text{HCS}}^{r} = \nu\left(1 - L^{-1}\psi_{\text{HCS}}\right).$$
 (5.25)

The last result gives the finite size correction of the cooling rate in the Haff's law. Obviously, if we consider that $\sigma = t/L \ll 1$ and retain only the linear terms in L^{-1} , the results of Eq. (5.19) are reobtained,

The renormalization of the Haff's law predicted by Eq. (5.25) is verified in Fig. 5.3: simulations made over long times $\nu t \psi_{\text{HCS}} \sim L$ show the exponential behavior of the rescaled temperature, as predicted from the multiple-scale analysis. Numerical results are in good agreement with the theoretical prediction (5.24). Nearest-neighbor correlations have been studied as in Fig. 5.1: Fig. 5.3 shows that for $\nu = 50$, 60 they converge to their expected value after a very short transient, whereas for $\nu = 70$ the stationary value is smaller than its theoretical prediction. It is here possible that next order corrections are becoming relevant when approaching the critical dissipation ν_c , where it is known that ψ_{HCS} is divergent.

5.3 Total Energy Fluctuations and Multiscaling

The distribution of the extensive energy $E(\tau) = \sum_l v_l^2(\tau)$ is a central problem in granular systems. Usually, granular models present non-Gaussian distributions that can be mostly characterized by the study of their fluctuations [4]. Within the same spirit of Sect. 5.1, this section aims to derive the total energy rescaled fluctuations $\Sigma(\tau)$, defined as

$$\Sigma^{2}(\tau) = \frac{\langle E^{2}(\tau) \rangle - \langle E(\tau) \rangle^{2}}{\langle E(\tau) \rangle^{2}}.$$
 (5.26)

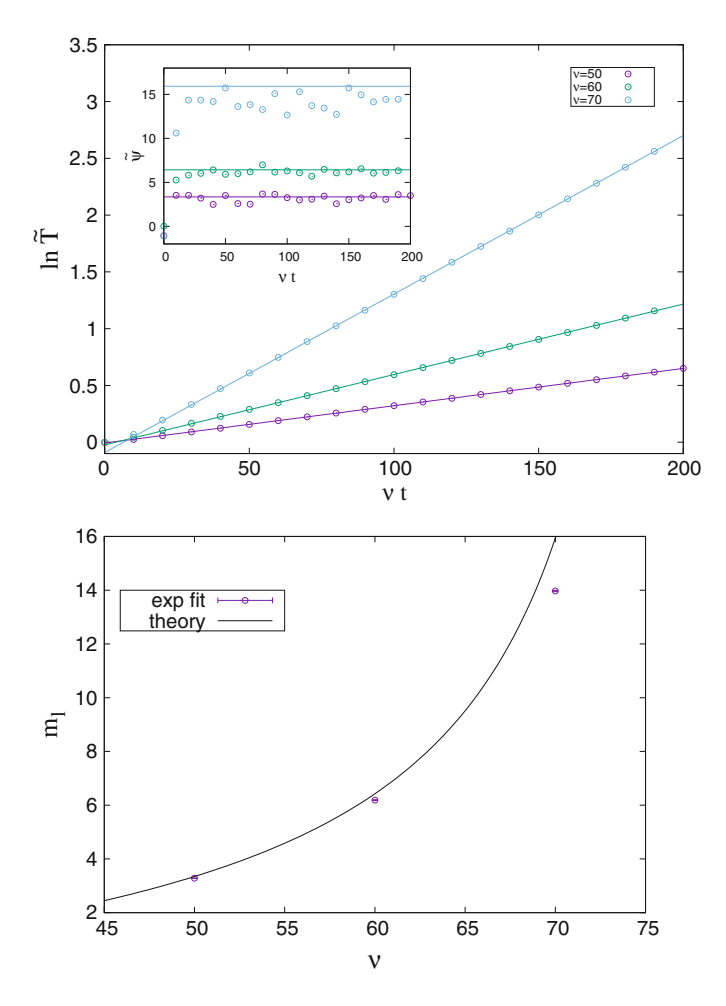


Fig. 5.3 Top panel: log-linear plot of the rescaled temperature. Simulated values are plotted for $\nu=50,60,70$ (circles), together with the fits upon the second part of the long trajectories (lines). The time evolution is clearly exponential as predicted from Eq. (5.24). Inset: time evolution of the nearest-neighbor rescaled correlations $\widetilde{\psi}(t)$ for long trajectories, simulations (circles) and theoretical stationary values (lines). Bottom panel: slope m_l of the time evolution of $\ln \widetilde{T}$. The fitted values from the top panel (squares) are shown together with the theoretical prediction (5.24) (black line). All the realizations have been done with L=1000 particles up to a maximum time $\nu t=200$

Assuming the Local Equilibrium Approximation (LEA) one immediately finds the constant solution $\Sigma^2(\tau)=2/L$. However, the time evolution of $\Sigma^2(\tau)$ numerically observed is clearly divergent from the LEA solution, as can be seen in Fig. 5.4.

This kind of anomalous behavior is generally associated with the presence of a multiscaling of the velocity moments [5], i.e. the moments are not scaling proportionally to the granular temperature $T(\tau) = \langle v^2(\tau) \rangle$. Notwithstanding, this phenomenon

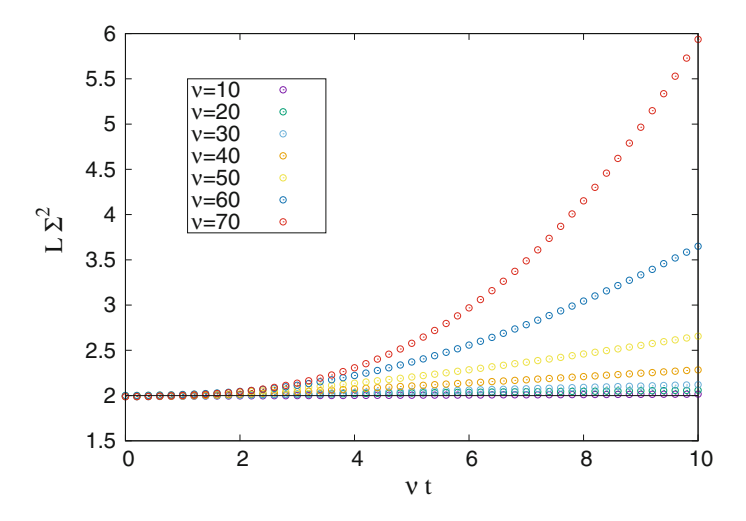


Fig. 5.4 Total energy rescaled fluctuations as a function of dimensionless time νt . Numerical results are plotted for $\nu=10,20,\ldots,70$, always with L=1000. The divergence from the expected LEA value is evident and grows with ν

can also be explained by a well-defined scaled distribution function with some divergent moments [6, 7]. Following the same approach of Sect. 5.1, we look for a direct calculation of the energy fluctuations by means of the evolution equations for the 4th order moments and correlations.

In the homogeneous case, the evolution equations read

$$\langle E^{2}(\tau) \rangle = \sum_{l=1}^{L} \langle v_{l}^{4}(\tau) \rangle + \sum_{l=1}^{L} \sum_{k=1}^{L-1} \langle v_{l}^{2}(\tau) v_{l+k}^{2}(\tau) \rangle$$

$$= L \langle v^{4}(\tau) \rangle + L \left[(L-1)T^{2}(\tau) + 2 \sum_{k=1}^{(L-1)/2} C_{k}^{2,2}(\tau) \right],$$

$$\langle E(\tau) \rangle = LT(\tau),$$
(5.27b)

having defined the two-particle squared velocity correlation function

$$C_k^{2,2}(\tau) = \langle v_l^2(\tau) v_{l+k}^2(\tau) \rangle - T^2(\tau), \quad k \neq 0.$$
 (5.28)

Therefore, the energy fluctuations dynamics is given by the dynamics of $T(\tau)$, $q(\tau) = \langle v^4(\tau) \rangle$ and $C_k^{2,2}(\tau)$ altogether.

Rescaled energy fluctuations hence read

$$L\Sigma^{2}(t) = 2 + a_{2}(t) + \frac{2}{T^{2}(t)} \int_{0}^{\frac{1}{2} - \frac{3}{2L}} D^{2,2}(x,t) dx,$$
 (5.29)

moving to continuum fields through the hydrodynamic scaling defined in Eq. (5.7) and introducing the excess kurtosis field $a_2(t)=q(t)/T^2(t)-3$. The correlation field $D^{2,2}=LC^{2,2}$ has been defined analogously with the scaling used in Sect. 5.1, and is expected to be finite in the large size limite. The evolution equations for these fields can be computed from the microscopic dynamics (4.15). A perturbative approach analogous to the one in Sect. 5.1 gives a set of equations similar to Eq. (5.14), coupling all the one-particle and two-particles fourth-degree fields, namely q(t), $D^{2,2}(x,t)$ and $D^{3,1}(x,t)$. The latter is the large-size limit of $D_k^{3,1}(\tau)=L\left\langle v_l^3(\tau)\,v_{l+k}(\tau)\right\rangle$. Also, these equations contain the three-particles velocity correlations, namely $C_{i,j}^{1,2,1}(\tau)=\left\langle v_{l-i}(\tau)\,v_l^2(\tau)\,v_{l+j}(\tau)\right\rangle$. To get a closed set, we need to make use of the *clustering ansatz*, i.e. the three-particles correlations $C^{1,2,1}$ are simplified through a cluster expansion and the purely correlated terms are neglected, namely

$$C_{i,j}^{1,2,1}(\tau) = \left\langle v_l^2(\tau) \right\rangle \left\langle v_{l-i}(\tau) v_{l+j}(\tau) \right\rangle + 2 \left\langle v_l(\tau) v_{l-i}(\tau) \right\rangle \left\langle v_l(\tau) v_{l+j}(\tau) \right\rangle + \mathcal{O}(L^{-3}) = \frac{1}{L} T(\tau) D_{|i+j|}(\tau) + \frac{2}{L^2} D_i(\tau) D_j(\tau) + \mathcal{O}(L^{-3}).$$

$$(5.30)$$

The derivation from microscopic dynamics is lengthy and painful but conceptually easy to understand: it relies on the expansion of correlation fields and moments, analogous to the one defined in Eq. (5.13). The main steps and the final results are here shown; in Appendix A.4 the reader will find the detailed calculations to obtain the results presented in the section.

Starting from the microscopic dynamics defined in Eq. (4.15) and moving to the continuum limit, with the clustering ansatz one gets to the lowest order

$$\frac{d}{dt}\tilde{q}_0(t) = 0, (5.31a)$$

$$\nu \left[\tilde{q}_0(t) + 3\tilde{T}_0^2 \right] + 8\partial_x \tilde{D}_0^{3,1}|_{x=0} = 0, \tag{5.31b}$$

$$\partial_t \widetilde{D}_0^{3,1} = \frac{\nu}{2} \left(\widetilde{D}_0^{3,1} + \widetilde{T}_0 \widetilde{D}_0 \right) + 2 \, \partial_{xx} \widetilde{D}_0^{3,1},$$
 (5.31c)

$$\partial_x \widetilde{D}_0^{3,1}|_{x=1/2} = 0, (5.31d)$$

$$\partial_x \widetilde{D}_0^{2,2}|_{x=0} = 0, (5.31e)$$

$$\partial_t \widetilde{D}_0^{2,2} = 2 \, \partial_{xx} \widetilde{D}_0^{2,2},\tag{5.31f}$$

$$\partial_x \widetilde{D}_0^{2,2}|_{x=1/2} = 0. {(5.31g)}$$

These equations can be readily solved. If the initial distribution is Gaussian, we have at any time $\tilde{q}_0 = 3 \, \tilde{T}_0^2$. Furthermore, in the long time limit $t \gg 1$, the stationary fields read

$$\widetilde{D}_0^{3,1}(x) = 3\,\widetilde{D}_0(x), \qquad \widetilde{D}_0^{2,2}(x) = 0,$$
(5.32)

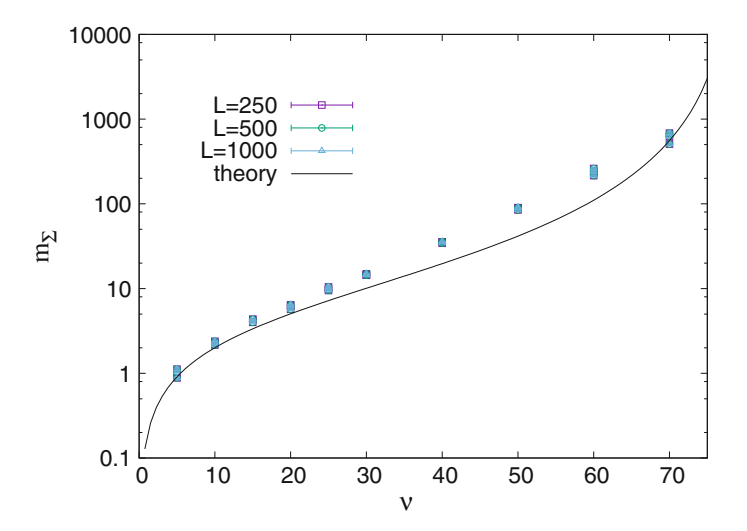


Fig. 5.5 Slope of the energy fluctuations in function of time. The fitted values (symbols) in the second part of the trajectories are compared with the theoretical prediction $m_{\Sigma}(\nu)$ in (5.38) (black line). Simulations are carried out as in Fig. 5.4 but with L=250,500,1000 particles

recalling that $\tilde{T}_0 = 1$. It must be noticed that these results do not lead to any multiscaling effect such as the one observed into the simulations.

In light of the above, it is necessary to compute the next perturbative order. The equations needed from the definition (5.29) are those for \tilde{q}_1 and $\widetilde{D}_1^{2,2}$, i.e.

$$\frac{\mathrm{d}}{\mathrm{d}t}\tilde{q}_1(t) = 2\nu\tilde{\psi}_0^{3,1}(t),\tag{5.33a}$$

$$\nu \widetilde{T}_0 \widetilde{\psi}_0 + \partial_x \widetilde{D}_1^{2,2}|_{x=0} = 0, \tag{5.33b}$$

$$\partial_t \widetilde{D}_1^{2,2} = 2 \, \partial_{xx} \widetilde{D}_1^{2,2} + 4 \, \nu \widetilde{D}_0^2,$$
 (5.33c)

$$\partial_x \widetilde{D}_1^{2,2}|_{x=1/2} = 0, (5.33d)$$

where $\widetilde{\psi}^{3,1}(t) = \lim_{x \to 0} \widetilde{D}^{3,1}(x,t)$. Equation (5.33a) can be easily solved for long times since $\widetilde{D}_0^{3,1}(x,t)$ is known from (5.32), yielding

$$\tilde{q}_1(t) = 2\nu \psi_0^{3,1} = 6\nu \psi_{\text{HCS}}.$$
 (5.34)

Looking at the $\tilde{D}_1^{2,2}$ field from Eq. (5.29), for our purposes it is sufficient to compute the integral $\Delta_1(t) = \int_0^1 dx \ \tilde{D}_1^{2,2}(x,t)$. Considering Eq. (5.33), we have that

$$\frac{d}{dt}\Delta_1(t) = 4\nu \left[\psi_0(t) + \int_0^1 dx \, \widetilde{D}_0^2(x, t) \right],\tag{5.35}$$

having used the boundary condition

$$\partial_x \widetilde{D}_1^{2,2}|_{x=1^-} = -\partial_x \widetilde{D}_1^{2,2}|_{x=0^+}. \tag{5.36}$$

Therefore, in the long time limit the stationary correlation profile $\widetilde{D}(x)$ from Eq. (5.15) yields a stationary growth of $\Delta_1(t)$, namely

$$\frac{d}{dt}\Delta_1(t) = 2\nu \left[\frac{\pi\sqrt{\nu/\nu_c}}{\sin\left(\pi\sqrt{\nu/\nu_c}\right)} \right]^2 \left[1 - \frac{\sin\left(2\pi\sqrt{\nu/\nu_c}\right)}{2\pi\sqrt{\nu/\nu_c}} \right]. \tag{5.37}$$

It is now possible to compute the energy fluctuations of Eq. (5.29). To the first order, from Eqs. (5.34) and (5.16) we can see that the excess kurtosis $a_2(t)$ vanishes for all times if it initially did so, so $a_2(t) = O(L^{-2})$. Therefore the steady-state linear divergence of the energy fluctuations (to the first order) is given by the $D^{2,2}$ correlations term in (5.37). Specifically, for $t \gg 1$, we have

$$\frac{d}{dt}\Sigma^{2}(t) = \frac{1}{L}\frac{d}{dt}\Delta_{1}(t) = \frac{\nu}{L}m_{\Sigma}(\nu), \tag{5.38}$$

where the factor $m_{\Sigma}(\nu) = d\Delta_1/d(\nu t)$ is the slope of the energy fluctuations in function of the dimensionless time νt .

In conclusion, it seems that the observed energy multiscaling stems from the multiscaling of two-particles and three-particles correlation fields, while the single-particle fourth moment still scales with the squared granular temperature. This theoretical result has been compared with simulations in Fig. 5.5. Although their agreement is slightly less accurate than in the previous cases - especially for high ν - we see that they both exhibit a similar trend over three decades of m_{Σ} values.

In order to improve the agreement between theory and simulations, a multiple scale analysis has also been performed, analogous to that in Sect. 5.2, keeping the clustering ansatz (5.30). Nevertheless, this step does not improve the agreement with the numerics, therefore the clustering ansatz may be the main responsible for the discrepancy observed.

References

- C.A. Plata, A. Manacorda, A. Lasanta, A. Puglisi, A. Prados, Lattice models for granular-like velocity fields: finite-size effects. J. Stat. Mech. (Theor. Exp.) 2016(9), 093203 (2016). http://stacks.iop.org/1742-5468/2016/i=9/a=093203, https://doi.org/10.1088/ 1742-5468/2016/09/093203
- 2. C.A. Plata, Ph.D. thesis, To be defended
- C.M. Bender, S.A. Orszag, in Advanced Mathematical Methods for Scientists and Engineers (Springer, Berlin, 1999)

- J.J. Brey, A. Domínguez, M.I. García de Soria, P. Maynar, Mesoscopic theory of critical fluctuations in isolated granular gases. Phys. Rev. Lett. 96, 158002 (2006). https://doi.org/10.1103/PhysRevLett.96.158002
- E. Ben-Naim, P.L. Krapivsky, Multiscaling in inelastic collisions. Phys. Rev. E 61, R5–R8 (2000). https://doi.org/10.1103/PhysRevE.61.R5
- A. Baldassarri, U.M.B. Marconi, A. Puglisi, Influence of correlations on the velocity statistics of scalar granular gases. EPL (Europhys. Lett.) 58(1), 14 (2002). https://doi.org/10.1209/epl/ i2002-00600-6
- G. Costantini, U.M.B. Marconi, A. Puglisi, Velocity fluctuations in a one-dimensional inelastic Maxwell model. J. Stat. Mech. Theory Exp. 2007(08), P08031 (2007). http://stacks.iop.org/ 1742-5468/2007/i=08/a=P08031, https://doi.org/10.1088/1742-5468/2007/08/P08031

Chapter 6 Active Lattice Fluctuating Hydrodynamics



It don't mean a thing
If it ain't got that swing

(D. Ellington)

The granular lattice model analyzed in the last chapters has shown to reproduce realistic physical phenomena and to lead towards new analytical results on nonequilibrium fluctuating hydrodynamics [1–3]. The generality of the method brought us to the formulation of a lattice model of active matter, which will be developed along the same lines [4].

Here we introduce a model of granular active particles (GAP) on the lattice where pairwise interactions combine excluded volume and dissipative alignment, quite similarly to the off-lattice model in [5] described in Sect. 2.3. The main result is a set of hydrodynamic equations for the density, momentum and energy fields with fluctuating currents and source terms, in analogy with granular lattice results in Chap. 4. An application of these general equations is given in the dilute limit, assuming local equilibrium [6], where they describe a gas-swarming phase transition through the linear instability of the homogeneous disordered state. The homogeneous swarming [7] state arises when either the noise amplitude is small enough or the aligning force is strong enough. Numerical simulations are in fair agreement with the theory - including predictions of the macroscopic noise amplitudes - for packing fraction smaller than 10%: they also suggest that the instability is discontinuous in the large volume limit. Simulations also display the emergence of clustering and phase separation at higher packing fraction, where our assumptions fail.

6.1 Definition of the Model

6.1.1 Microscopic Ingredients

We consider a square lattice in d dimensions of volume $V = L^d$, with $1 \ll N \leq V$ self-propelled particles moving on it. A lattice site $\mathbf{i} = (i_1, i_2, \dots, i_d) \in \{1, L\}^d = \Lambda$ can be occupied at most by one particle (excluded volume) and is described by its occupation number $n_{\mathbf{i}} \in \{0, 1\}$ and its "active velocity" $\mathbf{v_i} \in \mathbb{R}^d$ (the meaning of this variable is discussed later). The elementary moves that constitute the microscopic evolution of each particle, see Fig. 6.1, amount to

- hopping;
- nearest-neighbors interactions;
- self-propulsion;
- noise.

Hopping means that a particle at site \mathbf{i} can move to an adjacent site $\mathbf{i} + \sigma \mathbf{e}_l$, being \mathbf{e}_l the unit vector in the lth direction and $\sigma = \pm 1$ the orientation of the hop, with $l = 1, \ldots, d$. The probability of hopping per unit of time can generally be velocity-dependent.

Pairwise interactions are represented by a contact force: when two particles with active velocities \mathbf{v} and \mathbf{v}' are nearest-neighbors, they act on each other with a force

$$\mathbf{f}^{(2)}(\mathbf{v}, \mathbf{v}') = -\mathbf{f}^{(2)}(\mathbf{v}', \mathbf{v}), \qquad (6.1)$$

where $\mathbf{f}^{(2)}(\mathbf{v}, \mathbf{v}')$ represents the force transmitted from a particle with velocity \mathbf{v} to a particle with velocity \mathbf{v}' . The above relation implies the conservation of total momentum during interactions. The force can be dissipative or conservative; from Sect. 6.2 on we will focus on the dissipative case, in analogy with granular collisions.

Self-propulsion consists of a velocity-dependent force $\mathbf{f}^{(1)}(\mathbf{v})$: indeed, the speed of active particles $v = |\mathbf{v}|$ is not fixed and the self-propulsion acts to maintain the state of motion of the particles, typically pushing them towards a fixed point of the speed v_s . The self-propulsion is combined with a vectorial Wiener process $\Delta \mathbf{W_i}(t)$ independently acting upon each component of the velocity of each particle, with a velocity-diffusion tensor $\mathbf{B}(\mathbf{v})$.

The state of the system is completely determined by its microscopic configuration $\{n_i, \mathbf{v_i}\}$. The system evolves with a discretized time. The index $p \in \mathbb{N}$ denotes the number of performed time steps. Physical time reads $t = p\Delta t \in \mathbb{R}$, where Δt will go to zero when taking the continuum limit, as well as the physical distance between two lattice sites Δx .

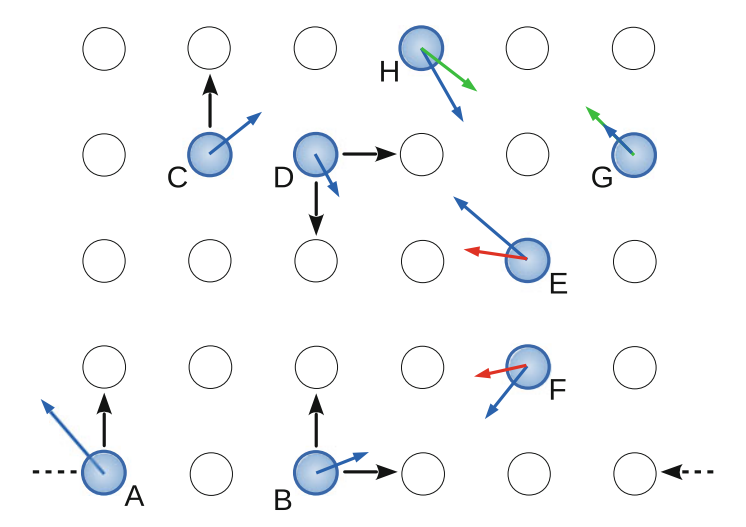


Fig. 6.1 Sketch of active particles in a 2*d* lattice. Particles A–D show hopping (black arrows) to neighbor sites according to the directions of their active velocity (blue arrows), including periodic conditions (A, dashed arrow) and excluded volume (C, D). Next-neighbors interact (E, F), with a force which aligns velocities (from blue to red arrows). Self-propulsion acts in the direction of the velocity and brings the speed toward a fixed value (G, from blue to green arrow). The velocity of a particle can be modified also by external noise (H, from blue to green). All the contributions are acting on every particle at the same time, but they are represented separately for the sake of clarity

6.1.2 Physical Interpretation

The model possesses the main features of active matter models described in Sect. 2.2. The interplay between an interaction rule and a self-propulsion is present [8], combined with a noise term which can be interpreted as the effect of hidden degrees of freedom like the action of surrounding fluid or the random exploration of space performed by active units [9-13]. Conversely from the granular case, the particles move on the lattice when hopping, similarly with the exclusion processes described in Sect. 3.3.1 [14–16]. Additionally, particles hop from one site to another depending on the active velocity degree of freedom directly entering in the hopping probabilities: indeed, with the "natural active velocity" hopping probability defined in the next subsection, a probe particle on an empty lattice follows a ballistic motion with $\langle \mathbf{x}(t) - \mathbf{x}(0) \rangle = \mathbf{v} t$, where v is constant in absence of self-propulsion, noise and interactions. However, this is not the case in a crowded environment: when all the adjacent sites are occupied, a particle with a non-vanishing active velocity does not move at all because of excluded volume. This is why we call $\mathbf{v_i}$ the active velocity of a particle in the site i: it represents the tendency of active particles to move with a given direction and speed provided that the direction of motion is not occupied by other particles. This behavior may reproduce the clustering behavior of bacteria or Janus particles [17, 18], when they all point towards the same direction and therefore

self-clustering arises. So, in our model it is generally wrong to say that $\dot{\mathbf{x}} = \mathbf{v}$, as in the case of Active Ornstein–Uhlenbeck particles introduced in Sect. 2.2.4 [19–22]. However, in the latter model this was the consequence of an overdamping of the motion equations; here, it directly stems from the presence of excluded volume: the equations for our model are *not overdamped* in any considered case.

6.1.3 Microscopic Balance Equations

We now write the microscopic evolution equations for occupation n_i , momentum $n_i \mathbf{v_i}$ and energy $e_i \equiv \frac{1}{2} n_i \sum_k v_{i,k}^2$. From now on, the index l is associated to the direction of hopping while the index k indicates a general component of vectorial quantities.

At each infinitesimal time step p two random vectors are extracted: the random site $\xi_p \in \Lambda$, determining the hopping particle, and the random direction $\zeta_p = \pm \mathbf{e}_l$ determining the direction and orientation of the hop. The probability of extraction satisfies

$$\overline{\delta_{\xi_p, \mathbf{i}} \delta_{\zeta_p, \sigma \mathbf{e}_l}} = n_{\mathbf{i}, p} (1 - n_{\mathbf{i} + \sigma \mathbf{e}_l, p}) g(\sigma v_{l, p}) \frac{\Delta t}{\Delta x} , \qquad (6.2)$$

where $\sigma=\pm 1$ and $\overline{\cdots}$ represents the average over the fast variables $\boldsymbol{\xi}_p, \boldsymbol{\zeta}_p$ conditioned by the actual microscopic configuration $\{n_{\mathbf{i},p},\mathbf{v}_{\mathbf{i},p}\}$ at time p. The first two factors in the rhs guarantee that hopping can only occur from an occupied to an empty site, as for SEP models. The projection function g relates the active velocity component l with the hopping probability in the lth direction: since $g(\sigma v_{l,p})\Delta t/\Delta x$ must be dimensionless, g must have the dimension of a velocity. In our model, we will choose it as proportional to the projection of \mathbf{v}_l along the direction l, namely

$$g(\sigma v_l) = \Theta(\sigma v_l) |\sigma v_l|, \qquad (6.3)$$

where $\Theta(x)$ is the Heaviside step function. We call this rule the "natural active velocity" prescription. Equations (6.2) and (6.3) provide that a free particle follows an average ballistic motion with $\langle \dot{\mathbf{x}} \rangle = \mathbf{v}$ if all the forces are absent. The hopping probability (6.2) also includes a constraint $\Delta t \ll \Delta x$ which will be analyzed later. The total hopping probability is generally under-normalized, i.e. there can be no hops during a time step.

The evolution of microscopic variables is given by *balance equations*: for each of the quantities above defined, we can compute the gain and loss terms at each time step. For instance, the occupation number n_i increases by 1 if a particle from an adjacent site hops into it, and vice versa if the occupying particle hops away from it. So,

$$n_{\mathbf{i},p+1} = n_{\mathbf{i},p} + \sum_{l=1}^{d} \sum_{\sigma=+1} \left(\delta_{\boldsymbol{\xi}_{p},\mathbf{i}-\sigma \mathbf{e}_{l}} \delta_{\boldsymbol{\zeta}_{p},\sigma \mathbf{e}_{l}} - \delta_{\boldsymbol{\xi}_{p},\mathbf{i}} \delta_{\boldsymbol{\zeta}_{p},\sigma \mathbf{e}_{l}} \right) . \tag{6.4}$$

The discrete continuity equation for occupation number reads

$$\Delta n_{\mathbf{i}} = -\sum_{l=1}^{d} \left(\mathbf{j}_{\mathbf{i}} - \mathbf{j}_{\mathbf{i} - \mathbf{e}_{l}} \right)_{l} , \qquad (6.5)$$

where $\Delta n_i \equiv n_{i,p+1} - n_{i,p}$ and the time dependence from now on is omitted because every variable in the rhs is evaluated at time p. Equation (6.5) defines the *density current* vector as

$$j_{\mathbf{i},l} \equiv \delta_{\boldsymbol{\xi}_p, \mathbf{i}} \delta_{\boldsymbol{\zeta}_p, \mathbf{e}_l} - \delta_{\boldsymbol{\xi}_p, \mathbf{i} + \mathbf{e}_l} \delta_{\boldsymbol{\zeta}_p, -\mathbf{e}_l} , \qquad (6.6)$$

which is either 1 if the particle is leaving the site \mathbf{i} in the "positive" direction (right, top...) or -1 if a particle is incoming from the same direction. The particles can not be created or destroyed, so the occupation number obeys an exact continuity equation.

Analogously, the evolution of the active velocity can be obtained through active momentum balance, i.e.

$$\Delta(n_{\mathbf{i}}\mathbf{v}_{\mathbf{i}}) = \sum_{l=1}^{d} \sum_{\sigma=\pm 1} \left[\delta_{\boldsymbol{\xi}_{p},\mathbf{i}-\sigma\mathbf{e}_{l}} \delta_{\boldsymbol{\zeta}_{p},\sigma\mathbf{e}_{l}} \mathbf{v}_{\mathbf{i}-\sigma\mathbf{e}_{l}} - \delta_{\boldsymbol{\xi}_{p},\mathbf{i}} \delta_{\boldsymbol{\zeta}_{p},\sigma\mathbf{e}_{l}} \mathbf{v}_{\mathbf{i}} + n_{\mathbf{i}} n_{\mathbf{i}-\sigma\mathbf{e}_{l}} \mathbf{f}^{(2)} \left(\mathbf{v}_{\mathbf{i}-\sigma\mathbf{e}_{l}}, \mathbf{v}_{\mathbf{i}} \right) \Delta t \right] + n_{\mathbf{i}} \left[\mathbf{f}^{(1)}(\mathbf{v}_{\mathbf{i}}) \Delta t + \mathsf{B}(\mathbf{v}_{\mathbf{i}}) \cdot \Delta \mathbf{W}_{\mathbf{i}}(t) \right],$$
(6.7)

or, writing the components explicitly,

$$\Delta(n_{\mathbf{i}}v_{\mathbf{i},k}) = -\sum_{l=1}^{d} \left(\mathbf{J}_{\mathbf{i}} - \mathbf{J}_{\mathbf{i}-\mathbf{e}_{l}} \right)_{kl} + n_{\mathbf{i}} \left[f_{k}^{(1)}(\mathbf{v}_{\mathbf{i}}) \Delta t + \sum_{l=1}^{d} B_{kl}(\mathbf{v}_{\mathbf{i}}) \Delta W_{\mathbf{i},l}(t) \right],$$
(6.8)

accounting for momentum transport through hopping and pairwise interactions and momentum injection by means of the self-propulsion $f^{(1)}$ and the random force $B(v_i) \cdot \Delta W_i$ acting on the unit. The transported momentum defines the *momentum current* tensor J, whose components read

$$J_{\mathbf{i},kl} \equiv \delta_{\boldsymbol{\xi}_{n},\mathbf{i}} \delta_{\boldsymbol{\zeta}_{n},\mathbf{e}_{l}} v_{\mathbf{i},k} - \delta_{\boldsymbol{\xi}_{n},\mathbf{i}+\mathbf{e}_{l}} \delta_{\boldsymbol{\zeta}_{n},-\mathbf{e}_{l}} v_{\mathbf{i}+\mathbf{e}_{l},k} + n_{\mathbf{i}} n_{\mathbf{i}+\mathbf{e}_{l}} f_{k}^{(2)}(\mathbf{v}_{\mathbf{i}},\mathbf{v}_{\mathbf{i}+\mathbf{e}_{l}}) \Delta t , \qquad (6.9)$$

representing the momentum in direction k transported in direction l.

The evolution of microscopic kinetic energy is given by

$$\Delta e_{\mathbf{i}} = (n_{\mathbf{i}}\mathbf{v}_{\mathbf{i}}) \cdot \Delta(n_{\mathbf{i}}\mathbf{v}_{\mathbf{i}}) + \frac{1}{2} \left[\sum_{l,\sigma} \left(\delta_{\boldsymbol{\xi}_{p},\mathbf{i}-\sigma\mathbf{e}_{l}} \delta_{\boldsymbol{\zeta}_{p},\sigma\mathbf{e}_{l}} \mathbf{v}_{\mathbf{i}-\sigma\mathbf{e}_{l}} - \delta_{\boldsymbol{\xi}_{p},\mathbf{i}} \delta_{\boldsymbol{\zeta}_{p},\sigma\mathbf{e}_{l}} \mathbf{v}_{\mathbf{i}} \right) \right]^{2} \\
+ \frac{1}{2} \left[n_{\mathbf{i}} \sum_{l=1}^{d} B_{kl}(\mathbf{v}_{\mathbf{i}}) \Delta W_{\mathbf{i},l}(t) \right]^{2} \\
= -\sum_{k,l} (n_{\mathbf{i}}v_{\mathbf{i},k}) \left(\mathbf{J}_{\mathbf{i}} - \mathbf{J}_{\mathbf{i}-\mathbf{e}_{l}} \right)_{kl} + \sum_{k=1}^{d} \left[(n_{\mathbf{i}}v_{\mathbf{i},k}) \left(f_{k}^{(1)}(\mathbf{v}_{\mathbf{i}}) \Delta t + \sum_{l=1}^{d} B_{kl}(\mathbf{v}_{\mathbf{i}}) dW_{\mathbf{i},l}(t) \right) \right. \\
+ \frac{1}{2} \sum_{l,\sigma} \left(\delta_{\boldsymbol{\xi}_{p},\mathbf{i}-\sigma\mathbf{e}_{l}} \delta_{\boldsymbol{\zeta}_{p},\sigma\mathbf{e}_{l}} v_{\mathbf{i}-\sigma\mathbf{e}_{l},k}^{2} + \delta_{\boldsymbol{\xi}_{p},\mathbf{i}} \delta_{\boldsymbol{\zeta}_{p},\sigma\mathbf{e}_{l}} v_{\mathbf{i},k}^{2} \right) + \frac{1}{2} n_{\mathbf{i}} \sum_{l=1}^{d} \left[B_{kl}(\mathbf{v}_{\mathbf{i}}) \right]^{2} \Delta t \right] \\
= -\sum_{l=1}^{d} \left(\mathbf{J}_{\mathbf{i}} - \mathbf{J}_{\mathbf{i}-\mathbf{e}_{l}} \right)_{l} + n_{\mathbf{i}} \mathbf{v}_{\mathbf{i}} \cdot \mathbf{B}(\mathbf{v}_{\mathbf{i}}) \cdot \Delta \mathbf{W}_{\mathbf{i}}(t) + D_{\mathbf{i}} \Delta t , \tag{6.10}$$

defining the energy current J_i as

$$\mathbf{J_{i}} = \mathbf{J_{i}^{(hops)}} + \mathbf{J_{i}^{(int)}},
J_{\mathbf{i},l}^{(hops)} = \delta_{\boldsymbol{\xi}_{p},\mathbf{i}}\delta_{\boldsymbol{\zeta}_{p},\mathbf{e}_{l}}e_{\mathbf{i}} - \delta_{\boldsymbol{\xi}_{p},\mathbf{i}+\mathbf{e}_{l}}\delta_{\boldsymbol{\zeta}_{p},-\mathbf{e}_{l}}e_{\mathbf{i}+\mathbf{e}_{l}},
J_{\mathbf{i},l}^{(int)} = \frac{1}{2}n_{\mathbf{i}}n_{\mathbf{i}+\mathbf{e}_{l}}(\mathbf{v_{i}} + \mathbf{v_{i}+\mathbf{e}_{l}}) \cdot \mathbf{f}^{(2)}(\mathbf{v_{i}}, \mathbf{v_{i}+\mathbf{e}_{l}}) \Delta t,$$
(6.11)

and the energy injection/dissipation terms

$$D_{\mathbf{i}} = D_{\mathbf{i}}^{(\text{int})} + D_{\mathbf{i}}^{(\text{self})} + D_{\mathbf{i}}^{(\text{noise})},$$

$$D_{\mathbf{i}}^{(\text{int})} = -\frac{1}{2} \sum_{l,\sigma} n_{\mathbf{i}} n_{\mathbf{i}+\sigma \mathbf{e}_{l}} (\mathbf{v}_{\mathbf{i}} - \mathbf{v}_{\mathbf{i}+\mathbf{e}_{l}}) \cdot \mathbf{f}^{(2)} (\mathbf{v}_{\mathbf{i}}, \mathbf{v}_{\mathbf{i}+\mathbf{e}_{l}}),$$

$$D_{\mathbf{i}}^{(\text{self})} = n_{\mathbf{i}} \mathbf{v}_{\mathbf{i}} \cdot \mathbf{f}^{(1)} (\mathbf{v}_{\mathbf{i}}),$$

$$D_{\mathbf{i}}^{(\text{noise})} = \frac{1}{2} n_{\mathbf{i}} \sum_{k,l}^{1,d} [B_{kl}(\mathbf{v}_{\mathbf{i}})]^{2} \equiv \frac{1}{2} n_{\mathbf{i}} B(\mathbf{v}_{\mathbf{i}}),$$

$$(6.12)$$

where the contributions from hopping, interactions, self-propulsion and noise have been written separately.

Equations (6.5), (6.8) and (6.10) are the microscopic balance equations of the system. Their validity is not restricted to any equilibrium approximation or hypothesis on the configuration distribution function. At this stage, they are equivalent to Eqs. (4.15) and (4.17) of the granular model.

6.2 Hydrodynamic Limit

The derivation of the hydrodynamic equations for the model can be done through a continuum limit of microscopic balance equations derived in the previous section. The hydrodynamic fields considered are density, momentum and temperature. The probability of a configuration $\{n_i, \mathbf{v_i}\}$ at time t is defined as $\mathcal{P}(\{n_i, \mathbf{v_i}\}; t)$. The 2-sites (\mathbf{i}, \mathbf{j}) and 1-site (\mathbf{i}) marginalized distributions are respectively given by $P_{\mathbf{i}, \mathbf{i}}^{(2)}(n_{\mathbf{i}}, n_{\mathbf{j}}, \mathbf{v_i}, \mathbf{v_j}; t)$ and $P_{\mathbf{i}}^{(1)}(n_{\mathbf{i}}, \mathbf{v_i}; t)$. Locally averaged fields are defined as

$$\rho_{\mathbf{i}}(t) = \langle n_{\mathbf{i}} \rangle \,, \tag{6.13a}$$

$$\rho_{\mathbf{i}}(t)u_{\mathbf{i},k}(t) = \langle n_{\mathbf{i}}v_{\mathbf{i},k}\rangle, \qquad (6.13b)$$

$$\rho_{\mathbf{i}}(t)T_{\mathbf{i}}(t) = \frac{1}{d} \langle n_{\mathbf{i}} | \mathbf{v}_{\mathbf{i}} - \mathbf{u}_{\mathbf{i}} |^{2} \rangle, \qquad (6.13c)$$

where

$$\langle f(n_{\mathbf{i}}, \mathbf{v}_{\mathbf{i}}) \rangle = \prod_{\mathbf{i} \in \Lambda} \left(\sum_{n_{\mathbf{i}} = 0, 1} \int_{\mathbb{R}} d\mathbf{v}_{\mathbf{i}} \right) \mathcal{P}(\{n_{\mathbf{i}}, \mathbf{v}_{\mathbf{i}}\}; t) f(n_{\mathbf{i}}, \mathbf{v}_{\mathbf{i}}),$$
 (6.14)

and in Eq. (6.13c) we assumed the isotropy of local temperature. From now on we make only use of continuous time $t = p\Delta t$. The temperature is related to the energy through the relation

$$T_{\mathbf{i}}(t) \equiv \frac{1}{d} \left\langle |\mathbf{v} - \mathbf{u}|^2 \right\rangle_{\mathbf{i}} = \frac{1}{d} \left(\frac{2}{\rho_{\mathbf{i}}(t)} \left\langle e_{\mathbf{i}}(t) \right\rangle - u_{\mathbf{i}}^2(t) \right). \tag{6.15}$$

We move to a large volume limit $L \to \infty$, $N \to \infty$ at constant number density $\phi = N/V$. In this limit the physical spacing between two adjacent lattice sites is sent to 0 as $\Delta x = 1/L$, such that a spatial position in the system is denoted by a continuous $\mathbf{x} \in [0, 1]^d$.

To get a closed set of equations, we make use of two assumptions

1. Molecular Chaos (expected to be valid in the dilute limit $\phi \to 0$) with isotropic velocity factorization:

$$P_{\mathbf{i},\mathbf{j}}^{(2)}(n_{\mathbf{i}}, n_{\mathbf{j}}, \mathbf{v}_{\mathbf{i}}, \mathbf{v}_{\mathbf{j}}; t) = P_{\mathbf{i}}^{(1)}(n_{\mathbf{i}}, \mathbf{v}_{\mathbf{i}}; t) P_{\mathbf{j}}^{(1)}(n_{\mathbf{j}}, \mathbf{v}_{\mathbf{j}}; t) , \qquad (6.16)$$

$$P_{\mathbf{i}}^{(1)}(n_{\mathbf{i}}, \mathbf{v}_{\mathbf{i}}; t) = p_{\mathbf{i}}(n_{i}; t) \prod_{k=1}^{d} P_{\mathbf{i}, k}(v_{\mathbf{i}, k}; t);$$
(6.17)

2. smoothness in space of averages of generic observables F(n, v):

$$\langle F \rangle_{\mathbf{i} \pm \mathbf{e}_{t}, t} = \langle F \rangle(\mathbf{x}, t) \pm \frac{1}{L} \frac{\partial}{\partial x_{t}} \langle F \rangle|_{(\mathbf{x}, t)} + O(1/L^{2}),$$
 (6.18)

being l a Cartesian direction $l \in \{1, d\}$.

With the hypothesis above stated, it is straightforward to perform averages and limits of the currents. At the first order, these read

$$\langle \mathbf{j}_{\mathbf{i},p} \rangle \to \frac{\Delta t}{\Delta x} \mathbf{j}^{\text{av}}(\mathbf{x},t) ,$$
 (6.19a)

$$\mathbf{j}^{\text{av}}(\mathbf{x},t) = \rho(\mathbf{x},t) \left[1 - \rho(\mathbf{x},t)\right] \mathbf{G}^{(0)}(\mathbf{x},t), \qquad (6.19b)$$

$$\langle \mathsf{J}_{\mathsf{i},p} \rangle \to \frac{\Delta t}{\Delta x} \mathsf{J}^{\mathrm{av}}(\mathbf{x},t) ,$$
 (6.20a)

$$\mathbf{J}^{\text{av}}(\mathbf{x},t) = \rho(\mathbf{x},t) \left[1 - \rho(\mathbf{x},t)\right] \mathbf{G}^{(1)}(\mathbf{x},t) , \qquad (6.20b)$$

$$\langle \mathbf{J}_{\mathbf{i},p} \rangle \to \frac{\Delta t}{\Delta x} \mathbf{J}^{\text{av}}(\mathbf{x},t) ,$$
 (6.21a)

$$\mathbf{J}^{\text{av}}(\mathbf{x},t) = \rho(\mathbf{x},t) \left[1 - \rho(\mathbf{x},t)\right] \mathbf{G}^{(2)}(\mathbf{x},t), \qquad (6.21b)$$

where $\mathbf{G}^{(0)}$, $\mathbf{G}^{(1)}$ and $\mathbf{G}^{(2)}$ are defined as the hop vectors and tensor, respectively accounting for transport of particles, momentum and energy. They read

$$G_l^{(0)}(\mathbf{x},t) \equiv \int d\mathbf{v} P(\mathbf{v};\mathbf{x},t) h(v_l) , \qquad (6.22a)$$

$$G_{kl}^{(1)}(\mathbf{x},t) \equiv \int d\mathbf{v} P(\mathbf{v};\mathbf{x},t) h(v_l) v_k , \qquad (6.22b)$$

$$G_l^{(2)}(\mathbf{x},t) \equiv \int d\mathbf{v} P(\mathbf{v};\mathbf{x},t) h(v_l) \frac{1}{2} v^2, \qquad (6.22c)$$

with $h(v_l) \equiv g(v_l) - g(-v_l)$.

We also take the averages of the gain/loss terms, which read

$$\langle n\mathbf{f}^{(1)}(\mathbf{v})(\mathbf{x},t)\rangle = \rho(\mathbf{x},t) \int d\mathbf{v} P(\mathbf{v};\mathbf{x},t)\mathbf{f}^{(1)}(\mathbf{v}) \equiv \rho(\mathbf{x},t)\mathbf{f}^{s}(\mathbf{x},t),$$
 (6.23)

$$\langle D^{(\text{int})}(\mathbf{x}, t) \rangle = -d\rho^{2}(\mathbf{x}, t) \int d\mathbf{v} d\mathbf{v}' P(\mathbf{v}; \mathbf{x}, t) P(\mathbf{v}'; \mathbf{x}, t) (\mathbf{v} - \mathbf{v}') \cdot \mathbf{f}^{(2)}(\mathbf{v}, \mathbf{v}')$$

$$\equiv -d\rho^{2}(\mathbf{x}, t) \Delta^{d}(\mathbf{x}, t) ,$$
(6.24)

$$\langle D^{(\text{self})}(\mathbf{x}, t) \rangle = \rho(\mathbf{x}, t) \int d\mathbf{v} P(\mathbf{v}; \mathbf{x}, t) \mathbf{v} \cdot \mathbf{f}^{(1)}(\mathbf{v}) \equiv d\rho(\mathbf{x}, t) \Delta_0^s(\mathbf{x}, t) ,$$
 (6.25)

$$\langle D^{\text{(noise)}}(\mathbf{x}, t) \rangle = \rho(\mathbf{x}, t) \int d\mathbf{v} P(\mathbf{v}; \mathbf{x}, t) B(\mathbf{v}) \equiv d\rho(\mathbf{x}, t) \Delta^{n}(\mathbf{x}, t) ,$$
 (6.26)

and - for the following - it is also useful to define

$$\Delta^{s}(\mathbf{x},t) \equiv \int d\mathbf{v} P(\mathbf{v};\mathbf{x},t) \left[\mathbf{v} - \mathbf{u}(\mathbf{x},t) \right] \cdot \mathbf{f}^{(1)}(\mathbf{v})/d.$$
 (6.27)

With the above assumptions and definitions, through a direct local averaging of Eqs. (6.5), (6.8) and (6.10) and in the large volume limit one gets the following hydrodynamic equations:

$$\partial_t \rho = -\nabla \cdot \mathbf{j},\tag{6.28a}$$

$$\rho \partial_t \mathbf{u} = -\nabla \cdot \mathbf{J} + \mathbf{u}(\nabla \cdot \mathbf{j}) + \rho \mathbf{f}^s, \tag{6.28b}$$

$$\rho \partial_t T = \left(T - \frac{u^2}{d} \right) \nabla \cdot \mathbf{j} + \frac{2}{d} \mathbf{u} \nabla : \mathbf{J} - \frac{2}{d} \nabla \cdot \mathbf{J}$$

$$-2\rho^2 \Delta^d + 2\rho (\Delta^s + \Delta^n).$$
(6.28c)

Equation (6.28) are the most general hydrodynamic equations which can be derived for our system. Since we retained only the first order gradients from the analytical expansion of averaged fields in Eq. (6.18), Eq. (6.28) are equivalent to the "Euler" hydrodynamic equations (3.20). At this stage their meaning is formal, because the actual expressions of currents and source terms are unknown. These can be computed only once the specific forms of projection function $g(\sigma v_l)$, interaction $\mathbf{f}^{(2)}$, self-propulsion $\mathbf{f}^{(1)}$ and diffusion tensor B are given. Furthermore, we will see that the one-particle distribution must be specified to close the hydrodynamic equations at this order.

It is remarkable that, without any assumption on the velocity distribution, the momentum current associated with interactions vanishes in Eq. (6.22b) at the leading order because of the interplay between Molecular Chaos ansatz and momentum conservation in continuum limit: indeed, if correlations are neglected, the exchange of momentum is symmetrical between two particles with the same one-particle distribution function at the leading order because of the smoothness ansatz (6.18). Thus, its expression is of the first order in spatial gradients and therefore subleading with respect to hopping terms. A clear derivation of this fact is given in Appendix B.2. The physical consequence of this result is the absence of viscosity in hydrodynamic equations at the leading order.

Let's now derive the hydrodynamic equations for some specific microscopic rules. For the "natural active velocity" prescription, we have

$$G_{l}^{(0)}(\mathbf{x},t) = \int d\mathbf{v} P(\mathbf{v};\mathbf{x},t) v_{l} = u_{l},$$

$$G_{kl}^{(1)}(\mathbf{x},t) = \int d\mathbf{v} P(\mathbf{v};\mathbf{x},t) v_{l} v_{k} = \langle v_{l} v_{k} \rangle,$$

$$G_{l}^{(2)}(\mathbf{x},t) = \int d\mathbf{v} P(\mathbf{v};\mathbf{x},t) v_{l} \frac{1}{2} v^{2} = \frac{1}{2} \sum_{k=1}^{d} \langle v_{l} v_{k}^{2} \rangle.$$

$$(6.29)$$

The above quantities can be further simplified by defining a "stress" tensor

$$Q_{kl}(\mathbf{x},t) \equiv G_{kl}^{(1)}(\mathbf{x},t) - u_k(\mathbf{x},t)\mathbf{G}_l^{(0)}(\mathbf{x},t) = \int d\mathbf{v} P(\mathbf{v};\mathbf{x},t)h(v_l) \left[v_k - u_k(\mathbf{x},t)\right],$$
(6.30)

and a "heat" vector

$$R_l(\mathbf{x},t) \equiv \int d\mathbf{v} P(\mathbf{v};\mathbf{x},t) h(v_l) \left[\frac{1}{d} |\mathbf{v} - \mathbf{u}(\mathbf{x},t)|^2 - T(\mathbf{x},t) \right].$$
 (6.31)

Within the "natural active velocity" prescription, we have

$$G_{kl}^{(1)}(\mathbf{x},t) = T(\mathbf{x},t)\delta_{kl} + u_k(\mathbf{x},t)u_l(\mathbf{x},t),$$

$$G_l^{(2)}(\mathbf{x},t) = \langle v_l^3 \rangle(\mathbf{x},t) + (d-1)u_l(\mathbf{x},t)T(\mathbf{x},t) + u_l(\mathbf{x},t)u^2(\mathbf{x},t) - u_l^3(\mathbf{x},t),$$

$$Q_{kl}(\mathbf{x},t) = T(\mathbf{x},t)\delta_{kl},$$

$$R_l(\mathbf{x},t) = \frac{1}{d} \left[\langle v_l^3 \rangle(\mathbf{x},t) - 3u_l(\mathbf{x},t)T(\mathbf{x},t) - u_l^3(\mathbf{x},t) \right],$$
(6.32)

provided that the Cartesian components of the active velocity are statistically independent and that the temperature is isotropic, i.e.

$$P(\mathbf{v}; \mathbf{x}, t) = \prod_{k=1}^{d} P_k(v_k; \mathbf{x}, t) \quad , \quad \langle (v_k - u_k)^2 \rangle = T \quad \forall k .$$
 (6.33)

With the additional assumption that central odd velocity moments are zero, we get

$$\langle (v_l - u_l)^3 \rangle = 0 \quad \Rightarrow \quad \langle v^3 \rangle = 3Tu_l + u_l^3 , \qquad (6.34)$$

and, as a consequence, $G_l^{(2)}$ and R_l simplify into

$$G_l^{(2)}(\mathbf{x},t) = \frac{1}{2}u_l(\mathbf{x},t)\left[(d+2)T(\mathbf{x},t) + u^2(\mathbf{x},t)\right], \quad R_l(\mathbf{x},t) = 0.$$
 (6.35)

In conclusion, in the continuous limit, the balance Eqs. (6.5), (6.7) and (6.10) with the average currents and noise terms for the choice of the "natural active velocity" read

$$\partial_t \rho = -\nabla \cdot [\rho (1 - \rho) \mathbf{u}] , \qquad (6.36a)$$

$$\rho \partial_t \mathbf{u} = -\left\{ \nabla \left[\rho \left(1 - \rho \right) T \right] + \rho \left(1 - \rho \right) \left(\mathbf{u} \cdot \nabla \right) \mathbf{u} \right\} + \rho \mathbf{f}^s , \tag{6.36b}$$

$$\rho \partial_t T = -\rho \left(1 - \rho \right) \left[\frac{2}{d} T \nabla \cdot \mathbf{u} + \left(\mathbf{u} \cdot \nabla \right) T \right] - 2\rho^2 \Delta^d + 2\rho \left(\Delta^s + \Delta^n \right) . \quad (6.36c)$$

These equations are completely analogous to Euler equations (3.20), except for the terms $\rho(1-\rho)$ appearing in the currents: their presence clarifies the meaning of our "active velocity" \mathbf{v}_i , which as explained above is not equivalent to the actual infinitesimal displacement of the particle. The excluded volume can be seen as a modification of the particles' mobility, which is vanishing in the dense case $\rho \to 1$. On the contrary, in the dilute limit $\rho \to 0$ this is not a relevant difference, but it can be appreciated at relatively moderate densities.

We now specify the interaction, self-propulsion and noise terms: the former is taken as

$$\mathbf{f}^{(2)}(\mathbf{v}, \mathbf{v}') = \omega_d(\mathbf{v} - \mathbf{v}'). \tag{6.37}$$

This choice deserves some justification: indeed, it reproduces a sort of "soft" interaction between velocities of nearest-neighbor particles. Actually, the force above-defined has two main properties

- 1. it mimics the behavior of Kuramoto and Vicsek aligning interactions, with a stable fixed point for $\mathbf{v} = \mathbf{v}'$;
- 2. it is a source of dissipation because, as it will be shown, it yields $\Delta^d > 0$.

The interaction in Eq. (6.37) is a deterministic force and the result of a compromise between Vicsek model and granular collisions. It must be stressed that the interactions are acting *continuously* instead than being *instantaneous* as for granular hard spheres: this is an important difference with respect to our previous granular model. Also, the characteristic frequency ω_d cannot be directly associated to the restitution coefficient α , and there is no elastic limit for this kind of interaction. However, the comparison between granular and active hydrodynamic equations allows a mapping of inelastic collisions into Vicsek-like force (6.37). Moreover, a further version of the active model may easily include granular collisions as an instantaneous process, with the same procedure described in Sects. 4.2.1 and 6.1.3.

Self-propulsion is taken as

$$\mathbf{f}^{(1)}(\mathbf{v}) = \omega_s \mathbf{v} \left(1 - \frac{v^2}{v_s^2} \right) , \qquad (6.38)$$

having the same form of the *Rayleigh-Helmoltz* viscosity introduced in Sect. 2.2.3. The effect of self-propulsion is to push the particles towards the stable fixed point $v = v_s$; on the contrary, the fixed point v = 0 is unstable. The self-propulsion doesn't change the direction or orientation of the velocity, but rather acts only on its magnitude. The analytical solution of the motion equation $\dot{\mathbf{v}} = \mathbf{f}^{(1)}(\mathbf{v})$ is given in Appendix B.1.

Finally, we choose an isotropic and constant diffusion tensor B(v), namely

$$B_{kl}(\mathbf{v}) = \sqrt{2D}\delta_{kl} \,, \tag{6.39}$$

defining the *diffusivity D*. For all these choice of microscopic features, the average source terms read

$$f_k^s(\mathbf{x},t) = \omega_s u_k(\mathbf{x},t) \left[1 - \frac{1}{v_s^2} \left((d+2)T(\mathbf{x},t) + u^2(\mathbf{x},t) \right) \right], \tag{6.40a}$$

$$\Delta^d(\mathbf{x}, t) = 2d \,\omega_d T(\mathbf{x}, t) \,, \tag{6.40b}$$

$$\Delta^{s}(\mathbf{x},t) = \omega_{s} T(\mathbf{x},t) \left[1 - \frac{d+2}{v_{s}^{2}} \left(T(\mathbf{x},t) + \frac{1}{d} u^{2}(\mathbf{x},t) \right) \right], \tag{6.40c}$$

$$\Delta^n(\mathbf{x}, t) = D \,, \tag{6.40d}$$

where the first and third equations, stemming from self-propulsion force (6.38), have been derived under the *Local Equilibrium assumption*, namely

$$P(\mathbf{v}; \mathbf{x}, t) = \left[2\pi T(\mathbf{x}, t)\right]^{-d/2} \exp\left[-|\mathbf{v} - \mathbf{u}(\mathbf{x}, t)|^2 / 2T(\mathbf{x}, t)\right], \tag{6.41}$$

because of the presence of $\langle v^4 \rangle$ terms in the averages.

Substituting the above expressions into Eq. (6.36) we get the average hydrodynamic equations with the above specified prescriptions and the Local Equilibrium assumption, which read

$$\partial_{t}\rho = -\nabla \cdot [\rho (1 - \rho) \mathbf{u}], \qquad (6.42a)$$

$$\rho \partial_{t} \mathbf{u} = -\{\nabla [\rho (1 - \rho) T] + \rho (1 - \rho) (\mathbf{u} \cdot \nabla) \mathbf{u}\} \qquad (6.42b)$$

$$+ \rho \omega_{s} \mathbf{u} \left[1 - \frac{1}{v_{s}^{2}} \left((d + 2)T + u^{2} \right) \right],$$

$$\rho \partial_{t}T = -\rho (1 - \rho) \left[\frac{2}{d} T \nabla \cdot \mathbf{u} + (\mathbf{u} \cdot \nabla) T \right] \qquad (6.42c)$$

$$-4d\omega_{d}\rho^{2}T + 2\rho\omega_{s}T \left[1 - \frac{d+2}{v_{s}^{2}} \left(T + \frac{1}{d}u^{2} \right) \right] + 2\rho D.$$

6.2.1 Homogeneous Fixed Points

We look at the fixed points of hydrodynamic equations (6.36). Our case of study is the homogeneous case, in analogy with the HCS described in the granular model. Homogeneity greatly simplify hydrodynamic equations, which now read

$$\dot{\rho} = 0, \qquad (6.43a)$$

$$\dot{\mathbf{u}} = \mathbf{f}^s \,, \tag{6.43b}$$

$$\dot{T} = -2\rho\Delta^d + 2\left(\Delta^s + \Delta^n\right). \tag{6.43c}$$

Thus, the homogeneous density is constant and equivalent to the packing fraction $\rho \equiv \phi$. The stationary velocity and temperature must satisfy the condition of vanishing self-propulsion and balancing energy source terms. For the specific choice of Eq. (6.40), one has

$$\dot{u} = \omega_s u \left\{ 1 - \frac{1}{v_s^2} \left[(d+2)T + u^2 \right] \right\} , \tag{6.44a}$$

$$\dot{T} = -4d \,\phi \omega_d T + 2\omega_s T \left[1 - \frac{d+2}{v_s^2} \left(T + \frac{1}{d} u^2 \right) \right] + 2D \,, \tag{6.44b}$$

where $u = |\mathbf{u}|$ is the speed field. Now, we move to adimensional variables, defining

$$\tilde{t} = \omega_s t ,$$

$$\tilde{x} = (\omega_s/v_s)x ,$$

$$\tilde{\mathbf{u}} = \mathbf{u}/v_s ,$$

$$\tilde{T} = t/v_s^2 ,$$

$$\gamma = \omega_d/\omega_s ,$$

$$\Gamma = D/(\omega_s v_s^2) ,$$
(6.45)

which will be used in the rest of the chapter, and the tilde will be omitted for the sake of simplicity. The physical parameters of our system can now be defined:

- 1. the packing fraction or density ϕ
- 2. the relative dissipation γ , i.e. the ratio of dissipation and self-propulsion characteristic frequencies
- 3. the relative noise Γ , measuring the amplitude of noise with respect to self-propulsion strength

Under the assumptions stated until now, the behavior of the system is completely determined by these parameters together with the boundary conditions (which we always take as periodic).

Homogeneous dimensionless equations have the same form of Eq. (6.44), because only constant coefficients have been redefined. We observe that there are three possible fixed points

1. A disordered fixed point (u_0, T_0) , where particles are moving with zero mean velocity but positive temperature, so that cooling is avoided. This is similar to a gas of granular particles in presence of a bulk driving, without collective motion. The fixed points read

$$u = 0$$
 , $T = T_0 = \frac{1 - 2d\phi\gamma + \sqrt{(1 - 2d\phi\gamma)^2 + 4(d+2)\Gamma}}{2(d+2)}$, (6.46)

The presence of noise is determinant: indeed, for $\Gamma=0$, the temperature is positive only until $\gamma<1/(2d\phi)$. For higher values of dissipation, the stationary solution reads T=0 and self-propulsion cannot prevent the system from cooling. On the contrary, when $\Gamma>0$ the disordered fixed point is always present.

2. Two *ordered* fixed points (u_{\pm}, T_{\pm}) , with $u_{\pm} > 0$. They exist if

$$\Gamma < \frac{(1+2d^2\phi\gamma)^2}{2d(d+2)},$$
(6.47)

and are given by

$$u_{\pm}^{2} = \frac{1}{2} \left(1 - 2d^{2}\phi\gamma \mp \sqrt{(1 + 2d^{2}\phi\gamma)^{2} - 2d(d+2)\Gamma} \right) ,$$

$$T_{\pm} = \frac{1 + 2d^{2}\phi\gamma \pm \sqrt{(1 + 2d^{2}\phi\gamma)^{2} - 2d(d+2)\Gamma}}{2(d+2)} .$$
(6.48)

The first point (u_-, T_-) exists only if $\gamma < 1/(2d^2\phi) \vee \Gamma < 4d/(d+2)\phi\gamma$. The second point (u_+, T_+) exists only if $\gamma < 1/(2d^2\phi) \wedge \Gamma > 4d/(d+2)\phi\gamma$.

The existence of fixed points with u>0 suggests the presence of a stationary *swarming* state, where a macroscopic collective motion arises spontaneously breaking the rotational symmetry because in every trajectory the units move together in a random direction. This is actually observed in simulations. However, it must be underlined that homogeneous equations (6.44) have been derived under the Local Equilibrium assumption with a Gaussian distribution, which may have nothing to do with the distribution of the swarming state. On the other hand, the Local Equilibrium assumption is expected to be physically consistent in the disordered state, so we focus on its stability.

6.2.2 Stability Analysis of the Disordered State

We introduce small, spatially dependent fluctuations around the fully disordered fixed point as

$$\delta \rho = \rho(\mathbf{x}, t) - \phi,$$

$$\delta \mathbf{u} = \mathbf{u}(\mathbf{x}, t),$$

$$\delta T = T(\mathbf{x}, t) - T_0.$$
(6.49)

The linearized hydrodynamic equations now read

$$\partial_t \delta \rho = -\phi \left(1 - \phi \right) \nabla \cdot \delta \mathbf{u} \,, \tag{6.50a}$$

$$\partial_{t}\delta\mathbf{u} = -\frac{1 - 2\phi}{\phi}T_{0}\nabla\delta\rho + C(\gamma, \Gamma)\delta\mathbf{u} - (1 - \phi)\nabla\delta T, \qquad (6.50b)$$

$$\partial_{t}\delta T = -4d\gamma T_{0}\delta\rho - \frac{2}{d}(1 - \phi)T_{0}\nabla\cdot\delta\mathbf{u} - 2r(\gamma, \Gamma)\delta T, \qquad (6.50c)$$

$$\partial_t \delta T = -4d\gamma T_0 \delta \rho - \frac{2}{d} (1 - \phi) T_0 \nabla \cdot \delta \mathbf{u} - 2r(\gamma, \Gamma) \delta T , \qquad (6.50c)$$

with

$$r(\gamma, \Gamma) = \sqrt{(1 - 2d\phi\gamma)^2 + 4(d + 2)\Gamma},$$

$$C(\gamma, \Gamma) = \frac{1}{2} (1 + 2d\phi\gamma - r(\gamma, \Gamma)).$$
(6.51)

After converting to Fourier space, decomposing $\hat{\boldsymbol{u}}_k$ in a parallel (to k) and d-1 transverse components $(\hat{u}_{\mathbf{k}}^{\parallel}, \hat{\mathbf{u}}_{\mathbf{k}}^{\perp})$, and defining $\hat{\Psi}_{\mathbf{k}} = (\hat{\rho}_{\mathbf{k}}, \hat{u}_{\mathbf{k}}^{\parallel}, \hat{\mathbf{u}}_{\mathbf{k}}^{\perp}, \hat{T}_{\mathbf{k}})$, the timeevolution of the modes linearized near that fixed point reads

$$\partial_t \hat{\Psi}_{\mathbf{k}} = \mathsf{L}(\mathbf{k}) \hat{\Psi}_{\mathbf{k}} \,, \tag{6.52}$$

with $L(\mathbf{k})$ equal to

$$\begin{pmatrix} 0 & -\phi(1-\phi)2\pi ik & 0 & 0\\ -\frac{1-2\phi}{\phi}T_02\pi ik & C(\gamma,\Gamma) & 0 & -(1-\phi)2\pi ik\\ 0 & 0 & C(\gamma,\Gamma) & 0\\ -4d\gamma T_0 & -\frac{2}{d}(1-\phi)T_02\pi ik & 0 & -2r(\gamma,\Gamma) \end{pmatrix}.$$
(6.53)

The first outcome is that the shear mode - which is reminiscent of swarming phases - separates from other modes and it is stable only when $C(\gamma, \Gamma) < 0$, i.e.

$$\Gamma > \frac{2d}{d+2}\phi\gamma. \tag{6.54}$$

Shear modes are stabilized by large noise Γ , and its threshold is linearly decreasing with the relative dissipation rate γ . At zero dissipation the shear mode is stable for any non-zero noise amplitude. Conversely, at zero noise amplitude, the shear mode is always unstable. Noticeably, in the absence of a k-dependent competing mechanism for stability (such as shear viscosity), stability of the shear mode is lost synchronously at any k. In Sect. 6.4 it will be numerically shown how shear instability is a strong signal of the appearance of a swarming state.

Numerical analysis of the eigenvalues of $L(\mathbf{k})$ reveals that at a given γ , at least in the range $0 < \gamma < 1/(2\phi)$, the eigenvalue associated with shear is the first to change sign when Γ is reduced, i.e. shear instability is the leading one. Being such a result the outcome of linear stability analysis, it does not imply that the bifurcation leads the system to a macroscopic shear-like state: we can only say that the fully disordered state is replaced by a different state which - at the beginning - looks ordered in the velocity field.

6.3 Fluctuating Hydrodynamics

The last analytical result on the active model is the derivation of fluctuating currents. Hydrodynamic equations (6.28) can be seen as fluctuating hydrodynamics equations; the microscopic currents \mathbf{j} , \mathbf{J} and \mathbf{J} depend both upon the "fast" variables $\boldsymbol{\xi}_p$, $\boldsymbol{\zeta}_p$ and the "slow" variables $n_{\mathbf{i},p}$, $\mathbf{v}_{\mathbf{i},p}$. Therefore, analogously with Sect. 4.4.1, at finite L the non-averaged currents can be written as the sum of their averages over the fast variables plus remainders. In particular we can write

$$j_l(\mathbf{x},t) = \overline{j_l}(\mathbf{x},t) + \sigma_l(\mathbf{x},t) , \qquad (6.55a)$$

$$\mathbf{J}_{kl}(\mathbf{x},t) = \overline{\mathbf{J}_{kl}}(\mathbf{x},t) + \varsigma_{kl}(\mathbf{x},t), \qquad (6.55b)$$

$$J_l(\mathbf{x}, t) = \overline{J_l}(\mathbf{x}, t) + \Sigma_l(\mathbf{x}, t). \tag{6.55c}$$

for density, momentum and energy respectively. The terms σ_l , ς_{kl} and Σ_l are current noises with zero average.

The current's noise correlations in Eq. (6.55) can be deduced from microscopic dynamics, analogously with the granular case in Sect. 4.4.2. We here focus on the fluctuations of density current, since the derivation of the others follows the same procedure. First of all, one has in discrete space and time variables

$$\langle \sigma_{\mathbf{i},p,l} \sigma_{\mathbf{i}',p',l'} \rangle \sim \langle j_{\mathbf{i},p,l} j_{\mathbf{i}',p',l'} \rangle$$
 (6.56)

With the definition in (6.6) and the "natural active velocity" prescription, only the diagonal terms are non vanishing and expanding fluctuations in Δt and Δx one obtains

$$\langle j_{\mathbf{i},p,l} j_{\mathbf{i}',p',l'} \rangle = \delta_{\mathbf{i},\mathbf{i}'} \delta_{p,p'} \delta_{l,l'} \rho_{\mathbf{i},p} (1 - \rho_{\mathbf{i},p}) \langle |v_l| \rangle_{\mathbf{i},p} \frac{\Delta t}{\Delta x}, \qquad (6.57)$$

hence the current's noise is white in space, time and components; its derivation can be found in Appendix B.3. This expression is meaningful if $\Delta t \ll \Delta x$, introducing a constraint in hydrodynamic scaling.

From Eq. (6.19a), the hydrodynamic limit of the currents reads

$$j_l(\mathbf{x},t) = \frac{\Delta x}{\Delta t} j_{\mathbf{i},p,l} , \qquad (6.58)$$

and the delta functions in continuum limit become

$$\delta_{\mathbf{i},\mathbf{i}'} = \delta(\mathbf{x} - \mathbf{x}')(\Delta x)^d$$
, $\delta_{p,p'} = \delta(t - t')\Delta t$, (6.59)

therefore Eq. (6.57) reads

$$\langle j_l(\mathbf{x},t)j_{l'}(\mathbf{x}',t)\rangle = \delta(\mathbf{x} - \mathbf{x}')\delta(t - t')\delta_{l,l'} \rho(\mathbf{x},t)[1 - \rho(\mathbf{x},t)] \langle |v_l| \rangle (\mathbf{x},t) (\Delta x)^{d+1}.$$
(6.60)

With the Gaussian velocity assumption, one finally finds

$$\langle \sigma_{l}(\mathbf{x}, t)\sigma_{l'}(\mathbf{x}', t')\rangle \sim \delta(\mathbf{x} - \mathbf{x}')\delta(t - t')\delta_{l, l'}\rho(\mathbf{x}, t)[1 - \rho(\mathbf{x}, t)]\sqrt{\frac{2}{\pi}T(\mathbf{x}, t)}(\Delta x)^{d+1}.$$
(6.61)

This result can be generalized to momentum and energy currents given by hopping particles; indeed, computing the current noise correlation $\eta_l^{(\chi)}$ for the generic transported quantity $\chi(n, v)$, with analogous steps one has

$$\left\langle \eta_l^{(\chi)}(\mathbf{x}, t) \eta_l^{(\chi)}(\mathbf{x}', t') \right\rangle \sim \delta(\mathbf{x} - \mathbf{x}') \delta(t - t') \delta_{l, l'} \left\langle n(1 - n) \chi^2(n, v) |v_l| \right\rangle (\mathbf{x}, t) \left\langle \Delta x \right\rangle^{d+1}, \tag{6.62}$$

always considering the leading term in Δt and Δx expansion. Interaction terms in Eq. (6.9), (6.11) are subleading and therefore do not appear at this level. The explicit expressions for momentum and energy are straightforward and read

$$\langle \varsigma_{l}(\mathbf{x},t)\varsigma_{l'}(\mathbf{x}',t')\rangle \sim \delta(\mathbf{x}-\mathbf{x}')\delta(t-t')\delta_{l,l'}\rho(\mathbf{x},t)[1-\rho(\mathbf{x},t)]\langle |v_{l}|v_{k}v_{k'}\rangle(\Delta x)^{d+1},$$
(6.63)

$$\left\langle \Sigma_{l}(\mathbf{x},t)\Sigma_{l'}(\mathbf{x}',t')\right\rangle \sim \delta(\mathbf{x}-\mathbf{x}')\delta(t-t')\delta_{l,l'}\rho(\mathbf{x},t)[1-\rho(\mathbf{x},t)]\left\langle |v_{l}|\left(\frac{v^{2}}{2}\right)^{2}\right\rangle (\Delta x)^{d+1},$$
(6.64)

Having shown that fluctuating currents are white and having found their amplitudes, we can show they are Gaussian. Again, the procedure adopted is equivalent to the one used in Sect. 4.4.3. Considering the rescaled current $\hat{j}_l = \hat{j}_l^{\text{av}} + \hat{\sigma}_l = (\Delta x)^{(d-1)/2} j_l$, from previous results we have that

$$\langle \hat{\sigma}_l(\mathbf{x}, t) \rangle = 0 \,, \tag{6.65a}$$

$$\langle \hat{\sigma}_l(\mathbf{x}, t) \hat{\sigma}_{l'}(\mathbf{x}', t') \rangle \sim \delta(\mathbf{x}, \mathbf{x}') \delta(t - t') \delta_{l,l'} \mathcal{A}_l^{(2)}(\mathbf{x}, t) ,$$
 (6.65b)

where $\mathcal{A}_{l}^{(2)}(\mathbf{x},t)$ is the rescaled amplitude of the second cumulant, which is finite when rescaling the current. For the generic cumulant of order n, we get

$$\left\langle \hat{\sigma}_{l_1}(\mathbf{x}_1, t_1) \cdots \hat{\sigma}_{l_n}(\mathbf{x}_n, t_n) \right\rangle \sim \prod_{i=1}^{n-1} \left[\delta(\mathbf{x}_i - \mathbf{x}_{i+1}) \delta(t_i - t_{i+1}) \delta_{l_i, l_{i+1}} \right]$$

$$\times \mathcal{A}_{l_1}^{(n)}(\mathbf{x}_1, t_1) \left(\Delta x \right)^{(d+1)(\frac{n}{2} - 1)},$$
(6.66)

which is non vanishing in the hydrodynamic limit only when n=2, because the amplitudes $\mathcal{A}_l^{(n)}$ are all finite. The rescaled noise $\hat{\sigma}_l$ is Gaussian in the large size limit and therefore the original noise σ_l is Gaussian too.

6.4 Numerical Results

Simulations of the system have shown the existence of two macroscopically ordered states:

- a swarming state, where particles align their velocities and walk across the lattice as a global swarm;
- 2. a *clustering* state, where a macroscopic fraction of the particles group and form a large, standing aggregate when they all point towards the center of the cluster.

A swarming and a clustering order parameters are defined and their evolution is studied and compared with linear stability analysis of Sect. 6.2.2. A preliminary study on the finite-size behavior suggests that the disorder-swarming transition may be discontinuous in the infinite size limit. Finally, the amplitude of the fluctuating density current is computed and compared with theoretical predictions.

6.4.1 General Simulation Strategy

The simulation strategy for the active model is analogous to the one used for the granular model. M stochastic trajectories of a system of N particles on a 2d periodic square lattice have been performed, locating each particle at a discrete position $\mathbf{r}_i(t) \in \Lambda$ and carrying a continuous 2d velocity $\mathbf{v}_i(t)$. For each trajectory, the system starts from a random configuration with uniform distribution of occupation numbers and normal distribution of velocities, with $\langle v_l \rangle = 0$ and $\langle v_l^2 \rangle = T_0$, being T_0 the stationary temperature of the disordered state defined in Eq. (6.46). At each time step Δt , a random number $\chi \in [0,1]$ is drawn to determine the particle eventually hopping, according to the "natural active velocity" prescription in (6.3): the normalization of the probability yields a constraint on the time interval, which we took $\Delta t \leq (10NL)^{-1}$ to guarantee that the total probability of a hop is $P_h \leq 1$, where P_h is defined as

$$P_h = \sum_{i=1}^{N} \sum_{\substack{l=1,2\\ \sigma=\pm 1}} (1 - n_{\mathbf{r}_i(t) \pm \sigma \mathbf{e}_l}) g(\sigma v_{i,l}) \frac{\Delta t}{\Delta x} . \tag{6.67}$$

The condition $P_h < 1$ has been verified throughout the simulations: it is reasonable to think that the self-propulsion force is lowering high-velocities tails. Simulations have been carried out for several values of γ and Γ and densities ϕ of 1, 5 and 10%, since we are interested in the dilute limit. The lattice size has been taken L=100 ($V=10^4$ sites), except the case of finite-size effects where the size is changed keeping the density constant.

6.4 Numerical Results 167

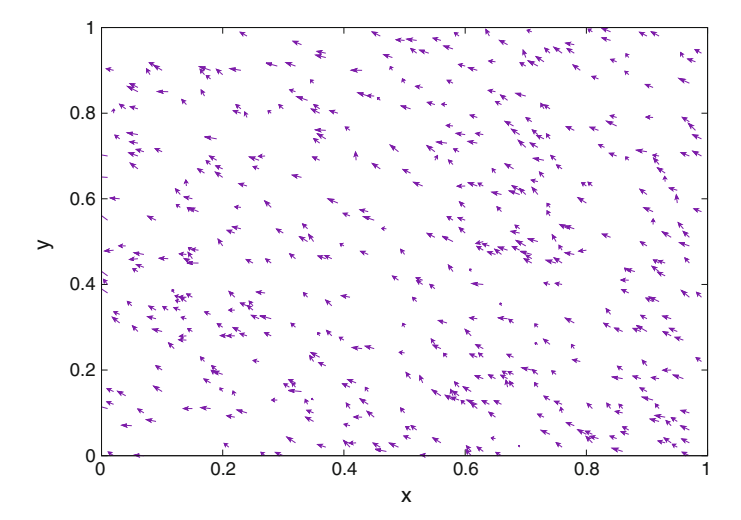


Fig. 6.2 A snapshot of the system configuration in the homogeneous swarming regime. Here $\phi = 0.05$, $\gamma = 9$, $\Gamma = 0.135$, and the order parameters result to be r = 0.994 (strong swarming) and C = 0.057 (negligible clustering)

6.4.2 Swarming Instability

Figure 6.2 displays the arising of swarming states in the model. These can be identified through the usual swarming order parameter r(t) identified to be

$$r(t) = \left| \frac{1}{N} \sum_{j=1}^{N} e^{i\theta_j(t)} \right|,$$
 (6.68)

where θ_j is the direction of velocity of the *j*th particle, so that $r(t) \approx 0$ in the fully disordered state and $r(t) \approx 1$ in the case of all particles' velocities aligned along the same direction.

Monitoring r(t) up to times $t_{\rm max}$ larger than the inverse of the minimum of the eigenvalues of $L(\mathbf{k})$ gives a reasonable idea of the fate of this initial condition and allows us to compare the system's phase diagram with the predictions of linear stability analysis. The swarming order is shown in Fig. 6.3 parameter r, averaged over the time interval $[t_{\rm max}/2, t_{\rm max}]$ so that the system has settled in the stationary regime, for three values of the density ϕ , together with the line predicted in Eq. (6.54). The comparison is fair at all values of ϕ , especially for $\phi=0.05$. It is likely that this value matches our analysis being the best compromise between the dilute and the large size limits at fixed volume V: on the contrary, for $\phi=0.01$ there are N=100 particles in the lattice, and for such a small value the fluctuations seem relevant; nevertheless, for $\phi=0.1$ we have N=1000 particles, so the fluctuations decrease but at the same time the system is moving away from the dilute limit.

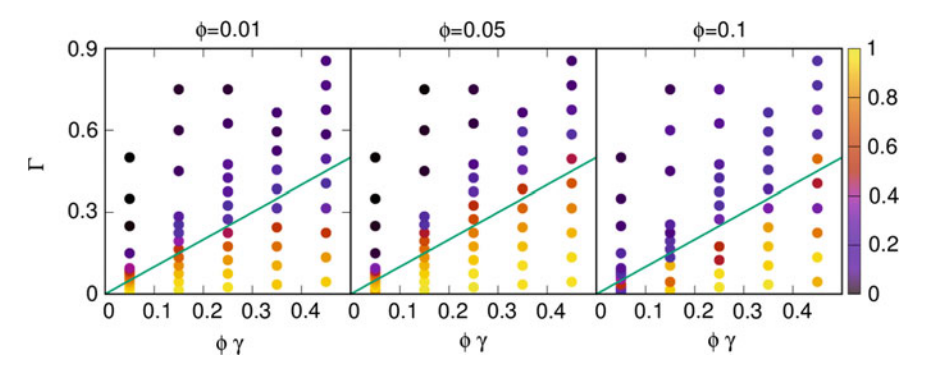


Fig. 6.3 Swarming phase parameter r (going from 0 in the disordered phase to 1 in the full swarming phase, see color legend on the right) as a function of relative noise amplitude Γ and rescaled relative dissipation rate $\phi\gamma$, for three different packing fractions ϕ . The solid lines indicate the theoretical transition, Eq. (6.54)

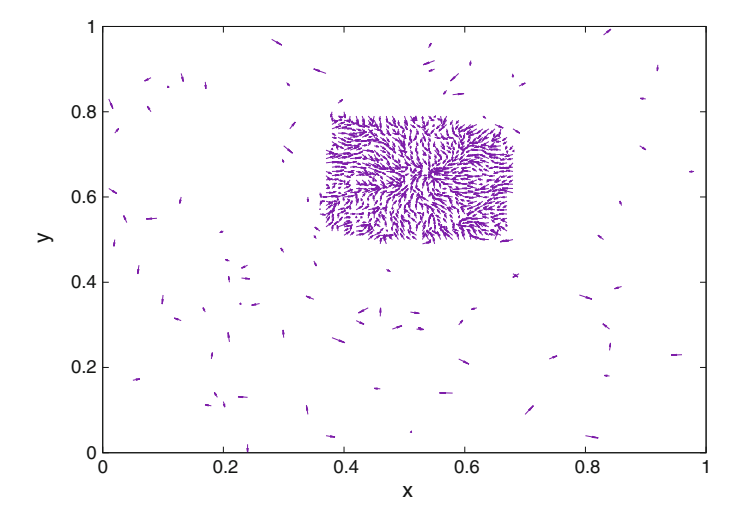


Fig. 6.4 A snapshot of the system configuration in the coexistence regime "cluster+gas". Here $\phi=0.1, \gamma=1.5, \Gamma=4.5$, and the order parameters result to be r=0.027 (negligible swarming) and C=0.874 (macroscopic clustering)

6.4.3 Clustering Instability

Clustering is another ordered phase observed in simulations. Contrarily from swarming, clustering is nonhomogeneous: typically, active units form a single, giant aggregate somewhere in the lattice while the rest of them swarm around, occasionally falling on the cluster or kicking away some particles at its borders. The typical clustered state in shown in Fig. 6.4.

6.4 Numerical Results 169

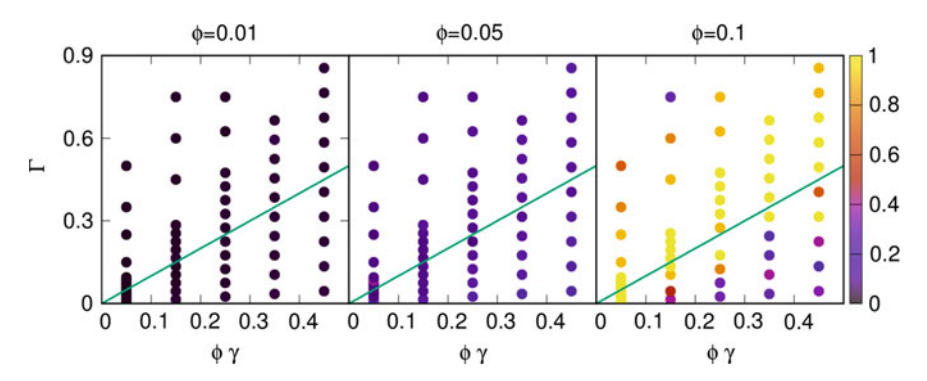


Fig. 6.5 Clustering phase parameter C (see color legend on the right) as a function of relative noise amplitude Γ and rescaled relative dissipation rate $\phi\gamma$. Same parameters of Fig. 6.3

In simulations, we can count the number $N_l(t)$ of pairs of first neighbors at time t, a number that goes from $N_l \approx 2\phi N$ in the unclustered case, up to $N_l \approx 2N$ in the fully clustered case, so that

$$C(t) = \frac{N_l(t)}{2N} \in [\phi, 1], \qquad (6.69)$$

is a good estimate of the clustering degree in the system. Of course, this parameter is significant only in dilute cases, with $\phi \ll 1$. As for the swarming state, a phase diagram in the $(\gamma - \Gamma)$ can be created, see Fig. 6.5.

It is clear that in the dilute cases, roughly speaking $\phi < 10\%$, there is no clustering in both disordered and swarming phases (i.e. above and below the solid line, see also Fig. 6.3).

On the contrary, at larger packing fraction $\phi \ge 10\%$ clustering arises as a stable phase *above* the critical noise amplitude for swarming. Looking at single configurations in the simulations - see Fig. 6.4 - we can attempt an interpretation: it seems that when swarming is possible (e.g. below the transition line), many particles in the dilute phase coordinate and erode efficiently the clusters. This is a sort of of "viscous heating" mechanism.

6.4.4 Finite-Size Effects Near the Transition

A preliminary study of the effect of lattice volume V has been performed to assess the quality of the observed gas-swarming transition in the dilute case. Choosing a dilute value of ϕ and an average value of γ , the swarming parameter $\langle r \rangle$ has been measured when moving from high noise $\Gamma > \Gamma_c(\gamma, \phi)$ to low noise $\Gamma < \Gamma_c(\gamma, \phi)$, where $\Gamma_c(\gamma, \phi) = \frac{2d}{d+2}\gamma\phi$ (see Eq. (6.54)), repeating this protocol for increasing values of V. If the transition is discontinuous in the continuum limit, we expect that the

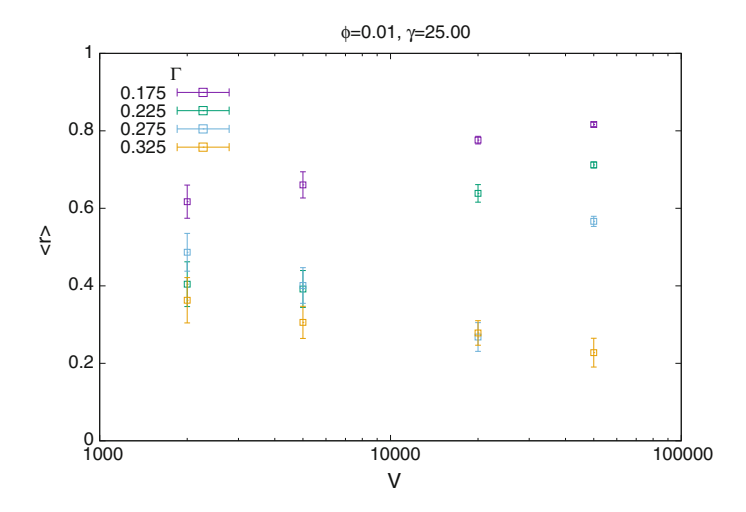


Fig. 6.6 Average value of the swarming parameter r, which goes from 0 in the disordered phase to 1 in the full swarming phase, as a function of the lattice volume V at a constant value of ϕ (dilute case) and γ , for four values of the relative noise amplitude Γ : two values are below the instability swarming threshold, two are above

separation between the swarming phase (high $\langle r \rangle$) and the disordered phase (low $\langle r \rangle$) increases with V. The result of the study is shown in Fig. 6.6. It indicates that the gap $r_+ - r_-$ between the value of r respectively slightly above and slightly below the transition tends to increase with V. This result gives the first hint that the observed transition may be discontinuous.

6.4.5 Fluctuating Currents

Numerical simulations have been also implemented in order to verify the prediction about current noises, defined in Eq. (6.55). In the case of Gaussian local velocity distribution, the noise correlation for the hopping current reads

$$\langle \sigma_l(\mathbf{x}, t) \sigma_{l'}(\mathbf{x}', t') \rangle = \delta(\mathbf{x} - \mathbf{x}') \delta(t - t') \delta_{l,l'} \phi(1 - \phi) \sqrt{\frac{2}{\pi} T(t)} (\Delta x)^{d+1} . \quad (6.70)$$

In the simulation the microscopic current $j_{i,p,l} = 0, \pm 1$ can be measured, representing the number of particles hopping - in the pth time step - from site i to its neighbors in the lth direction. In the homogeneous fully disordered state, Eq. (6.70) is equivalent, assuming ergodicity, to

6.4 Numerical Results 171

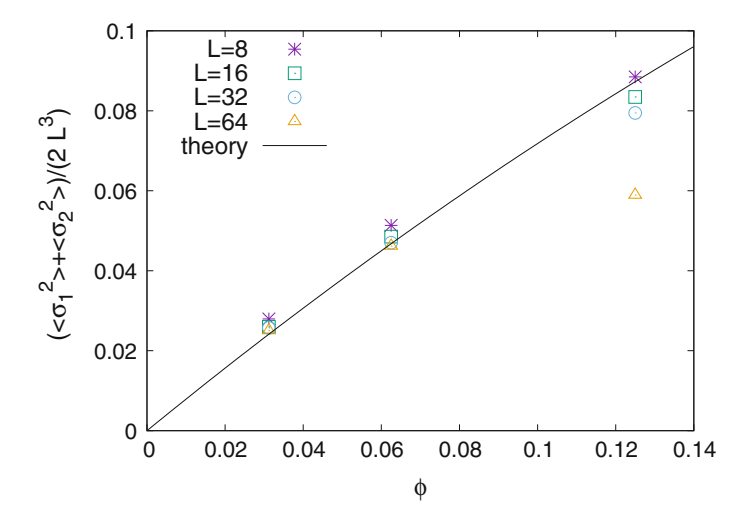


Fig. 6.7 Amplitude of fluctuations of the hopping current (symbols), and its theoretical prediction Eq. (6.70)–(6.71) (solid line), as function of ϕ for various sizes L. Here $\phi\gamma=0.25$, $\Gamma=4$ and the system is prepared at the steady temperature $T_0=1$. The fluctuations' amplitude is also averaged over its components, $\langle \sigma_1^2 \rangle$ and $\langle \sigma_2^2 \rangle$

$$\sum_{i,i'}^{1,V} \sum_{p,p'}^{1,t_{max}/\Delta t} j_{i,p,l} j_{i',p',l'} \simeq L^3 \phi (1-\phi) \sqrt{\frac{2}{\pi} T_0} t_{max}.$$
 (6.71)

The verification of this relation is shown in Fig. 6.7: we see that for $\phi < 10\%$ the numerical results tend to the theoretical value as $L \to \infty$. This trend is broken when $\phi > 10\%$, as expected in view of the used assumptions (Molecular Chaos and local Gaussian equilibrium) which are reasonable only in the dilute limit.

References

- A. Lasanta, A. Manacorda, A. Prados, Fluctuating hydrodynamics and mesoscopic effects of spatial correlations in dissipative systems with conserved momentum. New J. Phys. 17, 083039 (2015). https://doi.org/10.1088/1367-2630/17/8/083039
- A. Manacorda, C.A. Plata, A. Lasanta, A. Puglisi, A. Prados, Lattice models for granular-like velocity fields: hydrodynamic description. J. Stat. Phys. 164(4), 810–841 (2016). https://doi. org/10.1007/s10955-016-1575-z
- C.A. Plata, A. Manacorda, A. Lasanta, A. Puglisi, A. Prados, Lattice models for granular-like velocity fields: finite-size effects. J. Stat. Mech. (Theor. Exp.) 2016(9), 093203 (2016). http://stacks.iop.org/1742-5468/2016/i=9/a=093203, https://doi.org/10.1088/1742-5468/2016/09/093203
- A. Manacorda, A. Puglisi, Lattice model to derive the fluctuating hydrodynamics of active particles with inertia. Phys. Rev. Lett. 119, 208003 (2017). https://doi.org/10.1103/PhysRevLett. 119.208003

- D. Grossman, I.S. Aranson, E.B. Jacob, Emergence of agent swarm migration and vortex formation through inelastic collisions. New J. Phys. 10(2), 023036 (2008). http://stacks.iop. org/1367-2630/10/i=2/a=023036, https://doi.org/10.1088/1367-2630/10/2/023036
- T. Mora, A.M. Walczak, L. Del Castello, F. Ginelli, S. Melillo, L. Parisi, M. Viale, A. Cavagna, I. Giardina, Local equilibrium in bird flocks. Nat. Phys. 12(12), 1153–1157 (2016). https://doi. org/10.1038/nphys3846
- T. Vicsek, A. Zafeiris, Collective motion. Phys. Rep. 517(34), 71–140 (2012). http://www.sciencedirect.com/science/article/pii/S0370157312000968, https://doi.org/10.1016/j.physrep.2012.03.004
- T. Vicsek, A. Czirók, E. Ben-Jacob, I. Cohen, Novel type of phase transition in a system of self-driven particles. Phys. Rev. Lett. 75, 1226–1229 (1995). https://doi.org/10.1103/PhysRevLett. 75.1226
- 9. J. Tailleur, M.E. Cates, Statistical mechanics of interacting run-and-tumble bacteria. Phys. Rev. Lett. **100**, 218103 (2008). https://doi.org/10.1103/PhysRevLett.100.218103
- 10. L. Angelani, Run-and-tumble particles, telegraphers equation and absorption problems with partially reflecting boundaries. J. Phys. A Math. Theory **48**(49), 495003 (2015). http://stacks.iop.org/1751-8121/48/i=49/a=495003, https://doi.org/10.1088/1751-8113/48/49/495003
- R. Golestanian, Anomalous diffusion of symmetric and asymmetric active colloids. Phys. Rev. Lett. 102, 188305 (2009). https://doi.org/10.1103/PhysRevLett.102.188305
- J. Palacci, C. Cottin-Bizonne, C. Ybert, L. Bocquet, Sedimentation and effective temperature of active colloidal suspensions. Phys. Rev. Lett. 105, 088304 (2010). https://doi.org/10.1103/ PhysRevLett.105.088304
- A.P. Solon, M.E. Cates, Active Brownian particles and run-and-tumble particles: a comparative study. Eur. Phys. J. Spec. Top. 224(7), 1231–1262 (2015). https://doi.org/10.1140/epjst/e2015-02457-0
- B. Derrida, Y. Pomeau, Classical diffusion on a random chain. Phys. Rev. Lett. 48, 627–630 (1982). https://doi.org/10.1103/PhysRevLett.48.627
- B. Derrida, Velocity and diffusion constant of a periodic one-dimensional hopping model. J. Stat. Phys. 31(3), 433–450 (1983). https://doi.org/10.1007/BF01019492
- B. Derrida, Non-equilibrium steady states: fluctuations and large deviations of the density and of the current. J. Stat. Mech. (Theory Exp.) 2007(07), P07023 (2007). http://stacks.iop.org/ 1742-5468/2007/i=07/a=P07023, https://doi.org/10.1088/1742-5468/2007/07/P07023
- M.C. Marchetti, J.F. Joanny, S. Ramaswamy, T.B. Liverpool, J. Prost, M. Rao, R.A. Simha, Hydrodynamics of soft active matter. Rev. Mod. Phys. 85, 1143–1189 (2013). https://doi.org/ 10.1103/RevModPhys.85.1143
- C. Bechinger, R. Di Leonardo, H. Löwen, C. Reichhardt, G. Volpe, G. Volpe, Active particles in complex and crowded environments. Rev. Mod. Phys. 88, 045006 (2016). https://doi.org/ 10.1103/RevModPhys.88.045006
- N. Koumakis, C. Maggi, R. Di Leonardo, Directed transport of active particles over asymmetric energy barriers. Soft Matter 10, 5695–5701 (2014). https://doi.org/10.1039/C4SM00665H
- T.F.F. Farage, P. Krinninger, J.M. Brader, Effective interactions in active Brownian suspensions. Phys. Rev. E 91, 042310 (2015). https://doi.org/10.1103/PhysRevE.91.042310
- C. Maggi, U.M.B. Marconi, N. Gnan, R. Di Leonardo, Multidimensional stationary probability distribution for interacting active particles. Sci. Rep. 5, 10742 (2015). https://doi.org/10.1038/ srep10742
- U.M.B. Marconi, C. Maggi, Towards a statistical mechanical theory of active fluids. Soft Matter 11, 8768–8781 (2015). https://doi.org/10.1039/C5SM01718A

Chapter 7 Conclusions



In this thesis, we first of all reviewed the main properties of granular and active matter, underlining remarkable similarities between their physical behavior. The properties of their individual and collective motion have been analyzed in the framework of nonequilibrium statistical mechanics. Experiments and simulations suggested us a specularity between granular and active particles, especially because of the continuous energy exchanges driving the systems out of equilibrium and leading to the observed collective motion. Hydrodynamics has been introduced to describe the macroscopic behavior of fluid systems. Indeed, when many active or granular units are present, they can be seen as a flowing material under some assumptions. A derivation of hydrodynamics for conservative systems has been introduced and later extended to the granular case, while the recent developments on hydrodynamic descriptions of active matter have been reviewed. Finally, lattice models have been introduced as a powerful tool to analyze and foresee the behavior of nonequilibrium systems. My thesis' work has been focused on the analysis of granular and active matter through the formulation of two lattice models.

The first model we introduced is a lattice model of granular particles on a linear chain. A hydrodynamic description of the system has been derived: although some realism has been sacrificed in the formulation of the model, the latter has reproduced the average hydrodynamic equations derived from the kinetic theory of sheared granular gases. The characteristic granular states like the Homogeneous Cooling State, the Uniform Shear Flow and the Couette Flow have been derived and their hydrodynamic equations have been solved for each case, even in the transient or non-homogeneous state. The Homogeneous Cooling instability has been recovered, obtaining an exact expression for the critical value of dissipation and system size. We derived the fluctuating hydrodynamic currents and computed their noise properties at the leading order from microscopic dynamics, without the need of an equilibrium approximation: the latter has been used only in some cases of need to formulate the noise correlations in terms of hydrodynamic fields.

174 7 Conclusions

Interestingly, the interplay between momentum conservation and energy dissipation has shown several unforeseen properties: for finite systems, the global cooling contributes to the development of long-range spatial velocity correlations, which at the same time affect the temperature evolution. Velocity correlations between colliding particles are generally disregarded because of the Molecular Chaos ansatz. In our model, we can avoid this ansatz and obtain a closed set of equations for temperature and correlations from microscopic dynamics: both of them decay in time at the same rate, and the rescaled correlation profile tends to a steady value independent from initial conditions. Furthermore, the mesoscopic dissipation coefficient has been redefined through a multiple scales analysis. The fluctuations of rescaled total energy have shown a divergent behavior in time, an unexpected feature in our model: again, a microscopic derivation through average balance equations allowed the computation of the many-particles velocity moments and has shown a multiscaling behavior driving the fluctuations away from a stationary value. So, the model enables direct computations of fluctuating quantities under a few controlled assumptions, by means of a perturbative approach which may be easily extended to next orders, depending on the required accuracy.

The encouraging results on the granular lattice model inspired the formulation of a lattice model of active granular particles; the model was enhanced allowing hopping (and therefore compressibility) and moving to a general d > 1 case. Again, the model provided a clear and general derivation of hydrodynamic equations in the dilute limit from the microscopic rules of the model. For a specific choice of microscopic ingredients, hydrodynamic equations can be derived in the Local Equilibrium Approximation yielding the existence of homogeneous disordered and ordered states. The former has been proved to be unstable depending on the relative strength of noise, dissipation and self-propulsion: we derived a phase diagram, showing the competition between noise (fostering disorder) and dissipation (fostering order). When the disordered system is unstable, ordered phases like swarming or clustering arise. Two essential points must be underlined: first, hydrodynamic equations have shown that viscosity and heat transport are not required for the existence of a disorder-swarming transition. Second, when moving to the unstable region all the modes become simultaneously unstable: this is in contrast with HCS instability, which was actually caused by the first mode (longest wavelength) amplification and driven by viscosity, which is absent in our model of active matter. Furthermore, fluctuating currents have been computed also in the active case, and the theoretical results have shown a fair agreement with simulations.

The main result of this thesis is the development of a class of lattice models and a procedure to reproduce the average hydrodynamic equations of granular and active systems and derive their fluctuating hydrodynamics from microscopic behavior. In addition, the Molecular Chaos ansatz is not always needed because it is sometimes possible to compute the correlations in the system, as it has be shown for granular Maxwell Molecules: analytical results successfully explain the new phenomena observed in simulations. The procedure introduced may be applied to several other cases.

7 Conclusions 175

	Dissipation	Injection	Noise	Disordered state	Instability
Granular model	Inelasticity	Formal rescaling	absent	Homogeneous cooling state	Shear instability $\nu > \nu_c$
Active model	Aligning forces	Self- propulsion	White noise	Homogeneous disordered state	Swarming $\gamma > \gamma_c(\Gamma)$

Table 7.1 A comparative recap of granular and active models

The results obtained in the two models can be compared: indeed we have seen that strong analogies between granular and active model are present. In Table 7.1, the main features are presented both considering microscopic ingredients defining the models - dissipation, injection and noise terms - and concerning the most analyzed hydrodynamic states, namely the Homogeneous Cooling State and the homogeneous disordered state. Those are the most suitable for a direct comparison, which can be enhanced in further studies.

The models have shown to be adaptive, i.e. the rules determining their evolution can be easily changed separately. Further perspectives of the granular model include the generalization to d>1, a dilute case with hopping particles and the introduction of hard-spheres collisions. Also, adapting the model to the framework of Macroscopic Fluctuation Theory would be an intriguing challenge, since this has never been done for models with momentum conservation such as the one described here.

The active model can represent a basis for several possible developments: the first one is that the *ordered* phase still needs to be studied analytically. A next step may then be the hydrodynamic analysis of ordered phases such as swarming or clustering. It is probable that the Local Equilibrium Approximation will not be a good assumption any more for these states, so the development of a theory beyond Local Equilibrium and Molecular Chaos may be attempted, following the results derived for the granular model. Thereafter, the generality of the active system allows to introduce several choices for collisions, self-propulsion and all the physical parameters. A comparative study may clarify the role of microscopic parameters in macroscopic behavior, both in theoretical analysis and empirical observations. Further investigations may include the introduction of "Navier-Stokes" terms such as viscosity and heat conductivity.

The models presented can be seen as part of a wider framework, nonequilibrium statistical physics, and further studies may deal with several theoretical problems such as entropy production or fluctuation-dissipation relations. The theoretical achievements could be compared with further experimental evidences, pointing out new issues and research directions. The possibility of deriving new and more general results from the theoretical analysis here developed is still to be explored.

Appendix A

Analytical Results for the Granular Model

A.1 Microscopic Derivation of Balance Equations

Microscopic balance equations in Sect. 4.2.1 can be directly derived computing the gain and loss terms of local velocity $v_{l,p}$ as a stochastic processes in discrete time, writing a pseudo-Langevin equation. For our granular model, velocity $v_{l,p}$ evolves as

$$v_{l,p+1} = (1 - \delta_{y_p,l} - \delta_{y_p,l-1})v_{l,p} + \delta_{y_p,l} \left[v_{l,p} - \frac{1+\alpha}{2} \left(v_{l,p} - v_{l+1,p} \right) \right] + \delta_{y_p,l-1} \left[v_{l,p} + \frac{1+\alpha}{2} \left(v_{l-1,p} - v_{l,p} \right) \right],$$
(A.1)

where $\delta_{y_p,l}$ is selecting the colliding particle at the p-th time step. We can also write

$$v_{l,p+1} = v_{l,p} - \delta_{y_p,l} \frac{1+\alpha}{2} \left(v_{l,p} - v_{l+1,p} \right) + \delta_{y_p,l-1} \frac{1+\alpha}{2} \left(v_{l-1,p} - v_{l,p} \right)$$

$$= v_{l,p} - j_{l,p} + j_{l-1,p},$$
(A.2)

introducing the momentum current $j_{l,p}$, which for our system reads

$$j_{l,p} = \frac{1+\alpha}{2} \delta_{y_p,l} \left(v_{l,p} - v_{l+1,p} \right). \tag{A.3}$$

For the evolution of the kinetic energy, we square equation (A.2) and we obtain

$$v_{l,p+1}^{2} = v_{l,p}^{2} + \delta_{y_{p},l} \left[\left(\frac{1+\alpha}{2} \right)^{2} \left(v_{l,p} - v_{l+1,p} \right)^{2} - (1+\alpha) v_{l,p} \left(v_{l,p} - v_{l+1,p} \right) \right] + \delta_{y_{p},l-1} \left[\left(\frac{1+\alpha}{2} \right)^{2} \left(v_{l-1,p} - v_{l,p} \right)^{2} + (1+\alpha) v_{l,p} \left(v_{l-1,p} - v_{l,p} \right) \right],$$
(A.4)

© Springer International Publishing AG, part of Springer Nature 2018 A. Manacorda, *Lattice Models for Fluctuating Hydrodynamics in Granular and Active Matter*, Springer Theses, https://doi.org/10.1007/978-3-319-95080-8

which can be written as

$$v_{l,p+1}^{2} = v_{l,p}^{2} + \frac{\alpha^{2} - 1}{4} \left[\delta_{y_{p},l} \left(v_{l,p} - v_{l+1,p} \right)^{2} + \delta_{y_{p},l-1} \left(v_{l-1,p} - v_{l,p} \right)^{2} \right] - (v_{l,p} + v_{l+1,p}) j_{l,p} + (v_{l-1,p} + v_{l,p}) j_{l-1,p}. \tag{A.5}$$

We now compute the averages. For the velocity we have that

$$u_{l,p+1} - u_{l,p} = -\langle j_{l,p} - j_{l-1,p} \rangle,$$
 (A.6)

with

$$u_{l,p} = \langle v_{l,p} \rangle. \tag{A.7}$$

Reminding that $\langle \delta_{y_p,l} \rangle = 1/L$ in the MM case, we can compute the mean current

$$\langle j_{l,p} \rangle = \left\langle \frac{1+\alpha}{2} \delta_{y_p,l} \left(v_{l,p} - v_{l+1,p} \right) \right\rangle$$

$$= \frac{1+\alpha}{2L} \langle v_{l,p} - v_{l+1,p} \rangle$$

$$= \frac{1+\alpha}{2L} (u_{l,p} - u_{l+1,p}). \tag{A.8}$$

Then, the time evolution equation for the mean velocity is

$$u_{l,p+1} - u_{l,p} = \frac{1+\alpha}{2L}(u_{l+1,p} + u_{l-1,p} - 2u_{l,p}). \tag{A.9}$$

For the mean quadratic velocity, from Eq. (A.5) we have that

$$\langle v_{l,p+1}^{2} \rangle - \langle v_{l,p}^{2} \rangle = \frac{\alpha^{2} - 1}{4L} \left\langle \left(v_{l,p} - v_{l+1,p} \right)^{2} + \left(v_{l-1,p} - v_{l,p} \right)^{2} \right\rangle - \frac{1 + \alpha}{2L} \left\langle \left(v_{l,p} + v_{l+1,p} \right) \left(v_{l,p} - v_{l+1,p} \right) - \left(v_{l-1,p} + v_{l,p} \right) \left(v_{l-1,p} - v_{l,p} \right) \right\rangle.$$
(A.10)

Developing the terms on the rhs, we find

In order to close the rhs of the last equation, we factorize the 2-points correlations $\langle v_{l,p}v_{l\pm 1,p}\rangle=u_{l,p}u_{l\pm 1,p}$: this assumption correspond to the Molecular Chaos ansatz assumed in Sect. 4.2.1. Now, in the rhs of Eq. (A.5) we have

$$\begin{split} \left\langle v_{l,p+1}^{2} \right\rangle - \left\langle v_{l,p}^{2} \right\rangle &= -\frac{1 - \alpha^{2}}{L} \left[\left\langle v_{l,p}^{2} \right\rangle - \frac{1}{2} u_{l,p} (u_{l+1,p} + u_{l-1,p}) \right] \\ &+ \left(\frac{1 + \alpha}{2} \right)^{2} \frac{1}{L} \left(\left\langle v_{l+1,p}^{2} \right\rangle + \left\langle v_{l-1,p}^{2} \right\rangle - 2 \left\langle v_{l,p}^{2} \right\rangle \right). \end{split} \tag{A.12}$$

Equations (A.9) and (A.12) are the balance equations for our lattice system, with discrete sites l at discrete times p. Introducing the hydrodynamic scaling of Eq. (4.25)

$$x = \frac{l}{L}, \qquad \Delta x = \frac{1}{L}, \qquad \Delta t = \frac{1}{L^3}, \tag{A.13}$$

and by assuming that $u_{l,p}$ and $T_{l,p}$ are both smooth functions x = l/L, we can develop the following terms

$$u_{l\pm 1,p} = u_{l,p} \pm \frac{\partial u}{\partial x} \frac{1}{L} + \frac{1}{2} \frac{\partial^2 u}{\partial x^2} \frac{1}{L^2} + O(L^{-3})$$
(A.14)

$$\langle v_{l\pm 1,p}^2 \rangle = \langle v_{l,p}^2 \rangle \pm \frac{\partial \langle v^2 \rangle}{\partial x} \frac{1}{L} + \frac{1}{2} \frac{\partial^2 \langle v^2 \rangle}{\partial x^2} \frac{1}{L^2} + O(L^{-3}). \tag{A.15}$$

and with a similar development in $\Delta t = 1/L^3$ we have the evolution equations for the fields u(x,t) and $\langle v^2 \rangle(x,t)$

$$\frac{1}{L^3} \frac{\partial u}{\partial t} = \frac{1+\alpha}{2} \frac{1}{L^3} \frac{\partial^2 u}{\partial x^2} + O(L^{-4})$$
(A.16a)
$$\frac{1}{L^3} \frac{\partial \langle v^2 \rangle}{\partial t} = -\frac{1-\alpha^2}{L} (\langle v^2 \rangle - u^2) + \left(\frac{1+\alpha}{2}\right)^2 \frac{1}{L^3} \frac{\partial^2 \langle v^2 \rangle}{\partial x^2}$$

$$+ \frac{1-\alpha^2}{4} \frac{1}{L^3} 2u \frac{\partial^2 u}{\partial x^2} + O(L^{-4})$$
(A.16b)

We here introduce the macroscopic inelasticity coefficient ν , that in this case reads

$$\nu = L^2(1 - \alpha^2) > 0, (A.17)$$

and if we want ν to be finite we need $1 - \alpha = O(L^{-2})$. So, multiplying by L^3 and neglecting $O(L^{-1})$ terms, we have

$$\frac{\partial u}{\partial t} = \frac{1+\alpha}{2} \frac{\partial^2 u}{\partial x^2} \tag{A.18a}$$

$$\frac{\partial \langle v^2 \rangle}{\partial t} = -\nu(\langle v^2 \rangle - u^2) + \left(\frac{1+\alpha}{2}\right)^2 \frac{\partial^2 \langle v^2 \rangle}{\partial x^2} + \frac{1-\alpha^2}{4} 2u \frac{\partial^2 u}{\partial x^2}.$$
(A.18b)

Now, we find evolution equations for u(x, t) and T(x, t) by replacing $\langle v^2 \rangle(x, t) = T(x, t) + u^2(x, t)$ in Eq. (A.18b); the derivatives read

$$\frac{\partial \langle v^2 \rangle}{\partial t} = \frac{\partial T}{\partial t} + 2u \frac{\partial u}{\partial t} = \frac{\partial T}{\partial t} + \frac{1 + \alpha}{2} 2u \frac{\partial^2 u}{\partial x^2}$$
 (A.19a)

$$\frac{\partial^2 \langle v^2 \rangle}{\partial x^2} = \frac{\partial}{\partial x} \left(\frac{\partial T}{\partial x} + 2u \frac{\partial u}{\partial x} \right) = \frac{\partial^2 T}{\partial x^2} + 2\left(\frac{\partial u}{\partial x} \right)^2 + 2u \frac{\partial^2 u}{\partial x^2}$$
 (A.19b)

and substititung them into Eq. (A.18b), the $2u \frac{\partial^2 u}{\partial x^2}$ terms vanish and we have

$$\frac{\partial u}{\partial t} = \frac{1+\alpha}{2} \frac{\partial^2 u}{\partial x^2} \tag{A.20a}$$

$$\frac{\partial T}{\partial t} = -\nu T + \left(\frac{1+\alpha}{2}\right)^2 \left[\frac{\partial^2 T}{\partial x^2} + 2\left(\frac{\partial u}{\partial x}\right)^2\right],\tag{A.20b}$$

which are the evolution equations for u and T continuous in our model. Since the limit $L \to \infty$ yields $(1 + \alpha)/2 \to 1$, we finally have

$$\frac{\partial u}{\partial t} = \frac{\partial^2 u}{\partial x^2} \tag{A.21a}$$

$$\frac{\partial T}{\partial t} = -\nu T + \frac{\partial^2 T}{\partial x^2} + 2\left(\frac{\partial u}{\partial x}\right)^2. \tag{A.21b}$$

We found then that the velocity field u(x,t) follows a diffusion equation, while the temperature evolution equation (A.21b) shows the presence of sink, diffusion processes and viscous heating, represented respectively by the first, second and third term in Eq. (A.21b). The obtained results are equivalent to the ones discussed in Sect. 4.2.1: I presented an alternative derivation of hydrodynamic equations, without the need of a Boltzmann Equation, which has been our first derivation of hydrodynamic equations in this work.

A.2 Balance Equations for Moments with $n \ge 3$

Starting from the microscopic evolution equation (A.2), we can get the dynamic equations for any moment of the velocity with few considerations.

First of all, let's look at the δ -functions in Eq. (A.2); since we need to compute averages over trajectories, it is useful to see that for MM one has

$$\left\langle \delta_{y_p,l}^n \right\rangle = \left\langle \delta_{y_p,l} \right\rangle = \frac{1}{L}, \quad \left\langle \delta_{y_p,l}^n \delta_{y_p,l'}^m \right\rangle = 0 \quad \forall m, n > 1 \ (l \neq l')$$
 (A.22)

So, we can write

$$v_{l,p+1}^{n} - v_{l,p}^{n} = \sum_{k=1}^{n} {n \choose k} v_{lp}^{n-k} \left(j_{l-1,p} - j_{l,p} \right)^{k}$$

$$= \sum_{k=1}^{n} {n \choose k} v_{lp}^{n-k} \sum_{h=0}^{k} {k \choose h} \left(\frac{1+\alpha}{2} \right)^{k} \times \delta_{y_{n},l-1}^{k-h} \delta_{y_{n},l}^{h} \left(v_{l-1,p} - v_{l,p} \right)^{k-h} \left(v_{l+1,p} - v_{l,p} \right)^{h}. \quad (A.23)$$

When we average the two sides over the trajectories, we can exploit the properties in Eq. (A.22): the only terms remaining in the sum over h are for h = 0, k. Then, defining $\zeta = (1 + \alpha)/2$

$$\langle v_{l,p+1}^n \rangle - \langle v_{l,p}^n \rangle = \frac{1}{L} \sum_{k=1}^n \binom{n}{k} \zeta^k \left\langle v_{lp}^{n-k} \left[\left(v_{l-1,p} - v_{l,p} \right)^k + \left(v_{l+1,p} - v_{l,p} \right)^k \right] \right\rangle. \tag{A.24}$$

After some algebra, the term into square brackets reads

$$(v_{l-1,p} - v_{l,p})^k + (v_{l+1,p} - v_{l,p})^k = \sum_{j=0}^k {k \choose j} (-1)^{k-j} v_{l,p}^{k-j} \left(v_{l-1,p}^j + v_{l+1,p}^j \right),$$
(A.25)

then

$$\langle v_{l,p+1}^n \rangle - \langle v_{l,p}^n \rangle = \frac{1}{L} \sum_{k=1}^n \binom{n}{k} \zeta^k \sum_{j=0}^k \binom{k}{j} (-1)^{k-j} \left\langle v_{l,p}^{n-j} \left(v_{l-1,p}^j + v_{l+1,p}^j \right) \right\rangle. \tag{A.26}$$

We can now use the *Local Equilibrium approximation* to split the average into two parts: namely, the LEA is equivalent to

$$\langle v_{l,p}^{m} v_{l+1,p}^{n} \rangle_{LE} = \frac{1}{2\pi \sqrt{T_{l,p} T_{l+1,p}}} \int_{-\infty}^{+\infty} dv_{l} \int_{-\infty}^{+\infty} dv_{l+1} v_{l}^{m} v_{l+1}^{n}$$

$$\times \exp\left\{-\frac{(v_{l} - u_{l,p})^{2}}{2T_{l,p}}\right\} \exp\left\{-\frac{(v_{l+1} - u_{l+1,p})^{2}}{2T_{l+1,p}}\right\}$$

$$= \langle v_{l,p}^{m} \rangle_{LE} \langle v_{l+1,p}^{n} \rangle_{LE}, \qquad (A.27)$$

which includes not only Molecular Chaos but also the Gaussianity of the velocity distribution. This assumption allows us to compute all the moments independently. Furthermore, the expansion in Eq. (A.15) can be generalized and then

$$\left\langle v_{l,p+1}^{n}\right\rangle - \left\langle v_{l,p}^{n}\right\rangle = \frac{1}{L}\sum_{k=1}^{n}\sum_{j=0}^{k}\binom{n}{k}\binom{k}{j}\zeta^{k}(-1)^{k-j}\left\langle v_{l,p}^{n-j}\right\rangle \left[2\left\langle v_{l,p}^{j}\right\rangle + \frac{1}{L^{2}}\partial_{x}^{2}\left\langle v_{l,p}^{j}\right\rangle\right]. \tag{A.28}$$

We now move to the $L \to \infty$ limit: to lighten the notation, we introduce the momentum fields $u_n(x,t)$ defined as

$$u_n(x,t) = \lim_{L \to \infty} \left\langle v_{l,p}^n \right\rangle,\tag{A.29}$$

so that, with the continuum limit defined in Eqs. (A.13), (A.28) yields

$$\partial_t u_n(x,t) = \sum_{k=1}^n \sum_{j=0}^k \binom{n}{k} \binom{k}{j} \zeta^k (-1)^{k-j} u_{n-j}(x,t) \left[2L^2 u_j(x,t) + \partial_x^2 u_j(x,t) \right],$$
(A.30)

where the L^2 factor doesn't baffle us because the sum of the ζ^k will give the leading and also the subleading terms, knowing that $1 - \zeta = O(L^{-2})$. It is then possible to derive all the required moments, and to compute the central moments. For n = 1, 2, we recover the results of the previous paragraph; for $n \ge 3$, we have all the new dynamic equations we were looking for. For instance,

$$\partial_t u_3(x,t) = -\frac{3}{2}\nu \left[u_3(x,t) - u_1(x,t)u_2(x,t) \right] + \partial_x^2 u_3(x,t)$$
 (A.31a)

$$\partial_t u_4(x,t) = -2\nu \left[u_4(x,t) - u_1(x,t)u_3(x,t) \right] + \partial_x^2 u_4(x,t) \tag{A.31b}$$

... and so on.

The last equations are the first step of an infinite hierarchy. Interestingly, they are closed at each order: the equation for u_3 contains only $n \le 3$ fields, the equation for u_4 only $n \le 4$, etc. etc. So, starting from the equation for $u_1 \equiv u(x,t)$ one can solve the equations at any order for given boundary conditions. Equation (A.31) give us the evolution equations for central moments $\mu_n = \langle (v - u)^n \rangle$, which have been written in (4.36b).

A.3 Sum Rule

Here, we rigorously derive, in the continuum limit and up to $O(L^{-1})$, the sum rule (5.10) that stems from momentum conservation.

Our starting point is (5.5), which is equivalent to

$$T(t) + 2\sum_{k=1}^{\frac{L-1}{2}} D_k(t)\Delta x = 0, \quad \Delta x = L^{-1}.$$
 (A.32)

Now, we go to the continuum limit by making use of (5.7). To be precise, we denote here x = (k-1)/L by x_k . Then,

$$\int_{x_k}^{x_{k+1}} dx \, D(x,t) = L^{-1} D(x_k,t) + \frac{L^{-2}}{2} \partial_x D(x,t)|_{x_k} + O(L^{-3}). \tag{A.33}$$

Hence,

$$\sum_{k=1}^{\frac{L-1}{2}} \underbrace{D(x_k, t)}_{D_k(t)} \Delta x = \int_0^{\frac{1}{2} - \frac{1}{2L}} dx \ D(x, t) - \frac{L^{-1}}{2} \int_0^{\frac{1}{2} - \frac{1}{2L}} dx \ \partial_x D(x, t) + O(L^{-2})$$

$$= \int_0^{\frac{1}{2} - \frac{1}{2L}} dx \ D(x, t) - \frac{L^{-1}}{2} \left[D\left(\frac{1}{2} - \frac{1}{2L}, t\right) - D(0, t) \right] + O(L^{-2}). \tag{A.34}$$

The expression above can be further simplified to

$$\sum_{k=1}^{\frac{L-1}{2}} D_k(t) \Delta x = \int_0^{\frac{1}{2}} dx \, D(x,t) + \frac{L^{-1}}{2} \left[\psi(t) - 2\chi(t) \right] + O(L^{-2}), \tag{A.35}$$

where we have made use of the definitions of ψ and χ in (5.9). If we insert (A.35) into (A.32), we obtain (5.10) of the main text.

A.4 Energy Fluctuations

We here look at the normalized energy fluctuations for the granular model with Maxwell molecules. Our aim is a theoretical derivation of the quantity

$$\Sigma^{2}(t) \equiv \frac{\langle E^{2}(t) \rangle - \langle E(t) \rangle^{2}}{\langle E(t) \rangle^{2}}$$
 (A.36)

where $E(t) = \lim_{L \gg 1} E_p = \lim_{L \gg 1} \sum_{l=1}^{L} v_{lp}^2$.

From now on all our calculations will be done in the homogeneous state, i.e. where the system is invariant for space translation and inversion; hence, all the one-point fields become spatially flat fields, all the two-point fields become one-point fields, and so on.

If we assume local equilibrium, we have $\langle E(t) \rangle = LT(t)$ and $\langle E^2(t) \rangle = 3LT^2(t)$. So, local equilibrium prediction is $L\Sigma^2(t) = 2$. However, numerical results diverge from this value as time increases in trajectories. The numerical behavior of $L\Sigma^2(t)$ is shown in Fig. 5.4. This behavior cannot be explained with a local equilibrium assumption. We need to compute a result without using it, so let's go back to Eq. (A.36): we can see that

$$\langle E^{2}(t) \rangle = \left\langle \sum_{l,l'}^{1,L} v_{lp}^{2} v_{l'p}^{2} \right\rangle = \sum_{l=1}^{L} \left\langle v_{lp}^{4} \right\rangle + \sum_{l=1}^{L} \sum_{l' \neq l}^{1,L} \left\langle v_{lp}^{2} v_{l'p}^{2} \right\rangle$$

$$= L \left[q_{p} + \sum_{k=1}^{L-1} \left(C_{kp}^{22} + T_{p}^{2} \right) \right]$$
(A.37)

with the following definitions (the last will appear later)

$$\langle v_{l_p}^4 \rangle \equiv q_p,$$
 (A.38a)

$$\langle v_{ln}^2 v_{l+k,n}^2 \rangle \equiv C_{kn}^{22} + T_n^2,$$
 (A.38b)

$$\langle v_{lp}^3 v_{l\pm k,p} \rangle \equiv C_{kp}^{31},\tag{A.38c}$$

$$\langle v_{l \mp m,p} v_{lp}^2 v_{l \pm n,p} \rangle \equiv C_{mnp}^{121}. \tag{A.38d}$$

Hence, in the continuum limit we have

$$\Sigma^{2}(t) = \frac{1}{L^{2}T^{2}(t)} \left[Lq(t) + L(L-1)T^{2}(t) + L^{2} \int_{0}^{1} dx \, C^{22}(x,t) - L^{2}T^{2}(t) \right]$$

$$= \frac{1}{L} \frac{q(t) - T^{2}(t) + L \int_{0}^{1} dx \, C^{22}(x,t)}{T^{2}(t)}$$
(A.39)

From Sect. 5.1, we already know T(t) up to the L^{-1} order; we need to compute q(t) and $C^{22}(x, t)$ out of a local equilibrium approximation.

In Eq. (A.38) there are all the quartic fields that we will consider in these notes; they are all evolving in time with a Langevin equation that depends on the microscopic dynamics, as usual. For instance, reminding the velocity current definition

$$j_{lp} = \zeta \delta_{y_p,l} \left(v_{lp} - v_{l+1,p} \right) \quad \text{with } \zeta = \frac{1+\alpha}{2}$$
 (A.40)

for q_p we have

$$\begin{aligned} q_{p+1} &= \langle v_{l,p+1}^4 \rangle = \left\langle \left(v_{lp} - j_{lp} + j_{l-1,p} \right)^4 \right\rangle = \\ &= \langle v_{lp}^4 \rangle - 4 \left\langle v_{lp}^3 \left(j_{lp} - j_{l-1,p} \right) \right\rangle + 6 \left\langle v_{lp}^2 \left(j_{lp}^2 + j_{l-1,p}^2 \right) \right\rangle \\ &- 4 \left\langle v_{lp} \left(j_{lp}^3 - j_{l-1,p}^3 \right) \right\rangle + \left\langle j_{lp}^4 + j_{l-1,p}^4 \right\rangle = \\ &= q_p + \frac{1}{L} \left\{ - 4\zeta \left\langle v_{lp}^3 \left(v_{lp} - v_{l+1,p} - v_{l-1,p} + v_{lp} \right) \right\rangle \right. \\ &+ 6\zeta^2 \left\langle v_{lp}^2 \left[\left(v_{lp} - v_{l+1,p} \right)^2 + \left(v_{l-1,p}^2 - v_{lp} \right)^2 \right] \right\rangle \\ &- 4\zeta^3 \left\langle v_{lp} \left[\left(v_{lp} - v_{l+1,p} \right)^3 - \left(v_{l-1,p}^2 - v_{lp} \right)^3 \right] \right\rangle \\ &+ \zeta^4 \left\langle \left(v_{lp} - v_{l+1,p} \right)^4 + \left(v_{l-1,p}^2 - v_{lp} \right)^4 \right\} = \end{aligned}$$

$$= \cdots = q_p - \frac{4\zeta (1-\zeta)}{L} \left\{ [2-\zeta (1-\zeta)] \left(q_p - C_{1p}^{31} \right) + 3\zeta (1-\zeta) \left(C_{1p}^{31} - C_{1p}^{22} \right) \right\},$$
(A.41)

where we exploited the delta properties in the partial averages of the velocity current, which for Maxwell molecules read (from Eq. (A.40))

$$\langle f(\mathbf{v}_p) j_{lp} \rangle = \frac{\zeta}{L} \langle f(\mathbf{v}_p) \left(v_{lp} - v_{l+1,p} \right) \rangle$$
 (A.42a)

$$\left\langle f(\mathbf{v}_p) j_{lp} j_{l'p} \right\rangle = \frac{\zeta^2}{L} \delta_{l,l'} \left\langle f(\mathbf{v}_p) \left(v_{lp} - v_{l+1,p} \right)^2 \right\rangle \tag{A.42b}$$

$$\left\langle f(\mathbf{v}_p) \left(\prod_{i=1}^n j_{l_i,p} \right) \right\rangle = \frac{\zeta^n}{L} \left(\prod_{i=2}^n \delta_{l_1,l_i} \right) \left\langle f(\mathbf{v}_p) \left(v_{l_1,p} - v_{l_1+1,p} \right)^n \right\rangle. \tag{A.42c}$$

Equation (A.41) is very similar to Eq. (5.4) in Sect. 5.1. Indeed, for the temperature we had

$$T_{p+1} = T_p - \frac{4\zeta (1-\zeta)}{L} \left(T_p - C_{1p} \right) \tag{A.43}$$

where from its definition in Eq. (A.40) we have that 4ζ (1 – ζ) = 1 – $\alpha^2 = \nu L^{-2}$. We write Eq. (A.41) with its explicit dependence on L as

$$q_{p+1} - q_p = -\frac{2\nu}{L^3} \left[\left(1 - \frac{\nu}{8L^2} \right) \left(q_p - C_{1p}^{31} \right) + \frac{3\nu}{8L^2} \left(C_{1p}^{31} - C_{1p}^{22} \right) \right], \quad (A.44)$$

hence, neglecting $\mathcal{O}(L^{-2})$ terms in the rhs, for $L\gg 1$ we have the continuous equation

$$\dot{q}(t) = -2\nu \left[q(t) - \Gamma^{31}(t) \right] \tag{A.45}$$

using the same continuum limit of Sect. 5.1, i.e. $\Gamma^{31}(t) = \lim_{x\to 0} C^{31}(x,t)$ and $\Gamma^{22}(t) = \lim_{x\to 0} C^{22}(x,t)$.

Since we don't have any information about the magnitude of C^{31} and C^{22} , we perform a cluster expansion; in our homogenous case with $\langle v_{lp} \rangle = 0$, we have

$$\langle v_{lp}^{3} v_{l\pm k,p} \rangle = 3 \langle v_{lp}^{2} \rangle \langle v_{lp} v_{l\pm k,p} \rangle + g_{kp}^{31}$$

$$= 3T_{p}C_{kp} + g_{kp}^{31},$$
(A.46)

$$\langle v_{lp}^2 v_{l\pm k,p}^2 \rangle = \langle v_{lp}^2 \rangle \langle v_{l\pm k,p}^2 \rangle + 2 \langle v_{lp} v_{l\pm k,p} \rangle^2 + g_{kp}^{22}$$

$$= T_p^2 + 2C_{kp}^2 + g_{kp}^{22},$$
(A.47)

where g^{31} and g^{22} are the purely correlated terms. Then, continuous fields are

$$C^{31}(x,t) = 3T(t)C(x,t) + g^{31}(x,t), \tag{A.48}$$

$$C^{22}(x,t) = 2C^2(x,t) + g^{22}(x,t).$$
 (A.49)

The leading terms in the rhs of Eqs. (A.46), (A.47) are respectively $3TC = \mathcal{O}(T_0^2/L)$ and T^2 . Then, we assume that purely correlated terms are subleading with respect to previous ones, then $g^{31}(x,t) = \mathcal{O}(T_0^2/L^2)$ and $g^{22}(x,t) = \mathcal{O}(T_0^2/L)$. So, we have that both C^{31} and C^{22} are at most $\mathcal{O}(T_0^2/L)$. Then, Γ^{31} in Eq. (A.45) is a L^{-1} correction and introducing the same expansion of Sect. 5.1^2

$$q(t) = q_0(t) + \frac{1}{L}q_1(t) + \frac{1}{L^2}q_2(t) + \dots,$$
 (A.50a)

$$LC^{31}(x,t) \equiv D^{31}(x,t) = D_0^{31}(x,t) + \frac{1}{L}D_1^{31}(x,t) + \dots,$$
 (A.50b)

$$LC^{22}(x,t) \equiv D^{22}(x,t) = D_0^{22}(x,t) + \frac{1}{L}D_1^{22}(x,t) + \dots,$$
 (A.50c)

we can solve Eq. (A.45) at the zeroth order that is

$$\begin{cases} \dot{q_0} = -2\nu q_0 \\ q_0(t=0) = 3T_0^2(t=0) \end{cases} \Rightarrow q_0(t) = 3T_0^2(t=0)e^{-2\nu t}. \tag{A.51}$$

This solution is the local equilibrium solution that is exact when $L = \infty$. We see that the quartic velocity field is cooling as $T_0^2(t)$, so we introduce the usual rescaled fields

$$\tilde{q}(t) \equiv q(t)/T_0^2(t) = q(t)e^{2\nu t}/T_0^2(t=0),$$
 (A.52)

and analogously we define $\tilde{D^{31}}$ and $\tilde{D^{22}}$. The tilde represent the Haff's law scaling taking into account the dimension of the field, so $\tilde{T}(t)$ and $\tilde{D}(x,t)$ are still scaled with $T_0(t=0)e^{-\nu t}$.

Hence, we have the following equations for \tilde{q}_0 and \tilde{q}_1

$$\frac{\mathrm{d}}{\mathrm{d}t}\tilde{q_0} = 0,\tag{A.53}$$

$$\frac{\mathrm{d}}{\mathrm{d}t}\tilde{q}_1 = 2\nu\psi^{31}(t). \tag{A.54}$$

So we have $\tilde{q}_0 = 3$, and the first order correction for q(t) may be computed once we know $D^{31}(x, t)$.

¹Ansatz n.1.

²Where we use the rescaled fields D^{31} and D^{22} , which shouldn't necessarily vanish in the continuum limit, and we define $\psi^{31}=L\Gamma^{31},\,\psi^{22}=L\Gamma^{22}$.

We then move to the study of the time evolution of D^{31} and D^{22} : first, we introduce the following exact initial conditions for our model

$$T(t=0) = T_0(t=0) \left(1 - \frac{1}{L}\right),$$
 (A.55a)

$$D(x, t = 0) = -T_0(t = 0),$$
 (A.55b)

$$q(t=0) = 3T_0^2(t=0)\left(1 - \frac{1}{L}\right)^2,$$
 (A.55c)

$$D^{31}(x, t = 0) = -3T_0^2(t = 0)\left(1 - \frac{1}{L}\right),\tag{A.55d}$$

$$D^{22}(x, t = 0) = \frac{2}{L}T_0^2(t = 0).$$
 (A.55e)

which derivation can be found in Sect. A.4.1. Second, we derive evolution equations for D^{31} and D^{22} with the same technique used for D field; then, we write the difference in time for C_{1p}^{31} , C_{kp}^{31} , C_{1p}^{22} , C_{kp}^{22} (with $k \ge 2$); we neglect the equation for k = L/2 because the symmetry of the system yields a reflecting boundary at all orders at x = 1/2 (however I studied it in calculations, you can check this result if you wish).

After some painful algebra one gets

$$C_{1,p+1}^{31} = \left\langle \left(v_{lp} - j_{lp} + j_{l-1,p} \right)^{3} \left(v_{l+1,p} - j_{l+1,p} + j_{lp} \right) \right\rangle =$$

$$= \cdots =$$

$$= C_{1p}^{31} + \frac{1}{L} \left\{ -7\zeta \left(1 - \zeta \right) \left[1 - \frac{8}{7}\zeta \left(1 - \zeta \right) \right] C_{1p}^{31} + \right.$$

$$+ \left. \left(\zeta^{3} + \zeta \right) \left(C_{2p}^{31} - C_{1p}^{31} \right) + \right.$$

$$+ \zeta \left(1 - \zeta \right) \left[1 - 2\zeta \left(1 - \zeta \right) \right] \left(q_{p} + 3T_{p}^{2} + 3C_{1p}^{22} \right) + \right.$$

$$+ 3\zeta \left(1 - \zeta \right) \left[\left(1 - \zeta \right) C_{1,1,p}^{121} + \zeta C_{-2,1,p}^{121} \right] \right\}$$
(A.56)

$$C_{k,p+1}^{31} = \left\langle \left(v_{lp} - j_{lp} + j_{l-1,p} \right)^3 \left(v_{l+k,p} - j_{l+k,p} + j_{l+k-1,p} \right) \right\rangle =$$

$$= \cdots =$$

$$= C_{kp}^{31} + \frac{1}{L} \left\{ -6\zeta \left(1 - \zeta \right) C_{kp}^{31} + \left(\zeta^3 + \zeta \right) \left(C_{k+1,p}^{31} + C_{k-1,p}^{31} - 2C_{kp}^{31} \right) + C_{kp}^{31} \right\}$$

$$+3\zeta (1-\zeta) \left[(1-\zeta) \left(C_{-1,k,p}^{121} + C_{1,k,p}^{121} \right) + \right.$$

$$\left. + \zeta \left(C_{1,k-1,p}^{121} + C_{-1,k+1,p}^{121} \right) \right] \right\}$$
(A.57)

$$C_{1,p+1}^{22} = \left\langle \left(v_{lp} - j_{lp} + j_{l-1,p} \right)^{2} \left(v_{l+1,p} - j_{l+1,p} + j_{lp} \right)^{2} \right\rangle - T_{p+1}^{2} =$$

$$= \cdots =$$

$$= C_{1p}^{22} + \frac{1}{L} \left\{ -8\zeta \left(1 - \zeta \right) \left[1 - \frac{3}{4}\zeta \left(1 - \zeta \right) \right] C_{1p}^{22} + \right.$$

$$+ 2\zeta^{2} \left(C_{2p}^{22} - C_{1p}^{22} \right) - 8\zeta \left(1 - \zeta \right) T_{p} C_{1p} +$$

$$+ 4\zeta \left(1 - \zeta \right) \left[1 - 2\zeta \left(1 - \zeta \right) \right] C_{1p}^{31} +$$

$$+ 2\left[\zeta \left(1 - \zeta \right) \right]^{2} \left(q_{p} + 3T_{p}^{2} \right) + 4\zeta \left(1 - \zeta \right) C_{-2,1,p}^{121} +$$

$$- 16 \frac{\left[\zeta \left(1 - \zeta \right) \right]^{2}}{L} \left(T_{p} - C_{1p} \right)^{2} \right\}$$
(A.58)

$$C_{k,p+1}^{22} = \left\langle \left(v_{lp} - j_{lp} + j_{l-1,p} \right)^2 \left(v_{l+k,p} - j_{l+k,p} + j_{l+k-1,p} \right)^2 \right\rangle - T_{p+1}^2 =$$

$$= \cdots =$$

$$= C_{kp}^{22} + \frac{1}{L} \left\{ -8\zeta \left(1 - \zeta \right) \left(C_{kp}^{22} + T_p C_{1p} \right) + 2\zeta^2 \left(C_{k+1,p}^{22} + C_{k-1,p}^{22} - 2C_{kp}^{22} \right) + 4\zeta \left(1 - \zeta \right) \left(C_{-k,k-1,p}^{121} + C_{-(k+1),k,p}^{121} \right) + 16\frac{\left[\zeta \left(1 - \zeta \right) \right]^2}{L} \left(T_p - C_{1p} \right)^2 \right\}$$
(A.59)

where the · · · indicate long, painful but straightforward algebra.

These equations rule the time evolution of C^{31} and C^{22} ; before going to the continuum limit, we notice that they all contain the 3-point correlation function $C^{121}_{i,j,p} = \left\langle v_{l \mp i,p} v_{lp}^2 v_{l \pm j,p} \right\rangle$ defined in Eq. (A.38d). We *don't* want to derive ad hydrodynamic equation for this field too; so, we use a cluster expansion to approximate it, and we find

$$C_{ijp}^{121} = \langle v_{lp}^2 \rangle \langle v_{l \mp i,p} v_{l \pm j,p} \rangle + 2 \langle v_{lp} v_{l \mp i,p} \rangle \langle v_{lp} v_{l \pm j,p} \rangle + g_{i,j,p}^{121}$$

= $T_p C_{i+j,p} + 2 C_{ip} C_{jp} + g_{i,j,p}^{121}$ (A.60)

so we see that the leading term is $T_pC_{1p} = \mathcal{O}(L^{-1})$. To get a closed set of equations, we neglect $g_{i,j,p}^{121-3}$ and we write

$$C_{1,1,p}^{121} \simeq T_p C_{2p} + 2C_{1p}^2$$
 (A.61a)

$$C_{-2,1,p}^{121} \simeq T_p C_{1p} + 2C_{1p} C_{2p}$$
 (A.61b)

$$C_{-1,k,p}^{121} \simeq T_p C_{k-1,p} + 2C_{1p} C_{kp}$$
 (A.61c)

. .

... and so on.

With this second ansatz and the quasielastic limit 4ζ $(1-\zeta)=\nu L^{-2}$, through the usual hydrodynamic scaling for space and time

$$\Delta x = \frac{1}{L}, \quad x = \frac{k-1}{L} \tag{A.62a}$$

$$\Delta t = \frac{1}{L^3} \,, \quad t = \frac{p}{L^3} \tag{A.62b}$$

we get the continuous evolution equations for both fields:

$$\begin{split} \frac{1}{L^4} \partial_t \psi^{31}(t) &= \frac{1}{L^4} \left\{ -\frac{7\nu}{4} \left(1 - \frac{2\nu}{7L^2} \right) \psi^{31}(t) + \right. \\ &\quad + 2L \left(1 - \frac{\nu}{2L^2} + \mathcal{O}(L^{-4}) \right) \left(\partial_x D^{31}|_{x=0} + \frac{1}{2L} \partial_x^2 D^{31}|_{x=0} + \mathcal{O}(L^{-2}) \right) \\ &\quad + \frac{\nu}{4} \left(1 - \frac{\nu}{2L^2} \right) \left[L \left(q(t) + 3T^2(t) \right) + 3\psi^{22}(t) \right] + \\ &\quad + \frac{3\nu}{4} \left[\frac{\nu}{4L^2} \left(T(t) \left(\psi(t) + L^{-1} \partial_x D|_{x=0} + \mathcal{O}(L^{-2}) \right) + 2L^{-1} \psi^2(t) \right) + \\ &\quad + \left(1 - \frac{\nu}{4L^2} \right) \left(T(t) \psi(t) + 2L^{-1} \psi(t) \left(\psi(x, t) + L^{-1} \partial_x D|_{x=0} + \mathcal{O}(L^{-2}) \right) \right) \right] \right\} \end{split}$$

$$(A.63)$$

$$\begin{split} \frac{1}{L^4} \partial_t D^{31}(x,t) &= \frac{1}{L^4} \left\{ -\frac{3\nu}{2} D^{31}(x,t) + \right. \\ &+ 2 \left(1 - \frac{\nu}{2L^2} + \mathcal{O}(L^{-4}) \right) \left(\partial_x^2 D^{31} \right) + \\ &+ \frac{3\nu}{4} \left[\frac{\nu}{4L^2} \left(2T(t) D(x,t) + \mathcal{O}(L^{-2}) \right) + \right. \\ &\left. + \left(1 - \frac{\nu}{2L^2} \right) \left(2T(t) D(x,t) + 4L^{-1} \psi(t) D(x,t) + \mathcal{O}(L^{-2}) \right) \right] \right\} \end{split}$$

$$(A.64)$$

³Ansatz n.2.

$$\begin{split} \frac{1}{L^4} \partial_t \psi^{22}(t) &= \frac{1}{L^4} \left\{ -2\nu \left(1 - \frac{3\nu}{16L^2} \right) \psi^{22}(t) - \nu T(t) \psi(t) + \right. \\ &\quad + 2L \left(1 - \frac{\nu}{2L^2} + \mathcal{O}(L^{-4}) \right) \partial_x D^{22}|_{x=0} + \nu \left(1 - \frac{\nu}{2L^2} \right) \psi^{31}(t) + \\ &\quad + \frac{2\nu}{L} \psi(t) \left(\psi(t) + L^{-1} \partial_x D|_{x=0} + \mathcal{O}(L^{-2}) \right) + \\ &\quad + \frac{\nu^2}{8L} \left(q(t) + 3T^2(t) \right) - \frac{\nu^2}{L^2} \left(T(t) - \frac{1}{L} \psi(t) \right)^2 \bigg\} \end{split} \tag{A.65}$$

$$\frac{1}{L^4} \partial_t D^{22}(x,t) = \frac{1}{L^4} \left\{ -2\nu D^{22}(x,t) + \frac{4\nu}{L} D^2(x,t) + \mathcal{O}(L^{-2}) + 2\left(1 - \frac{\nu}{2L^2} + \mathcal{O}(L^{-4})\right) \left(\partial_x^2 D^{22} + \mathcal{O}(L^{-2})\right) + \frac{\nu^2}{L^2} \left(T(t) - \frac{1}{L}\psi(t)\right)^2 \right\}$$
(A.66)

Equations (A.63)–(A.66) are the coupled evolution equations for the 4th order correlations: they can be solved separately at each order, together with the perturbative solution of q(t) from Eq. (A.45). we then write the first order with the help of the expansion defined in Eq. (A.50), in terms of rescaled fields as defined in Eq. (A.52). So, we get

we get
$$\begin{cases}
\partial_t \tilde{D}_0^{31}(x,t) = 2\partial_x^2 \tilde{D}_0^{31}(x,t) + \frac{\nu}{2} \left[\tilde{D}_0^{31}(x,t) + 3\tilde{D}_0(x,t) \right] \\
\partial_x \tilde{D}_0^{31}(x,t)|_{x=0} = -\frac{3}{4}\nu \\
\partial_x \tilde{D}_0^{31}(x,t)|_{x=1/2} = 0 \\
\tilde{D}_0^{31}(x,t) = 0 = -3
\end{cases}$$
(A.67)

where we used the result $\tilde{T}_0 = 1$, and for long times we have the solution

$$\tilde{D_0^{31}}(x) = 3\tilde{D}_0(x) \tag{A.68}$$

which confirm that at the first order the clustering approximation is good. For $D_0^{22}(x, t)$ we have

$$\begin{cases} \partial_t \tilde{D}_0^{22}(x,t) = 2\partial_x^2 \tilde{D}_0^{22}(x,t) \\ \partial_x \tilde{D}_0^{22}(x,t)|_{x=0} = 0 \\ \partial_x \tilde{D}_0^{22}(x,t)|_{x=1/2} = 0 \\ \tilde{D}_0^{22}(x,t) = 0 \end{cases}$$
(A.69)

that immediately lead to the flat solution

$$\tilde{D}_0^{22}(x,t) \equiv 0 \tag{A.70}$$

So, we can compute the correction to the cooling of q(t) and solve Eq. (A.53): for long times we have

$$\tilde{q}_1(t) = \tilde{q}_1(t_s) + 6\tilde{\psi}_{\infty}\nu(t - t_s)$$
 (A.71)

where t_s is the time at which we have $\partial_t \tilde{D}(x, t)|_{t \ge t_s} = 0$.

The results of Eqs. (A.68), (A.70), (A.71) can be plugged into Eq. (A.39), yielding

$$\begin{split} L\sigma^{2}(t) &= \frac{\tilde{q}(t) + \int_{0}^{1} \mathrm{d}x \, \tilde{D}^{22}(x,t)}{\tilde{T}^{2}(t)} - 1 = \\ &= \frac{\tilde{q}_{0} + \int_{0}^{1} \mathrm{d}x \, \tilde{D}^{22}_{0} + L^{-1}\left(\tilde{q}_{1} + \int_{0}^{1} \mathrm{d}x \, \tilde{D}^{22}_{1}\right) + \cdots}{\tilde{T}_{0} + 2L^{-1}\tilde{T}_{0}\tilde{T}_{1} + \cdots} - 1 = \\ &= 2 + \frac{1}{L}\left[\tilde{q}_{1}(t_{s}) + 6\tilde{\psi}_{\infty}\nu(t - t_{s}) + \int_{0}^{1} \mathrm{d}x \, \tilde{D}^{22}_{1} - 6\left(\tilde{T}_{1}(t_{s}) + \tilde{\psi}_{\infty}\nu(t - t_{s})\right)\right] + \mathcal{O}(L^{-2}) \end{split}$$

$$(A.72)$$

Equation (A.72) shows that local equilibrium result is valid only at first order in L^{-1} ; corrections are found, but linearly increasing contributions vanish. So, the time dependence shown in Fig. 5.4 must come from $D_1^{22}(x, t)$; going to this order (now the leading order for D^{22}), from Eqs. (A.65), (A.66) we have that

$$\begin{cases} \partial_t \tilde{D}_1^{22} = 2\partial_x^2 \tilde{D}_1^{22}(x,t) + 4\nu \tilde{D}_0^2(x,t) \\ \partial_x \tilde{D}_1^{22}|_{x=0} = -\nu \tilde{\psi}_0(t) \\ \partial_x \tilde{D}_1^{22}|_{x=1/2} = 0 \\ \tilde{D}_1^{22}(x,t=0) = 2 \end{cases}$$
(A.73)

We don't know how to solve this system; however, all we need to know to compute the fluctuations is $\int_0^1 dx D_1^{22}(x, t) = \tilde{d}_1(t)$. So, integrating over x the first equation in Eq. (A.73), we have

$$\frac{\mathrm{d}}{\mathrm{d}t}\tilde{d}_{1}(t) = 2\left[\partial_{x}\tilde{D}_{1}^{22}|_{x=1^{-}} - \partial_{x}\tilde{D}_{1}^{22}|_{x=0^{+}}\right] + 4\nu \int_{0}^{1} \mathrm{d}x\,\tilde{D}_{0}^{2}(x,t) =
= 4\nu \left[\tilde{\psi}_{0}(t) + \int_{0}^{1} \mathrm{d}x\,\tilde{D}_{0}^{2}(x,t)\right]$$
(A.74)

when for long times we have

$$\tilde{D}_0(x,t) \underset{t \gg 1}{\longrightarrow} \tilde{D}_{\infty}(x) = -\frac{1}{2} \sqrt{\frac{\nu}{2}} \frac{\cos\left(\frac{1}{2}\sqrt{\frac{\nu}{2}}(1-2x)\right)}{\sin\left(\frac{1}{2}\sqrt{\frac{\nu}{2}}\right)} \tag{A.75}$$

$$\tilde{\psi}_0(t) \underset{t \gg 1}{\longrightarrow} \tilde{\psi}_\infty = -\frac{1}{2} \sqrt{\frac{\nu}{2}} \cot\left(\frac{1}{2} \sqrt{\frac{\nu}{2}}\right)$$
 (A.76)

hence the long times solution of Eq. (A.74) reads

$$\tilde{d}_{1}(t) = \tilde{d}_{1}(t_{s}) + 4 \left[-\frac{1}{2} \sqrt{\frac{\nu}{2}} \cot\left(\frac{1}{2} \sqrt{\frac{\nu}{2}}\right) + \frac{\nu}{16 \sin^{2}\left(\frac{1}{2} \sqrt{\frac{\nu}{2}}\right)} \left(1 + \frac{\sin\sqrt{\nu/2}}{\sqrt{\nu/2}}\right) \right] \nu(t - t_{s})$$

$$= \tilde{d}_{1}(t_{s}) + m_{\Sigma}(\nu)\nu(t - t_{s})$$
(A.77)

for which fluctuations can be written as

$$L\Sigma^{2}(t) = 2 + \frac{1}{L} \left(\tilde{q}_{1}(t_{s}) - 6\tilde{T}_{1}(t_{s}) + \tilde{d}_{1}(t_{s}) + m_{\Sigma}(\nu)\nu(t - t_{s}) \right) + \mathcal{O}(L^{-2})$$
(A.79)

We have derived an analytical prediction for the slope of $L\Sigma^2(t)$ for long times; the constant term depends on the transient evolution and cannot be computed at this stage. The final result is the slope of energy fluctuations

$$m(\nu) = \frac{\sqrt{\nu/2}}{\sin\left(\frac{1}{2}\sqrt{\frac{\nu}{2}}\right)} \left[\frac{\frac{1}{2}\sqrt{\frac{\nu}{2}}}{\sin\left(\frac{1}{2}\sqrt{\frac{\nu}{2}}\right)} - \cos\left(\frac{1}{2}\sqrt{\frac{\nu}{2}}\right) \right] \nu \tag{A.80}$$

leading to the result in (5.37).

The result has been derived through a linear perturbative expansion; however, a multiple-scales approach has been developed as well. The calculations are very complicated and don't lead to a improved agreement with simulation, so we don't report them here.

A.4.1 Initial Conditions in the Center of Mass Frame

To get the initial conditions in Eq. (A.55), we have to consider the correct velocity distribution to perform the averages.

At t = 0, we draw L velocities w_l with zero average and T_0 variance, hence their pdf is

$$P(\mathbf{w}) = \prod_{l=1}^{L} p(w_l)$$

with
$$p(w_l) = \exp(-w_l^2/2T_0)/\sqrt{2\pi T_0}$$
.

We move to the center of mass inertial frame, so we make a change of variables with the new ones

$$v_i = w_i - \frac{1}{L} \sum_{l=1}^{L} w_l$$

Then we can compute the averages: to compute the initial variance, for example, we have

$$\begin{split} \left\langle v_{i}^{2} \right\rangle &= \int \mathrm{d}w_{i} \; p(w_{i}) \left(w_{i} - \frac{1}{L} \sum_{l=1}^{L} w_{l} \right)^{2} \\ &= \int \mathrm{d}w_{i} \; p(w_{i}) \left(w_{i}^{2} - \frac{2}{L} w_{i} \sum_{l=1}^{L} w_{l} + \frac{1}{L^{2}} \sum_{l,l'}^{1,L} w_{l} w_{l'} \right) \\ &= \left\langle w_{i}^{2} \right\rangle - \frac{2}{L} \sum_{l=1}^{L} \left\langle w_{i} w_{l} \right\rangle + \frac{1}{L^{2}} \left(\sum_{l=1}^{L} \left\langle w_{l}^{2} \right\rangle + \sum_{l \neq l'}^{1,L} \left\langle w_{l} w_{l'} \right\rangle \right) \\ &= T_{0} - \frac{2}{L} \sum_{l=1}^{L} T_{0} \delta_{il} + \frac{1}{L^{2}} \sum_{l=1}^{L} T_{0} \\ &= T_{0} \left(1 - \frac{1}{L} \right) \end{split}$$

To compute the initial correlation function, we exploit the property that velocities are i.i.d., i.e. correlations are flat and all site pairs are equivalent; so, when $i \neq j$

$$\begin{split} \left\langle v_i v_j \right\rangle &= \int \mathrm{d}w_i \; p(w_i) \left(w_i - \frac{1}{L} \sum_{l=1}^L w_l \right) \left(w_j - \frac{1}{L} \sum_{l'=1}^L w_{l'} \right) \\ &= \left\langle w_i w_j \right\rangle - \frac{1}{L} \sum_{l=1}^L \left\langle \left(w_i + w_j \right) w_l \right\rangle + \frac{1}{L^2} \sum_{l,l'}^{1,L} \left\langle w_l w_{l'} \right\rangle \\ &= -\frac{1}{L} \sum_{l=1}^L T_0 \left(\delta_{il} + \delta_{jl} \right) + \frac{1}{L^2} \sum_{l=1}^L T_0 \\ &= -\frac{T_0}{L} \end{split}$$

Similarly all the initial fields can be computed with the right correction in powers of L^{-1} .

Appendix B

Analytical Results for the Active Model

B.1 Self-propulsion with Nonlinear Friction

The Rayleigh–Helmoltz friction (2.82b) used as a self-propulsion force in (6.38) is a first-order differential equation equivalent to the Cauchy problem

$$y'(x) = y(x)(1 - y^{2}(x))$$

 $y(0) = y_{0}$ (B.1)

in adimensional variables, namely $y = v/v_s$ and $x = \omega_s t$. The equation can be integrated by separating its variables, and the solution reads

$$y(x) = \frac{y_0 e^x}{\sqrt{1 + y_0^2 (e^{2x} - 1)}}$$
 (B.2)

when $|y_0| < 1$ and C is an integration constant. A similar solution showing exponential approach to the fixed point y = 1 can be found for $|y_0| > 1$. Note that the solutions are symmetrical when changing $y_0 \to -y_0$, then $y(x) \to -y(x)$. In Fig. B.1 the solutions for three different initial values $y_0 = -0.2$, 0.5, 4: it is worth remarking the absence of oscillations when approaching the fixed point y = 1 and the fast relaxation when $|y_0| > 1$ compared to the slow one for $|y_0| < 1$.

B.2 Absence of Viscosity at First-Order

The momentum current given by momentum transport in pairwise interaction is given by Eq. (6.9) and reads

$$J_{\mathbf{i}}^{(int)} \equiv n_{\mathbf{i}} n_{\mathbf{i}+\mathbf{e}_{l}} f_{k}^{(2)}(\mathbf{v}_{\mathbf{i}}, \mathbf{v}_{\mathbf{i}+\mathbf{e}_{l}}) \Delta t$$
 (B.3)

© Springer International Publishing AG, part of Springer Nature 2018 A. Manacorda, *Lattice Models for Fluctuating Hydrodynamics in Granular and Active Matter*, Springer Theses, https://doi.org/10.1007/978-3-319-95080-8

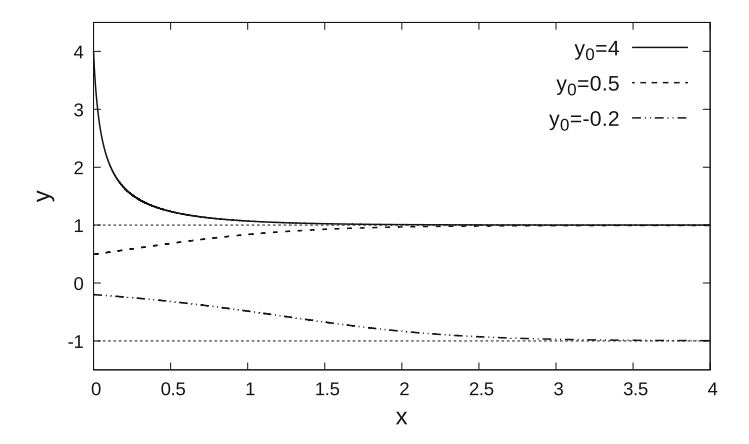


Fig. B.1 Solution of the differential equation in (B.1) for three different values of initial conditions, see legend

Its averaged value can be computed as

$$\left\langle J_{\mathbf{i},kl}^{(int)} \right\rangle = \rho_{\mathbf{i}} (1 - \rho_{\mathbf{i} + \mathbf{e}_{l}}) \int d\mathbf{v} \, d\mathbf{v}' \, P_{\mathbf{i}}(\mathbf{v}, t) \, P_{\mathbf{i} + \mathbf{e}_{l}}(\mathbf{v}', t) \, f_{k}^{(2)}(\mathbf{v}, \mathbf{v}') \, \Delta t \tag{B.4}$$

where we have used the Molecular Chaos assumption stated in (6.16) and the factorization in (6.17). Now we move to the continuum limit through the smoothness ansatz in (6.18), which is equivalent to

$$P_{\mathbf{i}+\mathbf{e}_l}(\mathbf{v},t) = P(\mathbf{v};\mathbf{x},t) \pm \frac{1}{L} \left. \frac{\partial P}{\partial x_l} \right|_{(\mathbf{x},t)} + O(1/L^2).$$
 (B.5)

This expansion can be introduced in Eq. (B.4), leading to

$$\left\langle J_{kl}^{(int)} \right\rangle (\mathbf{x}, t) = \rho [1 - \rho + O(1/L)]$$

$$\times \int d\mathbf{v} \, d\mathbf{v}' \, P(\mathbf{v}; \mathbf{x}, t) \left[P(\mathbf{v}; \mathbf{x}, t) \pm \frac{1}{L} \frac{\partial P}{\partial x_l} + O(1/L^2) \right] f_k^{(2)}(\mathbf{v}, \mathbf{v}') \Delta t$$
(B.6)

but the first term in the parenthesis vanishes because of momentum conservation in (6.1), $\mathbf{f}^{(2)}(\mathbf{v}, \mathbf{v}') = -\mathbf{f}^{(2)}(\mathbf{v}', \mathbf{v})$. So, one has $\left\langle J_{kl}^{(int)} \right\rangle(\mathbf{x}, t) = O(\Delta t/L)$ and $J_{kl}^{(int)}$ does not enter in the average momentum evolution equation (6.20b) at the first order $O(\Delta t)$.

B.3 Fluctuating Currents of Active Matter

The noise correlations of the density current can be derived substituting microscopic (fluctuating) density current from Eq. (6.6) into Eq. (6.56), yielding

$$\langle j_{\mathbf{i},p,l} j_{\mathbf{i}',p,l'} \rangle = \left\langle (\delta_{\boldsymbol{\xi}_p,\mathbf{i}} \delta_{\boldsymbol{\zeta}_p,\mathbf{e}_l} - \delta_{\boldsymbol{\xi}_p,\mathbf{i}+\mathbf{e}_l} \delta_{\boldsymbol{\zeta}_p,-\mathbf{e}_l}) (\delta_{\boldsymbol{\xi}_p,\mathbf{i}'} \delta_{\boldsymbol{\zeta}_p,\mathbf{e}_l'} - \delta_{\boldsymbol{\xi}_p,\mathbf{i}'+\mathbf{e}_l'} \delta_{\boldsymbol{\zeta}_p,-\mathbf{e}_l'}) \right\rangle$$
(B.7)

taking the current at equal time p = p' because fast variables ξ_p and ζ_p are independent at different times, so the correlations must vanish.

The only non vanishing terms are the product between the first and ones in the two parenthesis, because they respectively account for particles hopping in the positive or negative directions. One easily sees that

$$\left\langle \delta_{\boldsymbol{\xi}_{p},\mathbf{i}}\delta_{\boldsymbol{\zeta}_{p},\mathbf{e}_{l}}\delta_{\boldsymbol{\xi}_{p},\mathbf{i}'}\delta_{\boldsymbol{\zeta}_{p},\mathbf{e}'_{l}} \right\rangle = \delta_{\mathbf{i},\mathbf{i}'}\delta_{l,l'}\left\langle \delta_{\boldsymbol{\xi}_{p},\mathbf{i}}\delta_{\boldsymbol{\zeta}_{p},\mathbf{e}_{l}} \right\rangle \\
= \delta_{\mathbf{i},\mathbf{i}'}\delta_{l,l'}\left\langle n_{\mathbf{i}}(1-n_{\mathbf{i}+\mathbf{e}_{l}})\Theta(v_{\mathbf{i},l}|v_{\mathbf{i},l}|\right\rangle \frac{\Delta t}{\Delta x} \tag{B.8}$$

and analogously

$$\left\langle \delta_{\boldsymbol{\xi}_{p},\mathbf{i}+\mathbf{e}_{l}} \delta_{\boldsymbol{\zeta}_{p},-\mathbf{e}_{l}} \delta_{\boldsymbol{\xi}_{p},\mathbf{i}'+\mathbf{e}_{l}} \delta_{\boldsymbol{\zeta}_{p},-\mathbf{e}'_{l}} \right\rangle = \delta_{\mathbf{i},\mathbf{i}'} \delta_{l,l'} \left\langle n_{\mathbf{i}+\mathbf{e}_{l}} (1-n_{\mathbf{i}}) \Theta(-v_{\mathbf{i}+\mathbf{e}_{l},l}|v_{\mathbf{i}+\mathbf{e}_{l},l}|) \frac{\Delta t}{\Delta x}.$$
(B.9)

Separating the (independent) density and velocity contribution and using Molecular Chaos one has

$$\langle j_{\mathbf{i},p,l} j_{\mathbf{i}',p,l'} \rangle = \delta_{\mathbf{i},\mathbf{i}'} \delta_{p,p'} \delta_{l,l'} [\rho_{\mathbf{i}} (1 - \rho_{\mathbf{i}+\mathbf{e}_{l}}) \langle \Theta(v_{\mathbf{i},l}) | v_{\mathbf{i},l} | \rangle + \rho_{\mathbf{i}+\mathbf{e}_{l}} (1 - \rho_{\mathbf{i}}) \langle \Theta(-v_{\mathbf{i}+\mathbf{e}_{l},l}) | v_{\mathbf{i}+\mathbf{e}_{l},l} | \rangle].$$
(B.10)

Smoothness assumption on the probability distribution in (B.5) yields

$$\langle \Theta(-v_{\mathbf{i}+\mathbf{e}_{l},l})|v_{\mathbf{i}+\mathbf{e}_{l},l}|\rangle = \langle \Theta(-v_{\mathbf{i},l})|v_{\mathbf{i},l}|\rangle + O(1/L)$$
(B.11)

so the two terms in the rhs of Eq. (B.10) sum up and at the first order give

$$\langle j_{\mathbf{i},p,l} j_{\mathbf{i}',p,l'} \rangle \sim \delta_{\mathbf{i},\mathbf{i}'} \delta_{p,p'} \delta_{l,l'} \rho_{\mathbf{i}} (1-\rho_{\mathbf{i}}) \langle |v_{\mathbf{i},l}| \rangle \frac{\Delta t}{\Delta x}$$
 (B.12)

because $[\Theta(x) + \Theta(-x)]|x| = |x|$. The procedure shown is completely general and holds as well for momentum and energy currents: one simply has to compute the correlations through Eq. (B.7) substituting the current of the transported quantity $\chi(\mathbf{v})$, namely

$$J_{\mathbf{i},l}^{(\chi)} \equiv \delta_{\boldsymbol{\xi}_p,\mathbf{i}} \delta_{\boldsymbol{\zeta}_p,\mathbf{e}_l} \chi(\mathbf{v_i}) - \delta_{\boldsymbol{\xi}_p,\mathbf{i}+\mathbf{e}_l} \delta_{\boldsymbol{\zeta}_p,-\mathbf{e}_l} \chi(\mathbf{v_{i}+\mathbf{e}_l}). \tag{B.13}$$

Appendix C Videos

This appendix contains a collection of links to video showing experiments and simulations on granular matter, active matter and hydrodynamics, cited in Part II, which can be useful to clarify the meaning of the discussed phenomenology.

C.1 Granular Matter

- Granular jamming through a hopper: https://youtu.be/IWSJwZhqoQw, by J. Tang and R.P. Behringer, Duke Physics.
- A demonstration of possible applications of granular jamming: https://youtu.be/ZKOI_IVDPpw by Cornell Creative Machines Lab.
- Convection and segregation can be seen through an experimental realization of the Brazil-nut effect, see https://youtu.be/PGDP5DomhWc by Chung, Liaw and Ju.
- Pattern formation is shown at https://youtu.be/s0XYrW1X0ig (experiment and simulations) and https://youtu.be/CpZaRn0Bez0 (simulations), respectively made by Howard Duan at Toronto university and by Simons Foundation.
- A granular simulation showing clustering during cooling of a granular gas is shown at https://youtu.be/ObyE8mrDjRE, made by Stefan Luding at Twente University; another clustering simulation can be found at https://youtu.be/ap_PcMC2cdE, made by the MPIDS-DCF group.
- Experimental visualization and qualitative explaination of granular jets: https://youtu.be/Nt4jzVUEJjo, by Sixty Symbols with Roger Bowley.
- An experiment on a shaken granular showing several granular phases and Leidenfrost effect: https://youtu.be/ueCtAlHXxCU, by Bagnoli and Guarino at Florence University
- A granular rotor used to build a ratchet is shown at https://youtu.be/aHrdY4BC71k, made by the GranularChaos group in Rome.

200 Appendix C: Videos

C.2 Active Matter

 Synchronization of metronomes (Kuramoto): https://youtu.be/Aaxw4zbULMs, by Harvard Natural Science Lectures Demonstrations.

- Swarming bacteria: https://youtu.be/q27Jn3h4kpE by Matthew Copeland, University of Wisconsin.
- Bird flocks in Rome: https://youtu.be/8V6qUUWa4zk (Science Channel).
- Simulations showing active matter phase separation: https://youtu.be/JtY2rtw P9v0, ratchet effect: https://youtu.be/oOtKNO-AEbY and shepherding: https://youtu.be/aIcaAuqP_KY. Made by Danielle McDermott at Wabash University.

C.3 Hydrodynamic Instabilities

Here the main hydrodynamic instabilities connected with the

- The Rayleigh–Taylor instability: https://youtu.be/yabqo7VFTYs, by Jens Niemeyer at Göttingen University
- The Kelvin–Helmoltz instability is experimentally presented at https://youtu.be/ UbAfvcaYr00 and numerically shown at https://youtu.be/mZ19gLn6Fx4. Videos respectively made by the DAMTP, University of Cambridge, and by Jens Niemeyer.
- The Plateau—Rayleigh instability: https://youtu.be/UYRGEINpO50, by the BYUS-plashLab, Ira A. Fulton College.
- The Saffman–Taylor instability: https://youtu.be/FqC7VGTGh4U, by Fluid Dynamics students at Dalhousie University, lecturer David Barclay.